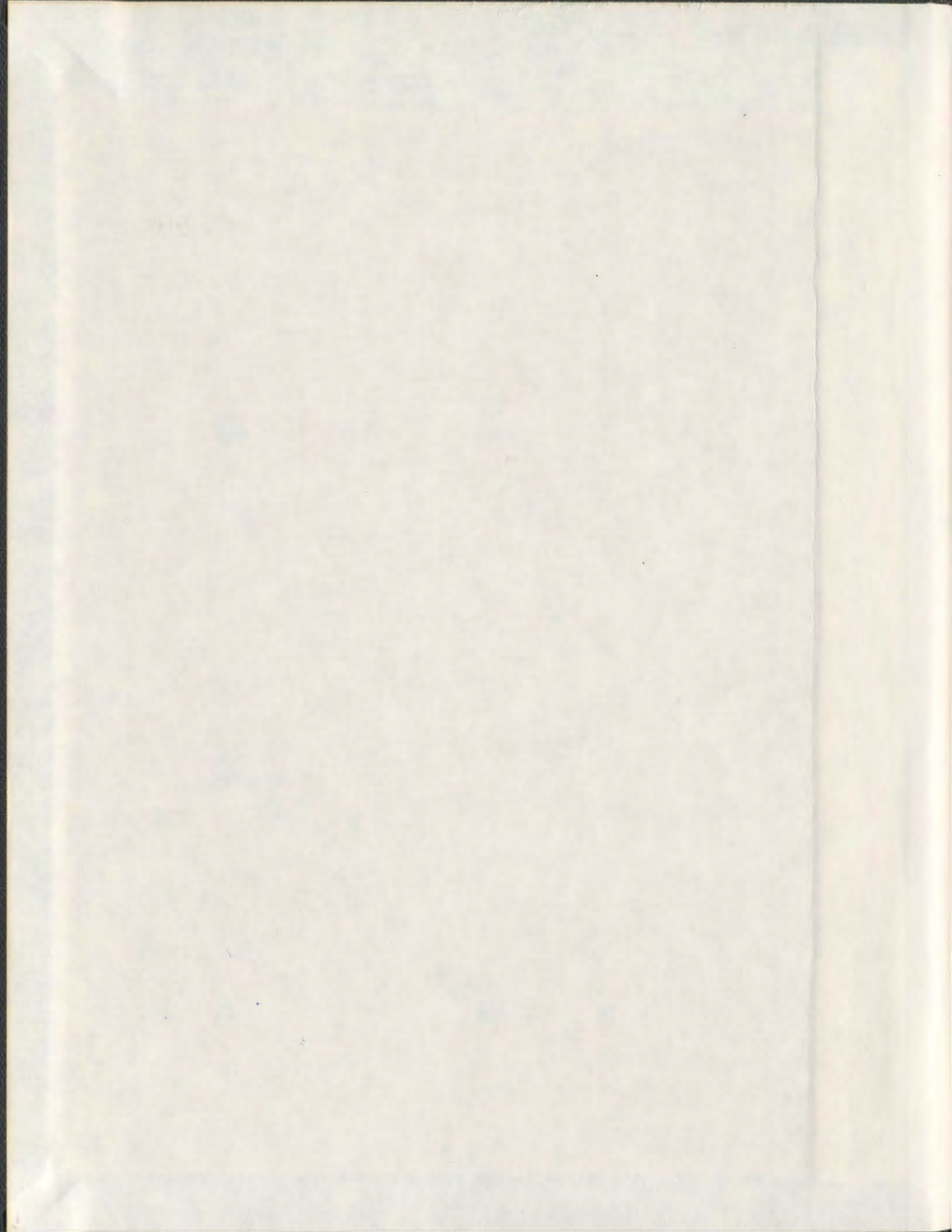


COMPUTATIONAL STUDIES OF REACTIONS INVOLVING  
1<sup>ST</sup>, 2<sup>ND</sup> AND 3<sup>RD</sup> ROW ELEMENTS AND THE  
PERFORMANCE OF THEORY

MOHAMMAD SHAHIDUL ISLAM



001311





**COMPUTATIONAL STUDIES OF REACTIONS INVOLVING  
1<sup>ST</sup>, 2<sup>ND</sup> AND 3<sup>RD</sup> ROW ELEMENTS AND THE  
PERFORMANCE OF THEORY**

**BY**

**MOHAMMAD SHAHIDUL ISLAM**

**A DISSERTATION  
IN PARTIAL FULFILMENT OF THE REQUIREMENTS FOR THE  
DEGREE OF DOCTOR OF PHILOSOPHY**

**DEPARTMENT OF CHEMISTRY  
MEMORIAL UNIVERSITY OF NEWFOUNDLAND**

**DECEMBER, 2007**

**ST. JOHN'S**

**NEWFOUNDLAND**

**CANADA**

## Abstract

This thesis has involved detailed computational studies of the mechanisms of several chemical reactions involving first, second and third row elements. Geometries of the relevant molecules were optimized at the HF, MP2 and B3LYP levels using the 6-31G(d), 6-31+G(d), 6-31G(d,p) and aug-cc-pVDZ basis sets. Gaussian-n theories such as G3MP2, G3MP2B3 and G3B3 were also used, as they are expected to adequately reproduce experimental data. The complete reaction pathways for all the mechanisms have been verified using intrinsic reaction coordinate (IRC) analysis.

The reactions of  $\text{SiH}_3\text{X}$  ( $\text{X} = \text{H}, \text{Cl}, \text{Br}, \text{I}$ ) with HCN were investigated and three different mechanisms were obtained. One of the mechanisms involves HX elimination by a one-step pathway producing  $\text{SiH}_3\text{CN}$ . The second mechanism consists of  $\text{H}_2$  elimination, producing  $\text{SiH}_2\text{XCN}$  via a one-step pathway or three multiple-step pathways. The third mechanism involves dissociation of  $\text{SiH}_3\text{X}$  to various products, which can then react with HCN.

We have found for the first time that the mechanism of the addition of bromine to alkenes involves reaction with two bromine molecules in non-polar aprotic solvents, while in polar protic solvents the mechanism involves reaction with a single bromine molecule mediated by a solvent molecule. For both cases, the calculated activation energies were found to be in excellent agreement with experiment. We proposed a kinetic

expression that accounts for the difference between bromination of alkenes in protic and aprotic solvents. We also found that bromination of adamantylideneadamantane should occur spontaneously in the gas phase as well as in some solvents with no reaction barrier.

We have found that for third row elements the BC6-31G basis set which is widely used as a 6-31G basis set in most of the commercial quantum chemistry packages does not meet the definition of the standard 6-31G basis set. A comparative study of the performance of the standard 6-31G and Binning-Curtiss (BC6-31G) basis sets for third row elements, Ga, Ge, As, Se, and Br, was carried out. Frequencies and thermodynamic values obtained by using the standard 6-31G basis set are better than those obtained using the BC6-31G basis set when compared to experiment and G3MP2. We recommend that the standard 6-31G basis set be used for calculations involving 3<sup>rd</sup> row elements.

The kinetic isotope effects (KIEs), a major experimental tool to determine the transition state (TS) structure, have been used to characterize the transition state structure of S<sub>N</sub>2 reactions. Chlorine leaving group  $k^{35}/k^{37}$ , nucleophile carbon  $k^{11}/k^{14}$  and secondary  $\alpha$ -deuterium  $[(k_H/k_D)_\alpha]$  kinetic isotope effects (KIEs) have been calculated for the S<sub>N</sub>2 reactions between *para*-substituted benzyl chlorides and cyanide ion and compared to the experimental results to determine whether these isotope effects can be used to determine the substituent effect on the structure of the transition state. It was found that both leaving group and nucleophile KIE vary with the TS structure. However, a correct and measurable substituent effect on leaving group KIEs will only be found for

a very reactant-like or for a very product-like TS. The substituent effect on nucleophile KIEs will only be found when the Nu-C<sub>α</sub> bond formation in the TS is well advanced i.e., in a product-like S<sub>N</sub>2 TS.

Nucleophile carbon  $k^{11}/k^{14}$  and secondary  $\alpha$ -deuterium  $[(k_H/k_D)_\alpha]$  kinetic isotope effects (KIEs) were also calculated for the S<sub>N</sub>2 reactions between tetrabutylammonium cyanide and ethyl iodide, bromide, chloride and tosylate and compared to the experimental results to determine whether these isotope effects can be used to determine the structure of the S<sub>N</sub>2 transition states. The results showed that the nucleophile carbon  $k^{11}/k^{14}$  KIEs can be used to determine the transition state structure in different reactions and the results suggest that changing to a poorer leaving group leads to a tighter transition state. The magnitude of the experimental secondary  $\alpha$ -deuterium KIE is related to the nucleophile – leaving group distance in the S<sub>N</sub>2 transition state ( $R_{TS}$ ) for reactions with a halogen leaving group. However, the calculated and experimental  $\alpha$ -deuterium KIEs show opposite trends with leaving group ability.

In conclusion, the results of my doctoral research have greatly increased our knowledge of the mechanisms, transition state structures and the thermodynamic properties of reactions involving 1<sup>st</sup>, 2<sup>nd</sup> and 3<sup>rd</sup> row elements.

## Acknowledgements

All praises to the Almighty, the Most Gracious and the Most Benevolent God (Allah) for his infinite mercy bestowed on me in completing this great task within the stipulated time and fulfilling my life dream.

In the eve of submitting this dissertation, I cannot but express my deepest sense of gratitude and indebtedness to my respected teacher and supervisor Prof. Raymond A. Poirier, Department of Chemistry, Memorial University, for his kind advice, indispensable guidance and thoughtful suggestions throughout the research work. I must confess that without his continuous inspiration and constant supervision, it would have been difficult to complete and present this dissertation in such a form.

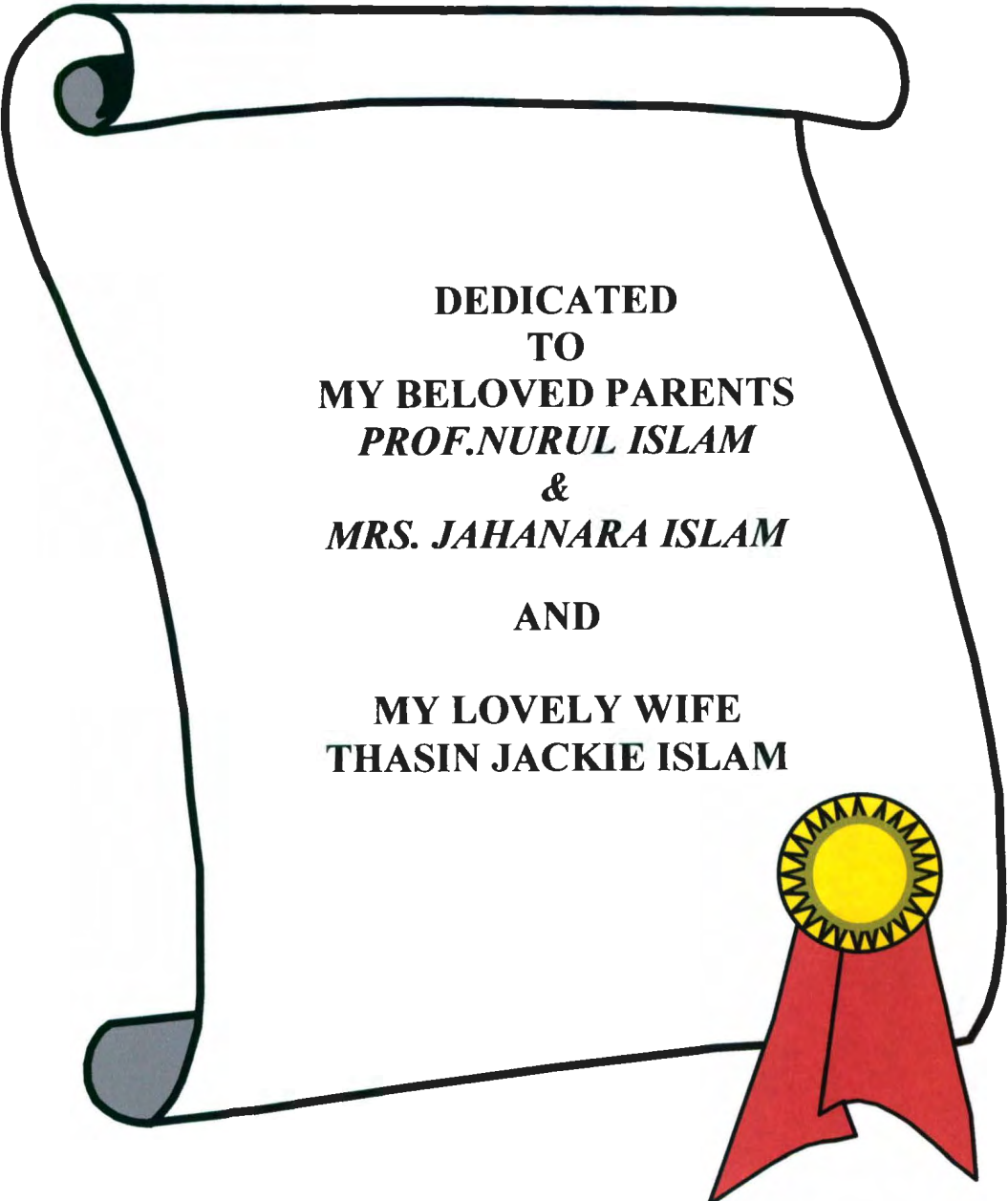
I would also like to thank Prof. Kenneth C. Westaway, Department of Chemistry and Biochemistry, Laurentian University for his valuable advice and various discussions during our study on kinetic isotope effect (KIE). I would also like to thank Prof. Olle Matsson, Uppsala University, Sweden for providing us experimental KIE results. Special thanks to Dr. Travis Fridgen for his valuable advice and suggestions.

I would like to thank my supervisory committee, Dr. Robert Davis and Dr. Christopher Flinn for their valuable suggestions and support in different ways throughout my research work and for proof reading the early version of this thesis.

I would also like to acknowledge each member of our vibrant computational chemistry group at Memorial University of Newfoundland (MUN) for cordial help, valuable advice, and continuous inspiration throughout the progress of this thesis work. I would like to give especial thanks to my friends and fellow colleagues, Joshua Hollett, Kushan Saputantri, Mansour Almatarneh, Aisha El-Sherbiny, Csaba Szakacs, Eva Simon, and Tammy Gosse for their sincere co-operation, many fruitful discussions and unconditional support.

I would also like to acknowledge the Department of Chemistry and the School of Graduate Studies at MUN and NSERC for financial support during my PhD program. I would also like to thank ACEnet for computer time and various agencies that have funded my conference trips.

At last, but not the least, I acknowledge my parents: my father, Prof. Md. Nurul Islam, who revealed the world of logic, and my mother, Mrs. Jahanara Islam, who revealed the world of life. My sincere gratitude is extended to them for their infinite contribution, prayer, and encouragement throughout my life. I am very grateful to my loving wife Thasin Islam for her help, inspiration, and encouragement during the period of my study. I am also grateful to my father and mother in law, my sisters Mrs. Fauzia Nur and Dr. Laila Nur, brothers Md. Zahedul Islam and Md. Kamrul Islam and brother in laws Golam Jilani and Jumar Islam for their constant inspiration, prayer, and encouragement. I would also like to extend my thanks to all my well-wishers.



**DEDICATED  
TO  
MY BELOVED PARENTS  
*PROF. NURUL ISLAM*  
&  
*MRS. JAHANARA ISLAM*  
AND  
MY LOVELY WIFE  
THASIN JACKIE ISLAM**

# Table of Contents

<b>Abstract</b>	ii
<b>Acknowledgements</b>	v
<b>Dedication</b>	vii
<b>Table of Contents</b>	viii
<b>List of Tables</b>	xv
<b>List of Figures</b>	xxiii
<b>List of Schemes</b>	xxviii
<b>List of Abbreviations and Symbols</b>	xxix
<b>List of Publications from This Thesis</b>	xxxiii
<b>Chapter 1 Introduction</b>	
1.1 Overall Goals and Objectives	1
1.2 Background	5
1.2.1 Transition State Theory	5
1.2.2 Kinetic Isotope Effect	7
1.2.3 Origin of Kinetic Isotope Effect	9
1.2.4 Calculation of Kinetic Isotope effect	10
1.2.5 The Molecular Hamiltonian	13
1.2.6 Born-Oppenheimer Approximation	14
1.2.7 The Hartree-Fock Approximation	15

1.2.8 The Basis Set Expansions	17
1.2.9 Post Hartree-Fock Methods	19
1.2.10 Moller-Plesset Perturbation Theory	19
1.2.11 Configuration Interaction	20
1.2.12 Density Functional Theory (DFT)	21
1.2.13 G3B3, G3MP2 and G3MP2B3 Theories	23
1.2.14 Solvation Models	25
1.2.15 The Onsager Model	26
1.2.4 Polarizable Continuum Model	27
1.3 References	27

**Chapter 2 Computational Study of the Reactions of SiH<sub>3</sub>X (X = H, Cl, Br, I)  
with HCN**

2.1 Introduction	37
2.2 Method	40
2.3 Results and Discussion	41
2.3.1 Activation energies and free energies of activation for the reaction of SiH <sub>3</sub> X with HCN	41
2.3.1.1 Reaction of SiH <sub>3</sub> X and HCN (Pathway A)	41
2.3.1.2 Reaction of SiH <sub>3</sub> X and HCN (H <sub>2</sub> elimination)	43
2.3.1.3 Decomposition of SiH <sub>3</sub> X and reaction with HCN	46
2.3.1.4 Summary of overall reaction mechanisms	48

investigated	
2.3.2 Thermodynamic results for the reaction of $\text{SiH}_3\text{X}$ with HCN	49
2.3.2.1 Thermodynamics of HX elimination	49
2.3.2.2 Thermodynamics of $\text{H}_2$ elimination	50
2.3.2.3 Thermodynamics for the thermal decomposition of $\text{SiH}_3\text{X}$ and $\text{SiHX} + \text{HCN}$	50
2.3.3 Performance of Theory/Basis set	51
2.3.4 Exploring Heats of Formation ( $\Delta H_f$ )	53
2. 4 Conclusions	55
2.5 References	57

### **Chapter 3 New insights into the bromination reaction for a series of alkenes -**

#### **A computational study**

3.1 Introduction	90
3.2 Method	93
3.3 Results and Discussions	94
3.3.1 Potential energy surfaces for the reaction of alkenes with $\text{Br}_2$	95
3.3.1.1 Perpendicular attack of $\text{Br}_2$ to $\text{C}=\text{C}$ : Pathway A	95
3.3.1.2 Sidewise attack of $\text{Br}_2$ to $\text{C}=\text{C}$ : Pathway B	96
3.3.2 Potential energy surfaces for the reaction of ethene with $2\text{Br}_2$	99
3.3.2.1 Pathway C	100
3.3.2.2 Pathway D	101

3.3.2.3 Pathway E	102
3.3.2.4 Pathway F	103
3.3.3 Summary of overall reaction mechanisms investigated	105
3.3.4 Comparison with Experiment	105
3.3.5 Thermodynamic results for the reaction of alkenes with Br <sub>2</sub>	109
3.3.6 Performance of Theory/Basis set	110
3.3.7 Exploring Heats of Formation ( $\Delta H_f$ )	112
3.4 Conclusions	113
3.5 References	114

**Chapter 4 The addition reaction of adamantylideneadamantane with Br<sub>2</sub> and 2Br<sub>2</sub> - A Computational Study**

4.1 Introduction	149
4.2 Method	152
4.3 Results and Discussions	153
4.3.1 Potential energy surface for the reaction of Ad-Ad + Br <sub>2</sub> :	153
Pathway A	
4.3.2 Potential energy surfaces for the reaction of Ad-Ad with 2Br <sub>2</sub>	155
4.3.2.1 Pathway B	155
4.3.2.2 Pathway C	156
4.3.2.3 Pathway D	157
3.3.3 Relative Stabilities	158

4.4. Conclusions	160
4.5 References	161

## **Chapter 5 A comparison of the Standard 6-31G and Binning-Curtiss Basis**

### **Sets for Third Row Elements**

4.1 Introduction	182
4.2 Method	184
4.3 Results and Discussions	185
5.3.1. Geometries of molecules containing 3 <sup>rd</sup> row elements	186
5.3. 2. Frequencies of molecules containing 3 <sup>rd</sup> row elements	187
5.3.3. Thermodynamic properties for the isogyric reactions involving 3 <sup>rd</sup> row elements	189
5.3.4. Exploring Heats of Formation ( $\Delta H_f$ )	193
5.4. Conclusions	194
5.5 References	196

## **Chapter 6 A new insight into using chlorine leaving group and nucleophile carbon kinetic isotope effects to determine substituent effects on the structure of S<sub>N</sub>2 transition states**

6.1 Introduction	227
6.2 Method	229
6.3 Results and Discussion	230
6.4 Conclusions	247

6.5 References	249
<b>Chapter 7 Can incoming nucleophile carbon kinetic isotope effects be used to determine the transition state structure for different <math>S_N2</math> reactions?</b>	
7.1 Introduction	267
7.2 Method	269
7.3 Results and Discussion	270
7.3.1. Experimental Nucleophile Carbon $k^{11}/k^{14}$ KIEs	271
7.3.2 Experimental Secondary $\alpha$ -Deuterium KIEs	272
7.3.3 The effect of changing the leaving group on the structure of the $S_N2$ transition state	274
7.3.4 Experimental vs calculated nucleophile $k^{11}/k^{14}$ carbon KIE	277
7.3.5 Experimental vs calculated $(k_H/k_D)_\alpha$ KIEs	278
7.3.6 Effect of Solvent	279
7.3.7 The implications of the theoretical study on using nucleophile carbon KIEs to determine the transition states of $S_N2$ reactions	281
7.4 Conclusions	283
7.5 References	284
<b>Chapter 8 Concluding Remarks</b>	298

<b>Appendix A</b>	309
<b>Appendix B</b>	311
<b>Appendix C</b>	317
<b>Appendix D</b>	324

## List of Tables

### Chapter 2

Table 2.1	Activation energies and free energies of activation for the reaction of $\text{SiH}_3\text{X}$ (X=H, Cl, Br, I) with HCN (HX elimination) and the isomerization of $\text{SiH}_3\text{CN}/\text{HX}$ (in $\text{kJ mol}^{-1}$ ) at 298.15K (Pathway A).	61
Table 2.2	Activation energies and free energies of activation for the reaction of $\text{SiH}_3\text{X}$ (X=H, Cl, Br, I) with HCN (in $\text{kJ mol}^{-1}$ ) at 298.15K ( $\text{H}_2$ elimination: Pathways B1, B* and B2).	63
Table 2.3	Activation energies and free energies of activation for the reaction of $\text{SiH}_3\text{X}$ (X=H, Cl, Br, I) with HCN (in $\text{kJ mol}^{-1}$ ) at 298.15K ( $\text{H}_2$ elimination: Pathways B3 and B4)	65
Table 2.4	Activation energies, activation enthalpies and free energies of activation for the thermal decomposition reaction of $\text{SiH}_3\text{X}$ (X=H, Cl, Br, I) (in $\text{kJ mol}^{-1}$ ) at 298.15K (Figure 9).	67
Table 2.5	Activation energies, enthalpies and free energies of activation for the reaction of $\text{SiHX}$ (X=H, Cl, Br, I) with HCN (in $\text{kJ mol}^{-1}$ ) at 298.15K (Figure 10).	69
Table 2.6	Thermodynamic properties for the reaction of $\text{SiH}_3\text{X}$ (X=H, Cl, Br, I) with HCN (in $\text{kJ mol}^{-1}$ ) at 298.15K (HX elimination reaction).	70
Table 2.7	Relative stabilities for the isomerization of $\text{SiH}_2\text{XCN}/\text{SiH}_2\text{XNC}$ (X=H, Cl, Br, I) (in $\text{kJ mol}^{-1}$ ) at 298.15K.	72

Table 2.8	Thermodynamic properties for the reaction of $\text{SiH}_3\text{X}$ (X = Cl, Br, I) with HCN ( $\text{H}_2$ elimination reaction) (in $\text{kJ mol}^{-1}$ ) at 298.15K.	74
Table 2.9	Thermodynamic properties for the thermal decomposition reaction of $\text{SiH}_3\text{X}$ (X = H, Cl, Br, I) (in $\text{kJ mol}^{-1}$ ) at 298.15K.	76
Table 2.10	Thermodynamic properties for the reaction of $\text{SiHX}$ (X = H, Cl, Br, I) with HCN (in $\text{kJ mol}^{-1}$ ) at 298.15K.	78
Table 2.11	Heat of formation ( $\Delta H_f$ ) (in $\text{kJ mol}^{-1}$ ) at 298.15K.	79

### Chapter 3

Table 3.1	Activation energies, free energies and enthalpies of activation ( $\text{kJ mol}^{-1}$ ) at 298.15K for the reaction of $\text{CH}_2=\text{CH}_2$ , $\text{CH}_3-\text{CH}_2=\text{CH}_2$ , $(\text{CH}_3)_2\text{CH}-\text{CH}_2$ , $\text{CH}_2=\text{CHF}$ , $\text{CH}_2=\text{CHCl}$ , (E)- $\text{CHF}=\text{CHF}$ and (E)- $\text{CHCl}=\text{CHCl}$ with $\text{Br}_2$ (Pathway A).	119
Table 3.2	Activation energies, free energies and enthalpies of activation ( $\text{kJ mol}^{-1}$ ) at 298.15K for the reaction of $\text{CH}_2=\text{CH}_2$ , $\text{CH}_3-\text{CH}_2-\text{CH}_2$ , $(\text{CH}_3)_2\text{CH}=\text{CH}_2$ , $\text{CH}_2=\text{CHF}$ and $\text{CH}_2=\text{CHCl}$ with $\text{Br}_2$ (Pathway B).	121
Table 3.3	Activation energies, free energies and enthalpies of activation ( $\text{kJ mol}^{-1}$ ) at 298.15K for the reaction of (E)- $\text{CHF}=\text{CHF}$ and (E)- $\text{CHCl}=\text{CHCl}$ with $\text{Br}_2$ (Pathway B).	125
Table 3.4	Activation energies, free energies and enthalpies of activation ( $\text{kJ mol}^{-1}$ ) at 298.15K for the reaction of $\text{CH}_2=\text{CH}_2$ and $2\text{Br}_2$ (Pathway C).	126
Table 3.5	Activation energies, free energies and enthalpies of activation ( $\text{kJ mol}^{-1}$ )	127

	<sup>1</sup> ) at 298.15K for the reaction of CH <sub>2</sub> -CH <sub>2</sub> and 2Br <sub>2</sub> (Pathway D).	
Table 3.6	Activation energies, free energies and enthalpies of activation (kJ mol <sup>-1</sup> ) at 298.15K for the reaction of CH <sub>2</sub> -CH <sub>2</sub> and 2Br <sub>2</sub> (Pathway E).	128
Table 3.7	Activation energies, free energies and enthalpies of activation (kJ mol <sup>-1</sup> ) at 298.15K for the reaction of CH <sub>2</sub> =CH <sub>2</sub> and 2Br <sub>2</sub> (Pathway F).	129
Table 3.8	The calculated overall free energies of activation (kJ mol <sup>-1</sup> ) at 298.15K for the reaction of CH <sub>2</sub> -CH <sub>2</sub> and 2Br <sub>2</sub> in solution at B3LYP/BC6-31G(d) (Pathway F) and experimental values.	130
Table 3.9	Thermodynamic properties (kJ mol <sup>-1</sup> ) at 298.15K for the reaction of CH <sub>2</sub> =CH <sub>2</sub> , CH <sub>3</sub> -CH <sub>2</sub> -CH <sub>2</sub> , (CH <sub>3</sub> ) <sub>2</sub> CH-CH <sub>2</sub> , CH <sub>2</sub> =CHF, CH <sub>2</sub> =CHCl, (E)-CHF=CHF and (E)-CHCl-CHCl with Br <sub>2</sub> .	131
Table 3.10	Heats of formation, ΔH <sub>f</sub> , (kJ mol <sup>-1</sup> ) at 298.15K.	134
 <b>Chapter 4</b>		
Table 4.1	Activation energies, free energies and enthalpies of activation (kJ mol <sup>-1</sup> ) at 298.15K for the reaction of adamantyldineadamantane with Br <sub>2</sub> (Pathway A).	165
Table 4.2	Activation energies, free energies and enthalpies of activation (kJ mol <sup>-1</sup> ) at 298.15K for the reaction of adamantyldineadamantane with 2Br <sub>2</sub> (Pathway B).	166
Table 4.3	Activation energies, free energies and enthalpies of activation (kJ mol <sup>-1</sup> ) at 298.15K for the reaction of adamantyldineadamantane with 2Br <sub>2</sub>	167

(Pathway C) in the gas phase.

Table 4.4	Activation energies, free energies and enthalpies of activation ( $\text{kJ mol}^{-1}$ ) at 298.15K for the reaction of adamantalydineadamantane with $2\text{Br}_2$ (Pathway D).	168
-----------	---	-----

Table 4.5	Relative Stabilities ( $\text{kJ mol}^{-1}$ ) at 298.15 K.	169
-----------	--	-----

## Chapter 5

Table 5.1	Optimized and experimental structural parameters for compounds containing 3 <sup>rd</sup> row elements (bond lengths in Å and angles in degrees).	201
-----------	---	-----

Table 5.2	Mean Absolute Deviations for bond lengths and angles (bond lengths in Å and angles in degrees).	205
-----------	---	-----

Table 5.3	Calculated and experimental frequencies ( $\text{cm}^{-1}$ ) for compounds containing 3 <sup>rd</sup> row elements.	206
-----------	---	-----

Table 5.4	Mean Absolute Deviations for frequencies ( $\text{cm}^{-1}$ ).	212
-----------	--	-----

Table 5.5	Thermodynamic properties for the reactions (1) and (2) ( $\text{kJ mol}^{-1}$ ) at 298.15K.	213
-----------	---	-----

Table 5.6	Thermodynamic properties for the reactions (3) and (4) ( $\text{kJ mol}^{-1}$ ) at 298.15K.	216
-----------	---	-----

Table 5.7	Thermodynamic properties for the reaction (5) ( $\text{kJ mol}^{-1}$ ) at 298.15K.	217
-----------	--	-----

Table 5.8	Mean Absolute deviations for the enthalpies of reaction involving 1 <sup>st</sup> and 3 <sup>rd</sup> row elements, reaction (1), and 1 <sup>st</sup> , 2 <sup>nd</sup> and 3 <sup>rd</sup> row elements.	218
-----------	---	-----

reaction (2) and (5), (in  $\text{kJ mol}^{-1}$ ).

Table 5.9	Heats of formation ( $\Delta H_f$ ) (in $\text{kJ mol}^{-1}$ ) at 298.15K.	219
-----------	--	-----

## Chapter 6

Table 6.1	The experimental secondary $\alpha$ -deuterium KIE for the $S_N2$ reactions between cyanide ion and benzyl- and <i>para</i> -chlorobenzyl chloride at $0^\circ\text{C}$ in THF.	254
Table 6.2	The secondary $\alpha$ -deuterium $(k_H/k_D)_\alpha$ KIEs for the $S_N2$ reactions between cyanide ion and five <i>para</i> -substituted benzyl chlorides at $25^\circ\text{C}$ using three different levels of theory.	255
Table 6.3	The experimental chlorine leaving group KIEs for the $S_N2$ reactions between cyanide ion and four <i>para</i> -substituted benzyl chlorides at $20^\circ\text{C}$ in THF.	256
Table 6.4	The calculated $C_\alpha$ -Cl bond length in five <i>para</i> -substituted benzyl chlorides at $25^\circ\text{C}$ using three different levels of theory.	257
Table 6.5	The calculated $C_\alpha$ -Cl and NC- $C_\alpha$ transition-state bond lengths for the $S_N2$ reactions between cyanide ion and five <i>para</i> -substituted benzyl chlorides at $25^\circ\text{C}$ using three different levels of theory.	258
Table 6.6	The chlorine $(k^{35}/k^{37})$ leaving group KIEs for the $S_N2$ reactions between cyanide ion and five <i>para</i> -substituted benzyl chlorides at $25^\circ\text{C}$ using four different levels of theory and un-scaled frequencies.	259
Table 6.7	The experimental chlorine $(k^{35}/k^{37})$ leaving group KIEs <sup>a, b</sup> for the $S_N2$	260

	reactions of <i>para</i> -substituted benzyl chlorides with various nucleophiles at 20°C.	
Table 6.8	The experimental nucleophile carbon $k^{11}/k^{14}$ KIEs for the $S_N2$ reactions between cyanide ion and three <i>para</i> -substituted benzyl chlorides at 20°C.	261
Table 6.9	The nucleophile carbon $k^{11}/k^{14}$ KIEs for the $S_N2$ reactions between cyanide ion and five <i>para</i> -substituted benzyl chlorides at 25°C using three different levels of theory.	262
Table 6.10	The individual contributions to the chlorine leaving group KIEs for the $S_N2$ reactions between cyanide ion and five <i>para</i> -substituted benzyl chlorides at 25°C in the gas phase at the B3LYP/aug-cc-pVDZ level of theory.	263
Table 6.11	Substituent effects on the transition structures and chlorine leaving group KIEs for different $S_N2$ reactions with a series of <i>para</i> -substituted benzyl chlorides at 25°C using the B3LYP/aug-cc-pVDZ level of theory.	264
Table 6.12	The individual contributions to the calculated nucleophile carbon ( $k^{11}/k^{14}$ ) KIEs for the $S_N2$ reactions between cyanide ion and five <i>para</i> -substituted benzyl chlorides at 25°C in the gas phase at the B3LYP/aug-cc-pVDZ level of theory.	265
Table 6.13	Substituent effects on the transition structures and nucleophile carbon $k^{11}/k^{14}$ and nitrogen $k^{14}/k^{15}$ KIEs for the $S_N2$ reactions between	266

cyanide ion and ammonia with a series of *para*-substituted benzyl chlorides, respectively, at 25°C using the B3LYP/aug-cc-pVDZ level of theory.

## Chapter 7

Table 7.1	The rate constants and the nucleophile carbon $k^{11}/k^{14}$ KIEs for the $S_N2$ reactions between cyanide ion and ethyl chloride, bromide, iodide and tosylate in anhydrous DMSO at 20°C.	288
Table 7.2	The secondary $\alpha$ -deuterium KIEs for the $S_N2$ reactions between cyanide ion and ethyl chloride, bromide, iodide and tosylate in anhydrous DMSO at 20°C.	289
Table 7.3	The calculated $C_\alpha$ -LG and NC- $C_\alpha$ transition-state bond lengths for the $S_N2$ reactions between cyanide ion and ethyl iodide, ethyl bromide, ethyl tosylate and ethyl chloride at 25°C.	290
Table 7.4	The nucleophile carbon ( $k^{11}/k^{14}$ ) KIEs for the $S_N2$ reactions between cyanide ion and ethyl iodide, ethyl bromide, ethyl tosylate and ethyl chloride at 25°C using three different levels of theory.	291
Table 7.5	The secondary $\alpha$ -deuterium $[(k_H/k_D)_{\alpha}]$ KIEs for the $S_N2$ reactions between cyanide ion and ethyl iodide, ethyl bromide, ethyl tosylate and ethyl chloride at 25°C using three different levels of theory	292
Table 7.6	Free energies of activation for the $S_N2$ reactions between cyanide ion and ethyl chloride, bromide, iodide and tosylate at 20°C	293

Table 7.7	The calculated C <sub>σ</sub> -LG and NC-C <sub>α</sub> transition-state bond lengths for the S <sub>N</sub> 2 reactions between cyanide ion and ethyl iodide, ethyl bromide, ethyl tosylate and ethyl chloride in DMSO at 30°C.	294
Table 7.8	The nucleophile carbon (k <sup>11</sup> /k <sup>14</sup> ) KIEs for the S <sub>N</sub> 2 reactions between cyanide ion and ethyl iodide, ethyl bromide, ethyl tosylate and ethyl chloride in DMSO at 30°C using three different levels of theory.	295
Table 7.9	The secondary α-deuterium (k <sub>H</sub> /k <sub>D</sub> ) <sub>α</sub> KIEs for the S <sub>N</sub> 2 reactions between cyanide ion and ethyl iodide, ethyl bromide, ethyl tosylate and ethyl chloride in DMSO at 30°C using three different levels of theory	296
Table 7.10	The individual contributions to the calculated nucleophile carbon (k <sup>11</sup> /k <sup>14</sup> ) KIEs for the S <sub>N</sub> 2 reactions between cyanide ion and ethyl iodide, ethyl bromide, ethyl tosylate and ethyl chloride at 25°C in the gas phase at the B3LYP/aug-cc-pVDZ level of theory.	297

# List of Figures

## Chapter 1

- Figure 1.1 Transition state structure for the  $S_N2$  reaction between an ethyl substrate and a nucleophile showing different kinetic isotope effects. Here, D represents deuterium. 33
- Figure 1.2 Origin of  $k_H/k_D$  in an exothermic reaction (early TS) 34
- Figure 1.3 Origin of low  $k_H/k_D$  in an endothermic reaction (late TS) 35
- Figure 1.4 Origin of large  $k_H/k_D$  in a thermoneutral reaction (symmetric TS) 36

## Chapter 2

- Figure 2.1 Mechanism for the reaction of  $\text{SiH}_3\text{X} + \text{HCN}$  (Pathway A). Only X = Cl is shown here, similar structures are found for X = Br and I. 80
- Figure 2.2 Reaction pathway for the reaction of  $\text{SiH}_3\text{X} + \text{HCN}$  (Pathway A) at G3MP2 level of theory (see Figure 1). 81
- Figure 2.3 Mechanism for the reaction of  $\text{SiH}_3\text{X} + \text{HCN}$  ( $\text{H}_2$  elimination). Only X = Cl is shown here, similar structures are found for X = H, Br and I. 82
- Figure 2.4 Mechanism for the reaction of  $\text{SiH}_3\text{X} + \text{HCN}$  forming the intermediate  $\text{II}^{\text{B}*}$  ( $\text{H}_2$  elimination). Only X = Cl is shown here, similar structures are found for X = H, Br and I. 83
- Figure 2.5 Reaction pathway B1 and B\* for the reaction of  $\text{SiH}_3\text{X} + \text{HCN}$  ( $\text{H}_2$  elimination) at G3MP2 level of theory (see Figure 3). 84
- Figure 2.6 Reaction pathway B2 for the reaction of  $\text{SiH}_3\text{X} + \text{HCN}$  ( $\text{H}_2$  85

	elimination) at G3MP2 level of theory (see Figure 4).	
Figure 2.7	Reaction pathway B3 for the reaction of $\text{SiH}_3\text{X} + \text{HCN}$ ( $\text{H}_2$ elimination) at G3MP2 level of theory (see Figure 4).	86
Figure 2.8	Reaction pathway B4 for the reaction of $\text{SiH}_3\text{X} + \text{HCN}$ ( $\text{H}_2$ elimination) at G3MP2 level of theory (see Figure 4).	87
Figure 2.9	Mechanism for thermal decomposition of $\text{SiH}_3\text{X}$ . Only X-H and Cl are shown here, similar structures to X-Cl are found for X-Br and I.	88
Figure 2.10	Mechanism for the addition reaction of $\text{SiHX} + \text{HCN}$ . Only X-Cl are shown here, similar structures are found for X-H, Br and I.	89

### Chapter 3

Figure 3.1	Pathway and barrier for the reaction of $\text{CH}_2=\text{CH}_2 + \text{Br}_2$ (Pathway A) at MP2/BC6-31G(d) level of theory. Although the IRC leads to $\text{I}^\ddagger$ no optimized structure was found.	135
Figure 3.2	Mechanism for the reaction of $\text{CH}_2=\text{CH}_2 + \text{Br}_2$ (Pathway B). Similar structures are found for the bromination of $\text{CH}_3\text{-CH}_2\text{-CH}_2$ , $(\text{CH}_3)_2\text{CH-CH}_2$ , $\text{CH}_2\text{-CHF}$ and $\text{CH}_2\text{-CHCl}$ .	136
Figure 3.3	Pathway for the reaction of $\text{CH}_2=\text{CH}_2 + \text{Br}_2$ (Pathway B) at MP2/BC6-31G(d) level of theory (see Figure 2 for structures).	137
Figure 3.4	Mechanism for the reaction of (E)- $\text{CHF-CHF} + \text{Br}_2$ (Pathway B). Similar structures are found for the bromination of (E)- $\text{CHCl-CHCl}$ .	138
Figure 3.5	Mechanism for the reaction of $\text{CH}_2\text{-CH}_2 + 2\text{Br}_2$ (Pathway C).	139

Figure 3.6	Pathway for the reaction of $\text{CH}_2=\text{CH}_2 + 2\text{Br}_2$ (Pathway C) at G3MP2B3 level of theory (see Figure 5 for structures).	140
Figure 3.7	Mechanism for the reaction of $\text{CH}_2=\text{CH}_2 + 2\text{Br}_2$ (Pathway D).	141
Figure 3.8	Pathway for the reaction of $\text{CH}_2=\text{CH}_2 + 2\text{Br}_2$ (Pathway D) at G3MP2B3 level of theory (see Figure 7 for structures).	142
Figure 3.9	Mechanism for the reaction of $\text{CH}_2=\text{CH}_2 + 2\text{Br}_2$ (Pathway E).	143
Figure 3.10	Pathway for the reaction of $\text{CH}_2=\text{CH}_2 + 2\text{Br}_2$ (Pathway E) at MP2/G3MP2large//HF/6-31G(d) level of theory (see Figure 9 for structures).	144
Figure 3.11	Mechanism for the reaction of $\text{CH}_2=\text{CH}_2 + 2\text{Br}_2$ (Pathway F).	145
Figure 3.12	Pathway for the reaction of $\text{CH}_2=\text{CH}_2 + 2\text{Br}_2$ (Pathway F) at G3MP2B3 level of theory (see Figure 11 for structures). For $\text{TS}_2^{\text{F}}$ , $\text{I}_2^{\text{F}}$ and $\text{I}_3^{\text{F}}$ the G3MP2B3 energies are calculated using HF/6-31G(d) by optimized geometries.	146
Figure 3.13	Mechanism for the reaction of $\text{Br}_2 + \text{Br}_2 \rightarrow \text{Br}_4$ .	147
Figure 3.14	Mechanism for the reaction of $\text{CH}_2=\text{CH}_2 + \text{Br}_2$ mediated by a $\text{CH}_3\text{OH}$ molecule (Pathway G).	148

## Chapter 4

Figure 4.1	Expected structure of the adamantylideneadamantane bromonium ion.	173
Figure 4.2	Mechanism for the reaction of $\text{Ad}=\text{Ad} + \text{Br}_2$ (Pathway A).	174

Figure 4.3	Reaction pathway for the reaction of Ad=Ad + Br <sub>2</sub> (Pathway A) at HF/6-31G(d) and B3LYP/6-31G(d) level of theory (see Figure 2 for structures).	175
Figure 4.4	Mechanism for the reaction of Ad=Ad + 2Br <sub>2</sub> (Pathway B).	176
Figure 4.5	Reaction pathway for the reaction of Ad=Ad + 2Br <sub>2</sub> (Pathway B) at HF/6-31G(d) and B3LYP/6-31G(d) level of theory (see Figure 4 for structures).	177
Figure 4.6	Mechanism for the reaction of Ad=Ad + 2Br <sub>2</sub> (Pathway C).	178
Figure 4.7	Reaction pathway for the reaction of Ad=Ad + 2Br <sub>2</sub> (Pathway C) at HF/6-31G(d) level of theory. For R <sup>C</sup> and TS <sup>C</sup> B3LYP/6-31G(d)//HF/6-31G(d) single point energies are indicated by dashed lines (see Figure 6 for structures).	179
Figure 4.8	Mechanism for the reaction of Ad=Ad + 2Br <sub>2</sub> (Pathway D).	180
Figure 4.9	Reaction pathway for the reaction of Ad=Ad + 2Br <sub>2</sub> (Pathway D) at HF/6-31G(d) level of theory. For R <sup>D</sup> and TS <sup>D</sup> B3LYP/6-31G(d)//HF/6-31G(d) single point energies are indicated by dashed lines (see Figure 8 for structures).	181
 <b>Chapter 5</b>		
Figure 5.1	Enthalpies of reaction (1) calculated at different levels of theory with the standard 6-31G(d,p) basis set.	220
Figure 5.2	Enthalpies of reaction (2) calculated at different levels of theory with	221

	the standard 6-31G(d,p) basis set.	
Figure 5.3	Difference between enthalpies of reaction (1) calculated at MP2 and B3LYP levels of theory with G3MP2.	222
Figure 5.4	Difference between enthalpies of reaction (2) calculated at MP2 and B3LYP levels of theory with G3MP2.	223
Figure 5.5	Enthalpy of reaction for $\text{CH}_3\text{Br} + \text{HCl} \rightarrow \text{CH}_3\text{Cl} + \text{HBr}$ calculated at different levels of theory and basis sets.	224
Figure 5.6	Enthalpy of reaction for $\text{SiH}_3\text{Br} + \text{HCl} \rightarrow \text{SiH}_3\text{Cl} + \text{HBr}$ calculated at different levels of theory and basis sets.	225
Figure 5.7	Enthalpy of reaction for $\text{PH}_2\text{Br} + \text{HCN} \rightarrow \text{PH}_2\text{CN} + \text{HBr}$ calculated at different levels of theory and basis sets.	226

## List of Schemes

### Chapter 4

- Scheme 4.1 Reaction of Adamantylideneadamantane (1) with bromine in  $\text{CCl}_4$  170  
forms adamantylideneadamantane bromonium ion with a  $\text{Br}^-$   
counterion (2).
- Scheme 4.2 Reaction of (E)-2,2,5,5-tetramethyl-3,4-diphenylhex-3-ene (3) with 171  
bromine forms a CTC complex only.
- Scheme 4.3 Tetraneopentylethylene (4) does not react with bromine in  $\text{CCl}_4$  172  
solution.

### Chapter 6

- Scheme 6.1 A possible mechanism for the reaction forming the largest side 253  
product from the reaction between tetrabutylammonium cyanide and  
*para*-nitrobenzyl chloride in THF at 20°C.

## List of Abbreviations and Symbols

Å	Ångström, $10^{-10}$ m
Anhydr.	Anhydrous
AO	Atomic orbital
B3LYP	Becke3-Lee-Yang-Parr
BC	Binning-Curtiss
Bz	Benzyl
Bu <sub>4</sub> NCN	Tetrabutylammonium cyanide
C	Concentration
CI	Configuration interaction
CIS	CI with single excitation
CISD	CI with single and double electronic excitations
CTC	Charge transfer complex
D	Deuterium
DFT	Density functional theory
DMSO	Dimethyl sulphoxide
DZP	Double zeta polarized (basis set)
E <sub>a</sub>	Activation energy
Et	Ethyl
Fc	Frozen core
G3	Gaussian-n-theory

G3MP2	Gaussian-n-theory
G3MP2B3	Gaussian-n-theory
G3B3	Gaussian-n-theory
GTF	Gaussian type functions
GTO	Gaussian type orbital
<i>h</i>	Planck's constant
HF	Hartree-Fock
I	Intermediate
ICR	Ion cyclotron resonance
IRC	Intrinsic reaction coordinate
IUPAC	International Union of Pure and Applied Chemistry
K	Rate constant
$k_B$	Boltzmann's constant
KIE	Kinetic isotope effect
KIE <sub>T</sub>	Contribution to the isotope effect from tunnelling
LCAO	Linear combination of atomic orbitals
LG	Leaving group
MAD	Mean absolute deviations
Me	Methyl
MO	Molecular orbital
MP <sub>n</sub>	Moller-Plesset perturbation theory of order n
MP2	Second order Møller-Plesset perturbation theory

MS	Mass spectrometry
NMR	Nuclear magnetic resonance
Nu	Nucleophile
OTs	Tosylate
PCM	Polarized continuum model
PES	Potential energy surface
Ps	Picoseconds
PS	Product state
QCI	Quadratic configuration interaction
QCISD	QCI including singles and doubles
QCISD(T)	QCISD with perturbative estimate for connected triples
R	Gas constant
r. c.	Reaction coordinate
RS	Reactant State
RHF	Restricted Hartree-Fock
SCF	Self consistent field
SCRFF	Self consistent reactions field
S <sub>N</sub> 2	Bimolecular nucleophilic substitution
STO	Slater type orbital
TDF	Temperature-dependent Factor
THF	Tetrahydrofuran
TIF	Temperature-independent factor

TS	Transition state
TST	Transition state theory
UA0	United atom
UFF	Universal (united) force field
ZPE	Zero-point energy
V	Velocity
E	Dielectric constant
H	Viscosity
N	Frequency
‡ or †	(Superscript) Relates to the transition state

## List of Publications from This Thesis

- I. Islam, S. M.; Hollett, J. W; Poirier R. A. Computational Study of the Reactions of  $\text{SiH}_3\text{X}$  (X = H, Cl, Br, I) with  $\text{HCN}$ , *Journal of Physical Chemistry A*, **2007**, *111*, 526-540 (Chapter 2).
- II. Islam, S. M.; Poirier, R. A. New insights into the bromination reaction for a series of alkenes - A computational study, *Journal of Physical Chemistry A*, **2007**, In Press (Chapter 3).
- III. Islam, S. M.; Poirier, R. A. The addition reaction of adamantylideneadamantane with  $\text{Br}_2$  and  $2\text{Br}_2$  - A Computational Study, *Journal of Physical Chemistry A*, **2007**, In Press (Chapter 4).
- IV. Islam, S. M.; Huelin, S. D.; Dawe, M.; Poirier, R. A. A comparison of the Standard 6-31G and Binning-Curtiss Basis Sets for Third Row Elements, *Journal of Chemical Theory and Computation*, **2007**, In Press (Chapter 5).
- V. Westaway, K. C.; Fang, Y.; MacMillar, S.; Matsson, O.; Poirier, R. A.; Islam, S. M. A new insight into using chlorine leaving group and nucleophile carbon kinetic isotope effects to determine substituent effects on the structure of  $\text{S}_{\text{N}}2$  transition states, *Journal of Physical Chemistry A*, **2007**, *111*, 8110-8120 (Chapter 6). Chapter 6 was mostly written by Dr. Kenneth C. Westaway, but I was actively

involved in all the interpretations and analysis of the data and I produced all the necessary figures and tables. I have performed all the computations, while Dr. Westaway's and Dr. Matsson's group performed the experiments.

- VI. Westaway, K. C.; Fang, Y.; MacMillar, S.; Matsson, O.; Poirier, R. A.; Islam, S. M. Can incoming nucleophile carbon kinetic isotope effects be used to determine the transition state structure for different  $S_N2$  reactions?, submitted to *Journal of Organic Chemistry* (Chapter 7). Chapter 7 was written jointly by Dr. Westaway, Dr. Poirier and I. I have performed all the calculations while the experimental work was done by Dr. Westaway's and Dr. Matsson's group.

# **CHAPTER 1**

## **Introduction**

### **1.1 Overall Goals and Objectives**

Quantum mechanical computational chemistry is a fast growing research area. Researchers use quantum chemistry calculations to predict and explain experimental results. Computational chemistry is used to study the structures, properties, and reactions of scientifically interesting systems. In principle, quantum mechanical computations can be very precise, because they can account for interactions between every electron and every proton in every atom. Experimental chemists have been investigating mechanisms of reactions for many years. However, it is very challenging to propose a reaction mechanism based on experimental observations because each step of the mechanism cannot be observed. The reactions are either very fast or cannot be carried out under normal conditions. The main purpose of this thesis is to investigate reaction mechanisms

computationally. Through computational methods, each step of a proposed reaction mechanism can be studied including the intermediates and transition states.

The reaction of bromine with alkenes is a well known organic reaction and many experimentalists have proposed possible mechanisms for the reaction under different reaction conditions. A survey of the literature reveals that very few theoretical studies<sup>1-5</sup> have been conducted for the bromination of alkenes. A computational study of the reactions of HCN with silanes and halosilanes has not been previously reported. These reactions are very difficult to carry out experimentally, however it is very likely that such reactions may occur in interstellar space where both HCN and silanes are abundant.<sup>6</sup> The reactions of silanes and halosilanes have also become a central focus in silicon chemistry for their usefulness in computers, semiconductors, polymer and glass industries.<sup>7-10</sup>

Although there has been rapid advancement in theoretical chemistry over the past two decades, there are still many improvements to be made to increase the accuracy, applicability, and efficiency of computational methods. The potential for such advances is increased further by the continuing development of computer technology. The accuracy of the level of theory and basis sets used in predicting the properties of a system is crucial. Therefore it is also necessary for computational chemists to compare the existing lower levels of theories, which are normally fast computationally, with higher level theories and with experiments. This will guide researchers in selecting the right level of theory and basis sets to use for their calculations. For 3<sup>rd</sup> row elements, the Binning-Curtiss (BC6-

31G) basis set<sup>11</sup> has been used as the 6-31G basis set in most electronic structure packages (for example, Gaussian<sup>12</sup> and GAMESS<sup>13</sup>), although this basis set does not actually meet the definition of the standard 6-31G basis set. Rassolov et al.<sup>14</sup> have constructed a standard 6-31G basis set for the third row elements to utilize in G3 theories.<sup>15</sup> There has been no comparative study of the performance of the standard 6-31G and BC6-31 basis sets and researchers are unaware of the advantages and weaknesses of these basis sets in predicting the properties of a system.

The kinetic isotope effect (KIE) is normally used by experimentalists to characterize the transition state (TS) structure of a reaction. However, there are still many limitations associated with this experimental tool to determine “the right” transition states. It is possible to obtain the transition state structure computationally. To better understand the origin of KIEs, more and more experimental researchers are now comparing their results with computationally obtained TS structures and KIEs.<sup>16-19</sup> However, more work needs to be done both experimentally and computationally to find and overcome the limitations associated with the KIE in predicting the TS structure successfully. This will allow one to use the KIE as a proper tool to characterize the TS structure for different reactions.

This thesis addresses each of the issues mentioned above. The broad objective of this thesis is given below in point form:

1. Identify the most plausible mechanism for the bromination reaction of alkenes by computational methods. The computational results will be compared to the data available from experiment.
2. Discover the likely mechanism for the reaction of HCN with  $\text{SiH}_3\text{X}$ , where  $\text{X} = \text{H}$ , Cl, Br, and I.
3. Determine the computationally least expensive level of theory that predicts reliable energies, by performing high level *ab initio* calculations and by comparing with experiment.
4. Determine the performance of the standard 6-31G and the Binning-Curtiss (BC6-31G) basis sets by studying the geometries, frequencies and thermodynamic properties for molecules containing 3<sup>rd</sup> row elements.
5. Characterize the transition states of  $\text{S}_{\text{N}}2$  reactions by calculating the KIE and comparing them with the experimental results.
6. Find the unknown heats of formation of different compounds which have not been reported in the literature.

This thesis is arranged in manuscript format and contains a total of eight chapters including this introduction. Chapter – 1 presents the general introduction of the overall thesis and is divided into two sections. The first section in the introduction contains the overall goal and objective of this research including an outline of the thesis and the second section contains a brief background on the theory and methods used in this thesis. All the chapters from 2 – 7 are arranged in manuscript format, each of which has its own

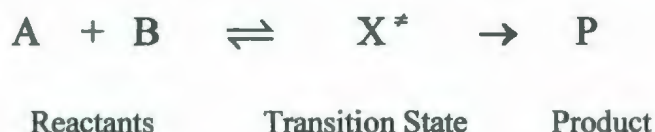
introduction, methodology, results & discussion, and conclusion summarizing the results. Chapter – 2 presents a detailed study of the reactions of  $\text{SiH}_3\text{X}$  ( $\text{X} = \text{H}, \text{Cl}, \text{Br}, \text{I}$ ) with HCN. Chapter - 3 describes a detailed mechanistic and thermodynamic study of the bromination reaction for a series of alkenes in the gas phase and in solution. Chapter – 4 presents a detailed study of the reaction of adamantylideneadamantane with  $\text{Br}_2$  and  $2\text{Br}_2$ . Chapter – 5 is a comparative study of the performance of the standard 6-31G and Binning-Curtiss (BC6-31G) basis sets for third row elements, Ga, Ge, As, Se, and Br. Chapter – 6 presents a detailed study of chlorine leaving group and nucleophile carbon kinetic isotope effects to determine substituent effects on the structure of  $\text{S}_{\text{N}}2$  transition states. Chapter – 7 is also a detailed study of the use of nucleophile carbon kinetic isotope effects to determine the transition state structure for different  $\text{S}_{\text{N}}2$  reactions. Finally, a summary of the entire research work is presented in Chapter 8. Except for the last chapter, each chapter has its own references at the end.

## **1.2 Background**

### **1.2.1 Transition State Theory**

Transition state theory (TST) is a powerful theory for translating molecular structure and energetics into predictions of chemical reaction rates.<sup>20</sup> In TST, the important criterion is that colliding molecules must have sufficient kinetic energy to overcome the activation energy barrier in order to react. The activation energy is the height of the potential energy barrier separating two minima on the potential energy

surface and the highest point is known as the transition state. The TS on such a surface is actually not a maximum but a saddle point. According to transition state theory, the transition state, also known as the activated complex,<sup>21</sup> is in equilibrium with the reactants,



According to the Arrhenius equation, the rate constant  $k$  is related to the activation energy  $E_a$  by the following equation,

$$k = A e^{-E_a/RT} \quad (1)$$

where,  $A$  is the pre-exponential factor,  $T$  represents the temperature and  $R$  is the gas constant.

The rate constant  $k$  of the elementary reaction is regulated by the difference in Gibbs' free energy between the reactant and the transition state,  $\Delta G^\ddagger$  and can also be represented by the following equation,

$$k = \frac{k_B T}{h} e^{-\Delta G^\ddagger/RT} \quad (2)$$

where  $k_B$ ,  $h$ ,  $T$  and  $R$  represent the Boltzmann's constant, Planck's constant, the absolute temperature, and the gas constant, respectively. Therefore, Eq. (2) can be used to convert the experimentally obtained rate constant to the free energy of activation and vice versa. Since the free energy of activation can be obtained by computational calculation, one can

compare the computationally obtained free energy of activation with the experimental free energy of activation. The computationally obtained free energies can also be converted to rate constants and compared to experiment.

The free energy of activation,  $\Delta G^\ddagger$ , can be represented by the enthalpy of activation,  $\Delta H^\ddagger$ , and the entropy of activation,  $\Delta S^\ddagger$ , by equation (3) as given below,

$$\Delta G^\ddagger = \Delta H^\ddagger - T\Delta S^\ddagger \quad (3)$$

The structure of the transition state is often based on the structural features of the reactants and products. According to Hammond's postulate,<sup>23</sup> two states (reactant and transition state or transition state and product) of an elementary reaction having similar energies should only need a minor structural reorganization in order to interconvert. Thus, a reactant-like transition state structure is expected for an exothermic reaction, whereas an endothermic reaction will have a product-like transition state. There also exists a third case where the transition state occurs near the centre of a reaction coordinate and the reaction is known to be thermoneutral.

### 1.2.2 Kinetic Isotope Effect

The substitution of an atom in a molecule by one of its isotopes can alter the rate at which the molecule reacts. The ratio of the reaction rates is called the kinetic isotope effect (KIE). A KIE involving light (L) and heavy (H) isotopes is represented as

$$\text{KIE} = \frac{k_L}{k_H} \quad (4)$$

where  $k_L$  is the rate constant for the molecule with the light isotope and  $k_H$  is the rate constant for the molecule with the heavy isotope. The KIE is normal when  $\frac{k_L}{k_H} > 1.0$ ,

inverse if  $\frac{k_L}{k_H} < 1.0$  and there is no isotope effect if  $\frac{k_L}{k_H} = 1.0$ .

Isotopic substitution is a very useful technique to obtain information about the mechanistic sequence of a chemical reaction and the associated transition state structures. The change of an isotope may cause the reaction rate to change in a number of ways, providing clues to the pathway of the reaction. For example, if the reacting molecule contains a C-H bond, then the reacting molecule will have a different reaction rate when protium is replaced by the heavier isotope deuterium, however, only if C-H is involved in the reaction. Because the zero-point energy of the C-D bond is lower than the C-H bond, a higher activation energy for C-D bond cleavage is required. The advantage of isotopic substitution is that this is the least disturbing structural change that can be effected in a molecule. Kinetic isotope effect is very useful to determine a transition state structure because it allows us to determine which bonds are forming or breaking in the transition state, and the amount of bond making and bond rupture that has occurred in the transition state. Primary KIEs result when bonds to the isotopically substituted atom are formed or broken in the rate determining step of a mechanism, while secondary KIEs result when the isotopically substituted atom influences the reaction rate but does not take part in the bond breaking/formation process. Figure 1.1 shows different types of KIEs from the

isotopic substitution in the reactants of an  $S_N2$  reaction. Some of these KIEs have been investigated in this thesis.

### 1.2.3 Origin of Kinetic Isotope Effect

Three situations can be considered for a reaction transition state structure, such as an early or reactant like TS, a late or product-like TS, and a symmetric or central TS. Figures 1.2, 1.3 and 1.4 illustrate the primary KIE for a proton (H) or deuteron (D) transfer from a carbon (C) atom to another atom A and show the potential energy surface along with the zero point energies (ZPEs) for the stretch of the reactant state (RS) and the TS.

ZPE is one of the dominant factors for hydrogen/deuterium KIEs. In the RS, the C-H and C-D species have different energy due to their difference in ZPE. As can be observed from Figure 1.2, when the reaction is exothermic the TS is early, i.e. the C-H or C-D bond will only be slightly broken in the TS. The vibrational frequencies of the stretching mode in the TS will be affected by the mass of the H or D atom. Therefore, the difference in the TS energy for the C-H or C-D species will be almost the same in the transition structure as in the reactant. The difference in activation energies for reactions with a C-H or C-D will be very small and  $k_H/k_D$  will be very close to unity. When the transition state is very late as for an endothermic reaction (Figure 1.3), the C-H or C-D bond will be almost broken and the A-H and A-D bond fully developed. If the difference in ZPE for the A-H or A-D in the TS is very close to the ZPE for the C-H or C-D bond in

the RS, the activation energy for abstracting a deuterium is very similar to that for abstracting a hydrogen atom and the KIE will be very small. In a thermoneutral reaction, the TS structure is symmetrical and the frequency of the symmetric stretching vibration of the TS is almost independent of isotopic substitution, i.e the frequency of the vibration depends very little on the mass of H or D. Therefore, the difference in isotopic ZPE in the RS will be fully expressed in the activation energies. As seen in Figure 1.4, the activation energy for deuterium ( $E_a^D$ ) will be larger than the activation energy for hydrogen ( $E_a^H$ ). Thus, there should be a significant primary KIE. Westheimer and Melander<sup>23, 24</sup> found that the maximum primary (1°) KIE will be seen if the TS is symmetrical. The magnitude of such a maximum for a 1° KIE is estimated to be 7–10.<sup>24,25</sup> In the above analysis of the origin of  $k_H/k_D$ , only stretching vibrations are considered and bending vibrations are completely ignored. But it is well known that the bending vibrations also play an important role in the magnitude of  $k_H/k_D$ .<sup>19,26</sup> Researchers are still working on different types of kinetic isotope effects (KIEs) to better understand their origin.<sup>16-19,27-28</sup>

#### 1.2.4 Calculation of Kinetic Isotope effect

Using the assumptions of transition state theory, if molecular masses  $M$ , moments of inertia  $A$ ,  $B$  and  $C$ , and isotopic vibrational frequencies  $\nu_i$  are known for both reactants,  $R$ , and transition states,  $\ddagger$ , the kinetic isotope effect can be represented by the following equation,<sup>24,29</sup>

$$\frac{k_L}{k_H} = \left( \frac{M_L^*}{M_H^*} \times \frac{M_H^R}{M_L^R} \right)^{3/2} \times \left( \frac{A_L^* B_L^* C_L^*}{A_H^* B_H^* C_H^*} \times \frac{A_H^R B_H^R C_H^R}{A_L^R B_L^R C_L^R} \right)^{1/2} \\ \times \prod_i^{3N-6} \frac{\sinh(\mu_{iL}^R / 2)}{\sinh(\mu_{iH}^R / 2)} \times \prod_i^{3N^*-7} \frac{\sinh(\mu_{iH}^* / 2)}{\sinh(\mu_{iL}^* / 2)} \quad (5)$$

where  $\mu_i = h\nu_i/k_B T$ ,  $h$  is Planck's constant,  $k_B$  is the Boltzmann constant,  $T$  is absolute temperature and  $L$  and  $H$  denote the light and heavy isotopes of the reactants. By applying the Teller-Redlich rule<sup>30</sup>, equation (5) can be represented by only the frequencies of the normal modes of vibration,

$$\frac{k_L}{k_H} = \left( \frac{v_L^*}{v_H^*} \right) \times \prod_i^{3N-6} \frac{\mu_{iH}^R \sinh(\mu_{iL}^R / 2)}{\mu_{iL}^R \sinh(\mu_{iH}^R / 2)} \times \prod_i^{3N^*-7} \frac{\mu_{iL}^* \sinh(\mu_{iH}^* / 2)}{\mu_{iH}^* \sinh(\mu_{iL}^* / 2)} \quad (6)$$

The above equation neglects the tunneling contribution to isotope effects. The significance of tunneling is that a light particle such as proton can cross an energy barrier with less energy than the activation energy, whereas a heavy particle such as deuterium cannot do so as easily. The tunneling effect which may be very important can be accounted for by the Wigner correction<sup>31</sup>, where the first two terms of the following expansion series are calculated,

$$Q_t = 1 + \frac{\mu_t^2}{24} + \dots \quad (7)$$

At 298K,

$$\mu_t = \frac{h\nu_i}{k_B T} \approx \frac{1.44}{T} \times \nu_i \approx 0.004828 \times \nu_i \quad (8)$$

where,  $\nu_i$  is the imaginary frequency of the transition state. The tunneling contribution to the KIE is obtained from the ratio of  $Q_t^L/Q_t^H$ . Tunneling is mainly important for the reactions with narrow reaction barriers. Tunneling is also favoured by low temperature and light nuclei. Therefore a kinetic isotope effect can be expressed as the product of three factors,  $KIE_T$ , TIF and TDF, according to equation (9),<sup>24,29</sup>

$$\frac{k_L}{k_H} = \underbrace{\left(\frac{k_L}{k_H}\right)_T}_{KIE_T} \times \underbrace{\left(\frac{\nu_L^*}{\nu_H^*}\right)}_{TIF} \times \underbrace{\prod_i^{3N-6} \frac{\mu_{iH}^R \sinh(\mu_{iL}^R/2)}{\mu_{iL}^R \sinh(\mu_{iH}^R/2)} \times \prod_i^{3N^*-7} \frac{\mu_{iL}^* \sinh(\mu_{iH}^*/2)}{\mu_{iH}^* \sinh(\mu_{iL}^*/2)}}_{TDF} \quad (9)$$

$KIE_T$  is the contribution from tunneling to the total KIE. The temperature independent factor (TIF) is the ratio of the imaginary frequencies for the isotopic transition states. The ratio of the total isotopic vibrational frequencies in the transition states to that of the reactant constitutes the temperature-dependent factor (TDF). TDF can also be represented by the products of the normal mode vibrational frequencies (VP), excited vibrational modes (EXC) and zero point energies of the vibrational modes (ZPE).<sup>29</sup>  $KIE_T$  is always normal as the lighter isotope is affected more by tunnelling than the heavier isotope.  $KIE_T$  may become very important when the magnitude of the KIE is small. Since the species containing the lighter isotope has the higher frequency, TIF will always be greater than unity. The change in the vibrational frequencies on going from the reactant state to the transition state determines the TDF. Therefore TDF will be inverse if the binding to the isotopically labeled atom is increased. For example, bond formation to a nucleophile

results in increased vibrational energy in the TS compared to the reactant. The TDF will be increasingly inverse with the degree of bond formation in the TS. Therefore, the magnitude of an incoming group KIE will be normal if there is a small amount of bond formation in the TS whereas it will be inverse if bond formation is far advanced in the TS.<sup>32-34</sup> This type of KIE can be very small and close to unity as the TIF and TDF have the opposite contributions to the total KIE.

### 1.2.5 The Molecular Hamiltonian

Finding an approximate solution of the Schrödinger equation is the main focus area of the computational chemist. The time-independent, non-relativistic Schrödinger equation is written as<sup>35,36</sup>

$$\hat{H}\Psi_i(\vec{r},\vec{R}) = E_i\Psi_i(\vec{r},\vec{R}) \quad (10)$$

where,  $\vec{r}$  and  $\vec{R}$  are the electronic and nuclear coordinates, respectively.  $\Psi_i$  is the wave function of the  $i$ 'th state of the system.  $\Psi_i$  depends on  $4N$  variables, three spatial variables (coordinates) and one spin variable for each of the  $N$  electrons, along with  $3M$  spatial coordinates of the nuclei.  $E_i$  represents the total energy of the system.  $\hat{H}$  is the Hamiltonian operator (or simply, the Hamiltonian) for a molecular system consisting of  $M$  nuclei and  $N$  electrons and contains all the terms that contribute to the total energy of the system. The Hamiltonian,  $\hat{H}$ , can be written in atomic units as:

$$\hat{H} = -\frac{1}{2} \sum_{i=1}^N \nabla_i^2 - \frac{1}{2} \sum_{A=1}^M \frac{\nabla_A^2}{M_A} - \sum_{i=1}^N \sum_{A=1}^M \frac{Z_A}{r_{iA}} + \sum_{i=1}^N \sum_{j>i}^N \frac{1}{r_{ij}} + \sum_{A=1}^M \sum_{B>A}^M \frac{Z_A Z_B}{R_{AB}} \quad (11)$$

The first two terms in the equation (11) describe the kinetic energy of the electrons and nuclei, respectively. The third term represents the attractive electrostatic interaction between the nuclei and the electrons (Coulomb attraction). The last two terms represent the repulsive potential due to the electron-electron and nucleus-nucleus interaction, respectively.  $\nabla_i^2$  and  $\nabla_A^2$  are the Laplacian operators resulting from the differentiation with respect to the coordinates of the electron and nucleus, respectively.  $Z_A$  and  $Z_B$  are the nuclear charge of nucleus A and B, respectively and the distances between the particles are denoted by  $r_{ij} = |\mathbf{r}_i - \mathbf{r}_j|$ ,  $r_{iA} = |\mathbf{r}_i - \mathbf{R}_A|$  and  $R_{AB} = |\mathbf{R}_A - \mathbf{R}_B|$ .

## 1.2.6 Born-Oppenheimer Approximation

Because the masses of the nuclei are several orders of magnitude greater than that of an electron, they move much slowly and can be considered stationary and separable while computing the electronic energies. This is the basis of the famous Born-Oppenheimer approximation.<sup>37</sup> Therefore, the Schrödinger equation can be written in terms of the electronic Hamiltonian operator as

$$\hat{H}_{\text{elec}} \Psi_{\text{elec}} = E_{\text{elec}} \Psi_{\text{elec}} \quad (12)$$

where the electronic Hamiltonian is the reduced form of the complete Hamiltonian given in Eq. (11),

$$\hat{H}_{\text{elec}} = -\frac{1}{2} \sum_{i=1}^N \nabla_i^2 - \sum_{i=1}^N \sum_{A=1}^M \frac{Z_A}{r_{iA}} + \sum_{i=1}^N \sum_{j>i}^N \frac{1}{r_{ij}} = \hat{T}_e + \hat{V}_{ne} + \hat{V}_{ee} \quad (13)$$

$\Psi_{\text{elec}}$  depends on the electron coordinates and parametrically on the nuclear coordinates.

Adding the constant nuclear repulsion term gives the total energy as

$$E_{\text{tot}} = E_{\text{elec}} + \sum_{A=1}^M \sum_{B>A}^M \frac{Z_A Z_B}{R_{AB}} = E_{\text{elec}} + V_{\text{nn}} \quad (14)$$

Therefore the electronic and nuclear parts of the Schrödinger equation can be solved separately by introducing the parametric dependence of the total energy on the nuclear coordinates. In more general terms, for a given set of nuclear configurations, the electronic Schrödinger equation is solved to find the total energy, allowing the energy to be studied as a function of the nuclear coordinates. This provides the potential energy surface (PES) of the system.

### 1.2.7 The Hartree-Fock Approximation

It is not possible to solve the electronic Schrödinger equation exactly with more than two interacting particles and therefore further simplification is required. One such simplification is the use of an approximate wave function, such as a single Slater determinant. This is known as the Hartree-Fock approximation. The formalism is outlined by Szabo and Ostlund<sup>35</sup> in detail. The HF energy can be represented in chemist's notation as

$$\begin{aligned} E_{\text{HF}} &= \int \Psi^* \hat{H} \Psi d\tau = \langle \Psi | \hat{H} | \Psi \rangle = 2 \sum_a^{N/2} \langle a | \hat{h} | a \rangle + \sum_a^{N/2} \sum_b^{N/2} 2 \langle aa | bb \rangle - \langle ab | ba \rangle \\ &= 2 \sum_a^{N/2} h_{aa} + \sum_a^{N/2} \sum_b^{N/2} 2J_{ab} - K_{ab} \end{aligned} \quad (15)$$

where  $\hat{H}$  is the full electronic Hamiltonian,  $N$  is the number of electrons,  $\Psi$  is the wave function and spatial orbitals are denoted by  $a$  and  $b$ . The first term in Eq. (15) is the one-electron integral as shown in Eq. (16),

$$(a|\hat{h}|a) = \int \psi_a^*(r_1) \left[ -\frac{1}{2} \nabla_1^2 - \sum_{\Lambda} \frac{Z_{\Lambda}}{r_{1\Lambda}} \right] \psi_a(r_1) dr_1 = h_{aa} \quad (16)$$

The above equation defines the contribution from the kinetic energy of an electron and the attractive electrostatic interaction between electron and nucleus.

The second term in Eq. (15) is defined as,

$$(aa|bb) = \int \psi_a^*(r_1) \psi_a(r_1) \frac{1}{r_{12}} \psi_b^*(r_2) \psi_b(r_2) dr_1 dr_2 = J_{ab} \quad (17)$$

$$(ab|ba) = \int \psi_a^*(r_1) \psi_b(r_1) \frac{1}{r_{12}} \psi_b^*(r_2) \psi_a(r_2) dr_1 dr_2 = K_{ab} \quad (18)$$

Eq. (17) and Eq. (18) represent the Coulomb integrals,  $J_{ab}$  and the exchange integrals,  $K_{ab}$ , respectively, between two electrons.

According to the variation principle, the best wave function is the one which gives the lowest possible energy ( $E_0$ ), i.e.,

$$E_0 = \langle \Psi_0 | \hat{H} | \Psi_0 \rangle \quad (19)$$

Minimizing  $E_0$  with respect to the spatial orbitals leads to the Hartree-Fock equations,

$$\hat{f}_i \psi_i = \epsilon_i \psi_i \quad i=1,2,\dots,N \quad (20)$$

where  $\hat{f}$  is called Fock operator which acts on the molecular orbital  $\psi_i$ .

The  $\hat{f}$  is an effective one-electron operator defined as:

$$\hat{f}(i) = -\frac{1}{2}\nabla_i^2 - \sum_A^M \frac{Z_A}{r_{iA}} + v^{\text{HF}}(i) = h(i) + v^{\text{HF}}(i) \quad (21)$$

Where,  $h(i)$  is the core-Hamiltonian operator and  $v^{\text{HF}}(i)$  is the effective one-electron potential operator called the Hartree-Fock potential which represents the average repulsive potential experienced by the  $i$ 'th electron due to the presence of all the other electrons.

## 1.2.8 The Basis Set Expansion

It is necessary to specify the form of spatial orbitals  $\psi_i(\mathbf{r})$  to carry out calculations on molecular systems. The orbitals may be expressed as a linear combination of a set of basis functions  $\{\phi_\mu, \mu = 1, 2, \dots, K\}$ :

$$\psi_i(\mathbf{r}) = \sum_{\mu=1}^K C_{\mu i} \phi_\mu(\mathbf{r}) \quad (22)$$

where  $\phi_\mu(\mathbf{r})$  are basis functions,  $C_{\mu i}$  are the molecular orbital expansion coefficients. Roothaan's equation can be written as a single matrix equation,<sup>35, 36</sup>

$$FC = \epsilon SC \quad (23)$$

where  $F$  is the Fock matrix where each element can be written as:

$$F_{\mu\nu} = \int \phi_\mu^*(\mathbf{r}_1) \hat{f}(\mathbf{r}_1) \phi_\nu(\mathbf{r}_1) d\mathbf{r}_1 \quad (24)$$

$S$  is the overlap matrix where each element can be written as:

$$S_{\mu\nu} = \int \phi_\mu^*(\mathbf{r}_1) \phi_\nu(\mathbf{r}_1) d\mathbf{r}_1 \quad (25)$$

C and  $\epsilon$  are the molecular orbital coefficients and orbital energies (eigenvalues), respectively. The equation is solved by the Self-Consistent-Field (SCF) procedure which is an iterative process starting with the initial guess of the molecular orbital coefficients C which are used to construct the Fock matrix, F. Roothaan's equation is then solved for new MO coefficients which can then be used to determine a new Fock matrix. This process is repeated until the Fock matrix converges to a desired accuracy.

In general, basis functions,  $\phi$ 's, are a linear combination of Gaussian Type Functions (GTF),

$$\phi_{\mu}^t = \sum_{r=1}^{N_g} d_r g_r^t(\alpha_r) \quad (26)$$

where  $N_g$  is typically, 1 to 6;  $d_r$  is a contraction coefficient; and  $g_r^t(\alpha_r)$  is a Gaussian primitive function, with exponent  $\alpha_r$ , of a given type t(s,p,d,...). The Gaussian type orbitals or functions have the general form,

$$g_{l,m,n}(\alpha_r) = N_r (X - A_x)^l (Y - A_y)^m (Z - A_z)^n \exp(-\alpha_r r_A^2) \quad (27)$$

where, (X, Y, Z) are coordinates of the electrons; ( $A_x$ ,  $A_y$ ,  $A_z$ ) are nuclear coordinates (origin of Gaussian);  $N_r$  is a normalization factor; and  $\alpha_r$  is the Gaussian exponent.  $r_A^2$  is represented as,

$$r_A^2 = (X - A_x)^2 + (Y - A_y)^2 + (Z - A_z)^2 \quad (28)$$

## 1.2.9 Post Hartree-Fock Methods

Since the HF method uses a single determinant wave function, its main drawback is neglect of electron correlation. In the HF method, electrons with the same spin are correlated, but electrons with opposite spins are not correlated. The correlation energy,  $E_{\text{corr}}$ , can be described as,

$$E_{\text{corr}} = E_0 - E_{\text{HFL}} \quad (29)$$

where,  $E_0$  is the exact non-relativistic energy of the system and  $E_{\text{HFL}}$  is the Hartree-Fock limit energy which represents the HF energy obtained in the limit that the basis set approaches completeness. There are many methods that compute  $E_{\text{corr}}$ , and some are collectively called Post-Hartree-Fock methods. Some of the post Hartree-Fock methods used in this thesis are briefly described in sections 1.2.10 and 1.2.11.

## 1.2.10 Møller-Plesset Perturbation Theory

In perturbation theory (PT), the exact Hamiltonian is expressed as a sum of a known term  $\hat{H}^{(0)}$  and a perturbation,  $\lambda\hat{V}$ , as shown in Eq. (30),<sup>36</sup>

$$\hat{H} = \hat{H}^{(0)} + \lambda\hat{V} \quad (30)$$

where  $\hat{V}$  is the perturbation operator with  $\lambda$  being an arbitrary parameter. The energy is expanded as a power series, as shown in Eq. (31),

$$E = E^{(0)} + \lambda E^{(1)} + \lambda^2 E^{(2)} + \dots \quad (31)$$

where  $E^{(1)}$  and  $E^{(2)}$  denote first- and second-order corrections to the zeroth-order (unperturbed) energy. Møller and Plesset have applied perturbation theory by defining  $\hat{V}$  which treats electron correlation effects.

$$\hat{V} = \sum_{i < j} \frac{1}{r_{ij}} - \sum_i v^{\text{HF}}(i) \quad (32)$$

Various levels of MP theory exist, each offering a subsequent correction to the Hartree-Fock energy, the most commonly used being MP2:

$$E = E^{(0)} + E^{(1)} + E^{(2)} = E_{\text{HF}} + E^{(2)} \quad (33)$$

### 1.2.11 Configuration Interaction

Another way to partially overcome the deficiencies of the Hartree-Fock approximation, which is a single determinant method, is to include more than one determinant in the wave function. The determinants for other electron configurations allow the wave function to include the effects of correlation between electrons of opposite spin. Different configurations are excitations of one or more electrons from occupied to virtual orbitals. In configuration interaction (CI) different electronic configurations are mixed. The full CI wave function is represented as

$$|\Psi_{\text{CI}}\rangle = C_0 |\Psi_0\rangle + \sum_{ar} C_a^r |\Psi_a^r\rangle + \sum_{\substack{a < b \\ r < s}} C_{ab}^{rs} |\Psi_{ab}^{rs}\rangle + \sum_{\substack{a < b < c \\ r < s < t}} C_{abc}^{rst} |\Psi_{abc}^{rst}\rangle + \dots \quad (34)$$

Since the CI wave function has more variational parameters,  $(C_0, C_a^r, C_{ab}^{rs}, \dots)$ , the CI energy is lower than that calculated by the HF method. Full CI is only feasible for small

molecules and modest basis sets. Single excitations (CIS) includes only one expansion term, as in Eq. (35),

$$\Psi_{\text{CI}} = C_0 \Psi_0 + \sum_{ar} C_a^r |\Psi_a^r\rangle \quad (35)$$

The inclusion of single and double excitations yields a wave function which contains the additional terms  $\sum_{\substack{a<b \\ r<s}} C_{ab}^{rs} |\Psi_{ab}^{rs}\rangle$ .

The most common truncated CI methods are CISD, QCISD and QCISD(T), where QCISD(T) stands for Quadratic Configuration Interaction with Single and Double Excitations and Triple Excitations added Perturbatively. MP calculations are much faster than CI calculations and moderately effective in correcting electron correlation effects, but are not variational methods and so can produce energy below the exact energy.

## 1.2.12 Density Functional Theory

Density functional theory (DFT) also accounts for electron correlation effects. In DFT, all the properties of a molecular system can be determined from the ground-state electron density  $\rho(r)$ .<sup>38-42</sup> The electron density is an observable and can be measured experimentally by X-ray diffraction. The energy of a system is a function of the density function, often called a functional:

$$E = E_0[\rho(r)] \quad (36)$$

Therefore, the ground state energy can be derived from the density function. Kohn and Sham (KS) devised a practical method for finding ground-state densities  $\rho_0$  and ground

state energies  $E_0$  by virtue of the fact that the true ground state electron density minimizes the energy functional, just as the true ground state wave function minimizes the energy. The energy density functional has the form

$$E[\rho] = T_s[\rho] + V_{ne}[\rho] + V_{ee}[\rho] + \Delta T[\rho] + \Delta V_{ee}[\rho] \quad (37)$$

where  $T_s$  is the kinetic energy for the reference system of non-interacting electrons (uniform electron gas or Jellium). The density for the reference system is written as:

$$\rho_s = \sum_{i=1}^N |\Psi_i^{KS}|^2 \quad (38)$$

where  $\Psi_i^{KS}$  are the Kohn-Sham orbitals.

$V_{ne}[\rho]$  represents the classical potential energy in terms of the density, which is written as:

$$V_{ne}[\rho] = \sum_A^M \int \frac{Z_A}{|\mathbf{r} - \mathbf{r}_A|} \rho(\mathbf{r}) d\mathbf{r} \quad (39)$$

$V_{ee}[\rho]$  represents the classical expression for the electrostatic electron-electron repulsion function, written as:

$$V_{ee}[\rho] = \frac{1}{2} \iint \frac{\rho(\mathbf{r}_1)\rho(\mathbf{r}_2)}{|\mathbf{r}_1 - \mathbf{r}_2|} d\mathbf{r}_1 d\mathbf{r}_2 \quad (40)$$

The last two terms in Eq. (37) are corrections to the kinetic energy of the non-interacting electrons and all the non-classical corrections to the electron-electron repulsion energy, respectively. These two terms are combined together in one term as:

$$E_{xc}[\rho] = \Delta T[\rho] + \Delta V_{ee}[\rho] \quad (41)$$

where  $E_{xc}[\rho]$  is the exchange-correlation energy functional. Eq. (37) can then be written as:

$$E[\rho] = T_s[\rho] + V_{ne}[\rho] + V_{ee}[\rho] + E_{xc}[\rho] \quad (42)$$

A good approximation to  $E_{xc}$  is required to get an accurate energy from DFT calculations.  $E_{xc}$  is written as the sum of an exchange-energy functional and a correlation-energy functional as:

$$\epsilon_{xc}[\rho] = \epsilon_x[\rho] + \epsilon_c[\rho] \quad (43)$$

Different functionals (X: exchange functional and C: correlation functional) are available.<sup>12,45-48</sup> Some of the widely used and fairly reliable functionals are B3LYP, B3PW91, B3P86, etc. DFT does not directly solve the Schrödinger equation and therefore it is not strictly an *ab initio* method. DFT is widely used since it is only slightly more time consuming than a Hartree-Fock calculation and has relatively good accuracy.

### 1.2.13 G3B3, G3MP2 and G3MP2B3 Theories

In general, Gaussian-n theories<sup>15,49-53</sup> including the Gaussian-3 theories,<sup>15,49,50</sup> G3B3, G3MP2 and G3MP2B3 consist of several high level *ab initio* calculations which are combined to give reliable energetics which closely match experimental values. The G3B3<sup>50</sup> and G3MP2B3<sup>50</sup> theories are based on an optimized geometry at B3LYP/6-31G(d), while the G3MP2<sup>49</sup> theory is based on an optimized geometry at MP2(FULL)/6-31G(d).

The G3B3 energy at 0 K is written as,

$$E_0(\text{G3B3}) = E[\text{MP4(FC)}/6-31\text{G(d)}] + \Delta E(+)+\Delta E(2\text{df},\text{p}) \\ +\Delta E(\text{QCI})+\Delta E+\Delta E(\text{SO})+\Delta E(\text{HLC})+\text{ZPE} \quad (44)$$

where,

$$\Delta E(+)=E[\text{MP4(FC)}/6-31+\text{G(d)}]-E[\text{MP4(FC)}/6-31\text{G(d)}],$$

$$\Delta E(2\text{df},\text{p})=E[\text{MP4(FC)}/6-31\text{G}(2\text{df},\text{p})]-E[\text{MP4(FC)}/6-31\text{G(d)}],$$

$$\Delta E(\text{QCI})=E[\text{QCISD(T,FC)}/6-31\text{G(d)}]-E[\text{MP4(FC)}/6-31\text{G(d)}],$$

$$\Delta E=E[\text{MP2(FU)}/\text{G3large}]-E[\text{MP2(FC)}/6-31\text{G}(2\text{df},\text{p})]-E[\text{MP2(FC)}/6-31+\text{G(d)}] \\ +E[\text{MP2}/6-31\text{G(d)}]$$

The G3MP2 energy at 0 K is written as,

$$E_0(\text{G3MP2})=E[\text{QCISD(T,FC)}/6-31\text{G(d)}/\text{MP2(FULL)}/6-31\text{G(d)}] \\ +\Delta E(\text{MP2})+\Delta E(\text{HLC})+\text{ZPE}+\Delta E(\text{SO}) \quad (45)$$

$\Delta E(\text{MP2})$  is given by:

$$\Delta E(\text{MP2})=E[\text{MP2(FC)}/\text{G3MP2large}/\text{MP2(FULL)}/6-31\text{G(d)}] \\ -E[\text{MP2(FC)}/6-31\text{G(d)}/\text{MP2(FULL)}/6-31\text{G(d)}]$$

The G3MP2B3 also follows Eq. (45) except that the geometry and ZPE are calculated at B3LYP/6-31G(d).

$\Delta E(\text{HLC})$ , used in all the theories, represents the higher level correction, given by:

$$\Delta E(\text{HLC})=-A n_{\beta}-B(n_{\alpha}-n_{\beta}) \quad (46)$$

$n_{\alpha}$  and  $n_{\beta}$  are the number of  $\alpha$  and  $\beta$  valence electrons, respectively, with  $n_{\alpha} \geq n_{\beta}$ . The A and B values are chosen to give the smallest average absolute deviation for the test set of experimental energies. The values are available in the literature.<sup>50</sup>  $\Delta E(\text{SO})$  is a spin-

orbit correction which is also taken from experimental results and is required for atomic species only.

For G3B3 and G3MP2B3,  $ZPE = 0.92 \times ZPE[B3LYP/6-31G(d)]$  and for G3MP2,  $ZPE = 0.8929 \times ZPE[HF/6-31G(d)]$

Gaussian-3 theories were developed mainly due to the fact that they are computationally less expensive than Gaussian-1<sup>51,52</sup> and Gaussian-2<sup>53</sup> theories and have been found to be more accurate as well. Within the Gaussian-3 theories, the average mean absolute deviation (MAD) for G3 theory from experiment for 299 energies is 4.2 kJ mol<sup>-1</sup>.<sup>15</sup> Although G3 theory predicts energies very well, it is also computationally demanding as the geometries are obtained from MP2(FULL)/6-31G(d). G3B3 theory overcomes this problem in which both the geometries and zero-point energies are obtained from B3LYP/6-31G(d). The mean absolute deviation for G3B3 energies from experiment is 4.1 kJ mol<sup>-1</sup> for 299 energies. The G3MP2 and G3MP2B3 theories also give reliable energies as the mean absolute deviations from experiment for 299 energies are 5.4 and 5.2 kJ mol<sup>-1</sup>, respectively. There are few single point calculations in G3MP2 and G3MP2B3 theories which represent a significant savings of computational time.

### 1.2.14 Solvation Models

Most of the chemical reactions in nature occur in the presence of solvent which may play a major role in the overall reaction mechanism and thermodynamics. Molecular

wave functions and electron densities in solution will differ to some extent from the gas phase. To deal with the solvent effect, a solute molecule is considered to be surrounded by many solvent molecules.<sup>36</sup> Inclusion of solvent effects is very important as it allows direct comparison with experiment and with the true nature of the system. Generally, the solvent effect is included in calculations by modelling the solvent as a continuous dielectric surrounding a cavity containing the solute molecule. Some of the solvent models used in this thesis are briefly discussed in sections 1.2.15 and 1.2.16.

### 1.2.15 The Onsager model

According to this model, the molecular cavity is considered spherical with a fixed radius and the electric dipole is located at the centre of the cavity. The electric field in the cavity is written as,<sup>36</sup>

$$E_R = \frac{2(\epsilon_r - 1)}{(2\epsilon_r + 1)a^3} \mu \quad (47)$$

Where,  $\epsilon_r$  is the dielectric constant of the solvent,  $a$  is the radius of the cavity,  $\mu$  is the electric dipole moment.

The potential energy due to electrostatic interaction between  $\mu$  and the reaction field  $E_R$  is represented as,

$$\hat{V}_{\text{int}} = -\hat{\mu} \cdot E_R \quad (48)$$

where,  $\hat{\mu}$  is the electric dipole moment operator.  $\hat{V}_{\text{int}}$  is added to the molecular electronic Hamiltonian  $\hat{H}_M^{(0)}$  obtained from the gas phase calculation.

### 1.2.16 Polarizable Continuum Model

Tomasi and co-workers initially developed the Polarizable Continuum Model (PCM) in which the cavity is created via a series of overlapping spheres.<sup>53,54</sup> In the PCM model, the molecular cavity is more realistic. For example, in a simple PCM model, each atomic nucleus in the solute molecule is surrounded by a sphere of radius 1.2 times the van der Waals radius of that atom.<sup>36</sup> In the Gaussian 03 quantum mechanical package, the molecular cavity can be specified by different cavity models such as UA0, UFF, PAULING, BONDI, etc. By default, the program builds up the cavity using the United Atom (UA0) model, i.e., by putting a sphere around each solute heavy atom and the hydrogen atoms are enclosed in the sphere of the atom to which they are bonded. The solvent used is also specified in the input of the Gaussian calculation. An example of an input keyword and an output summary for the solvent phase (CCl<sub>4</sub>) optimization of ethene at B3LYP/6-31G(d) is shown in appendix (A). The same procedure is followed for the calculations at MP2 and B3LYP levels of theory, however, it should be noted that the free energy of solvation at MP2 is the value saved in the Gaussian archive.

## 1.3 References

- (1) Yamabe, S.; Minato, T.; Inagaki, S., *J. Chem. Soc., Chem. Commun.*, **1988**, 532.
- (2) Hamilton, T. P.; Schaefer, H. F., *J. Am. Chem. Soc.*, **1990**, *112*, 8260.

- (3) Cammi, R.; Mennucci, B.; Pomelli, C.; Cappelli, C.; Corni, S.; Frediani, L.; Trucks, G. W.; Frisch, M., *J. Theor. Chem. Acc.*, **2004**, *111*, 66.
- (4) Hamilton, T. P.; Schaefer, H. F., *J. Am. Chem. Soc.*, **1991**, *113*, 7147.
- (5) Chiappe, C.; Lenoir, D.; Pomelli, C. S.; Bianchini, R., *Phys. Chem. Chem. Phys.*, **2004**, *6*, 3235.
- (6) McCarthy, M. C., Gottlieb, C. A., Thaddeus, P., *Mol. Phys.*, **2003**, *101*, 697.
- (7) Gershevitz O., Sukenik C. N., Ghabboun J., Cahen D., *J. Am. Chem. Soc.*, **2003**, *125*, 4730.
- (8) Koinuma H., Manako T., Natsuaki H., Fujioka H., Fueki, K., *J. Non-Cryst. Solids*, **1985**, *77*, 801.
- (9) Matsuda A., Yagii K., Kaga T., Tanaka K., *Jpn. J. Appl. Phys.*, **1984**, *23*, 576.
- (10) Sato K., Hirano T., Natsuaki H., Fueki K., Koinuma H., *Appl. Phys. Lett.*, **1984**, *45*, 1324.
- (11) Binning Jr, R. C.; Curtiss, L. A. *J. Comp. Chem.*, **1990**, *11*, 1206.
- (12) Frisch, M. J.; Trucks, G. W.; Schlegel, H. B.; Scuseria, G. E.; Robb, M. A.; Cheeseman, J. R.; Montgomery, Jr., J. A.; Vreven, T.; Kudin, K. N.; Burant, J. C.; Millam, J. M.; Iyengar, S. S.; Tomasi, J.; Barone, V.; Mennucci, B.; Cossi, M.; Scalmani, G.; Rega, N.; Petersson, G. A.; Nakatsuji, H.; Hada, M.; Ehara, M.; Toyota, K.; Fukuda, R.; Hasegawa, J.; Ishida, M.; Nakajima, T.; Honda, Y.; Kitao, O.; Nakai, H.; Klene, M.; Li, X.; Knox, J. E.; Hratchian, H. P.; Cross, J. B.; Bakken, V.; Adamo, C.; Jaramillo, J.; Gomperts, R.; Stratmann, R. E.; Yazyev, O.; Austin, A. J.; Cammi, R.; Pomelli, C.; Ochterski, J. W.; Ayala, P. Y.; Morokuma, K.; Voth, G. A.; Salvador, P.; Dannenberg, J.

- J.; Zakrzewski, V. G.; Dapprich, S.; Daniels, A. D.; Strain, M. C.; Farkas, O.; Malick, D. K.; Rabuck, A. D.; Raghavachari, K.; Foresman, J. B.; Ortiz, J. V.; Cui, Q.; Baboul, A. G.; Clifford, S.; Cioslowski, J.; Stefanov, B. B.; Liu, G.; Liashenko, A.; Piskorz, P.; Komaromi, I.; Martin, R. L.; Fox, D. J.; Keith, T.; Al-Laham, M. A.; Peng, C. Y.; Nanayakkara, A.; Challacombe, M.; Gill, P. M. W.; Johnson, B.; Chen, W.; Wong, M. W.; Gonzalez, C.; Pople, J. A. Gaussian 03, Revision B.05, Gaussian, Inc., Wallingford CT, 2004. <http://www.gaussian.com> (accessed on Oct 3, 2007)
- (13) Schmidt, M. W.; Baldridge, K. K.; Boatz, J. A.; Elbert, S. T.; Gordon, M. S.; Jensen, J. J.; Koseki, S.; Matsunaga, N.; Nguyen, K. A.; Su, S.; Windus, T. L.; Dupuis, M.; Montgomery, J. A. *J. Comput. Chem.*, **1993**, *14*, 1347-1363. GAMESS Version = 22 Feb 2006 (R5) from Iowa State University.
- (14) Rassolov, V. A.; Ratner, M. A.; Pople, J. A.; Redfern, P. C.; Curtiss, L. A. *J. Comput. Chem.*, **2001**, *22*, 976.
- (15) Curtiss, L. A.; Raghavachari, K.; Redfern, P. C.; Rassolov, V.; Pople, J. A. *J. Chem. Phys.*, **1998**, *109*, 7764.
- (16) Dybala-Defratyka, A.; Rostkowski, M.; Matsson, O.; Westaway, K. C.; Paneth, P., *J. Org. Chem.*, **2004**, *69*, 4900.
- (17) Fang, Y.; S. MacMillar, S.; Eriksson, J.; Kołodziejska-Huben, M.; Dybala-Defratyka, A.; Paneth, P.; Matsson, O.; Westaway, K. C., *J. Org. Chem.*, **2006**, *71*, 4742 – 4747.
- (18) Fang, Y.; Gao, Y.; Ryberg, P.; Eriksson, J.; Kolodziejska-Huben, M.; Dybala-Defratyka, A.; Madhavan, S.; Danielsson, R.; Paneth, P.; Matsson, O.; Westaway, K. C., *Chem. Eur. J.*, **2003**, *9*, 2696.

- (19) Poirier R. A.; Wang Y.; Westaway K. C., *J. Am. Chem. Soc.*, **1994**, *116*, 2526.
- (20) Garrett, B.C.; Truhlar, D. G. *Encyclopedia of Computational Chemistry: Transition State Theory*, John Wiley and Sons, Ltd., Chichester, England, 1998, 3094.
- (21) Atkins, P.; De Paula, Julio. *Physical Chemistry*, 7th ed.; W. H. Freeman and Company, NY, 2002.
- (22) Hammond, G. S. *J. Am. Chem. Soc.* **1955**, *77*, 334.
- (23) Westheimer, F. H. *Chem. Rev.* **1961**, *61*, 265.
- (24) Melander, L. *Isotope Effects on Reaction Rates*; The Ronald Press: New York, 1960.
- (25) Sühnel, J.; Schowen, R. L. In *Enzyme Mechanism from Isotope Effects*; Cook, P. F., Ed.; CRD Press, Inc.: Boca Ranton, 1991, pp 3-36.
- (26) Wiberg, K. B. *Physical Organic Chemistry*; Wiley: NY, 1964, pp. 352.
- (27) Westaway, K. C.; Fang, Y., MacMillar, S.; Matsson, O.; Poirier, R. A.; Islam, S. M., *J. Phys. Chem. A*, **2007**, *111*, 8110.
- (28) Westaway, K. C.; Fang, Y., MacMillar, S.; Matsson, O.; Poirier, R. A.; Islam, S. M., *J. Org. Chem.* (submitted).
- (29) Melander, L.; Saunders, W. H., Jr. *Reaction Rates of Isotopic Molecules*; 2ed.; Wiley-Interscience: New York, 1980.
- (30) Redlich, O. *Z. Phys. Chem. B*, **1935**, *28*, 371-382.
- (31) Wigner, E., *Z. Phys. Chem. B*, **1932**, *19*, 203.
- (32) Matsson, O.; Persson, J.; Axelsson, B. S.; Langstrom, B.; Fang, Y.; Westaway, K. C. *J. Am. Chem. Soc.* **1996**, *118*, 6350.

- (33) Anderson, V. E.; Cassano, A. G.; Harris, M. E. In *Isotope Effects in Chemistry and Biology*; Kohen, A., Limbach, H.-H., Eds.; Taylor & Francis: Boca Raton, 2006; pp 893-914.
- (34) Paneth, P.; O'Leary, M. H. *J. Am. Chem. Soc.* **1991**, *113*, 1691.
- (35) Szabo, A.; Ostlund, N. *Modern Quantum Chemistry*, Dover Publications, INC., New York, 1996.
- (36) Levine, I.N. *Quantum Chemistry*, Prentice-Hall, Inc., New Jersey, 2000.
- (37) Born, M.; Oppenheimer, R. *Ann Phys.* **1927**, *84*, 457.
- (38) Gross, E.K.U.; Dreizler, R.M. *Density Functional Theory*, Plenum Press, New York, 1995.
- (39) Fiolhais, C.; Nogueira, F.; Marques, M. *A Primer in Density Functional Theory*, Springer-Verlag, Berlin, Germany, 2003.
- (40) Labanowski, J.K.; Andzelm, J.W. *Density Functional Methods in Chemistry*. Springer-Verlag, New York, 1991.
- (41) Sahni, V. *Quantal Density Functional Theory*, Springer, Berlin, Germany, 2004.
- (42) Holthausen, M.C.; Koch, W. *A Chemist's Guide to Density Functional Theory*, Wiley-VCH, Weinheim, Germany, 2001.
- (43) Chong, D.P. *Recent Advances in Density Functional Methods*. Vol.1, World Scientific, Ltd., Singapore, 1997.
- (44) Schleyer, M.F. *Encyclopedia of Computational Chemistry*, John Wiley and Sons, New York, 1998.
- (45) Becke, A. D. *Phys. Rev. A*, **1988**, *38*, 3098.

- (46) Lee, C.; Yang, W.; Parr, R. G. *Phys. Rev. B*, **1988**, *37*, 785.
- (47) Perdew, J. P. *Phys. Rev. B*, **1986**, *33*, 8822.
- (48) Perdew, J. P.; Burke, K.; Wang, Y. *Phys. Rev. B*, **1996**, *54*, 16533.
- (49) Curtiss, L.A.; Redfern, P. C.; Raghavachari, K.; Rassolov, V. Pople J. A. *Journal of Chem. Phys.*, **1999**, *110*, 4703.
- (50) Baboul A. G., Curtiss, L.A.; Redfern, P. C.; Raghavachari, K. *Journal of Chem. Phys.*, **1999**, *110*, 7650.
- (51) Pople, J. A.; Head-Gordon, M., Fox, D. J.; Raghavachari, K.; Curtiss, L.A. *Journal of Chem. Phys.* **1989**, *90*, 5622.
- (52) Curtiss, L.A.; Jones, C.; Trucks, G. W.; Raghavachari, K., Pople, J. A. *Journal of Chem. Phys.* **1990**, *93*, 2537.
- (53) Curtiss, L.A.; Raghavachari, K.; Trucks, G. W.; Pople, J. A. *Journal of Chem. Phys.* **1991**, *94*, 7221.
- (53) Miertus, S.; Scrocco, E., Tomasi, J. *Chem. Phys.* **1981**, *55*, 117.
- (54) Miertus, S. ; Tomasi, J. *Chem. Phys.* **1982**, *65*, 117.

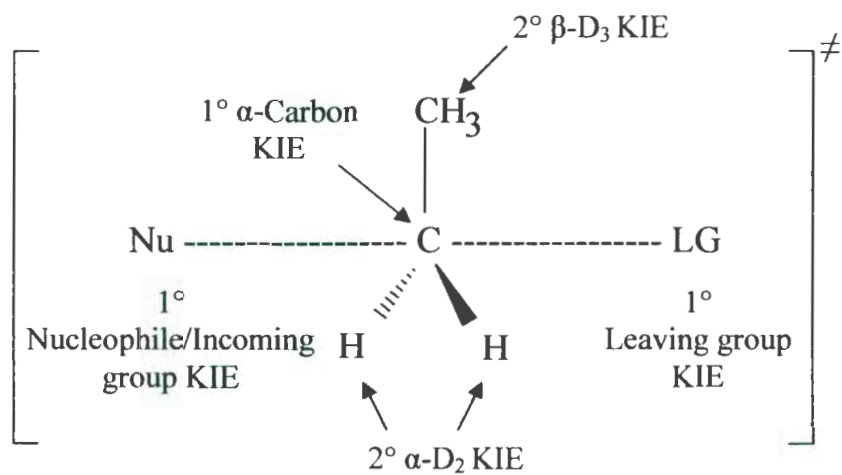


Figure 1.1 Transition state structure for the  $S_N2$  reaction between an ethyl substrate and a nucleophile showing different kinetic isotope effects. Here, D represents deuterium.

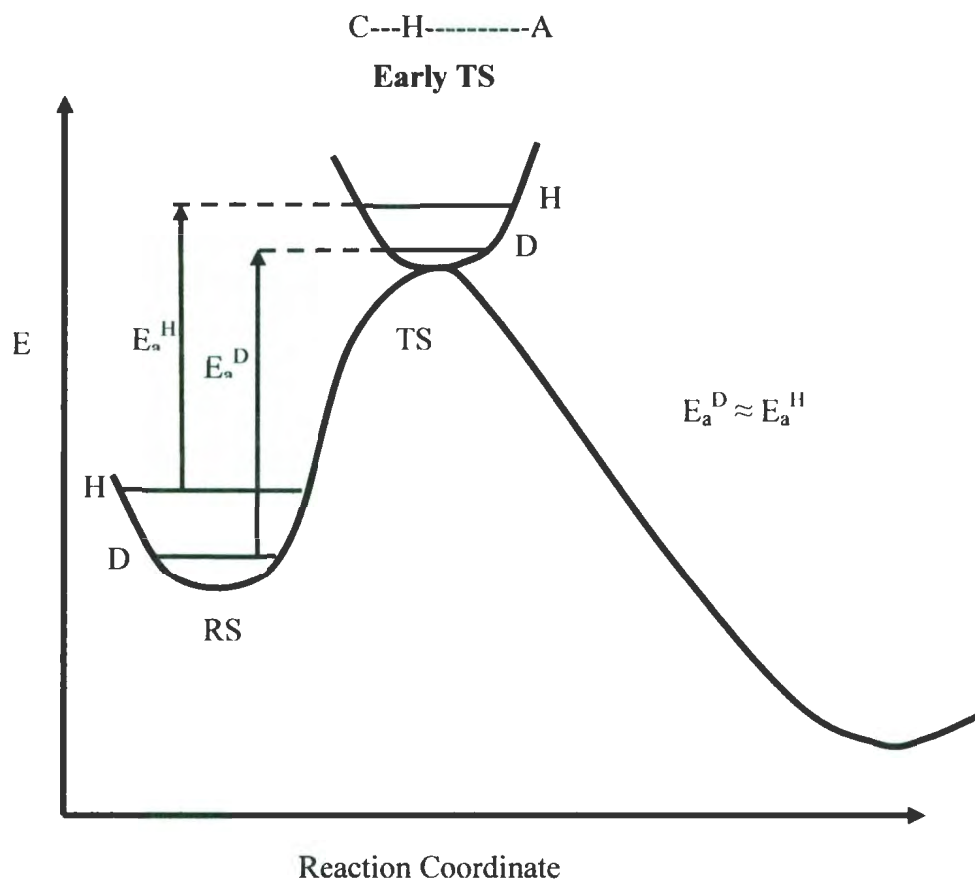


Figure 1.2 Origin of  $k_H/k_D$  in an exothermic reaction (early TS)

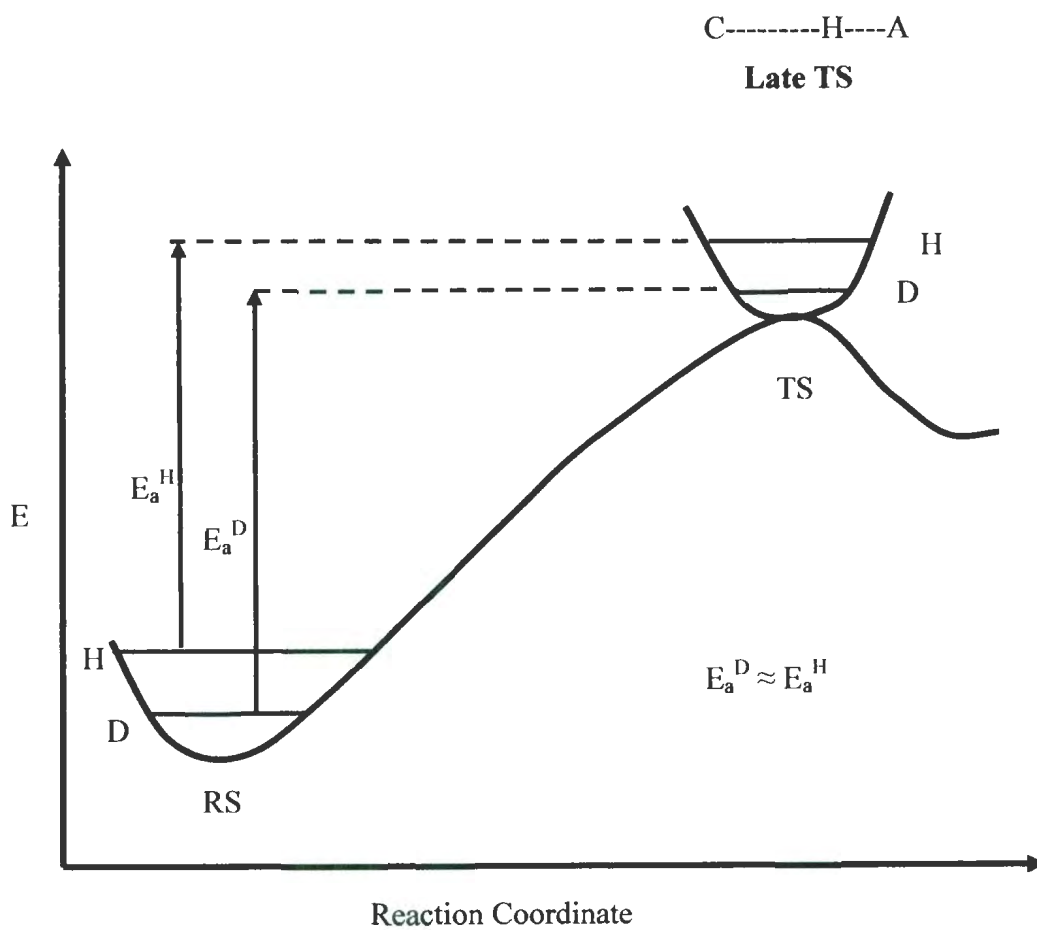


Figure 1.3 Origin of  $k_H/k_D$  in an endothermic reaction (late TS)

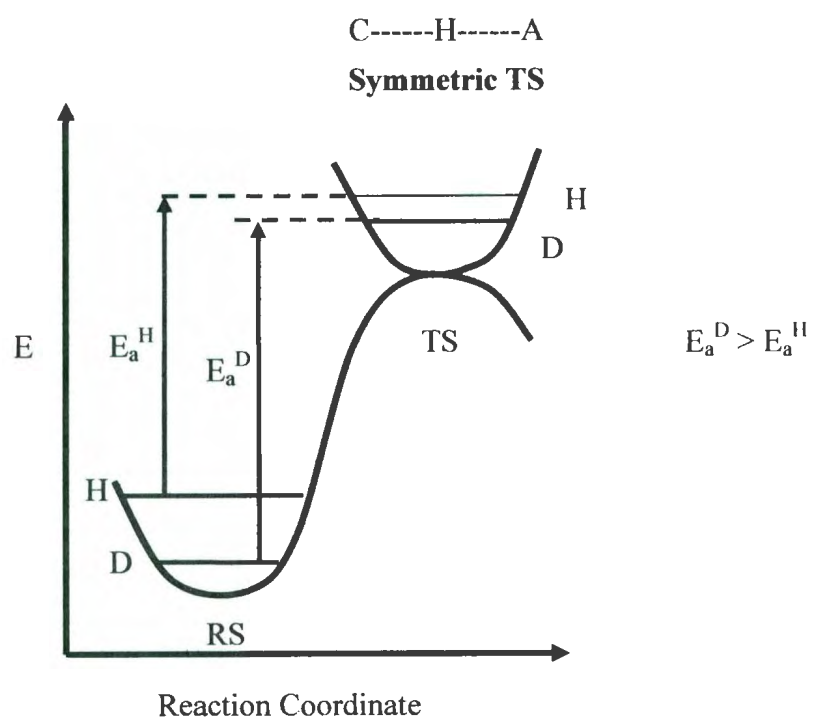


Figure 1.4 Origin of large  $k_H/k_D$  in a thermoneutral reaction (symmetric TS)

## CHAPTER 2

### Computational Study of the Reactions of $\text{SiH}_3\text{X}$

( $\text{X} = \text{H, Cl, Br, I}$ ) with HCN

#### 2.1 Introduction

In recent years, silanes ( $\text{SiH}_4$ ) and halosilanes ( $\text{SiH}_3\text{X}$ ) have drawn considerable attention because of their importance in the semiconductor, glass, and polymer industries.<sup>1-4</sup> The physical and chemical properties of most silyl compounds are quite different from those of their methyl analogues. Although silicon and carbon are isovalent, silicon can have coordinations greater than four. Silicon also interacts with the  $\pi$ -bonds of elements in groups V, VI, and VII. Unlike carbon, silicon does not favor formation of multiple bonds. Silane and halosilanes can react with small molecules, such as  $\text{NH}_3$ <sup>5</sup> and  $\text{H}_2\text{O}$ ,<sup>6</sup> to form various

intermediates and products under suitable conditions. Similar reactions may be possible in interstellar space where Si is relatively abundant.<sup>7</sup> As a consequence, a number of researchers have focused on the reactions of silane and halosilanes, both experimentally and theoretically.<sup>7-14</sup>

The gas-phase reactions of silane with ammonia and water were studied using ab initio methods by Hu et al.<sup>5,6</sup> The reaction with NH<sub>3</sub> was found to proceed in a single step to the most stable product silylamine (SiH<sub>3</sub>NH<sub>2</sub>). The reaction involves H<sub>2</sub> elimination from the weakly bonded reactant complex H<sub>3</sub>N/SiH<sub>4</sub>. The activation energy was found to be 206.1 kJ mol<sup>-1</sup> at the CCSD(T)/6-311++G(d,p)//MP2/6-31+G(d) level. This barrier was the lowest among various pathways investigated for the reaction. For the gas-phase reaction between SiH<sub>4</sub> and H<sub>2</sub>O, 40 equilibrium and 27 transition state structures were found on the potential energy surface of the reaction. The reaction, SiH<sub>4</sub> + H<sub>2</sub>O → SiH<sub>3</sub>OH + H<sub>2</sub> has an energy barrier of 194.8 kJ mol<sup>-1</sup> and ΔE<sub>rxn</sub> of -45.3 kJ mol<sup>-1</sup> at CCSD(T)/6-311++G(d,p)//MP2/6-31+G(d). It was found that SiH<sub>4</sub>/H<sub>2</sub>O can also eliminate H<sub>2</sub> to produce SiH<sub>2</sub>/H<sub>2</sub>O with an energy barrier of 242.8 kJ mol<sup>-1</sup>. The products can further eliminate H<sub>2</sub> or H, producing smaller molecules SiHOH, SiH<sub>2</sub>-O, Si-H<sub>2</sub>O, and SiO, and SiH<sub>2</sub>-OH, SiH-H<sub>2</sub>O, HSiO, and HOSi radicals.

Silanes have been found both experimentally and theoretically to complex with the lone-paired electrons of ammonia, amine, arsine, phosphorus or phosphine to form pentacoordinated adducts.<sup>15-21</sup> Feng et al.<sup>22</sup> investigated the adducts H<sub>3</sub>SiX/NH<sub>3</sub> (X = F, Cl,

Br, I) with ab initio calculations at the G2MP2 level, and discussed the influence of halogen atoms on the structure and stability of this type of species. Schlegel et al.<sup>23, 24</sup> studied the thermal decomposition of SiH<sub>4</sub> and SiH<sub>3</sub>Cl at HF/6-31G(d) and MP2/6-31G(d,p). They found that for the decomposition of SiH<sub>4</sub>, SiH<sub>2</sub> + H<sub>2</sub> is favored over SiH<sub>3</sub> + H and for SiH<sub>3</sub>Cl, SiHCl + H<sub>2</sub> is preferred over SiH<sub>2</sub> + HCl. Calculations have also shown that in the gas phase, SiH<sub>4</sub> and Ga in its first excited <sup>2</sup>S state, react to form SiH<sub>3</sub> radicals, H atoms, GaH and GaSiH<sub>3</sub>.<sup>25</sup>

The number of known Si-containing molecules is very small compared to C or N containing species and few compounds containing all three are known. In interstellar space, only the simplest radicals, SiCN and SiNC, have been detected.<sup>26</sup> In the laboratory, HSiCN and HSiNC<sup>27</sup> have been detected, along with the SiCN and SiNC<sup>28</sup> radicals. More hydrogenated species H<sub>3</sub>CNSi, H<sub>3</sub>SiCN, and H<sub>3</sub>SiNC were also characterized by IR spectra.<sup>29</sup> A G3B3 investigation of the singlet [H<sub>3</sub>, Si, N, C] isomers<sup>30</sup> resulted in 26 isomers and 45 interconversion transition state structures. The three lowest-lying isomers, H<sub>3</sub>SiCN (0.0 kJ mol<sup>-1</sup>), H<sub>3</sub>SiNC (20.5 kJ mol<sup>-1</sup>), and H<sub>3</sub>CNSi (30.9 kJ mol<sup>-1</sup>) were found to be kinetically stable with the lowest conversion barrier at 98.0 kJ mol<sup>-1</sup>. Fourteen new isomers with considerable kinetic stability were also predicted. To date, no experimental or theoretical heats of formation have been reported for H<sub>3</sub>SiCN and H<sub>3</sub>SiNC.

No computational studies have been reported for the reaction of silanes and halosilanes with HCN. To ensure the reliability of our results, wave function and DFT

calculations were performed. One of the main objectives of this study was to select the lowest level of theory/basis set that would give reliable energetics for these reactions. Because of the size of the system, it is possible to perform the calculations at high levels of theory, such as the G3MP2 and G3B3 levels, which are known to give reliable energetics.<sup>31</sup>

32

## 2.2 Method

All the electronic structure calculations were carried out with Gaussian03,<sup>33</sup> except for TS1<sup>A</sup>, X = Br, where the HF structure was optimized with MUNgauss.<sup>34</sup> The geometries of all reactants, transition states, intermediates and products were fully optimized at the HF, second-order Møller–Plesset (MP2) and B3LYP levels of theory using the 6-31G(d) and 6-31G(d,p) basis sets. From previous work,<sup>35</sup> it was found that the activation energies and the enthalpies of reaction calculated using Gaussian-n theories (G1, G2, G2MP2, G3, G3MP2, G3B3, and G3MP2B3) all agreed to within 10 kJ mol<sup>-1</sup>. For this study, G3MP2 and G3B3 theories have been selected due to their reliability<sup>31,32</sup> and the fact that they provide a contrast between wave function and density functional theories. For Br, the G3MP2large basis set,<sup>36,37</sup> which is not yet incorporated in Gaussian03, was used for G3MP2 calculations. The standard 6-31G(d) bromine basis set<sup>38</sup> has been used throughout and compared with the Binning-Curtiss<sup>39</sup> bromine basis set available in Gaussian03. For iodine, the Huzinaga double zeta basis set<sup>40</sup> was used. Frequencies were calculated for all structures to ensure the absence of imaginary frequencies in the minima and for the presence of only one imaginary

frequency in the transition states. The complete reaction pathways for all the mechanisms discussed in this paper have been verified using intrinsic reaction coordinate (IRC) analysis for all transition states. Structures at the last IRC points have been optimized to positively identify the reactant and product to which each transition state is connected. Heats of formation ( $\Delta H_f$ ) of  $\text{SiH}_3\text{CN}$ ,  $\text{SiH}_3\text{NC}$ ,  $\text{SiH}_2\text{ClCN}$ ,  $\text{SiH}_2\text{BrCN}$ ,  $\text{SiH}_2\text{ICN}$ ,  $\text{SiHCl}$ ,  $\text{SiHBr}$  and  $\text{SiHI}$  were calculated using computed enthalpies of reaction and available experimental heats of formation ( $\Delta H_f$ ).

## 2.3 Results and Discussions

The results for the reactions of  $\text{SiH}_3\text{X}$  ( $\text{X} = \text{H}, \text{Cl}, \text{Br}, \text{I}$ ) with  $\text{HCN}$  are given in Tables 2.1–2.10 and the heats of formation of some energetically stable compounds are presented in Table 2.11.

### 2.3.1 Activation energies and free energies of activation for the reaction of $\text{SiH}_3\text{X}$ with $\text{HCN}$

The results for the reaction of  $\text{SiH}_3\text{X}$  ( $\text{X} = \text{H}, \text{Cl}, \text{Br}, \text{I}$ ) with  $\text{HCN}$  will be discussed in the following order: 1)  $\text{HX}$  elimination, 2)  $\text{H}_2$  elimination, and 3) reaction of  $\text{HCN}$  with  $\text{SiH}_3\text{X}$  dissociation products.

#### 2.3.1.1 Reaction of $\text{SiH}_3\text{X}$ and $\text{HCN}$ (Pathway A):

Pathway A consists of an  $\text{HX}$  elimination reaction followed by isomerization of the

SiH<sub>3</sub>CN product:



The structures of pathway A are shown in Figure 2.1 for the reaction of SiH<sub>3</sub>Cl + HCN. Similar structures are also observed for the reaction of SiH<sub>4</sub>, SiH<sub>3</sub>Br, and SiH<sub>3</sub>I with HCN and hence are not shown here. The relative energies of reactants, transition states, and products are shown in Figure 2.2. In all cases, SiH<sub>3</sub>X and HCN react in a single-step to form SiH<sub>3</sub>CN and HX.

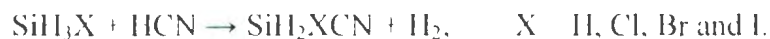
The reactant complex of SiH<sub>3</sub>X and HCN is a weak complex of the form SiH<sub>3</sub>X---HCN except for X = H, which has the form H<sub>4</sub>Si---NCH. The transition state (TS1<sup>A</sup>) involves two bond ruptures (Si-X and H-C) and two bond formations (Si-C and H-X). In the reactant complex R<sup>A</sup>, the Si-X bond distances for X = H, Cl, Br, and I at MP2/6-31G(d) level of theory are 1.482, 2.070, 2.242, and 2.486 Å, respectively, while in TS1<sup>A</sup>, they increase to 1.687, 2.449, 2.726, and 3.179 Å respectively. Similarly, the C-H bond distance of 1.070 Å in R<sup>A</sup> for X = H, Cl, Br, and I increase to 1.613, 1.455, 1.304, and 1.191 Å, respectively, in TS1<sup>A</sup>. The intrinsic reaction coordinate (IRC) analysis confirmed that TS1<sup>A</sup> leads to the SiH<sub>3</sub>X/HCN and SiH<sub>3</sub>CN/HX complexes. The activation energies for the HX elimination reaction along with the isomerization of SiH<sub>3</sub>CN/HX to SiH<sub>3</sub>NC/HX are listed in Table 2.1. The activation energies ( $\Delta E_{a, \text{TS1}^A}$ ) and free energies of activation ( $\Delta G_{\text{TS1}^A}^\ddagger$ ) are relatively high. Activation energy ( $\Delta E_{a, \text{TS1}^A}$ ) for the reaction of SiH<sub>3</sub>X and HCN decrease in the order X = H > Cl > Br > I with G3MP2 (B3LYP/6-31G(d,p) for X = I) activation energies of 280.7,

265.5, 261.1, and 256.0 kJ mol<sup>-1</sup>, respectively.

The SiH<sub>3</sub>CN/HX product can isomerize to form SiH<sub>3</sub>NC/HX. The transition state structure (TS2<sup>Δ</sup>) is a three-membered ring, consisting of C, N and SiH<sub>3</sub>. The vibrational analysis shows the Si-N bond shortening and Si-C bond lengthening and vice versa. The activation energy (ΔE<sub>a,TS2<sup>Δ</sup></sub>) for the isomerization reaction is low compared to the elimination reaction and can proceed to form the SiH<sub>3</sub>NC/HX complex. The barriers (ΔE<sub>a,TS2<sup>Δ</sup></sub>) for isomerization of SiH<sub>3</sub>CN/HX to SiH<sub>3</sub>NC/HX are 115.1, 121.2, and 119.7 kJ mol<sup>-1</sup> at G3MP2 level for X = H, Cl and Br and 129.1 kJ mol<sup>-1</sup> at B3LYP/6-31G(d,p) for X = I. The G3MP2 and G3B3 barriers differ by only 4.0 and 4.7 kJ mol<sup>-1</sup> for X = H and Cl, respectively. The G3MP2 values are also found to be close to those obtained at B3LYP/6-31G(d,p) and differ by no more than 9.6 kJ mol<sup>-1</sup> for HX elimination (X = H) and 10.6 kJ mol<sup>-1</sup> for isomerization (X = Cl).

### 2.3.1.2 Reaction of SiH<sub>3</sub>X and HCN (H<sub>2</sub> elimination):

There are four possible pathways for the H<sub>2</sub> elimination reaction:



The four pathways are designated as pathway B1 (one-step) and pathways B2, B3 and B4 (multiple-steps). Pathways B2, B3, and B4, all lead to intermediate I1<sup>B\*</sup>, which proceeds to product via pathway B\*. Reactants, intermediates, transition states, and products involved in the H<sub>2</sub> elimination reaction of SiH<sub>3</sub>Cl with HCN are shown in Figures 2.3 and 2.4. Similar

structures are also observed for the reaction of HCN with SiH<sub>4</sub>, SiH<sub>3</sub>Br and SiH<sub>3</sub>I and hence are not shown. The relative energies of reactants, intermediates, transition states, and products for pathways B1 and B\* are shown in Figure 2.5. Similarly, the relative energies in pathways B2, B3 and B4 are shown in Figures 2.6, 2.7, and 2.8, respectively. Activation energies and free energies of activation for pathways B1, B\*, and B2 are given in Table 2.2 and pathways B3 and B4 are given in Table 2.3.

Pathway B1 is a one-step mechanism in which a complex of SiH<sub>2</sub>XCN and H<sub>2</sub> is formed via transition state TS1<sup>B1</sup>, where the HCN carbon is attacking the Si and the hydrogen of HCN is simultaneously combining with a hydrogen of SiH<sub>3</sub>X to form H<sub>2</sub>. In TS1<sup>B1</sup>, the Si-C bond distance decreases in the order X = H > Cl > Br > I, with the Si-C bond distances of 2.329, 2.223, 2.217, and 2.213 Å, respectively, at MP2/6-31G(d) level of theory. The ∠H-Si-H bond angle remain relatively constant for X = H, Cl, Br, and I with values of 30.0, 31.3, 31.4 and 31.5°, respectively, at MP2/6-31G(d) level of theory. The activation energies ( $\Delta E_{a,TS1}^{B1}$ ) at G3MP2 for X = H, Cl, and Br are 280.7, 252.8 and 256.1 kJ mol<sup>-1</sup>, respectively. For the reaction of HCN and SiH<sub>3</sub>I, the activation energies at MP2/6-31G(d,p) and B3LYP/6-31G(d,p) are 296.8 and 272.0 kJ mol<sup>-1</sup>, respectively. Activation energies obtained at G3MP2 and G3B3 levels are within 1.1 kJ mol<sup>-1</sup> for the reactions of HCN with SiH<sub>4</sub> and SiH<sub>3</sub>Cl. Also, for X = H, Cl, and Br, the activation energies obtained at B3LYP/6-31G(d,p) differ from the G3 values by no more than 10.9 kJ mol<sup>-1</sup> (X = Cl, G3B3).

In pathway B2, intermediate  $I1^{B^*}$  is formed via  $TS1^{B2}$  in a single-step, which involves a proton transfer from  $SiH_3X$ . The activation energies ( $\Delta E_{a,TS1^{B2}}$ ) at G3MP2 are 265.4, 236.6, and 239.0  $\text{kJ mol}^{-1}$  for  $X = H, Cl$  and  $Br$ , respectively. For  $X = I$ , the activation energy is 245.8  $\text{kJ mol}^{-1}$  at B3LYP/6-31G(d,p). Pathway B3 is a three-step process, where intermediate  $I1^{B3}$  is formed via  $TS1^{B3}$ , which also involves a proton transfer from  $SiH_3X$ . The activation energies ( $\Delta E_{a,TS1^{B3}}$ ) are 268.6 and 271.0  $\text{kJ mol}^{-1}$  at G3MP2 and 274.6  $\text{kJ mol}^{-1}$  at B3LYP/6-31G(d,p) for  $X = Cl, Br$  and  $I$ , respectively. Then intermediate  $I2^{B3}$ , a conformational isomer of  $I1^{B3}$ , is formed via  $TS2^{B3}$ , with activation energies of only 6.0 and 6.4  $\text{kJ mol}^{-1}$  at G3MP2 and 11.0  $\text{kJ mol}^{-1}$  at B3LYP/6-31G(d,p) for  $X = Cl, Br$ , and  $I$ , respectively. Finally, intermediate  $I1^{B^*}$  is formed via  $TS3^{B3}$ , which involves rotation about the C-N bond. The activation energies ( $\Delta E_{a,TS3^{B3}}$ ) are 176.5 and 176.0  $\text{kJ mol}^{-1}$  at G3MP2 and 190.5  $\text{kJ mol}^{-1}$  at B3LYP/6-31G(d,p) for  $X = Cl, Br$ , and  $I$ , respectively. Pathway B4 is a two-step process leading to intermediate  $I1^{B^*}$ . First, intermediate  $I1^{B4}$  is formed via  $TS1^{B4}$ , where a hydride shift occurs from  $SiH_3X$ , with activation energies of 260.7 and 261.4  $\text{kJ mol}^{-1}$  at G3MP2 and 268.2  $\text{kJ mol}^{-1}$  at B3LYP/6-31G(d,p) for  $X = Cl, Br$ , and  $I$ , respectively. Finally, the intermediate  $I1^{B^*}$  is formed via  $TS2^{B4}$ , which involves rotation about the Si-N bond, with very low activation energy (Table 2.3). Note that pathways B3 and B4 do not exist for  $X = H$ .

In pathway  $B^*$  (Figures 2.3 and 2.5), a common pathway for B2, B3 and B4, intermediate  $I1^{B^*}$  eliminates  $H_2$ , (one H from the C atom and one from the N atom) via  $TS1^{B^*}$  to form a  $SiH_2XNC/H_2$  complex. In the intermediate  $I1^{B^*}$ , the H-H bond distance for  $X = H, Cl, Br$  and

I are 2.253, 2.240, 2.235, and 2.550 Å, respectively, at MP2/6-31G(d) level of theory, while in TS1<sup>B\*</sup>, they decrease to 1.022, 1.035, 1.037, and 1.039 Å. The activation energies ( $\Delta E_{a,TS1}^{B*}$ ) are 262.3, 258.7, and 256.4 kJ mol<sup>-1</sup> at G3MP2 for X = H, Cl and Br and the barrier ( $\Delta E_{a,TS1}^{B*}$ ) for X = I is 297.4 kJ mol<sup>-1</sup> at the B3LYP/6-31G(d,p) level. Finally, pathway B\* is connected to pathway B1 by the isomerization of SiH<sub>2</sub>XNC/H<sub>2</sub> via TS2<sup>B\*</sup> with activation energies of 97.3, 107.2 and 106.2 kJ mol<sup>-1</sup> at G3MP2 and 107.4 kJ mol<sup>-1</sup> at B3LYP/6-31G(d,p) for X = H, Cl, Br, and I, respectively. Therefore, of the four pathways, B1, B2, B3, and B4, pathway B1 is the most energetically favorable. However, formation of a new intermediate H<sub>2</sub>XSi-NHCH (I1<sup>B\*</sup>) is possible via pathways B2, B3, and B4.

### 2.3.1.3 Decomposition of SiH<sub>3</sub>X and reaction with HCN:

At elevated temperatures, SiH<sub>4</sub>, SiH<sub>3</sub>Cl, SiH<sub>3</sub>Br and SiH<sub>3</sub>I can dissociate to form various products:



It is well-known<sup>23, 24</sup> that SiH<sub>4</sub> → SiH<sub>2</sub> + H<sub>2</sub> is favored over SiH<sub>4</sub> → SiH<sub>3</sub> + H and SiH<sub>3</sub>Cl → SiHCl + H<sub>2</sub> is favored over SiH<sub>3</sub>Cl → SiH<sub>2</sub> + HCl. The pathway for the decomposition of SiH<sub>4</sub> and SiH<sub>3</sub>Cl are shown in Figure 2.9. Structures similar to the SiH<sub>3</sub>Cl decomposition are also observed for the decomposition of SiH<sub>3</sub>Br and SiH<sub>3</sub>I. The activation energies, activation enthalpies and free energies of activation for the decomposition of SiH<sub>4</sub>, SiH<sub>3</sub>Cl, SiH<sub>3</sub>Br and SiH<sub>3</sub>I are given in Table 2.4. The activation energies for SiH<sub>3</sub>X → SiHX + H<sub>2</sub> at G3MP2 are 233.1, 257.6, and 252.3 kJ mol<sup>-1</sup> for X = H, Cl and Br, respectively, and 267.3 kJ mol<sup>-1</sup> for X

= I at B3LYP/6-31G(d). The products of the dissociation, SiHX + H<sub>2</sub>, can react further to form SiH<sub>2</sub> + HX, by a one-step process. The barriers for SiHX + H<sub>2</sub> → SiH<sub>2</sub> + HX are lower than the barriers for dissociation of SiH<sub>3</sub>X (X = Cl, Br and I). For X = Cl and Br, the barriers are 128.7 and 118.5 kJ mol<sup>-1</sup> at the G3MP2 level and 108.7 kJ mol<sup>-1</sup> for X = I at B3LYP/6-31G(d).

The dissociation products (SiH<sub>2</sub> and SiHX) can react with HCN by a one-step mechanism leading to SiH<sub>3</sub>CN and SiH<sub>2</sub>XCN, respectively,



The transition state (TS3) involves one bond rupture (C-H) and two bond formations (Si-H and Si-C). The C-H bond distance of HCN in SiHX/HCN for X = H, Cl, Br, and I have a relatively constant value of 1.073 Å at MP2/6-31G(d) level of theory, which increase to 1.416, 1.478, 1.473, and 1.463 Å, respectively, in TS3. The Si-C bond distance in TS3 is almost constant (1.856 Å) for X = Cl, Br, and I, while for X = H, the Si-C bond distance is 1.868 Å at MP2/6-31G(d) level of theory. The activation energies, activation enthalpies and free energies of activation for the reaction of SiH<sub>2</sub> and SiHX (X = Cl, Br, I) with HCN are given in Table 2.5. The activation energies are found to be significantly lower, 152.7 kJ mol<sup>-1</sup> ( $\Delta E_{a,TS1}^A$  (X = I), B3LYP/6-31G(d)) to 255.9 kJ mol<sup>-1</sup> ( $\Delta E_{a,TS1}^A$  (X = H), G3MP2), than the activation energies of direct reactions between SiH<sub>3</sub>X and HCN,  $\Delta E_{a,TS1}^A$  and  $\Delta E_{a,TS1}^{BI}$  (Table 2.1 and 2.2). The G3MP2 and G3B3 values differ by no more than 4.5 kJ mol<sup>-1</sup> (X = H) and the B3LYP/6-31G(d) values agree well with the G3 values, differing by no more than

17.3 kJ mol<sup>-1</sup> (X = Cl, G3MP2). The barriers for the reaction SiHX + HCN → SiH<sub>2</sub>XCN generally increase in the order X = H < Br < Cl < I, with values of 24.8, 90.5, and 92.4 kJ mol<sup>-1</sup> at G3MP2, for X = H, Br and Cl, respectively, and 107.0 kJ mol<sup>-1</sup> at B3LYP/6-31G(d) for X = I. Thus the formation of SiH<sub>3</sub>CN is favored over the formation of SiH<sub>2</sub>XCN.

#### 2.3.1.4 Summary of overall reaction mechanisms investigated:

The favoured mechanism of the reaction of SiH<sub>3</sub>X with HCN depends upon the substituent, X. For X = H, decomposition has the lowest barrier, 233 kJ mol<sup>-1</sup> at the G3MP2 level, producing SiH<sub>2</sub> + H<sub>2</sub>. Therefore, SiH<sub>3</sub>CN could be formed from the reaction of SiH<sub>2</sub> and HCN, which has an activation energy of only 25 kJ mol<sup>-1</sup> at the G3MP2 level. For X = Cl, the H<sub>2</sub> elimination reaction is slightly favoured over the decomposition reaction by 5 kJ mol<sup>-1</sup> at the G3MP2 level (Tables 2.2 and 2.4) and the decomposition reaction is slightly favoured over the HCl elimination reaction by 8 kJ mol<sup>-1</sup> at the G3MP2 level (Tables 2.1 and 2.4). For X = Br, the decomposition reaction is favoured over H<sub>2</sub> elimination and HBr elimination by 4 and 9 kJ mol<sup>-1</sup>, respectively, at the G3MP2 level (Table 2.1, 2.2 and 2.4). The most likely mechanism of reaction for X = I, is HX elimination, with activation energy of 260 kJ mol<sup>-1</sup> at the B3LYP/6-31G(d) level of theory, producing SiH<sub>3</sub>CN and HI. The SiH<sub>3</sub>I decomposition reaction could also form SiH<sub>3</sub>CN, since the decomposition barrier is 267 kJ mol<sup>-1</sup> at the B3LYP/6-31G(d) level of theory. Within the error limit for B3LYP/6-31G(d) level of theory, the formation of SiH<sub>2</sub>ICN by the H<sub>2</sub> elimination reaction cannot be eliminated, since the activation energy is 287 kJ mol<sup>-1</sup> at B3LYP/6-31G(d).

## 2.3.2 Thermodynamic results for the reaction of SiH<sub>3</sub>X with HCN

### 2.3.2.1 Thermodynamics of HX elimination:

The thermodynamic properties of the reaction  $\text{SiH}_3\text{X} + \text{HCN} \rightarrow \text{SiH}_3\text{CN} + \text{HX}$  (X = H, Cl, Br, I) are listed in Table 2.6. For X = H, the reaction is found to be exothermic for all levels of theory and basis set (with enthalpies of -32.9 and -30.5 kJ mol<sup>-1</sup> at G3MP2 and G3B3, respectively). The MP2/6-31G(d,p) enthalpy is in better agreement with the G3 theories than the HF and B3LYP enthalpies. The free energies of reaction at G3MP2 and G3B3 are -26.2 and -23.7 kJ mol<sup>-1</sup>, respectively. For X = Cl, Br, and I, the reactions are found to be endothermic for all levels of theory and basis set. For X = Cl and Br, the B3LYP/6-31G(d,p) enthalpies are in better agreement with the G3 theories than the HF and MP2 enthalpies. For X = Cl and Br, the enthalpies of reaction are 46.3 and 43.6 kJ mol<sup>-1</sup> at G3MP2 and 33.9 kJ mol<sup>-1</sup> at B3LYP/6-31G(d,p) for X = I. All the levels of theory predict the reaction to be endergonic. The free energies of reaction for X = Cl and Br, are 46.5 and 43.8 kJ mol<sup>-1</sup> at G3MP2 and 34.6 kJ mol<sup>-1</sup> at B3LYP/6-31G(d,p) for X = I. For X = Br, the thermodynamic values obtained using Binning-Curtiss bromine basis set were found to be quite different compared to G3MP2 and all the other levels. However, the values obtained using recently developed 6-31G(d) bromine basis set<sup>38</sup> were found to agree very well with G3MP2 results. The relative energies of the SiH<sub>2</sub>XCN and SiH<sub>2</sub>XNC isomers are given in Table 2.7. All levels of theory (except HF) predict the SiH<sub>2</sub>XCN isomer to be more stable,

with G3MP2 enthalpies of isomerization of 17.3, 9.8, 11.6 kJ mol<sup>-1</sup>, for X = H, Cl, and Br, respectively and 20.4 kJ mol<sup>-1</sup> for X = I at B3LYP/6-31G(d,p). The B3LYP/6-31G(d,p) enthalpies are consistently in better agreement with the G3 theories than the HF and MP2 enthalpies.

### 2.3.2.2 Thermodynamics of H<sub>2</sub> elimination:

The thermodynamic properties of the reaction  $\text{SiH}_3\text{X} + \text{HCN} \rightarrow \text{SiH}_2\text{XCN} + \text{H}_2$  are listed in Table 2.8. The enthalpies of reaction for X = Cl and Br are -30.5 and -29.8 kJ mol<sup>-1</sup> at G3MP2 and -27.2 and -17.6 kJ mol<sup>-1</sup> at MP2/6-31G(d,p) and B3LYP/6-31G(d,p) for X = I. With the exception of HF/6-31G(d), all levels of theory predict the reactions to be exergonic. For X = Cl and Br, the free energies of reaction are -26.3 and -25.5 kJ mol<sup>-1</sup> at G3MP2 level. For X = I, the free energy of reaction is -22.8 kJ mol<sup>-1</sup> at MP2/6-31G(d,p) and -13.1 kJ mol<sup>-1</sup> at B3LYP/6-31G(d,p). For both enthalpies and free energies of reaction, it is found that MP2/6-31G(d,p) values agree the best with G3 values.

### 2.3.2.3 Thermodynamics for the thermal decomposition of SiH<sub>3</sub>X and SiHX + HCN:

The thermodynamic properties for the decomposition of SiH<sub>3</sub>X, X = H, Cl, Br and I are given in Table 2.9. For all levels of theory and basis sets, the reactions are highly endothermic. The G3MP2 enthalpies of decomposition for X = H and Cl (228.1 and 184.3 kJ mol<sup>-1</sup>) are found to agree well with previous calculations<sup>23</sup>. For X = Br, the G3MP2 enthalpy is 205.3 kJ mol<sup>-1</sup> and 174.2 kJ mol<sup>-1</sup> for X = I at B3LYP/6-31G(d). The subsequent

reactions,  $\text{SiHX} + \text{H}_2 \rightarrow \text{SiH}_2 + \text{HX}$  are also endothermic at all levels of theory. The decomposition reactions are all endergonic, with free energies of reaction for  $\text{X} = \text{H}, \text{Cl},$  and  $\text{Br}$  of 192.0, 145.5 and 166.5  $\text{kJ mol}^{-1}$  at G3MP2 and 135.2  $\text{kJ mol}^{-1}$  for  $\text{X} = \text{I}$  at B3LYP/6-31G(d). The reaction of the dissociated products is found to be less endergonic, with free energies of reaction for  $\text{X} = \text{Cl}$  and  $\text{Br}$  of 119.3, and 95.6  $\text{kJ mol}^{-1}$  at G3MP2 and 117.2  $\text{kJ mol}^{-1}$  for  $\text{X} = \text{I}$  at B3LYP/6-31G(d).

The products from thermal decomposition can also react with HCN. The reaction  $\text{SiH}_2 + \text{HCN} \rightarrow \text{SiH}_3\text{CN}$  is found to be highly exothermic with enthalpies of reaction of -260.9 and -262.5  $\text{kJ mol}^{-1}$  at G3MP2 and G3B3 respectively (Table 2.10). All the levels of theory also predict the reaction to be exergonic (-218.2  $\text{kJ mol}^{-1}$  at G3MP2). Similar results are seen for the reactions  $\text{SiHX} + \text{HCN} \rightarrow \text{SiH}_2\text{XCN}$ . For  $\text{X} = \text{Cl}$  and  $\text{Br}$ , the free energies of reaction are -171.7, and -192.0  $\text{kJ mol}^{-1}$  at G3MP2 and -148.5  $\text{kJ mol}^{-1}$  at B3LYP/6-31G(d) for  $\text{X} = \text{I}$ . These reactions are less exergonic than the reaction of  $\text{SiH}_2$  and HCN. Hence, formation of  $\text{SiH}_3\text{CN}$  is favored over formation of  $\text{SiH}_2\text{XCN}$  from the decomposition reaction pathway of  $\text{SiH}_3\text{X}$  and HCN.

### 2.3.3 Performance of Theory/Basis set:

All the reactions studied in this work are isogyric. When the HF results are compared with other levels of theory, it is evident that electron correlation is quite important in these

reactions. For both kinetics and thermodynamics, the G3MP2 and G3B3 theories differ by no more than  $6.7 \text{ kJ mol}^{-1}$  for activation energies ( $X = \text{H}$ ,  $\Delta E_{a, \text{TS1}}^{\text{B2}}$ ) and  $5.3 \text{ kJ mol}^{-1}$  for reaction enthalpies and free energies ( $\Delta H$  of  $\text{SiH}_3\text{Cl} \rightarrow \text{SiHCl} + \text{H}_2$ ). However, for the lower levels of theory, performance depends on the reaction type. Compared to MP2, activation energies calculated using B3LYP consistently agree better with the G3 values. Barriers predicted by both B3LYP and MP2 are always larger than the G3 values, except for the isomerization step in pathway B\*,  $\Delta E_{a, \text{TS2}}^{\text{B*}}$  (Table 2.2), where the MP2 values are lower. For all reactions with  $X = \text{Br}$ , activation energies calculated using the standard 6-31G(d) bromine basis set do not differ by more than  $10.1 \text{ kJ mol}^{-1}$  (G3MP2, HX elimination reaction) compared to the Binning-Curtiss basis set results.

Thermodynamic values calculated using B3LYP and MP2 levels of theory are more comparable. For the majority of cases, B3LYP provides reaction enthalpies and free energies that are in better agreement with G3 values. However, MP2 gives better results for the  $\text{H}_2$  elimination reactions (and HX elimination reaction,  $X = \text{H}$ ) (Tables 2.6 and 2.8). The enthalpies and free energies of reaction calculated using MP2 are also in better agreement with G3 values for the decomposition of  $\text{SiH}_3\text{Br}$  (Table 2.9) and the reaction  $\text{SiHBr} + \text{HCN} \rightarrow \text{SiH}_2\text{BrCN}$  (Table 2.10). Thermodynamic values determined using HF theory do not agree with G3 theories as well as MP2 and B3LYP. HF performs very poorly on the isomerization (Table 2.7) and  $\text{H}_2$  elimination reactions (Table 2.8). However, HF does perform well on the reactions of the  $\text{SiHX} + \text{HCN} \rightarrow \text{SiH}_2\text{XCN}$  (Table 2.10). Unlike kinetics, the

thermodynamics for some of the reactions change significantly with the change of bromine basis set. For HBr elimination, the enthalpies and free energies of reaction differ by 17-24 kJ mol<sup>-1</sup> at HF, MP2 and B3LYP level of theory with a change of bromine basis set. Similarly for SiHBr + H<sub>2</sub> → SiH<sub>2</sub> + HBr, the enthalpies and free energies of reaction differ by 18-20 kJ mol<sup>-1</sup> at HF, MP2 and B3LYP level of theory. In all cases, the results with the standard 6-31G(d) bromine basis set are closer to the G3MP2 results.

Most barriers were lowered by the addition of p-polarization functions to hydrogen, due to the involvement of hydrogen atoms in the transition states, but this had little effect on thermodynamic values. There was little to no effect on the barriers in which hydrogen atoms were not directly involved in the transition states, such as  $\Delta E_{a,1S2}^A$  (Table 2.1) and  $\Delta E_{a,1S2}^{B*}$  (Table 2.2).

### 2.3.4 Exploring Heats of Formation ( $\Delta H_f$ ):

No experimental or theoretical heats of formation ( $\Delta H_f$ ) have been reported for SiH<sub>3</sub>CN and SiH<sub>3</sub>NC. Part of this is due to the difficulty of carrying out such an experiment. In this study, the enthalpies of reaction for reactions between SiH<sub>3</sub>X and HCN have been obtained. From this data, it is possible to calculate heats of formation for SiH<sub>3</sub>CN, SiH<sub>3</sub>NC, SiH<sub>2</sub>ClCN, SiH<sub>2</sub>BrCN, SiH<sub>2</sub>ICN, SiH<sub>2</sub>, SiHCl, SiHBr, and SiH at a high level of theory. The  $\Delta H_f$  values obtained in this study are given in Table 2.11. From the G3MP2 enthalpy of reaction of SiH<sub>4</sub>

+ HCN  $\rightarrow$  SiH<sub>3</sub>CN + H<sub>2</sub> and the most recent and reliable experimental heats of formation for SiH<sub>4</sub> and HCN (given in Table 2.11),  $\Delta H_f$  for SiH<sub>3</sub>CN is calculated to be 133.5 kJ mol<sup>-1</sup>. The  $\Delta H_f$  for SiH<sub>3</sub>CN can also be calculated using the G3MP2 enthalpy of reaction of SiH<sub>3</sub>Cl + HCN  $\rightarrow$  SiH<sub>3</sub>CN + HCl and most recent experimental heats of formation for SiH<sub>3</sub>Cl, HCN, and HCl (given in Table 2.11). The resulting  $\Delta H_f$  is 134.5 kJ mol<sup>-1</sup>, both values being in excellent agreement. However, since the experimental heat of formation for SiH<sub>4</sub> is more reliable, the heat of formation of SiH<sub>3</sub>CN calculated using the first reaction is most likely more reliable. Similarly,  $\Delta H_f$  for SiH<sub>3</sub>NC (150.8 kJ mol<sup>-1</sup>) is obtained by using the G3MP2 enthalpy of isomerization for SiH<sub>3</sub>CN to SiH<sub>3</sub>NC (Table 2.7) and the calculated  $\Delta H_f$  for SiH<sub>3</sub>CN (133.5 kJ mol<sup>-1</sup>). Heats of formation of SiH<sub>2</sub>ClCN, SiH<sub>2</sub>BrCN, and SiH<sub>2</sub>ICN are calculated using the enthalpies of reaction for SiH<sub>3</sub>Cl + HCN  $\rightarrow$  SiH<sub>2</sub>ClCN + H<sub>2</sub> (-30.5 kJ mol<sup>-1</sup> at G3MP2), SiH<sub>3</sub>Br + HCN  $\rightarrow$  SiH<sub>2</sub>BrCN + H<sub>2</sub> (-29.8 kJ mol<sup>-1</sup> at G3MP2) and SiH<sub>3</sub>I + HCN  $\rightarrow$  SiH<sub>2</sub>ICN + H<sub>2</sub> (-17.6 kJ mol<sup>-1</sup> at B3LYP/6-31G(d,p)), along with experimental heats of formation for SiH<sub>3</sub>Cl, SiH<sub>3</sub>Br, SiH<sub>3</sub>I, and HCN (given in Table 2.11). The  $\Delta H_f$  for SiHX (X = Cl, Br, I) can be calculated using G3MP2 enthalpies of reaction from both the SiH<sub>3</sub>X  $\rightarrow$  SiHX + H<sub>2</sub> reaction and the SiHX + H<sub>2</sub>  $\rightarrow$  SiH<sub>2</sub> + HX reaction (Table 2.9), along with experimental  $\Delta H_f$  for SiH<sub>3</sub>Cl, SiH<sub>3</sub>Br, SiH<sub>3</sub>I, SiH<sub>2</sub>, HCl, HBr, and HI obtained from the literature (Table 2.11). Schlegel et al.<sup>41</sup> obtained a  $\Delta H_f$  for SiHCl of 62.8 kJ mol<sup>-1</sup> compared to 48.7 (54.0) and 58.7 (63.2) kJ mol<sup>-1</sup> obtained from the G3MP2 (G3B3) enthalpies of reaction for SiH<sub>3</sub>Cl  $\rightarrow$  SiHCl + H<sub>2</sub> and SiHCl + H<sub>2</sub>  $\rightarrow$  SiH<sub>2</sub> + HCl, respectively. The  $\Delta H_f$  of

48.7 kJ mol<sup>-1</sup> is recommended for SiHCl, since only  $\Delta H_f(\text{SiH}_3\text{Cl})$  and  $\Delta H_{\text{rxn}}$  are required. The  $\Delta H_f(\text{SiHBr})$  values obtained by using  $\text{SiH}_3\text{Br} \rightarrow \text{SiHBr} + \text{H}_2$  and  $\text{SiHBr} + \text{H}_2 \rightarrow \text{SiH}_2 + \text{HBr}$  are found to be 127.1 and 138.4 kJ mol<sup>-1</sup>, respectively; while  $\Delta H_f(\text{SiHI})$  is found to be 179.8 and 178.9 kJ mol<sup>-1</sup>, using  $\text{SiH}_3\text{I} \rightarrow \text{SiHI} + \text{H}_2$  and  $\text{SiHI} + \text{H}_2 \rightarrow \text{SiH}_2 + \text{HI}$ , respectively. Heats of formation calculated using  $\text{SiH}_3\text{X} \rightarrow \text{SiHX} + \text{H}_2$  are considered more reliable because only one experimental  $\Delta H_f$  is required. Heats of formation were also calculated, where possible, for SiH<sub>4</sub>, SiH<sub>3</sub>Cl, HCl, SiH<sub>3</sub>Br, HBr, and SiH<sub>2</sub>, for which experimental  $\Delta H_f$  values are available for comparison. All the  $\Delta H_f$  values are in excellent agreement with the experimental values except for the  $\Delta H_f$  value for SiH<sub>2</sub>, where the calculated  $\Delta H_f(\text{SiH}_2)$  is found to be 262.8 kJ mol<sup>-1</sup> compared to the experimental values of  $273.8 \pm 4.2$  kJ mol<sup>-1</sup>.

## 2. 4 Conclusions

Three possible mechanisms of reaction between SiH<sub>3</sub>X and HCN have been investigated: HX elimination, H<sub>2</sub> elimination, and reaction of HCN with SiH<sub>3</sub>X dissociation products. Reaction via H<sub>2</sub> elimination can involve several different pathways, and HCN can also react with the decomposition products of SiH<sub>3</sub>X. The activation energies for the rate-determining step of each mechanism suggest that for X = H, the decomposition mechanism ( $\text{SiH}_4 \rightarrow \text{SiH}_2 + \text{H}_2$ ) is preferred and in this case SiH<sub>3</sub>CN can be formed by reaction of SiH<sub>2</sub> with HCN. For X = Cl, H<sub>2</sub> elimination ( $\text{SiH}_3\text{Cl} + \text{HCN} \rightarrow \text{SiH}_2\text{ClCN} + \text{H}_2$ ) is slightly favoured where as for X = Br, the decomposition reaction ( $\text{SiH}_3\text{Br} \rightarrow \text{SiHBr} + \text{H}_2 \rightarrow \text{SiH}_2$

+HBr) is favoured. For  $X = I$ , mainly the  $\text{SiH}_3\text{CN}$  product could be formed via an HX elimination reaction ( $\text{SiH}_3\text{I} + \text{HCN} \rightarrow \text{SiH}_3\text{CN} + \text{HI}$ ) and a decomposition reaction ( $\text{SiH}_3\text{I} \rightarrow \text{SiHI} + \text{H}_2 \rightarrow \text{SiH}_2 + \text{HI}$ ). When considering thermodynamics, it is noticed that the HX elimination reaction is endothermic and endergonic, except for  $X = \text{H}$ , while the  $\text{H}_2$  elimination reaction is exothermic and exergonic for all X.

For both kinetics and thermodynamics, the G3 theories are generally in good agreement ( $X = \text{H}$  and  $\text{Cl}$ ). Values calculated using MP2 or B3LYP levels of theory are generally in better agreement with G3 theories than HF values. For the reactions studied here, B3LYP/6-31G(d,p) gives barriers similar to G3 values and MP2/6-31G(d,p) gives the best results for thermodynamics with the exception of the dissociation reactions. The kinetic and thermodynamic values obtained by using the standard 6-31G(d) bromine basis set are in much better agreement with the G3MP2 values compared to those obtained using Binning-Curtiss bromine basis set. Therefore, we recommend that the standard 6-31G(d) bromine basis set be used for calculations involving bromine.

It has also been shown that the reaction enthalpies, along with existing experimental data can be used to calculate heats of formation, which are otherwise unknown. Since high level calculations, such as G3MP2 and G3B3, are used to calculate reaction enthalpies, relatively good estimates of heats of formation are obtained.

## 2.5 References

- (1) Gershevitz, O.; Sukenik, C. N.; Ghabboun, J.; Cahen, D. *J. Am. Chem. Soc.* **2003**, *125*, 4730.
- (2) Koinuma, H.; Manako, T.; Natsuaki, H.; Fujioka, H.; Fueki, K. *J. Non-Cryst. Solid* **1985**, *77*, 801.
- (3) Matsuda, A.; Yagii, K.; Kaga, T.; Tanaka, K. *Jpn. J. Appl. Phys.* **1984**, *23*, 576.
- (4) Sato, K.; Hirano, T.; Natsuaki, H.; Fueki, K.; Koinuma H. *Appl. Phys. Lett.* **1984**, *45*, 1324.
- (5) Hu, S.; Wang, Y.; Wang, X.; Chu, T.; Liu, X.; *J. Phys. Chem. A* **2003**, *107*, 9189.
- (6) Hu, S.; Wang, Y.; Wang, X.; Chu, T.; Liu, X.; *J. Phys. Chem. A* **2004**, *108*, 1448.
- (7) McCarthy, M. C.; Gottlieb, C. A.; Thaddeus, P. *Mol. Phys.* **2003**, *101*, 697.
- (8) Stannowski, B.; Rath, J. K.; Schropp, R. E. *J. Appl. Phys.* **2003**, *93*, 2618.
- (9) Patil, S. B.; Kumbha, A.; Waghmare, P.; Rao, V. R.; Dusane, R. O. *Thin Solid Films*, **2001**, *395*, 270.
- (10) Boehme, C. ; Lucovsky, G. *J. Vac. Sci. Technol. A* **2001**, *19*, 2622.
- (11) Gleskova, H. ; Wagner, S. ; Gasparik, V. ; Kovac, P. *Appl. Surf. Sci.* **2001**, *175*, 12.
- (12) Santana, G. ; Morales-Acevedo, A. *Sol. Energ. Mat. Sol. C* **2000**, *60*, 135.
- (13) Ghosh, S. ; Dutta, P. K.; Bose D. N., *Mater. Sci. Semicond. Proc.* **1999**, *2*, 1.
- (14) Sahu, S.; Kavecky, S.; Szepvolgyi, J., *J. Eur. Ceram. Soc.* **1995**, *15*, 1071.
- (15) Du, Z. D.; Chen, J. H.; Bei, X. L.; Zhou, C. G., *Organosilicon Chemistry*; Advanced

Education Press: Beijing, 1990, p 80.

(16) Du, Z.D.; Chen, J. H.; Bei, X. L.; Zhou, C. G. *Organosilicon Chemistry*; Advanced Education Press: Beijing, 1990, p 101.

(17) Burg, A. B. *J. Am. Chem. Soc.* **1954**, *76*, 2654.

(18) Campbell-Ferguson, H. J.; Ebsworth, E. A. V. *Chem. Ind.* **1965**, 301.

(19) Aylett, B. J.; Sinclair, R.A. *Chem. Ind.* **1965**, 301.

(20) Aylett, B. J.; Emeleus, H. J.; Maddock, A. G. *J. Inorg. Nucl. Chem.* **1955**, *1*, 187.

(21) Campbell-Ferguson, H. J.; Ebsworth, E. A. V. *J. Chem. Soc. (A)* **1966**, 1508.

(22) Feng, S.; Feng, D.; Li, M.; Zhao, Y.; Wang, P. G. *J. Mol. Struct.* **2002**, *618*, 51.

(23) Su, M. ; Schlegel, H. B. *J. Phys. Chem.* **1993**, *97*, 9981.

(24) Gordon, M. S.; Schlegel, H. B.; Francisco, J. S. Reaction Energetics in Silicon Chemistry. *Adv. in Silicon Chemistry*", **1993**, *2*, 137.

(25) Pacheco-Sanchez, J. H. P. ; Luna-Garcia, H. ; Castillo, S. ; *J. Chem. Phys.* **2004**, *121*, 5777.

(26) Guelin, M. ; Muller, S. ; Cernicharo, J. ; Apponi, A. J. ; McCarthy, M. C. ; Gottlieb, C. A. ; Thaddeus, P. *Astron. Astrophys.* **2000**, *363*, L9.

(27) Sanz, E. M.; McCarthy, M. C.; Thaddeus, P. *Astrophys. J.* **2002**, *577*, 71.

(28) Apponi, A. J.; McCarthy, M. C.; Gottlieb, C. A.; Thaddeus, P. *Astrophys. J.* **2000**, *536*, L55.

(29) Maier, G.; Reisenauer, H. P.; Egenolf, H.; Glatthaar, J. *Eur. J. Org. Chem.*, **1998**, 1307.

(30) Wang, Q.; Ding, Y.; Sun, C. *J. Phys. Chem. A* **2004**, *108*, 10602.

- (31) Curtiss, L. A.; Redfern, P.C.; Raghavachari, K.; Rassolov, V.; Pople, J. A. *J. Chem. Phys.* **1999**, *110*, 4703.
- (32) Baboul, A. G.; Curtiss, L. A.; Redfern, P. C.; Raghavachari, K. *J. Chem. Phys.* **1999**, *110*, 7650.
- (33) GAUSSIAN03, Revision A. 9. Gaussian Inc.; Pittsburgh, PA, 2003.
- (34) Poirier, R. A. MUNgauss (Fortran 90 version), Chemistry Department, Memorial University of Newfoundland, St. John's, NL, A1B 3X7. With contributions from Bungay, S. D.; El-Sherbiny, A.; Gosse, T.; Hollett, J.; Keefe, D.; Kelly, A.; Pye, C.C.; Reid, D.; Shaw, M.; Wang, Y; and Xidos, J.
- (35) Almatarneh, M. H.; Flinn, C. G.; Poirier, R. A. *Can. J. Chem.* **2005**, *83*, 2082.
- (36) Curtiss, L. A.; Redfern, P. C.; Rassolov, V.; Kedziora, G. S.; Pople, J. A. *J. Chem. Phys.* **2001**, *114*, 9287.
- (37) <http://chemistry.anl.gov/compmat/compherni.html>
- (38) Rassolov, V. A.; Ratner, M. A.; Pople, J. A.; Redfern, P. C.; Curtiss, L. A. *J. Comput. Chem.* **2001**, *22*, 976.
- (39) Binning, R. C., Jr., Curtiss, L. A. *J. Comput. Chem.* **1990**, *11*, 1206.
- (40) Andzelm, J.; Klobukowski, M.; Radzio-andzelm, E.; Sakai, Y.; Tatewaki, H. In *Physical Sciences Data 16 Gaussian Basis Sets for Molecular Calculations*; Huzinaga S., Elsevier Science Publishers: Amsterdam, 1984, p 295.
- (41) Su, M. ; Schlegel, H. B. *J. Phys. Chem.* **1993**, *97*, 8732.

- (42) Gurvich, I. V.; Veyts, I. V.; Alcock, C. B. *Thermodynamic Properties of Individual Substances*; Hemisphere: New York, 1991; Vol. 2, Part I.
- (43) Chase, M. W. *NIST-JANAF Thermochemical Tables*, 4th ed., Monograph 9., *J. Phys. Chem. Ref. Data* 1998, 1-1951.
- (44) Hansel, A.; Scheiring, C.; Glantschnig, M.; Lindinger, W. *J. Chem. Phys.* **1998**, *109*, 1748.
- (45) Farber, M.; Srivastava, R. D. *J. Chem. Therm.* **1979**, *11*, 939.
- (46) *CRC Handbook of Chemistry and Physics*; CRC: Boca Raton, FL, 1977-1978; Vol. 58.
- (47) McBride, B. J.; Zehe, M. J.; Gordon, S. *NASA Glenn Coefficients for Calculating Thermodynamic Properties of Individual Species*; Glenn Research Center: Cleveland, OH, 2002.
- (48) Moffat, H. F.; Jensen, K. F.; Carr, R. W. *J. Phys. Chem.* **1991**, *95*, 145.

**TABLE 2.1: Activation energies and free energies of activation for the reaction of  $\text{SiH}_3\text{X}$  ( $\text{X} = \text{H}, \text{Cl}, \text{Br}, \text{I}$ ) with  $\text{HCN}$  (HX elimination) and the isomerization of  $\text{SiH}_3\text{CN}/\text{HX}$  (in  $\text{kJ mol}^{-1}$ ) at 298.15K (Pathway A)<sup>a</sup>.**

X	Level/Basis Set	HX Elimination		Isomerization	
		$\Delta E_{a,\text{TS1}}^{\text{A}}$	$\Delta G_{\text{TS1}}^{\ddagger\text{A}}$	$\Delta E_{a,\text{TS2}}^{\text{A}}$	$\Delta G_{\text{TS2}}^{\ddagger\text{A}}$
H	HF/6-31G(d)	374.7	387.6	127.7	122.2
	HF/6-31G(d, p)	353.3	367.1	127.8	121.9
	MP2/6-31G(d)	332.1	342.8	134.6	134.6
	MP2/6-31G(d, p)	311.5	322.3	133.9	138.4
	B3LYP/6-31G(d)	305.3	315.0	123.7	122.4
	B3LYP/6-31G(d, p)	290.3	300.9	123.8	122.9
	G3MP2	280.7	296.4	115.1	114.6
	G3B3	279.6	294.6	119.1	113.4
Cl	HF/6-31G(d)	376.0	368.5	137.5	125.8
	HF/6-31G(d, p)	360.5	348.3	137.5	121.1
	MP2/6-31G(d)	315.6	310.9	142.9	137.4
	MP2/6-31G(d, p)	295.8	291.7	141.5	136.3
	B3LYP/6-31G(d)	273.9	280.7	132.4	115.3
	B3LYP/6-31G(d, p)	264.3	266.4	131.8	115.5
	G3MP2	265.5	264.3	121.2	116.7
	G3B3	269.7	262.0	125.9	115.0
Br	HF/6-31G(d)	374.5 (373.9)	373.0 (367.8)	135.9 (131.1)	128.0 (127.8)
	HF/6-31G(d, p)	364.6 (364.0)	363.4 (347.0)	136.0 (131.1)	128.5 (128.1)
	MP2/6-31G(d)	306.7 (312.8)	310.7 (309.5)	142.0 (137.3)	137.4 (137.9)
	MP2/6-31G(d, p)	295.4 (300.3)	298.6 (290.6)	140.7 (135.7)	136.3 (136.2)
	B3LYP/6-31G(d)	265.8 (274.7)	269.5 (279.8)	131.1 (127.7)	127.9 (128.7)

	B3LYP/6-31G(d, p)	260.1 (267.0)	264.6 (264.8)	130.8 (124.0)	127.9 (121.6)
	G3MP2	261.1 (271.2)	275.9 (283.5)	119.7 (120.1)	117.1 (121.7)
I	MP2/6-31G(d)	302.8	320.4	140.4	139.2
	MP2/6-31G(d, p)	297.3	301.1	139.1	137.7
	B3LYP/6-31G(d)	259.7	289.3	129.3	121.6
	B3LYP/6-31G(d, p)	256.0	275.0	129.1	128.9

The values in parentheses are calculated by using the Binning-Curtiss bromine basis set from reference 39.

<sup>a</sup> Mechanistic pathway and barriers as defined in Figures 2.1 and 2.2, respectively.

TABLE 2.2: Activation energies and free energies of activation for the reaction of SiH<sub>3</sub>X (X = H, Cl, Br, I) with HCN (in kJ mol<sup>-1</sup>) at 298.15K (H<sub>2</sub> elimination: Pathways B1, B\* and B2).

X	Level/Basis Set	Pathway B1 <sup>a</sup>		Pathway B* <sup>a</sup>				Pathway B2 <sup>b</sup>	
		$\Delta E_{a,TS1}^{B1}$	$\Delta G_{TS1}^{\ddagger B1}$	$\Delta E_{a,TS1}^{B*}$	$\Delta G_{TS1}^{\ddagger B*}$	$\Delta E_{a,TS2}^{B*}$	$\Delta G_{TS2}^{\ddagger B*}$	$\Delta E_{a,TS1}^{B2}$	$\Delta G_{TS1}^{\ddagger B2}$
H	HF/6-31G(d)	374.7	387.6	392.1	362.5	129.7	122.6	385.2	400.7
	HF/6-31G(d, p)	353.3	367.1	364.3	337.1	129.8	122.5	299.2	321.1
	MP2/6-31G(d)	332.1	342.8	317.9	291.5	92.2	87.9	336.4	353.1
	MP2/6-31G(d, p)	311.5	322.3	293.1	268.2	92.3	87.6	334.5	350.9
	B3LYP/6-31G(d)	305.3	315.0	313.6	286.8	99.4	97.0	271.0	287.0
	B3LYP/6-31G(d, p)	290.3	300.9	293.1	268.1	99.5	94.5	270.2	286.4
	G3MP2	280.7	296.4	262.3	261.6	97.3	94.6	265.4	283.8
	G3B3	279.6	294.6	267.6	266.9	97.2	99.1	272.1	290.3
Cl	HF/6-31G(d)	363.9	368.5	392.6	364.6	142.0	134.1	358.6	366.8
	HF/6-31G(d, p)	342.3	348.3	364.7	338.9	142.0	133.7	355.6	364.7
	MP2/6-31G(d)	306.1	310.9	315.2	290.6	102.2	97.4	310.4	320.1
	MP2/6-31G(d, p)	286.4	291.7	290.2	267.0	102.5	97.2	308.6	318.7
	B3LYP/6-31G(d)	277.7	280.7	308.7	283.7	110.0	106.2	241.8	250.6
	B3LYP/6-31G(d, p)	262.7	266.4	288.3	265.1	110.1	106.1	240.0	249.0
	G3MP2	252.8	264.3	258.7	258.6	107.2	103.8	236.6	250.1
	G3B3	251.8	262.0	264.8	264.8	107.2	110.7	242.7	255.0

Br	HF/6-31G(d)	368.2 (363.5)	373.1 (367.8)	391.2 (392.6)	363.7 (364.2)	141.4 (140.4)	133.5 (132.7)	361.7 (360.6)	370.4 (368.7)
	HF/6-31G(d, p)	346.6 (341.9)	352.2 (347.0)	363.5 (364.9)	338.0 (338.6)	141.6 (140.6)	133.2 (132.4)	358.6 (357.6)	367.6 (366.0)
	MP2/6-31G(d)	309.9 (306.2)	313.8 (309.5)	312.4 (313.4)	288.6 (288.9)	101.0 (100.3)	96.6 (95.8)	311.9 (310.8)	320.9 (319.1)
	MP2/6-31G(d, p)	290.0 (286.5)	294.7 (290.6)	287.5 (288.6)	265.1 (265.6)	101.3 (100.6)	96.3 (95.2)	310.2 (309.1)	319.8 (318.1)
	B3LYP/6-31G(d)	281.4 (277.7)	283.7 (279.8)	306.0 (308.3)	282.0 (282.8)	109.0 (108.5)	105.6 (104.6)	244.2 (243.4)	252.5 (251.4)
	B3LYP/6-31G(d, p)	266.2 (262.6)	268.9 (264.8)	285.7 (288.0)	263.6 (264.3)	109.2 (108.6)	104.8 (104.2)	242.4 (241.7)	250.8 (249.4)
	G3MP2	256.1 (256.3)	267.6 (267.3)	256.4 (256.4)	256.7 (255.9)	106.2 (106.2)	102.7 (103.0)	239.0 (238.9)	252.5 (251.8)
	I	MP2/6-31G(d)	316.9	320.4	325.4	300.4	99.2	94.8	314.2
	MP2/6-31G(d, p)	296.8	301.1	299.9	276.1	99.4	94.3	312.6	322.3
	B3LYP/6-31G(d)	287.3	289.3	317.5	291.8	107.3	102.2	247.5	256.1
	B3LYP/6-31G(d, p)	272.0	275.0	297.4	273.3	107.4	101.8	245.8	254.9

The values in parentheses are calculated by using the Binning-Curtiss bromine basis set from reference 39.

<sup>a</sup> Mechanistic pathway and barriers as defined in Figure 2.3 and 2.5, respectively.

<sup>b</sup> Mechanistic pathway and barriers as defined in Figure 2.4 and 2.6, respectively.

**TABLE 2.3: Activation energies and free energies of activation for the reaction of SiH<sub>3</sub>X (X = H, Cl, Br, I) with HCN (in kJ mol<sup>-1</sup>) at 298.15K (H<sub>2</sub> elimination: Pathways B3 and B4)<sup>a</sup>**

X	Level/Basis Set	Pathway B3 <sup>b</sup>				Pathway B4 <sup>c</sup>					
		$\Delta E_{a,TS1}^{B3}$	$\Delta G_{TS1}^{\ddagger B3}$	$\Delta E_{a,TS2}^{B3}$	$\Delta G_{TS2}^{\ddagger B3}$	$\Delta E_{a,TS3}^{B3}$	$\Delta G_{TS3}^{\ddagger B3}$	$\Delta E_{a,TS1}^{B4}$	$\Delta G_{TS1}^{\ddagger B4}$	$\Delta E_{a,TS2}^{B4}$	$\Delta G_{TS2}^{\ddagger B4}$
Cl	HF/6-31G(d)	387.7	394.8	9.0	11.9	173.5	162.7	381.7	387.9	-5.6	-3.1
	B3LYP/6-31G(d)	272.2	280.7	7.9	11.3	190.2	180.3	268.6	276.7	-3.9	-1.2
	B3LYP/6-31G(d, p)	269.7	278.1	7.9	11.6	189.3	179.5	266.1	274.3	-3.8	-0.8
	G3MP2	268.6	282.0	6.0	9.7	176.5	177.1	260.7	272.2	-2.3	1.4
Br	HF/6-31G(d)	390.1	397.9	9.5	12.5	173.1	162.4	383.2	390.0	6.9	8.8
		(389.6)	(396.7)	(8.8)	(11.5)	(173.6)	(162.6)	(382.5)	(388.3)	(6.1)	(8.0)
	HF/6-31G(d, p)	386.5	394.5	9.6	12.7	172.0	161.3	377.4	383.1	-5.7	-2.9
	MP2/6-31G(d)	353.3	361.9	8.2	11.6	196.8	186.2	342.0	350.4	-5.9	-3.3
	MP2/6-31G(d, p)	350.4	359.7	8.1	11.5	196.1	185.2	338.1	347.2	-5.4	-2.6
	B3LYP/6-31G(d)	273.8	281.6	9.8	13.7	191.1	181.8	269.8	277.5	-1.7	1.7
	B3LYP/6-31G(d, p)	271.3	279.2	10.0	13.9	190.3	180.9	267.0	274.6	-1.4	2.1
	(271.2)	(278.3)	(7.8)	(11.1)	(189.1)	(179.3)	(265.9)	(272.6)	(12.2)	(13.7)	
	G3MP2	271.0	284.4	6.4	10.2	176.0	176.7	261.4	272.9	-1.5	1.0
		(270.9)	(283.7)	(5.3)	(8.7)	(175.9)	(176.3)	(262.0)	(272.7)	(2.4)	(4.9)
I	HF/6-31G(d)	394.3	402.4	9.8	12.9	172.5	162.1	385.3	392.3	7.1	9.0
	B3LYP/6-31G(d, p)	274.6	283.1	11.0	8.8	190.5	180.7	268.2	276.4	31.2	32.0

The values in parentheses are calculated by using Binning-Curtiss bromine basis set from reference 39.

<sup>a</sup> Mechanistic pathways as defined in Figure 2.4; B3LYP/6-31G(d,p) values are shown for all X, since they agree the best with G3 values.

<sup>b</sup> Barriers as defined in Figure 2.7.

<sup>c</sup> Barriers as defined in Figure 2.8.

**TABLE 2.4: Activation energies, activation enthalpies and free energies of activation for the thermal decomposition reaction of SiH<sub>3</sub>X (X = H, Cl, Br, I) (in kJ mol<sup>-1</sup>) at 298.15K (Figure 2.9).**

Level/Basis Set	$\Delta E_a$	$\Delta H^\ddagger$	$\Delta G^\ddagger$	$\Delta E_a$	$\Delta H^\ddagger$	$\Delta G^\ddagger$
	SiH <sub>4</sub> → SiH <sub>2</sub> + H <sub>2</sub>			SiH <sub>3</sub> Cl → SiHCl + H <sub>2</sub>		
HF/6-31G(d)	334.7	322.7	319.8	367.4	356.0	352.9
MP2/6-31G(d)	282.7	270.7	267.8	312.9	299.8	296.7
B3LYP/6-31G(d)	256.6	244.8	241.9	281.8	268.9	265.7
G3MP2	233.1	233.2	230.3	257.6	257.8	254.7
G3B3	235.6	235.6	232.7	260.8	261.1	257.8
	250.8 <sup>a</sup>			280.1 <sup>a</sup>		
	SiH <sub>3</sub> Br → SiHBr + H <sub>2</sub>			SiH <sub>3</sub> I → SiHI + H <sub>2</sub>		
HF/6-31G(d)	361.3 (362.2)	348.7 (349.7)	345.7 (346.6)	350.2	337.9	334.9
MP2/6-31G(d)	305.0 (304.9)	292.1 (292.0)	289.0 (288.9)	294.4	281.8	278.7
B3LYP/6-31G(d)	275.9 (275.8)	263.2 (263.3)	259.9 (260.1)	267.3	254.9	251.7
G3MP2	252.3 (252.2)	252.5 (252.3)	249.4 (252.0)			
<b>Further Reactions:</b>	SiHCl + H <sub>2</sub> → SiH <sub>2</sub> +HCl			SiHBr + H <sub>2</sub> → SiH <sub>2</sub> + HBr		
HF/6-31G(d)	194.9	192.6	218.8	177.2 (175.6)	174.2 (172.7)	200.2 (196.4)
MP2/6-31G(d)	171.8	168.8	191.1	155.9 (154.4)	151.7 (150.5)	173.3 (170.3)
B3LYP/6-31G(d)	129.1	124.9	142.7	117.1 (117.0)	112.1 (112.5)	130.2 (131.3)
G3MP2	128.7	119.6	146.9	118.5 (119.0)	109.4 (110.0)	136.5 (134.8)

G3B3	124.4	116.9	135.0
	SiH <sub>3</sub> + H <sub>2</sub> → SiH <sub>2</sub> + H <sub>2</sub>		
HF/6-31G(d)	162.2	157.6	183.3
MP2/6-31G(d)	144.2	138.5	160.1
B3LYP/6-31G(d)	108.7	102.6	121.6

The values in parentheses are calculated by using Binning-Curtiss bromine basis set from reference 39.

<sup>a</sup> The values obtained from reference 23.

**TABLE 2.5: Activation energies, enthalpies and free energies of activation for the reaction of SiHX (X = H, Cl, Br, I) with HCN (in kJ mol<sup>-1</sup>) at 298.15K (Figure 2.10).**

Level/Basis Set	$\Delta E_a$	$\Delta H^\ddagger$	$\Delta G^\ddagger$	$\Delta E_a$	$\Delta H^\ddagger$	$\Delta G^\ddagger$
	$\text{SiH}_2 + \text{HCN} \rightarrow \text{SiH}_3\text{CN}$			$\text{SiHCl} + \text{HCN} \rightarrow \text{SiH}_2\text{ClCN}$		
HF/6-31G(d)	155.5	147.0	168.3	222.2	210.8	235.9
MP2/6-31G(d)	53.3	45.0	63.4	131.8	120.9	141.9
B3LYP/6-31G(d)	34.3	26.1	45.7	109.7	98.8	121.4
G3MP2	24.8	18.0	39.8	92.4	86.0	111.6
G3B3	29.3	22.7	42.6	96.3	90.2	112.9
	$\text{SiHBr} + \text{HCN} \rightarrow \text{SiH}_2\text{BrCN}$			$\text{SiHI} + \text{HCN} \rightarrow \text{SiH}_2\text{ICN}$		
HF/6-31G(d)	221.3 (215.9)	209.8 (204.5)	235.6 (229.8)	216.0	204.4	230.6
MP2/6-31G(d)	129.4 (125.0)	118.4 (114.0)	140.0 (135.6)	122.0	111.0	132.8
B3LYP/6-31G(d)	109.9 (104.6)	98.8 (93.7)	121.3 (115.5)	107.0	95.8	118.2
G3MP2	90.5 (90.2)	84.2 (83.8)	110.5 (109.6)			

The values in parentheses are calculated by using Binning-Curtiss bromine basis set from reference 39.

**TABLE 2.6: Thermodynamic properties for the reaction of SiH<sub>3</sub>X (X = H, Cl, Br, I) with HCN (in kJ mol<sup>-1</sup>) at 298.15K (HX elimination reaction).**

Level/Basis Set	$\Delta E$	$\Delta H$	$\Delta G$	$\Delta E$	$\Delta H$	$\Delta G$
	SiH <sub>4</sub> +HCN→SiH <sub>3</sub> CN+H <sub>2</sub>			SiH <sub>3</sub> Cl+HCN→SiH <sub>3</sub> CN+HCl		
HF/6-31G(d)	-2.4	-13.2	-6.0	63.6	56.8	57.4
HF/6-31G(d, p)	-5.5	-16.0	-8.9	52.3	45.7	46.3
MP2/6-31G(d)	-28.4	-37.5	-30.8	60.1	54.6	54.8
MP2/6-31G(d, p)	-23.6	-32.7	-26.0	45.5	40.2	40.4
B3LYP/6-31G(d)	-15.5	-24.5	-17.5	55.8	49.7	50.2
B3LYP/6-31G(d, p)	-15.5	-24.4	-17.4	47.6	41.6	42.1
G3MP2	-35.8	-32.9	-26.2	44.4	46.3	46.5
G3B3	-33.3	-30.5	-23.7	43.8	45.6	45.9
					45.2 <sup>a</sup>	
	SiH <sub>3</sub> Br+HCN→SiH <sub>3</sub> CN+HBr			SiH <sub>3</sub> I+HCN→SiH <sub>3</sub> CN+HI		
HF/6-31G(d)	58.2 (82.0)	50.1 (73.5)	50.6 (73.9)	53.1	43.5	44.1
HF/6-31G(d, p)	51.0 (71.0)	43.3 (63.2)	43.9 (63.6)	46.8	37.6	38.2
MP2/6-31G(d)	58.4 (79.6)	51.8 (72.6)	51.9 (72.6)	54.9	46.7	47.0
MP2/6-31G(d, p)	49.5 (68.7)	43.1 (62.1)	43.3 (62.2)	47.7	39.7	40.0
B3LYP/6-31G(d)	50.7 (72.1)	43.6 (64.6)	44.1 (64.9)	45.8	37.6	38.2
B3LYP/6-31G(d, p)	46.2 (63.8)	39.3 (56.8)	39.8 (57.2)	41.9	33.9	34.6
G3MP2	42.0 (40.4)	43.6 (42.0)	43.8 (42.1)			
		29.6 <sup>b</sup>			29.8 <sup>c</sup>	

The values in parentheses are calculated by using Binning-Curtiss bromine basis set from

reference 39.

<sup>a</sup> The value is calculated from  $\Delta H_f$  of  $\text{SiH}_3\text{Cl}$ ,  $\text{HCN}$ ,  $\text{SiH}_3\text{CN}$  and  $\text{HCl}$  given in Table 2.11.

<sup>b</sup> The value is calculated from  $\Delta H_f$  of  $\text{SiH}_3\text{Br}$ ,  $\text{HCN}$ ,  $\text{SiH}_3\text{CN}$  and  $\text{HBr}$  given in Table 2.11.

<sup>c</sup> The value is calculated from  $\Delta H_f$  of  $\text{SiH}_3\text{I}$ ,  $\text{HCN}$ ,  $\text{SiH}_3\text{CN}$  and  $\text{HI}$  given in Table 2.11.

**TABLE 2.7: Relative stabilities for the isomerization of SiH<sub>2</sub>XCN/SiH<sub>2</sub>XNC (X = H, Cl, Br, I) (in kJ mol<sup>-1</sup>) at 298.15K.**

Level/Basis Set	$\Delta E$	$\Delta H$	$\Delta G$	$\Delta E$	$\Delta H$	$\Delta G$
	SiH <sub>3</sub> CN → SiH <sub>3</sub> NC			SiH <sub>2</sub> ClCN → SiH <sub>2</sub> CINC		
HF/6-31G(d)	-1.8	-2.5	-3.3	-10.7	-11.7	-12.4
HF/6-31G(d, p)	-1.8	-2.5	-3.3	-10.7	-11.6	-12.4
MP2/6-31G(d)	42.7	43.3	42.9	36.4	36.8	36.4
MP2/6-31G(d, p)	41.9	42.5	42.0	35.9	36.3	35.9
B3LYP/6-31G(d)	24.9	24.5	23.8	17.3	16.8	16.2
B3LYP/6-31G(d, p)	24.9	24.6	23.9	17.3	16.8	16.2
G3MP2	16.9	17.3	16.5	9.5	9.8	9.0
G3B3	20.6	20.9	20.3	13.3	13.6	13.0
	20.5 <sup>a</sup>					
	SiH <sub>2</sub> BrCN → SiH <sub>2</sub> BrNC			SiH <sub>2</sub> ICN → SiH <sub>2</sub> INC		
HF/6-31G(d)	-9.1 (-8.6)	-10.1 (-9.6)	-10.9 (-10.3)	-6.7	-7.7	-8.5
HF/6-31G(d, p)	-9.1 (-8.6)	-10.0 (-9.5)	-10.8 (-10.3)	-6.8	-7.7	-8.5
MP2/6-31G(d)	38.0 (38.0)	38.4 (38.4)	38.0 (38.1)	40.5	40.9	40.6
MP2/6-31G(d, p)	37.5 (37.6)	37.9 (37.9)	37.5 (37.6)	40.0	40.4	40.0
B3LYP/6-31G(d)	18.8 (19.1)	18.2 (18.5)	17.7 (18.1)	21.0	20.4	19.8
B3LYP/6-31G(d, p)	18.8 (19.1)	18.3 (18.6)	17.7 (18.1)	21.0	20.4	19.8
G3MP2	11.2 (11.4)	11.6 (11.8)	10.8 (11.1)			

The values in parentheses are calculated by using Binning-Curtiss bromine basis set from

reference 39.

"The values obtained from reference 30.

**TABLE 2.8: Thermodynamic properties for the reaction of  $\text{SiH}_3\text{X}$  ( $\text{X} = \text{Cl}, \text{Br}, \text{I}$ ) with  $\text{HCN}$  ( $\text{H}_2$  elimination reaction) (in  $\text{kJ mol}^{-1}$ ) at 298.15K.**

Level/Basis Set	$\Delta\text{E}$	$\Delta\text{H}$	$\Delta\text{G}$
$\text{SiH}_3\text{Cl} + \text{HCN} \rightarrow \text{SiH}_2\text{ClCN} + \text{H}_2$			
HF/6-31G(d)	7.5	-4.6	0.3
HF/6-31G(d, p)	4.4	-7.4	-2.4
MP2/6-31G(d)	-24.7	-34.9	-30.5
MP2/6-31G(d, p)	-19.8	-29.9	-25.5
B3LYP/6-31G(d)	-10.3	-20.3	-15.8
B3LYP/6-31G(d, p)	-10.4	-20.3	-15.7
G3MP2	-34.4	-30.5	-26.3
G3B3	-32.0	-28.2	-23.8
$\text{SiH}_3\text{Br} + \text{HCN} \rightarrow \text{SiH}_2\text{BrCN} + \text{H}_2$			
HF/6-31G(d)	9.3 (6.4)	-2.8 (-5.8)	2.2 (-1.0)
HF/6-31G(d, p)	6.3 (3.4)	-5.5 (-8.5)	-0.5 (-3.6)
MP2/6-31G(d)	-23.2 (-25.2)	-33.3 (-35.5)	-28.9 (-31.3)
MP2/6-31G(d, p)	-18.4 (-20.3)	-28.4 (-30.5)	-24.0 (-26.2)
B3LYP/6-31G(d)	-8.9 (-11.9)	-18.9 (-22.0)	-14.3 (-17.6)
B3LYP/6-31G(d, p)	-9.0 (-11.9)	-18.8 (-21.8)	-14.3 (-17.5)
G3MP2	-33.8 (-33.9)	-29.8 (-29.9)	-25.5 (-23.0)
$\text{SiH}_3\text{I} + \text{HCN} \rightarrow \text{SiH}_2\text{ICN} + \text{H}_2$			

HF/6-31G(d)	10.8	-1.1	3.8
HF/6-31G(d, p)	7.9	-3.7	1.2
MP2/6-31G(d)	-22.0	-32.1	-27.7
MP2/6-31G(d, p)	-17.2	-27.2	-22.8
B3LYP/6-31G(d)	-8.0	-17.8	-13.2
B3LYP/6-31G(d, p)	-7.9	-17.6	-13.1

---

The values in parentheses are calculated by using Binning-Curtiss bromine basis set from reference 39.

**TABLE 2.9: Thermodynamic properties for the thermal decomposition reaction of  $\text{SiH}_3\text{X}$  (X = H, Cl, Br, I) (in  $\text{kJ mol}^{-1}$ ) at 298.15K.**

Level/Basis Set	$\Delta E$	$\Delta H$	$\Delta G$	$\Delta E$	$\Delta H$	$\Delta G$
	$\text{SiH}_4 \rightarrow \text{SiH}_2 + \text{H}_2$			$\text{SiH}_3\text{Cl} \rightarrow \text{SiHCl} + \text{H}_2$		
HF/6-31G(d)	258.7	240.1	203.8	225.5	208.9	169.7
MP2/6-31G(d)	251.6	234.1	197.8	206.5	191.1	152.0
B3LYP/6-31G(d)	249.6	233.0	196.7	199.4	184.9	145.8
G3MP2	220.0	228.1	192.0	176.5	184.3	145.5
G3B3	223.9	232.0	195.8	181.8	189.6	150.6
		238.2 <sup>a</sup>			196.4 <sup>a</sup>	
	$\text{SiH}_3\text{Br} \rightarrow \text{SiHBr} + \text{H}_2$			$\text{SiH}_3\text{I} \rightarrow \text{SiHI} + \text{H}_2$		
HF/6-31G(d)	220.4 (223.5)	204.2 (207.0)	165.0 (167.8)	216.1	200.2	161.1
MP2/6-31G(d)	201.1 (203.3)	186.0 (187.9)	147.0 (148.8)	196.6	181.9	142.9
B3LYP/6-31G(d)	193.5 (196.6)	179.4 (182.2)	140.3 (143.1)	188.0	174.2	135.2
G3MP2	197.5 (197.5)	205.3 (205.3)	166.5 (169.3)			
<b>Further Reactions:</b>	$\text{SiHCl} + \text{H}_2 \rightarrow \text{SiH}_2 + \text{HCl}$			$\text{SiHBr} + \text{H}_2 \rightarrow \text{SiH}_2 + \text{HBr}$		
HF/6-31G(d)	99.2	101.2	97.4	98.8 (119.6)	99.2 (119.8)	95.4 (115.9)
MP2/6-31G(d)	133.7	135.2	131.4	137.4 (156.4)	137.4 (156.3)	133.5 (152.3)
B3LYP/6-31G(d)	121.4	122.3	118.6	122.2 (140.5)	121.6 (139.8)	118.0 (136.0)
G3MP2	123.6	122.9	119.3	100.2 (98.5)	99.2 (97.6)	95.6 (93.9)
G3B3	119.2	118.4	114.8			

	SiHl + H <sub>2</sub> → SiH <sub>2</sub> + Hl		
HF/6-31G(d)	98.0	96.5	92.7
MP2/6-31G(d)	138.4	136.5	132.7
B3LYP/6-31G(d)	122.9	120.8	117.2

---

The values in parentheses are calculated by using Binning-Curtiss bromine basis set from reference 39.

<sup>a</sup> The value is obtained from reference 23.

**TABLE 2.10: Thermodynamic properties for the reaction of SiHX (X = H, Cl, Br, I) with HCN (in kJ mol<sup>-1</sup>) at 298.15K.**

Level/Basis Set	$\Delta E$	$\Delta H$	$\Delta G$	$\Delta E$	$\Delta H$	$\Delta G$
	SiH <sub>2</sub> + HCN → SiH <sub>3</sub> CN			SiHCl + HCN → SiH <sub>2</sub> ClCN		
HF/6-31G(d)	-261.1	-253.3	-209.7	-218.0	-213.5	-169.4
MP2/6-31G(d)	-280.1	-271.7	-228.6	-231.2	-225.9	-182.5
B3LYP/6-31G(d)	-265.0	-257.4	-214.2	-209.8	-205.2	-161.6
G3MP2	-255.7	-260.9	-218.2	-210.9	-214.9	-171.7
G3B3	-257.2	-262.5	-219.5	-213.8	-217.8	-174.5
	SiHBr + HCN → SiH <sub>2</sub> BrCN			SiHI + HCN → SiH <sub>2</sub> ICN		
HF/6-31G(d)	-211.1 (-217.1)	-206.9 (-212.8)	-162.8 (-168.8)	-205.2	-201.3	-157.2
MP2/6-31G(d)	-224.3 (-228.5)	-219.4 (-223.4)	-175.9 (-180.1)	-218.7	-214.0	-170.6
B3LYP/6-31G(d)	-202.5 (-208.5)	-198.2 (-204.2)	-154.7 (-160.7)	-195.9	-192.0	-148.5
G3MP2	-231.3 (-231.5)	-235.1 (-235.2)	-192.0 (-192.2)			

The values in parentheses are calculated by using Binning-Curtiss bromine basis set from reference 39.

**TABLE 2.11: Heat of formation ( $\Delta H_f$ ) (in  $\text{kJ mol}^{-1}$ ) at 298.15K.**

	Experimental	Present work		Present work <sup>a</sup>
$\text{SiH}_4$	34.7 <sup>b</sup>	35.8 <sup>i</sup>	$\text{SiH}_3\text{CN}$	133.5 (134.6) <sup>i</sup>
$\text{HCN}$	131.67 <sup>c</sup>		$\text{SiH}_3\text{NC}$	150.8
$\text{SiH}_3\text{Cl}$	-135.6 <sup>d</sup>	-136.7 <sup>k</sup>	$\text{SiH}_2\text{ClCN}$	-34.4
$\text{HCl}$	-92.21 <sup>e</sup>	-91.1 <sup>k</sup>	$\text{SiH}_2\text{BrCN}$	23.7
$\text{SiH}_3\text{Br}$	-78.24 <sup>f</sup>	-78.0 <sup>k</sup>	$\text{SiH}_2\text{ICN}$	102.4
$\text{HBr}$	-36.2 <sup>e</sup>	-36.5 <sup>k</sup>	$\text{SiHCl}$	48.7
$\text{SiH}_3\text{I}$	-2.09 + 2 <sup>g</sup>		$\text{SiHBr}$	127.1
$\text{HI}$	25.92 <sup>e</sup>		$\text{SiHI}$	179.8
$\text{SiH}_2$	273.8 ± 4.2 <sup>h</sup>	262.8 <sup>i</sup>		

<sup>a</sup> See text for explanation.

<sup>b</sup> Reference 42; <sup>c</sup> Reference 44; <sup>d</sup> Reference 45; <sup>e</sup> Reference 46,47; <sup>f</sup> Reference 43; <sup>g</sup> Reference 47; <sup>h</sup> Reference 48.

<sup>i</sup> The value in parentheses is obtained by using the heat of reaction of  $\text{SiH}_3\text{Cl} + \text{HCN} \rightarrow \text{SiH}_3\text{CN} + \text{HCl}$  and experimental  $\Delta H_f$  of  $\text{SiH}_3\text{Cl}$ ,  $\text{HCN}$  and  $\text{HCl}$ .

<sup>j</sup> The value is obtained by using the heat of reaction of  $\text{SiH}_4 + \text{HCN} \rightarrow \text{SiH}_3\text{CN} + \text{H}_2$  and  $\Delta H_f(\text{SiH}_3\text{CN}) = 134.6 \text{ kJ mol}^{-1}$ .

<sup>k</sup> The values are obtained by using the heat of reaction of  $\text{SiH}_3\text{X} + \text{HCN} \rightarrow \text{SiH}_3\text{CN} + \text{HX}$  ( $\text{X} = \text{Cl}$  and  $\text{Br}$ ) and experimental  $\Delta H_f$  values for  $\text{SiH}_3\text{X}$ ,  $\text{HCN}$  and  $\text{HX}$  and the calculated  $\Delta H_f(\text{SiH}_3\text{CN}) = 133.5 \text{ kJ mol}^{-1}$ .

<sup>l</sup> The value is obtained by using the heat of reaction of  $\text{SiH}_4 \rightarrow \text{SiH}_2 + \text{H}_2$  and the experimental  $\Delta H_f$  value for  $\text{SiH}_4$ .

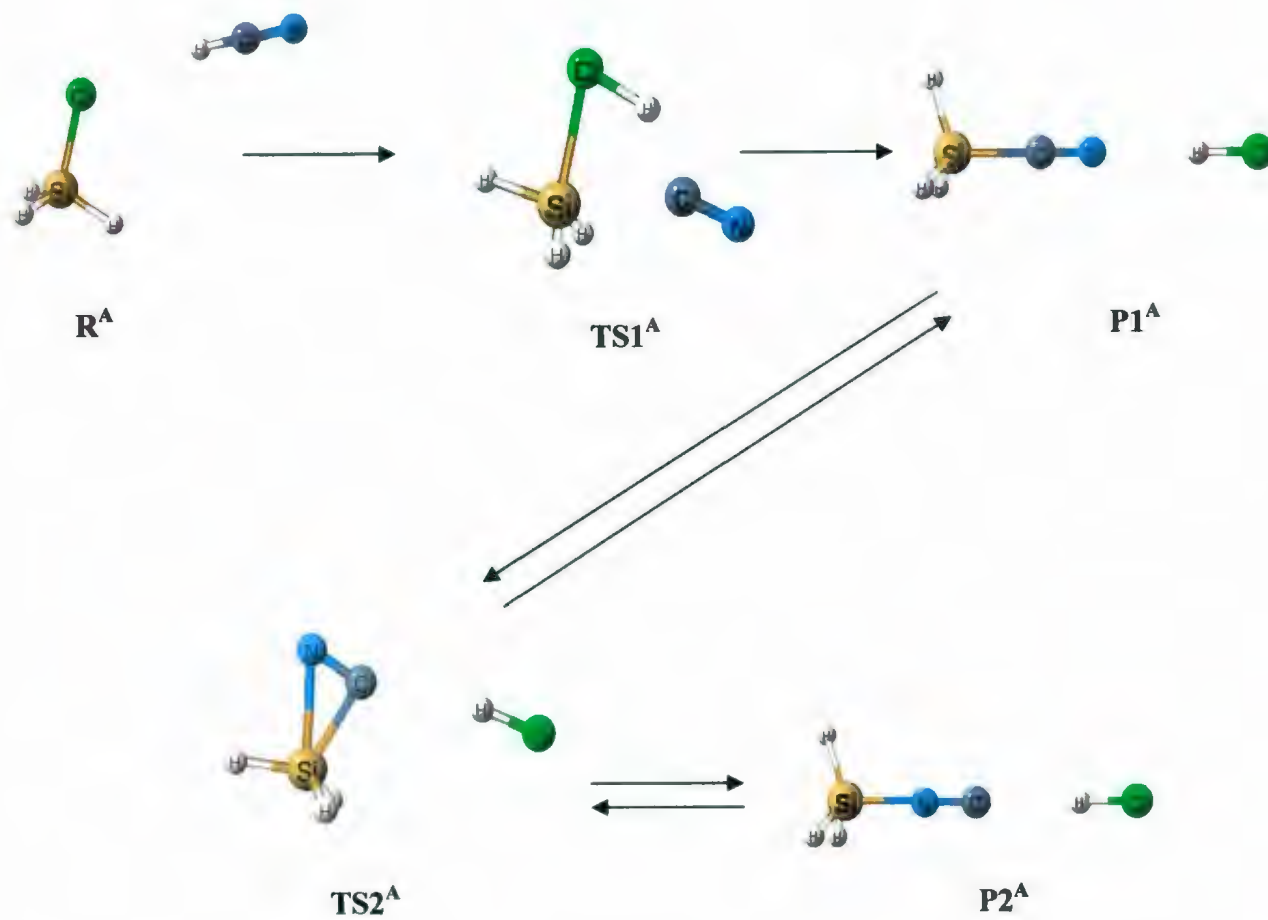


Figure 2.1. Mechanism for the reaction of  $\text{SiH}_3\text{X} + \text{HCN}$  (Pathway A). Only  $\text{X}=\text{Cl}$  is shown here, similar structures are found for  $\text{X}=\text{Br}$  and  $\text{I}$ .

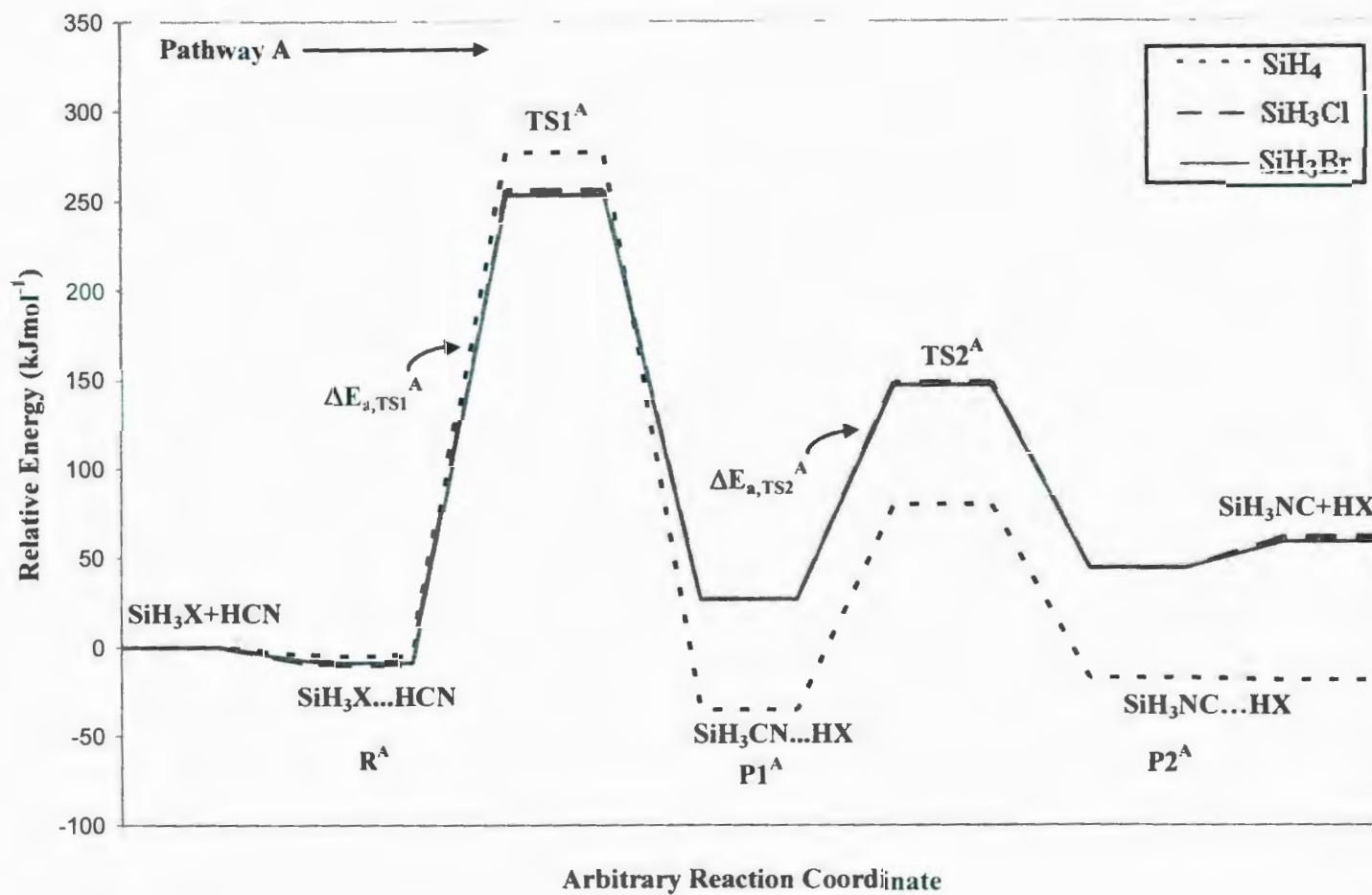


Figure 2.2. Reaction pathway for the reaction of  $\text{SiH}_3\text{X} + \text{HCN}$  (Pathway A) at G3MP2 level of theory (see Figure 2.1).

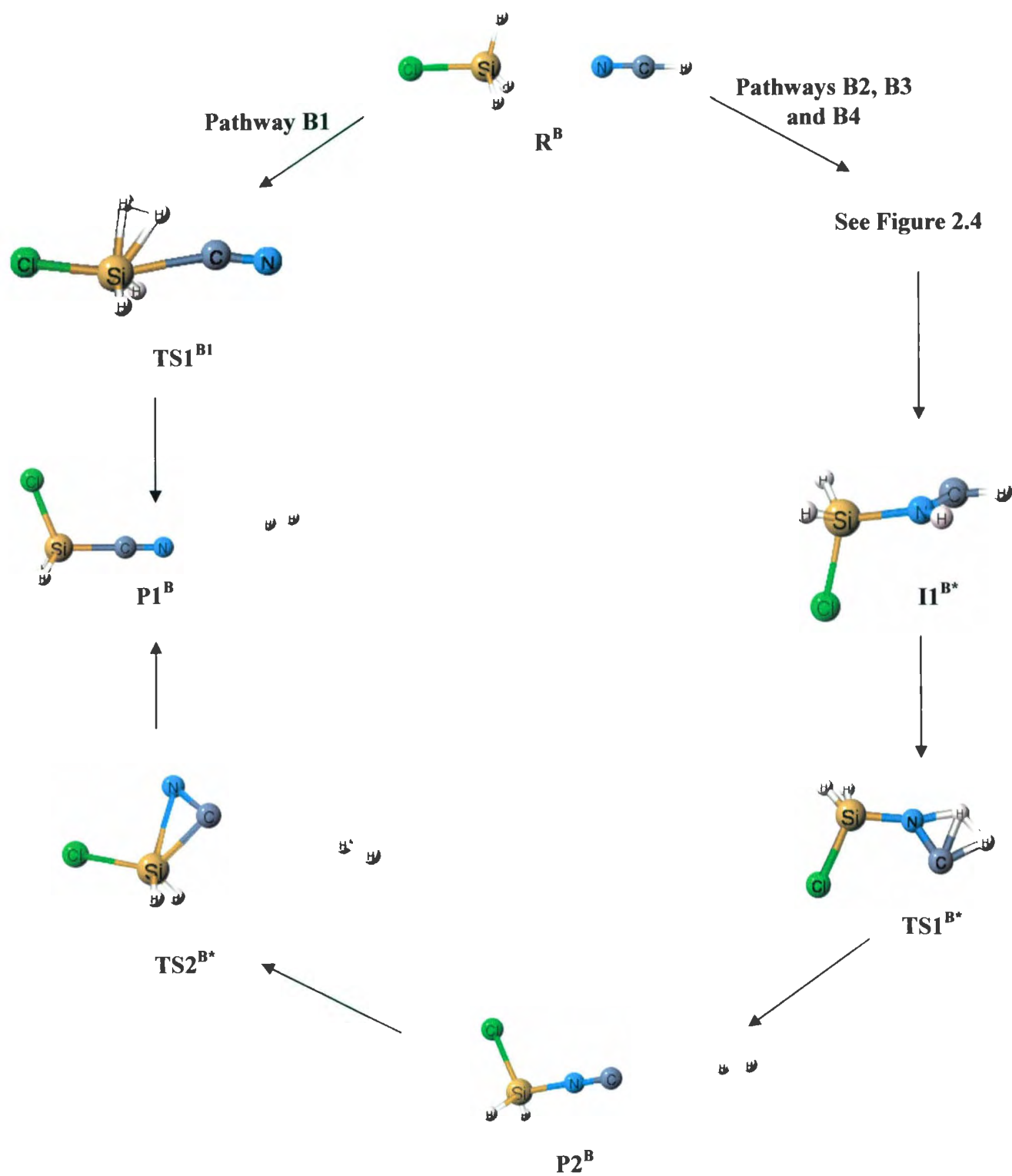


Figure 2.3. Mechanism for the reaction of  $\text{SiH}_3\text{X} + \text{HCN}$  ( $\text{H}_2$  elimination). Only  $\text{X} = \text{Cl}$  is shown here, similar structures are found for  $\text{X} = \text{H}$ , Br and I.

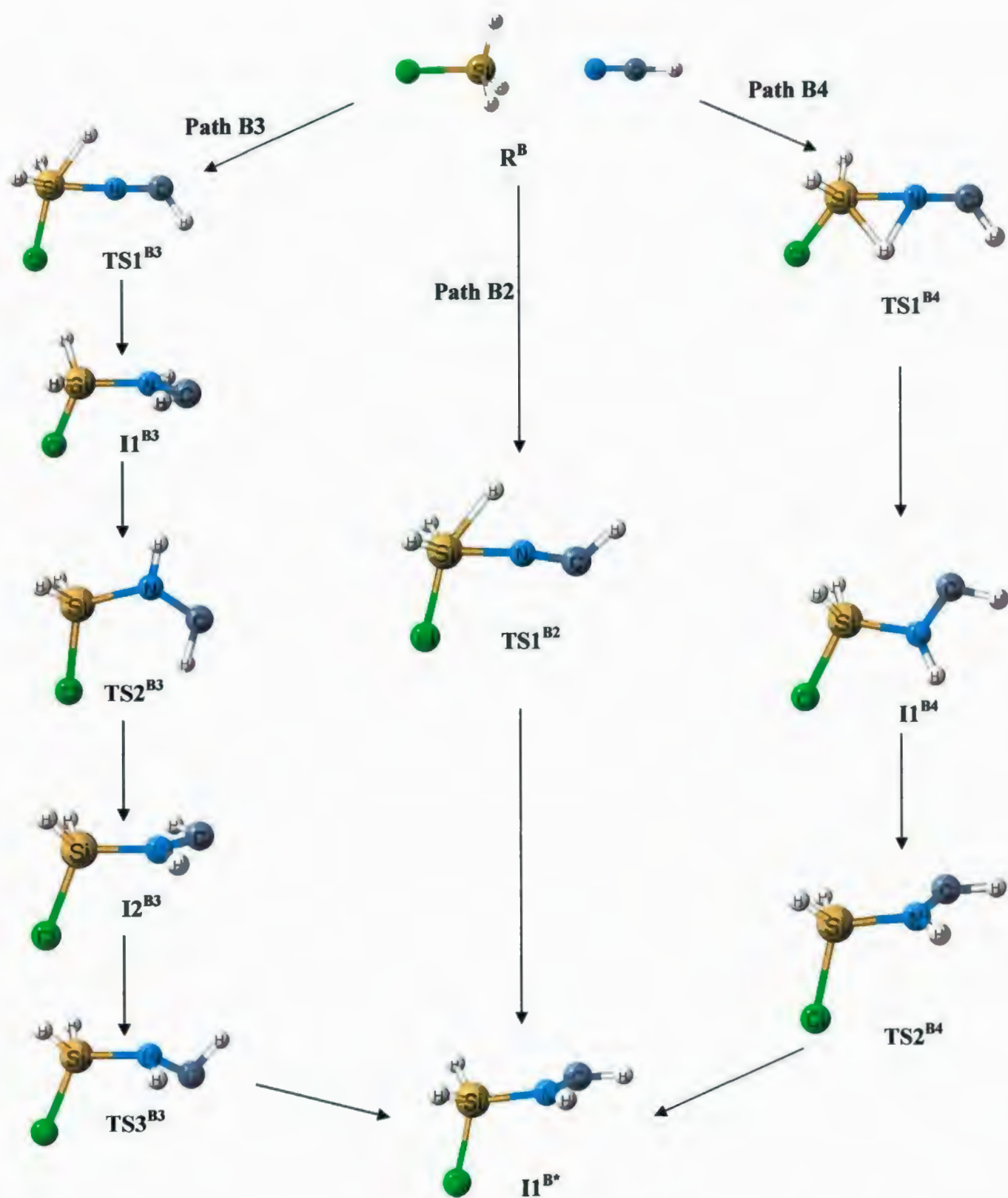


Figure 2.4. Mechanism for the reaction of  $\text{SiH}_3\text{X} + \text{HCN}$  forming the intermediate  $\text{II}^{\text{B}*}$  ( $\text{H}_2$  elimination). Only  $\text{X}=\text{Cl}$  is shown here, similar structures are found for  $\text{X}=\text{H}$ ,  $\text{Br}$  and  $\text{I}$ .

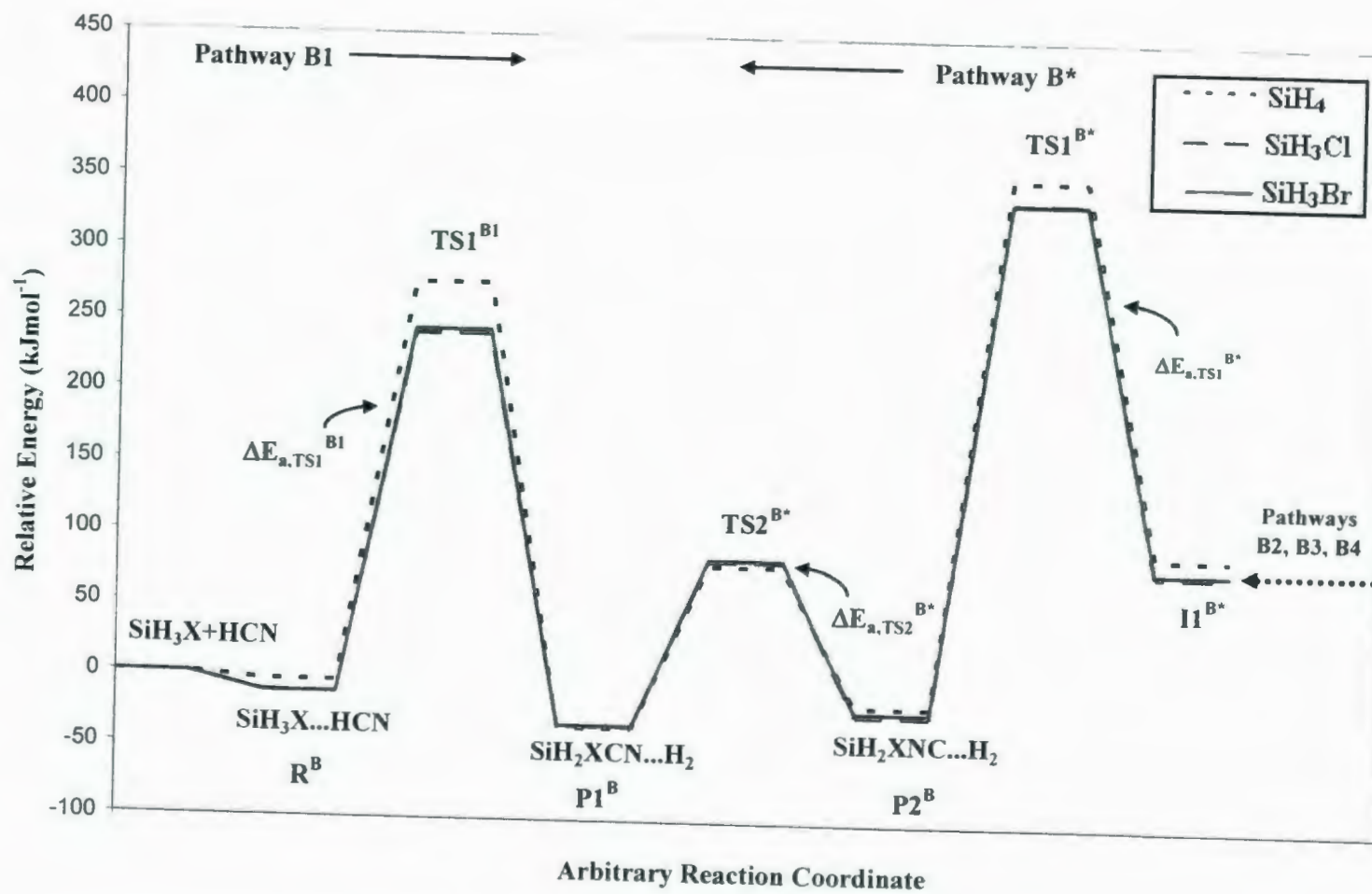


Figure 2.5. Reaction pathway B1 and B\* for the reaction of  $\text{SiH}_3\text{X} + \text{HCN}$  ( $\text{H}_2$  elimination) at G3MP2 level of theory (see Figure 2.3).

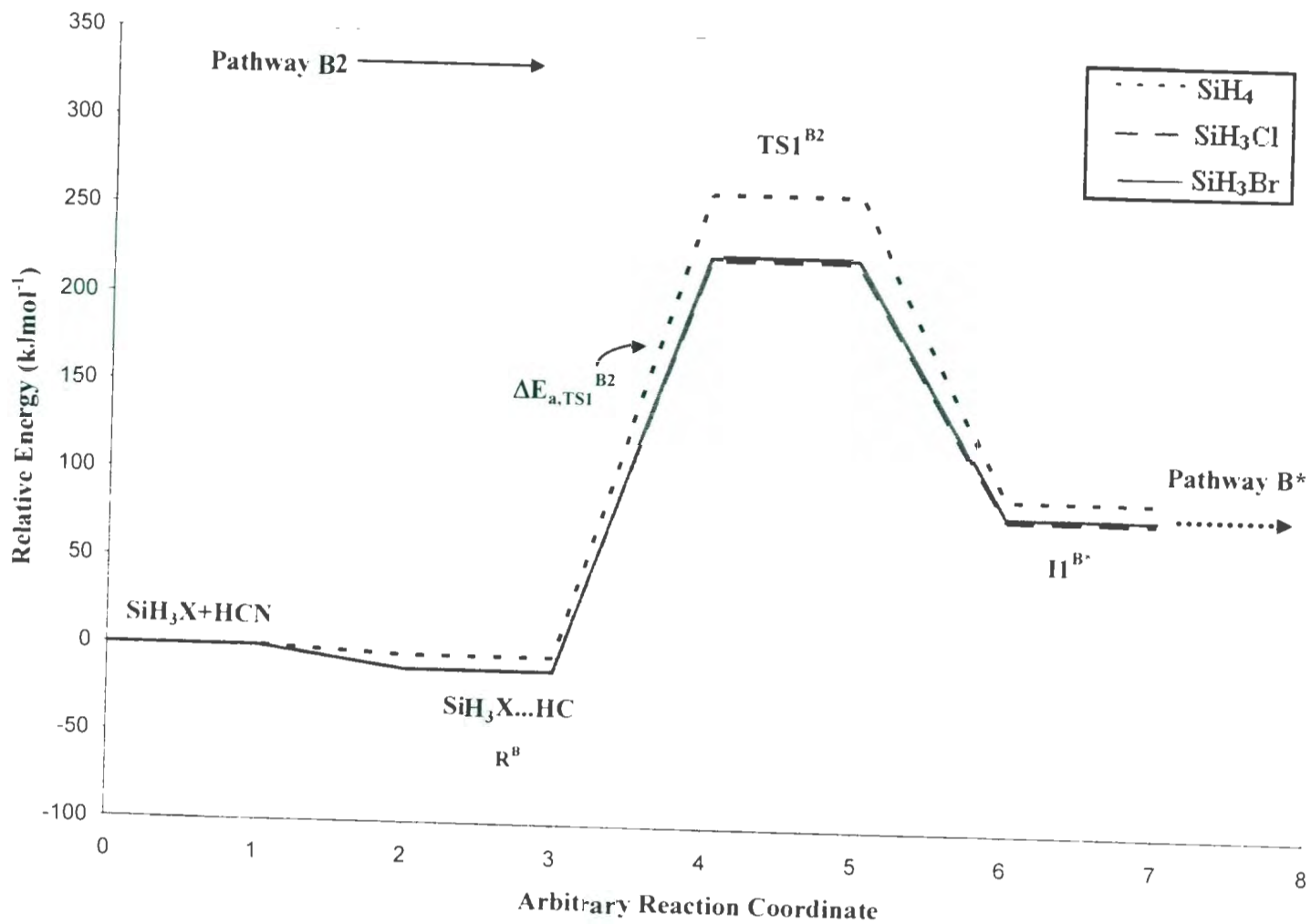


Figure 2.6. Reaction pathway B2 for the reaction of  $\text{SiH}_3\text{X} + \text{HCN}$  ( $\text{H}_2$  elimination) at G3MP2 level of theory (see Figure 2.4).

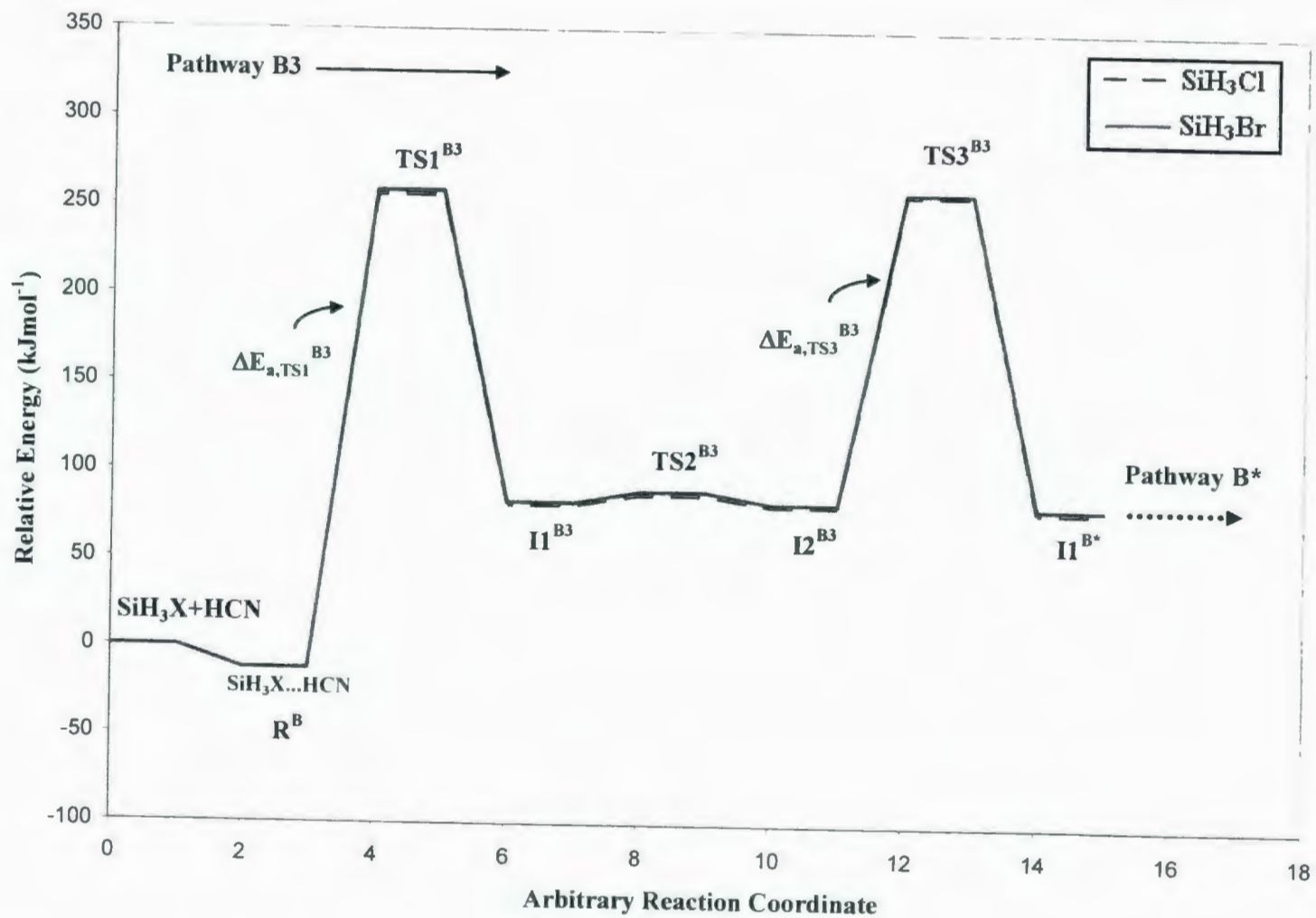


Figure 2.7. Reaction pathway B3 for the reaction of  $\text{SiH}_3\text{X} + \text{HCN}$  ( $\text{H}_2$  elimination) at G3MP2 level of theory (see Figure 2.4).

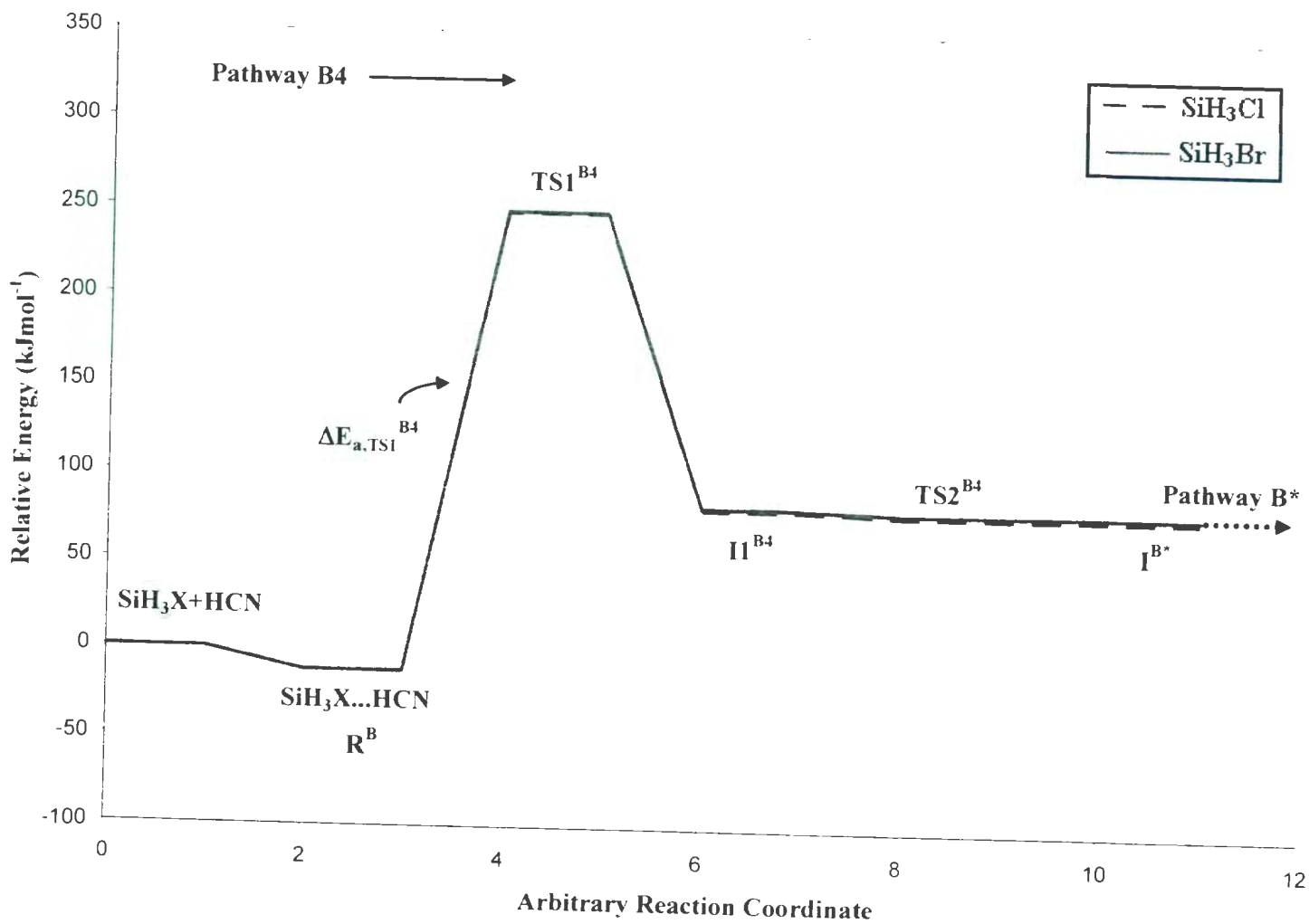


Figure 2.8. Reaction pathway B4 for the reaction of  $\text{SiH}_3\text{X} + \text{HCN}$  (H<sub>2</sub> elimination) at G3MP2 level of theory (see Figure 2.4).

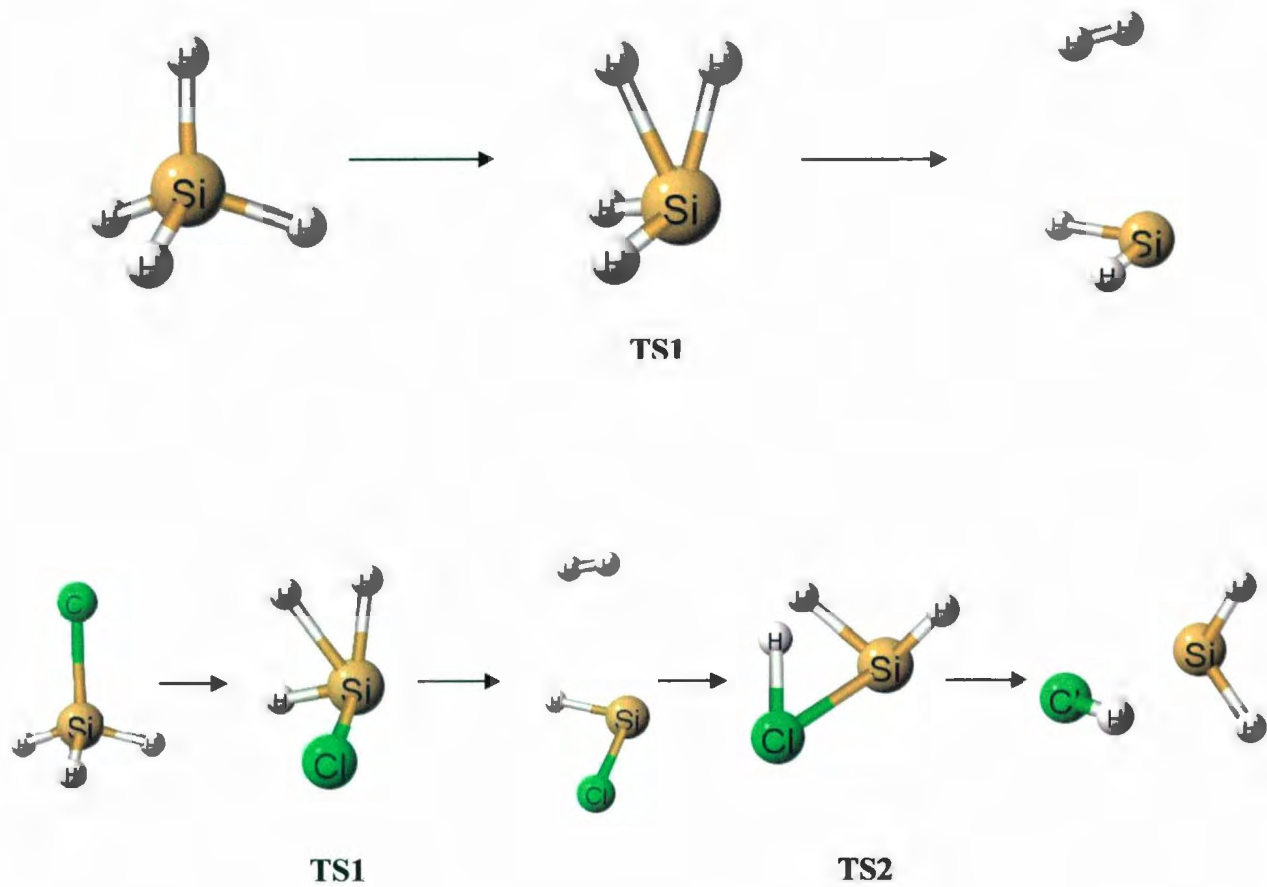


Figure 2.9. Mechanism for thermal decomposition of  $\text{SiH}_3\text{X}$ . Only  $\text{X}=\text{H}$  and  $\text{Cl}$  are shown here, similar structures to  $\text{X}=\text{Cl}$  are found for  $\text{X}=\text{Br}$  and  $\text{I}$ .

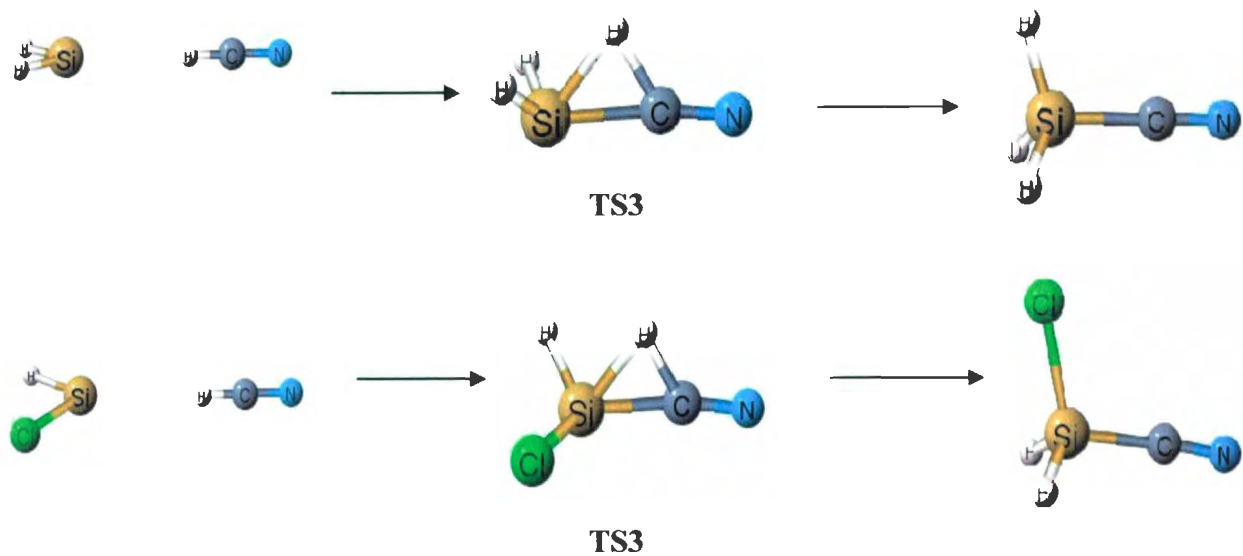


Figure 2.10. Mechanism for the addition reaction of SiHX + HCN. Only X=Cl are shown here, similar structures are found for X=H, Br and I.

## CHAPTER 3

# New insights into the bromination reaction for a series of alkenes - A computational study

### 3. 1 Introduction

The electrophilic addition of  $\text{Br}_2$  to alkenes is a well known organic reaction.<sup>1-2</sup> The reaction mechanism has been extensively studied experimentally and the generally accepted reaction scheme consists of several steps.<sup>2-7</sup> Studies of this reaction go back to as early as 1937 from the work of Roberts and Kimball.<sup>8</sup> Their work suggested the existence of a cyclic bromonium ion intermediate, which was shown in the late 1960s using NMR, by Olah and co-workers,<sup>9,10</sup> to be the actual reactive species. However, there was no structural evidence for the existence of a cyclic bromonium ion because the reaction is too fast. There have been many experimental attempts by a variety of techniques to confirm the occurrence of cyclic

bromonium ions in the gas phase, including photoionization,<sup>11</sup> ion cyclotron resonance,<sup>11-14</sup> radiolytic technique,<sup>15</sup> and conventional mass spectrometry.<sup>16,17</sup> Although some experiments suggest the formation of a bromonium ion, no conclusive evidence could be provided for its actual structure. Strating et al.<sup>18</sup> first produced a bromonium ion tribromide in the lab by reacting adamantylideneadamantane (Ad<sup>+</sup> Ad) with Br<sub>2</sub> in CCl<sub>4</sub>. Slebocka-Tilk et al.<sup>19</sup> for the first time obtained the X-ray structure of adamantylideneadamantane bromonium ion with a Br<sub>3</sub><sup>-</sup> counterion. In this case, because back-side attack by Br<sup>-</sup> is sterically hindered, bromination stops at the adamantylideneadamantane bromonium ion. (E)-2,2,5,5-Tetramethyl-3,4-diphenylhex-3-ene is the first reported example of an olefin whose interaction with bromine is limited to  $\pi$  complex formation.<sup>20</sup> Similarly, tetraneopentylethylene does not react with bromine in CCl<sub>4</sub> and on the basis of the <sup>13</sup>C NMR spectrum there is no evidence of formation of a  $\pi$  complex.<sup>21</sup> Thus the reactivity of olefins toward bromine depends on their steric hindrance. A study of the product of bromination of ethene in dichloroethane by <sup>1</sup>H and <sup>2</sup>H NMR spectra indicates that the addition gives trans-1,2-dibromoethane.<sup>22</sup> Chretien et al.<sup>23</sup> studied the selectivity of alkene bromination by using stereo-, regio-, and chemo- selectivity. It is believed that the electrophilic bromination of alkenes follows a mechanism that has three successive steps: (i) fast-equilibrated formation of an olefin-bromine charge-transfer complex, (ii) rate-limiting ionization of this  $\pi$  complex into a  $\sigma$  complex, the so-called bromonium ion, and finally, (iii) fast product formation by nucleophilic trapping of the ionic intermediate.<sup>24-26</sup>

In comparison to experimental studies, there have been a limited number of theoretical studies on the bromination of alkenes. Yamabe et al.<sup>27</sup> studied the electrophilic addition reactions,  $X_2 + C_2H_4 \rightarrow C_2H_4X_2$  ( $X = F, Cl, \text{ and } Br$ ) at the MP3/3-21G//RHF/3-21G level of theory. Their study shows that the fluorination of ethene occurs via a four-center transition state, while chlorination and bromination give zwitterionic three-center transition states. The activation energies were found to be 212.5, 212.1, and 256.9  $\text{kJ mol}^{-1}$  for  $X = F, Cl$  and  $Br$ , respectively. Hamilton and Schaefer<sup>28</sup> in their study on the structure and energetics of  $C_2H_4Br^+$  isomers proposed that the transition state for the bromination reaction is a three-membered bromonium ion with a nearby counter bromide ion. Later, Cammi et al.<sup>29</sup> conducted a detailed MP2 study from the charge-transfer complex (CTC) to the transition state (TS) for the addition of  $Br_2$  to ethene both in the gas phase and in water. At the MP2/CEP-121G(aug) level the structures of the CTC and the TS were found to have  $C_{2v}$  symmetry both in the gas phase and in water. They also found that the structure of the CTC is not very different in the gas phase and in water but the TS structure is largely affected by the presence of the solvent where the solvated TS has an earlier character with a  $Br-Br$  bond much shorter than that in the gas phase. At the MP2/CEP-121G(aug) level the barrier was found to be 250.8  $\text{kJ mol}^{-1}$ . The first step in electrophilic bromination of ethene in water was also investigated by Strnad et al.<sup>30</sup> by molecular dynamics simulations. Hamilton and Schaefer<sup>28,31</sup> studied the structure and energetics of  $C_2H_4Br^+$ ,  $C_2H_2Br^+$  and  $C_2H_2Cl^+$  using ab initio quantum mechanical techniques and found that the cyclic bromonium ion is more stable than the acyclic 1-bromoethyl cation by 6.3  $\text{kJ mol}^{-1}$  with a barrier of 104.5  $\text{kJ mol}^{-1}$  for the interconversion of these two forms. Cossi et al.<sup>32</sup> found the positive charge to be

delocalized over the Br atom and the two olefinic carbons in the bromonium ion. The CTC formed during the first step of the bromination reaction was also investigated.<sup>33-35</sup>

It is difficult to extract conclusive information about the mechanistic pathways from experiments only. Thus, quantum chemical calculations are the only source for a detailed characterization of the potential energy surface along the reaction path. However, no computational studies have been reported for the complete potential energy surface for the bromination of alkenes. To ensure the reliability of our results, wavefunction and density functional theory (DFT) calculations were performed. Because of the size of the system, it is possible to also perform some calculations at high levels of theory, such as G3MP2 and G3MP2B3, which are known to give reliable energetics.<sup>36, 37</sup>

### 3.2 Method

All of the electronic structure calculations were carried out with Gaussian03.<sup>38</sup> The geometries of all reactants, transition states, intermediates and products were fully optimized at the HF, MP2, and B3LYP levels of theory. From previous work,<sup>39</sup> it was found that for some reactions involving 3<sup>rd</sup> row elements energetics obtained using the standard 6-31G bromine basis set<sup>40</sup> showed better agreement with G3 theories compared to the Binning-Curtiss<sup>41</sup> bromine (BC6-31G) basis set. Therefore both the standard 6-31G(d) and BC6-31G(d) bromine basis sets are used in this study. Because the reaction of Br<sub>2</sub> with alkenes is known to proceed through formation of charged species the standard 6-31+G(d) and BC6-

31+G(d) basis sets were also used. B3P86 and B3PW91 density functional calculations were also performed where B3LYP failed to give an optimized structure along a reaction pathway. Single-point energies required for G3MP2, G2MP2B3 and G3MP2B3(BC) levels were obtained using the MP2(FULL)/6-31G(d), B3LYP/6-31G(d) and B3LYP/BC6-31G(d) optimized geometries, respectively. For Br, the G3MP2large basis set,<sup>42, 43</sup> which is not yet incorporated in Gaussian03, was used for G3MP2 and G3MP2B3 calculations. Frequencies were calculated for all structures to ensure the absence of imaginary frequencies in the minima and for the presence of only one imaginary frequency in the transition states. The complete reaction pathways for all the mechanisms discussed in this paper have been verified using intrinsic reaction coordinate (IRC) analysis. Structures obtained from IRC have been optimized to positively identify the reactant and product to which each transition state is connected. Free energies of activation and of reaction for the addition reaction of bromine to alkenes in CCl<sub>4</sub>, CH<sub>2</sub>Cl<sub>2</sub>, CH<sub>2</sub>Cl-CH<sub>2</sub>Cl and CH<sub>3</sub>OH were calculated with the polarizable continuum model (PCM) as implemented in Gaussian03. All free energy calculations involving solvation were performed using the optimized solution-phase structures. By default, the PCM model builds up the cavity using the united atom (UA0) model, i.e., putting a sphere around each solute heavy atom; hydrogen atoms are enclosed in the sphere of the atom to which they are bonded.

### 3.3 Results and Discussion

The results for the reaction of alkenes with Br<sub>2</sub> and 2Br<sub>2</sub> are given in Tables 3.1–3.9

and the heats of formation of some energetically stable compounds are presented in Table 3.10.

### 3.3.1 Potential energy surfaces for the reaction of alkenes with Br<sub>2</sub>

The results for the reaction of alkenes and Br<sub>2</sub> will be discussed in the following order: 1) perpendicular attack of Br<sub>2</sub> to C=C (pathway A) and 2) sidewise attack of Br<sub>2</sub> to C=C (pathway B).

#### 3.3.1.1 Perpendicular attack of Br<sub>2</sub> to C=C: Pathway A

Although this pathway has been investigated previously,<sup>29,30</sup> the studies involved the reaction of ethene with a single Br<sub>2</sub>. The structures of pathway A, perpendicular attack of Br<sub>2</sub> on the C=C bond, along with the relative energies of reactants, transition states, intermediates and products are shown in Figure 3.1 for ethene + Br<sub>2</sub>. Similar structures are also observed for the reaction of Br<sub>2</sub> with propene, isobutene, fluoroethene, chloroethene, (E)-1,2-difluoroethene and (E)-1,2-dichloroethene and are not shown here. The first step is the formation of a weak alkene/Br<sub>2</sub> (R<sup>A</sup>) T-shaped charge-transfer complex with the Br<sub>2</sub> molecule perpendicular to the C=C bond. In all cases, the transition state structure, which is only found at the MP2 level of theory, also retains the T-shaped structure. The transition state (TS1<sup>A</sup>) involves the rupture of the Br-Br bond and the formation of two C-Br bond. In the reactant complex R<sup>A</sup>, the Br-Br bond distance at MP2/BC6-31G(d) level of theory is 2.347 Å, while in TS<sup>A</sup>, it increases to 4.339 Å. However, the C-Br bond distances decrease from

2.962 to 2.906 Å. The IRC analysis confirmed that  $TS^A$  leads to  $R^A$  and to the bromonium/bromide ion complex,  $I^A$ . However, optimization of  $I^A$  failed for both the gas phase and in  $CCl_4$  for all alkenes investigated. However, an optimized structure for  $I^A$  was obtained in  $H_2O$  solution. The activation energies for the reaction of  $Br_2$  with ethene, propene, isobutene, fluoroethene, chloroethene, (E)-1,2-difluoroethene, (E)-1,2-dichloroethene in pathway A are listed in Table 3.1. In all cases, the activation energies ( $\Delta E_{a,TS^A}$ ), free energies ( $\Delta G_{TS^A}^\ddagger$ ) and enthalpies ( $\Delta H_{TS^A}^\ddagger$ ) of activation are relatively high. Activation energies range from 254.9 to 268.5  $\text{kJ mol}^{-1}$  at the MP2/G3MP2large//MP2(FULL)/6-31G(d) level of theory. This pathway does not lead to trans-1, 2-dibromoalkane which is known<sup>22</sup> to be the product of most simple alkenes.

### 3.3.1.2 Sidewise attack of $Br_2$ to $C=C$ : Pathway B

The structures for pathway B are shown in Figure 3.2 for the reaction of ethene and  $Br_2$ . Similar structures are also observed for the reaction of  $Br_2$  with propene, isobutene, fluoroethene and chloroethene. The relative energies of reactants, intermediates, transition states, and products are shown in Figure 3.3. Activation energies, free energies and enthalpies of activation for the reaction of  $Br_2$  with ethene, propene, isobutene, fluoroethene and chloroethene are given in Table 3.2. In addition to the previously reported CTC,  $R^A$ , a second alkene/ $Br_2$  complex ( $R^B$ ) was found. For the ethene/ $Br_2$  and propene/ $Br_2$  complexes, the perpendicular complex is more stable by 9.0 and 12.8  $\text{kJ mol}^{-1}$  at the G3MP2B3 level, respectively. Unlike pathway A, with few exceptions, the structures exist at all levels of

theory and basis sets investigated in this case. Pathway B is a multiple-step process. In the first step, a bromonium ion/ $\text{Br}^-$  intermediate  $\text{I1}^{\text{B}}$  is formed via  $\text{TS1}^{\text{B}}$ . For ethene, the Br-Br bond distance in the reactant complex  $\text{R}^{\text{B}}$  is 2.311 Å at the MP2/BC6-31G(d) level of theory, while in  $\text{TS1}^{\text{B}}$ , the distance increases to 2.963 Å. The IRC analysis confirmed that  $\text{TS1}^{\text{B}}$  leads to  $\text{R}^{\text{B}}$  and  $\text{I1}^{\text{B}}$ . The activation energies, free energies and enthalpies of activation calculated using the BC6-31G(d) and standard 6-31G(d) basis set are very similar at all the levels of theory (Table 3.2). Due to convergence failure in the QCISD(T) calculation, no G3 results were obtained for the reaction of  $\text{Br}_2$  with ethene and propene. However, for isobutene the QCISD(T) did converge and the activation energies obtained at the MP2/BC6-31G(d) and G3MP2B3 levels are found to be within 1.9  $\text{kJ mol}^{-1}$ . Hence, the activation energies at MP2/BC6-31G(d) level of theory should agree well with G3 theories for the first step of pathway B. Inclusion of a larger basis set does not change the barrier significantly (Table 3.2). The activation energies for the reaction of  $\text{Br}_2$  with ethene and propene are 247.3 and 200.4  $\text{kJ mol}^{-1}$  at MP2/BC6-31G(d) level of theory, respectively. Although, it was observed that the IRC leads from  $\text{TS1}^{\text{B}}$  to  $\text{R}^{\text{B}}$  and  $\text{I1}^{\text{B}}$  for all DFT methods, for some functionals no structure for  $\text{I1}^{\text{B}}$  was found. All attempts at optimizing the intermediate  $\text{I1}^{\text{B}}$  converged to the trans-1, 2-dibromoalkane product. For the reaction of ethene and propene, optimized structures for  $\text{I1}^{\text{B}}$  were obtained with B3PW91/BC6-31G(d) and B3P86/BC6-31G(d) levels of theory. It was also possible to obtain an optimized structure for  $\text{I1}^{\text{B}}$  in the case of ethene at the B3LYP/BC6-31G(d) level by decreasing the default maximum step size in the optimization from MaxStep=30 to MaxStep=1. For cases in which no DFT structures for  $\text{I1}^{\text{B}}$

were obtained, single point calculations were performed using MP2/6-31G(d) geometries (Table 3.2). In the second step of pathway B, a gauche dibromoalkane intermediate ( $I2^B$ ) is formed via  $TS2^B$ . The corresponding activation energy ( $\Delta E_{a,TS2^B}$ ) at G3MP2B3 for propene is  $37.0 \text{ kJ mol}^{-1}$  which again agrees very well with the MP2/BC6-31G(d) ( $45.0 \text{ kJ mol}^{-1}$ ) level of theory. Similar agreement is also expected for the other alkenes. The activation energies ( $\Delta E_{a,TS2^B}$ ) for the reaction of  $Br_2$  with ethene and isobutene are  $58.3$  and  $54.2 \text{ kJ mol}^{-1}$  at MP2/BC6-31G(d), respectively. Finally, the trans-1,2-dibromoalkane product ( $P^B$ ), a conformational isomer of  $I2^B$ , is formed via  $TS3^B$ , which involves rotation about the C-C bond with activation energies of  $13.9$  and  $22.0 \text{ kJ mol}^{-1}$  for (E)-1,2-dibromoethene and (E)-1,2-dibromopropene, respectively at G3MP2B3. Solvation ( $CCl_4$ ) has no effect on the reaction mechanism at the MP2/6-31G(d) and B3LYP/6-31G(d) levels of theory. The solvent model used in this study predicts the free energies of activation for the rate-determining step to be  $262.9$  and  $191.0 \text{ kJ mol}^{-1}$  at MP2/6-31G(d) and B3LYP/6-31G(d), respectively, for ethene and  $233.5$  and  $165.9 \text{ kJ mol}^{-1}$  at MP2/6-31G(d) and B3LYP/6-31G(d), respectively, for propene.

In the cases of fluoro- and chloroethene,  $Br_2$  can attack from two different directions (syn and anti). For syn attack (substituent side) the activation energies ( $\Delta E_{a,TS1^B}$ ) are  $224.2$  and  $206.1 \text{ kJ mol}^{-1}$  for F and Cl, respectively at the MP2/BC6-31G(d) level of theory whereas for anti attack the activation energies are  $238.4$  and  $240.1 \text{ kJ mol}^{-1}$  for F and Cl, respectively. The activation energies ( $\Delta E_{a,TS2^B}$ ) in step two of the  $Br_2$  reaction with fluoroethene and

chloroethene are 33.6 and 6.8 kJ mol<sup>-1</sup> at MP2/BC6-31G(d) level for syn addition and 23.0 and 27.2 kJ mol<sup>-1</sup> for anti addition. The last step involves rotation around the C-C bond with all of the levels predicting a low barrier (Table 3.2). The barriers for the rate-determining step decrease in the order ethene > fluoroethene > chloroethene > propene > isobutene, with values of 247.3, 224.2, 206.1, 200.4 and 189.3 kJ mol<sup>-1</sup> at the MP2/BC6-31G(d) level, respectively. This is consistent with experiment<sup>44, 45</sup> where the relative rates of bromination follow the order (CH<sub>3</sub>)<sub>2</sub>C=C(CH<sub>3</sub>)<sub>2</sub> > CH<sub>3</sub>CH<sub>2</sub>CH=CH<sub>2</sub> > CH<sub>2</sub>=CH<sub>2</sub>.

Reaction of Br<sub>2</sub> with (E)-1,2-difluoroethene and (E)-1,2-dichloroethene is a four-step process. The corresponding activation energies, free energies and enthalpies of activation are given in Table 3.3. All of the structures for this mechanism are shown in Figure 3.4. The activation energies of the rate-determining step are 220.1 kJ mol<sup>-1</sup> for (E)-1,2-difluoroethene and 217.1 kJ mol<sup>-1</sup> for (E)-1,2-dichloroethene at MP2/BC6-31G(d). The corresponding activation energies for step two are 69.0 and 91.9 kJ mol<sup>-1</sup>. Intermediate I3<sup>B</sup>, a rotamer of I2<sup>B</sup>, is formed via TS3<sup>B</sup>, with activation energies of 25.8 and 27.9 kJ mol<sup>-1</sup> at G3MP2B3 for 1,2-difluoroethene and dichloroethene, respectively. Similarly, product P<sup>B</sup>, which is also a conformational isomer of I3<sup>B</sup>, is formed via TS4<sup>B</sup>, with activation energies of 30.7 and 50.8 kJ mol<sup>-1</sup> at G3MP2B3 for difluoro- and dichloroethene, respectively.

### 3.3.2 Potential energy surfaces for the reaction of ethene with 2Br<sub>2</sub>

In this case, we investigate pathways for the reaction with ethene only. The results for

the reaction of ethene and  $2\text{Br}_2$  will be discussed in the following order: 1) pathway C, 2) pathway D, 3) pathway E, and 4) pathway F. For pathways C and D and channel 1 of pathway E, intermediate  $\text{I2}^{\text{X}}$  and  $\text{TS3}^{\text{X}}$  are labeled as X because they are common to these pathways.

### 3.3.2.1 Pathway C:

The structures of reactants, intermediates, transition states and products of pathway C are shown in Figure 3.5. The relative energies of reactants, intermediates, transition states and products are shown in Figure 3.6. Activation energies, free energies and enthalpies of activation for pathway C are given in Table 3.4. Ethene +  $2\text{Br}_2$  can form two possible complexes, R1 and R2. Complex R2 reacts through  $\text{TS1}^{\text{C}}$  to form intermediate  $\text{I1}^{\text{C}}$  which is a bromonium/tribromide ion pair. The Br-Br bond distance in the  $\text{Br}_2$  adding to  $\text{C}=\text{C}$  goes from 2.302 Å in the R2 complex to 2.940 Å in  $\text{TS1}^{\text{C}}$  at MP2/6-31G(d). The IRC analysis confirmed that  $\text{TS1}^{\text{C}}$  leads to R2 and  $\text{I1}^{\text{C}}$ . The activation energy ( $\Delta E_{\text{a,TS1}^{\text{C}}}$ ) is 207.3 kJ mol<sup>-1</sup> at the G3MP2B3 level. MP2 appears to overestimate while DFT appears to be underestimating the barrier for this reaction. The activation energy ( $\Delta E_{\text{a,TS1}^{\text{C}}}$ ) obtained by MP2/6-31G(d) is higher than the G3MP2B3 value by 25.5 kJ mol<sup>-1</sup>, while the activation energies obtained by B3LYP are lower by 47.0 and 39.5 kJ mol<sup>-1</sup> at 6-31G(d) and 6-31+G(d), respectively. However, activation energies do not depend significantly on the choice of basis set. Activation energies at MP2/6-31G(d) (232.8 kJ mol<sup>-1</sup>) and at MP2/G3MP2large//B3LYP/6-31G(d) (232.1 kJ mol<sup>-1</sup>) differ by only 0.7 kJ mol<sup>-1</sup> and B3LYP/6-31G(d) (160.3 kJ mol<sup>-1</sup>)

and B3LYP/6-31+G(d) ( $167.8 \text{ kJ mol}^{-1}$ ) differ by only  $7.5 \text{ kJ mol}^{-1}$ . The activation energies, free energies and enthalpies of activation calculated using the BC6-31G(d) bromine basis set and the standard 6-31G(d) basis set are also found to be very similar at all levels of theory (Table 3.4). In the next step, intermediate  $I2^X$  is formed via  $TS2^C$ , where a Br atom from  $Br_3^-$  attacks the bromonium ion resulting in a gauche 1,2- dibromoethane/ $Br_2$  complex. The corresponding activation energy ( $\Delta E_{a,TS2^C}$ ) is  $50.7 \text{ kJ mol}^{-1}$  at G3MP2B3. The activation energy obtained by MP2/6-31G(d) ( $55.1 \text{ kJ mol}^{-1}$ ) again gives the best agreement with G3MP2B3. Finally, the product, trans-1,2-dibromoethane (P) is formed via transition state  $TS3^X$ , which involves rotation about the C-C bond. The activation energy for this last step ( $\Delta E_{a,TS3^X}$ ) is  $15.6 \text{ kJ mol}^{-1}$  at G3MP2B3. All structures for pathway C were also obtained for the reaction in  $CCl_4$  solution at MP2/6-31G(d). The free energy of activation for the rate-determining step in  $CCl_4$  decreases by  $7.9 \text{ kJ mol}^{-1}$ .

### 3.3.2.2 Pathway D:

The structures of pathway D are shown in Figure 3.7. The relative energies of reactants, intermediates, transitions states and products are shown in Figure 3.8. Activation energies, free energies and enthalpies of activation are given in Table 3.5. The first step of pathway D involves formation of an interesting stable intermediate, trans-1-bromo-2-tribromoethane ( $I1^D$ ).  $I1^D$  is formed via transition state  $TS1^D$ , with an activation energy ( $\Delta E_{a,TS1^D}$ ) of  $204.3 \text{ kJ mol}^{-1}$  at the G3MP2B3 level. In  $TS1^D$  one Br atom adds to one of the C atoms of  $C=C$ , while  $Br_3^-$  adds to the other C resulting in a trans configuration (Figure 3.7).

The IRC analysis confirmed that TS1<sup>D</sup> leads to R2 and I1<sup>D</sup>. Intermediate I1<sup>D</sup> is converted to intermediate I2<sup>X</sup> via TS2<sup>D</sup>, with an activation energy of 180.2 kJ mol<sup>-1</sup> at the G3MP2B3 level of theory. The transition state (TS2<sup>D</sup>) structure consists of two bond ruptures (Br-Br and C-Br) and one bond formation (C-Br). The last step, I2<sup>X</sup> → P is the same as for pathway C (Figures 3.5 and 3.6). A similar mechanism is found in CCl<sub>4</sub> solution for this reaction. The solvent model used in this study predicts that the free energy of activation for this pathway would be reduced in CCl<sub>4</sub>. For the rate-determining step, ΔG<sup>‡</sup> is lowered by 9.4 and 15.4 kJ mol<sup>-1</sup> at the MP2/6-31G(d) and B3LYP/6-31G(d) levels, respectively.

### 3.3.2.3 Pathway E:

The geometries for the reactants, intermediates, transition states, and products involved in pathway E are shown in Figure 3.9. The relative energies of reactants, intermediates, transition states, and products for pathway E are shown in Figure 3.10. The activation energies, free energies of activation and enthalpies of activation are given in Table 3.6. Pathway E involves a perpendicular attack by one Br<sub>2</sub> and a sidewise attack by the other Br<sub>2</sub> (TS1<sup>E</sup>) which leads to intermediate I1<sup>F</sup> (Figure 3.9). I1<sup>F</sup> can lead to product P through two different channels (1 and 2). The first step of pathway E and the first step of channel 1 are only obtained at the HF level of theory. However, the activation energies for the first step of this pathway are extremely high (476.0 and 315.6 kJ mol<sup>-1</sup> at the HF/6-31G(d) and MP2/G3MP2large//HF/6-31G(d) levels of theory, respectively). The results are simply presented here for completeness.

### 3.3.2.4 Pathway F:

The structures of reactants, intermediates, transition states and products of pathway F are shown in Figure 3.11. The relative energies of reactants, intermediates, transition states and products are shown in Figure 3.12. The activation energies, free energies and enthalpies of activation for the first step of pathway F and for the overall reaction are given in Table 3.7. All of the optimized structures of pathway F were obtained at the HF level, except for  $TS1^F$  despite several attempts. It was possible to obtain an optimized structure for  $TS1^F$  using MP2 and B3LYP. In addition to the two reactant complexes R1 and R2, a third ethene/ $2Br_2$  complex (R3) was found. For the ethene/ $2Br_2$  complexes, R1 and R3 have one  $Br_2$  perpendicular to  $C=C$  and both R1 and R3 are energetically more stable than R2. Pathway F is a multiple-step process. In the first step, complex R3 reacts through  $TS1^F$  to form intermediate  $I1^F$ . In R3 the Br-Br bond distance for the  $Br_2$  attacking  $C=C$  is the 2.345 Å at MP2/BC6-31G(d) level of theory while it increases to 2.815 Å in  $TS1^F$ . The IRC analysis at the MP2 and B3LYP levels confirmed that  $TS1^F$  leads to R3 and  $I1^F$ . The activation energy ( $\Delta E_{a,TS1^F}$ ) is 119.0 kJ mol<sup>-1</sup> at the G3MP2B3 level. Intermediate  $I1^F$  can also form from the direct attack by a  $Br_4$  molecule to ethene. However, the activation energy for the formation of  $Br_4$  ( $Br_2 + Br_2 \rightarrow Br_4$ ) (Figure 3.13) is high (174.6 kJ mol<sup>-1</sup> at G3MP2B3). Therefore ethene will more likely react with  $2Br_2$  than  $Br_4$ . All of the optimized structures from  $TS1^F$  to  $TS3^F$  (the last step) of pathway F involve bromonium/ $Br_3^-$  ion pairs all very close in energy (Figure 3.12). However,  $TS3^F$  has a slightly higher energy than  $TS1^F$  (7 kJ mol<sup>-1</sup> at G3MP2B3(BC)).

In the second step,  $I2^F$  is formed via  $TS2^F$  with an activation energy ( $\Delta E_{a,TS2^F}$ ) of only 2 kJ mol<sup>-1</sup> at HF/BC6-31G(d) level. Optimization of  $TS2^F$ ,  $I2^F$  and  $I3^F$  failed with MP2 and B3LYP. The structure of intermediate  $I2^F$  is very similar to intermediate  $I3^F$  with the only difference being in the position of the  $Br_3^-$ . Finally, the product (P) is formed via transition state  $TS3^F$ , which involves one C-Br bond rupture from the bromonium ion and a trans addition of Br from  $Br_3^-$  to the C. The IRC analysis confirmed that  $TS3^F$  leads to  $I3^F$  and P for all levels of theory. However, optimization of  $I3^F$  leads to reactant complex R3 at both MP2 and B3LYP. It has been found that the overall activation energy ( $\Delta E_{a,TS3^F}$ ) calculated from R3 to  $TS3^F$  is higher than the activation energy of the first step ( $\Delta E_{a,TS1^F}$ ) in pathway F for all levels of theory (Table 3.7). The overall reaction barriers in pathway F are 151.9, 111.6, 101.8 and 122.7 kJ mol<sup>-1</sup> at the HF/BC6-31G(d), MP2/BC6-31G(d), B3LYP/BC6-31G(d), and G3MP2B3 levels of theory, respectively. Unlike other pathways, the overall activation energy obtained at MP2 agrees well with that obtained at B3LYP. The activation energies, free energies and enthalpies of activation calculated using the BC6-31G(d) and standard 6-31G(d) basis sets differ by no more than 15.4 kJ mol<sup>-1</sup> ( $\Delta H_{TS1^F}^\ddagger$ ) and it is interesting to note that the B3LYP/6-31G(d) and MP2/BC6-31G(d) results are in excellent agreement (Table 3.7). Structures similar to those in gas phase were also obtained in CCl<sub>4</sub> solution at the MP2 and B3LYP levels. The overall free energy of activation in CCl<sub>4</sub> (Table 3.8) decreases by 49.7 and 32.7 kJ mol<sup>-1</sup> at the MP2/BC6-31G(d) and B3LYP/BC6-31G(d) levels from that of the gas phase.

### 3.3.3 Summary of overall reaction mechanisms investigated:

The most likely mechanism for the reaction of alkenes with one Br<sub>2</sub> is pathway B. The activation energies of the rate-determining step of pathway B for the reaction with ethene, propene, isobutene, flouroethene, chloroethene, (E)-1,2-difluoroethene and (E)-1,2-dichloroethene are 247.3, 200.4, 189.3, 224.2, 206.1, 220.1 and 217.1 kJ mol<sup>-1</sup>, respectively at MP2/BC6-31G(d) level of theory, while the barriers for pathway A are 256.4, 249.8, 244.8, 247.6, 244.9, 243.4 and 249.3 kJ mol<sup>-1</sup>, respectively. For the reaction of 2Br<sub>2</sub> with ethene, pathways C and D have almost the same barrier for the rate-determining step with G3MP2B3 activation energies of 207.3 and 204.4 kJ mol<sup>-1</sup>, respectively. Pathway E is predicted to have a high activation energy (315.6 kJ mol<sup>-1</sup> at MP2/G3MP2large//HF/6-31G(d)). The most likely mechanism for the reaction of ethene with 2Br<sub>2</sub> is pathway F with an overall barrier of 122.7 kJ mol<sup>-1</sup> at G3MP2B3. By Comparison of the most likely pathway for the reaction with one Br<sub>2</sub> (pathway B) and most likely pathway for the reaction with two Br<sub>2</sub> (pathway F), bromination should be mediated via 2Br<sub>2</sub> where the second Br<sub>2</sub> assists in the ionization of the reactant complex to form a bromonium/Br<sub>3</sub><sup>-</sup> ion pair.

### 3.3.4 Comparison with Experiment:

A general kinetic equation for the addition of bromine to alkenes is given as,<sup>4</sup>

$$-d[\text{Br}_2]/dt = k_2[\text{Br}_2][\text{A}] + k_3[\text{Br}_2]^2[\text{A}] + k_3[\text{Br}_3^-][\text{A}] \quad (1)$$

where [A] = [alkene].

Modro et al.<sup>10</sup> found that in the absence of bromide ion and at low bromine concentrations

( $[\text{Br}_2] < 10^{-3} \text{ M}$ ) in  $\text{CH}_3\text{COOH}$ , equation 1 reduces to the form

$$-\text{d}[\text{Br}_2]/\text{dt} = k_2[\text{Br}_2][\text{A}] \quad (2)$$

and under the same conditions in  $\text{CCl}_2\text{H}-\text{CCl}_2\text{H}$  a third-order rate dependence was found

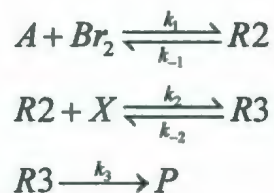
$$-\text{d}[\text{Br}_2]/\text{dt} = k_3[\text{Br}_2]^2[\text{A}] \quad (3)$$

The free energies of activation in  $\text{CH}_3\text{COOH}$  and in  $\text{CCl}_2\text{H}-\text{CCl}_2\text{H}$  were calculated from the experimental<sup>46</sup> rate constants obtained by equations 2 and 3. Equation 2 was also used by Dubois and Mouvier<sup>45</sup> to determine the rate constant for the bromination of ethene in  $\text{CH}_3\text{OH}$ . These experimental free energies of activation are given in Table 3.8. To compare our findings to experiment, four solvents with increasing polarity were chosen namely  $\text{CCl}_4$ ,  $\text{CH}_2\text{Cl}_2$ ,  $\text{CH}_2\text{Cl}-\text{CH}_2\text{Cl}$  and  $\text{CH}_3\text{OH}$ . The calculated overall free energies of activation for the most likely pathway (pathway F) in the reaction of ethene with  $2\text{Br}_2$  in  $\text{CCl}_4$ ,  $\text{CH}_2\text{Cl}_2$ ,  $\text{CH}_2\text{Cl}-\text{CH}_2\text{Cl}$  and  $\text{CH}_3\text{OH}$  are also given in Table 3.8. It has been found that the overall free energies of activation decrease with the increase of polarity of the solvent. The experimental values are also known<sup>47</sup> to decrease with the polarity of solvent. Although the experimental free energies in  $\text{CH}_3\text{COOH}$ ,  $\text{CCl}_2\text{H}-\text{CCl}_2\text{H}$  and  $\text{CH}_3\text{OH}$  were obtained from two different conditions, they also show decreasing free energies with increasing polarity from  $\text{CH}_3\text{COOH}$  to  $\text{CH}_3\text{OH}$  (Table 3.8). The calculated free energy of activation for the reaction of ethene with  $2\text{Br}_2$  in  $\text{CH}_2\text{Cl}_2$  is in excellent agreement with the experimental value obtained in  $\text{CCl}_2\text{H}-\text{CCl}_2\text{H}$ , differing by only  $1.8 \text{ kJ mol}^{-1}$  at B3LYP/BC6-31G(d). In this case, the two solvents,  $\text{CH}_2\text{Cl}_2$  and  $\text{CCl}_2\text{H}-\text{CCl}_2\text{H}$  have almost identical dielectric constants with values of 8.93 and 8.2, respectively. Similarly, the calculated activation energy in  $\text{CH}_2\text{Cl}-\text{CH}_2\text{Cl}$  (52.7

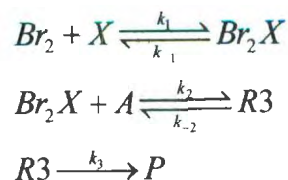
kJ mol<sup>-1</sup>) and the experimental activation energy in CCl<sub>2</sub>H-CCl<sub>2</sub>H (66.4 kJ mol<sup>-1</sup>) differ by only 13.7 kJ mol<sup>-1</sup> where the dielectric constant for CH<sub>2</sub>Cl-CH<sub>2</sub>Cl is 10.36 vs. 8.2 for CCl<sub>2</sub>H-CCl<sub>2</sub>H. As expected, a more polar solvent would result in a lower ΔG<sup>‡</sup>. It is worth mentioning here that the solvent models for CCl<sub>2</sub>H-CCl<sub>2</sub>H have not yet been implemented in Gaussian03 and hence CH<sub>2</sub>Cl-CH<sub>2</sub>Cl and CH<sub>2</sub>Cl<sub>2</sub> solvents were used in this study because these two solvents have almost similar structural features and dielectric constants compared to CCl<sub>2</sub>H-CCl<sub>2</sub>H.

The experimental free energy of activation obtained from the rate constant for the bromination of ethene in methanol is 64.6 kJ mol<sup>-1</sup> and found to be first order in Br<sub>2</sub>.<sup>45</sup> This barrier is significantly higher than the computed free energy of activation for the reaction with 2Br<sub>2</sub> (39.2 kJ mol<sup>-1</sup> at B3LYP/BC6-31G(d)). This disagreement may be explained in a number of ways. One possibility is that perhaps due to the relatively high polarity of CH<sub>3</sub>OH (dielectric constant of 32.63), both Br<sub>2</sub> and 2Br<sub>2</sub> mechanisms occur simultaneously and the observed experimental free energy values would correspond to an average of the two. Alternatively and more likely, the mechanism in polar protic solvents may be different. We propose the following two cases:

Case 1:



Case 2:



where X can be Br<sub>2</sub> or a solvent molecule.

Both cases lead to the same rate expression [See Appendix D],

$$\frac{dP}{dt} = \frac{k_1 k_2 k_3}{k_{-1} k_{-2}} [\text{A}][\text{Br}_2][\text{X}]$$

When [X] = [Br<sub>2</sub>],

$$\frac{dP}{dt} = \left( \frac{k_1 k_2 k_3}{k_{-1} k_{-2}} \right) [\text{A}][\text{Br}_2]^2 \quad (4)$$

When [X] = [S],

$$\frac{dP}{dt} = \left( \frac{k_1 k_2 k_3}{k_{-1} k_{-2}} \right) [\text{S}][\text{A}][\text{Br}_2] \quad (5)$$

where, [S] = solvent.

Therefore for [X] = [Br<sub>2</sub>],

$$k_{\text{eff}} = \left( \frac{k_1 k_2}{k_{-1} k_{-2}} \right) k_3 \text{ and the reaction is third-order.}$$

For [X]=[S],

$$k_{\text{eff}} = \left( \frac{k_1 k_2 [\text{S}]}{k_{-1} k_{-2}} \right) k_3 \text{ and the reaction is second-order.}$$

Assuming  $\left( \frac{k_1 k_2}{k_{-1} k_{-2}} \right) \cong 1 \text{ mol}^{-1}$ , on the basis of the agreement between the calculated

and the experimental free energies for the reaction in a non-polar solvent (Table 3.8),  $k_{eff} \cong k_3[S]$  for equation (5). In this case, to compare the calculated and the experimental free energies of activation, the experimental rate constant must be divided by [S]. The resulting  $\Delta G^\ddagger_{exptl}$  is found to be 72.5 kJ mol<sup>-1</sup> which is in much better agreement with the calculated value (75.5 kJ mol<sup>-1</sup> at B3LYP/BC6-31G(d)) obtained from the reaction of ethene with Br<sub>2</sub> mediated by a single CH<sub>3</sub>OH molecule in CH<sub>3</sub>OH solution (pathway G) as shown in Figure 3.14. This is the first evidence that a solvent molecule also takes part in the bromination reaction for polar protic solvents such as CH<sub>3</sub>OH.

### 3.3.5 Thermodynamic results for the reaction of alkenes with Br<sub>2</sub>

The thermodynamic properties for the bromination reaction investigated are listed in Table 3.9. All of the reactions are found to be exothermic at all levels of theory and basis sets. The  $\Delta H$  values for the reaction of Br<sub>2</sub> with ethene and propene are -125.7 and -129.0 kJ mol<sup>-1</sup> at G3MP2B3 and -126.0, -91.7, -123.3, -121.0 and -94.4 kJ mol<sup>-1</sup> for isobutene, fluoroethene, chloroethene, (E)-1,2-difluoroethene and (E)-1,2-dichloroethene, respectively, at G3MP2B3(BC). The enthalpies of reaction at G3MP2 and G3MP2B3 levels for the reaction of Br<sub>2</sub> with ethene and propene differ by no more than 1.8 kJ mol<sup>-1</sup>. There is also excellent agreement between G3 theories and experimental<sup>48</sup> enthalpies for the reaction of Br<sub>2</sub> with ethene, propene and isobutene differing by no more than 7.5 kJ mol<sup>-1</sup> (CH<sub>3</sub>-CH<sub>2</sub>=CH<sub>2</sub> + Br<sub>2</sub> → trans-CH<sub>3</sub>-CH<sub>2</sub>Br-CH<sub>2</sub>Br). However, the G3MP2B3(BC) enthalpy for

(E)-1, 2-dichloroethene differs by  $22.0 \text{ kJ mol}^{-1}$  from experiment. On the basis of the agreement between experimental and calculated enthalpies at G3 theories, the error is most likely in the experimental value. All of the reactions were also exergonic at all the levels of theory and basis sets. The free energies of reaction with ethene and propene are  $-84.3$  and  $-83.8 \text{ kJ mol}^{-1}$  at G3MP2B3 and  $-79.9$ ,  $-43.5$ ,  $-78.8$ ,  $-75.6$  and  $-47.8 \text{ kJ mol}^{-1}$  for isobutene, fluoroethene, chloroethene, (E)-1,2,-difluoroethene and (E)-1,2-dichloroethene, respectively at G3MP2B3(BC). In general, B3LYP provides reaction enthalpies and free energies that are in better agreement with G3 theories than HF and MP2. However, for chloroethene and (E)-1, 2-dichloroethene, the thermodynamic values obtained using G3MP2B3(BC) fall between MP2 and B3LYP values. For the reaction with ethene, the gas-phase free energies of reaction at MP2/6-31G(d) and B3LYP/6-31G(d) levels are  $-110.5$  and  $-81.3 \text{ kJ mol}^{-1}$ , which decrease to  $-111.1$  and  $-92.2 \text{ kJ mol}^{-1}$  in  $\text{CCl}_4$ . Similarly, the MP2/6-31G(d) and B3LYP/6-31G(d) free energies for the reaction with propene are  $-107.1$  and  $-68.7 \text{ kJ mol}^{-1}$  in the gas phase, which decrease to  $-109.0$  and  $-77.8 \text{ kJ mol}^{-1}$  in  $\text{CCl}_4$ .

### 3.3.6 Performance of Theory/Basis set:

All of the reactions studied in this work are isogyric. When comparing the HF results with other levels of theory, it is evident that electron correlation is quite important in these reactions for activation energies. However, it is not that significant for reaction enthalpies and free energies. In general, activation energies calculated using MP2 consistently agree better with the G3 theories, while B3LYP appears to underestimate some activation energies.

However, for pathway F, which is the likely pathway for the reaction of  $2\text{Br}_2$  with ethene, both MP2 and B3LYP agree well with the G3 results. Activation energies calculated using the standard 6-31G(d) bromine basis set differ by no more than  $16.8 \text{ kJ mol}^{-1}$  (HF, pathway C) compared to the BC6-31G(d) basis set results and the differences decrease from HF to MP2 and B3LYP levels of theory. There was little to no effect on the barriers by the addition of diffuse functions when compared to G3 theories. Even use of the G3MP2large basis set does not improve the barriers.

For thermodynamics, the G3MP2 and G3MP2B3 theories differ by no more than  $3 \text{ kJ mol}^{-1}$  for reaction enthalpies and free energies ( $\Delta G$  for  $\text{CH}_2=\text{CH}_2 + \text{Br}_2 \rightarrow \text{CH}_2\text{Br}-\text{CH}_2\text{Br}$ ). The G3 theories are also in excellent agreement with experiment, except in the case of  $\text{CHCl}-\text{CHCl} + \text{Br}_2 \rightarrow \text{CHClBr}-\text{CHClBr}$ , where B3LYP/BC6-31G(d) differs by only  $3 \text{ kJ mol}^{-1}$ , whereas G3MP2B3(BC) differs by  $22 \text{ kJ mol}^{-1}$  from experiment<sup>48</sup>. In comparison to MP2, thermodynamic values calculated using B3LYP provide reaction enthalpies and free energies that are consistently in better agreement with G3 values. Thermodynamic values calculated using the standard 6-31G(d) bromine basis set differ by no more than  $8.1 \text{ kJ mol}^{-1}$  (B3P86,  $\text{CH}_3-\text{CH}_2=\text{CH}_2 + \text{Br}_2 \rightarrow \text{CH}_3-\text{CH}_2\text{Br}-\text{CH}_2\text{Br}$ ) compared to the Binning-Curtiss 6-31G(d) basis set results. However, the reaction enthalpies and free energies differ significantly when diffuse functions are added to the two basis sets. For example, the enthalpy for  $\text{CH}_3-\text{CH}_2-\text{CH}_2 + \text{Br}_2 \rightarrow \text{CH}_3-\text{CH}_2\text{Br}-\text{CH}_2\text{Br}$  calculated at the B3LYP 6-31+G(d) and B3LYP/BC6-31+G(d) levels of theory differs by  $32.1 \text{ kJ mol}^{-1}$ .

### 3.3.7 Exploring Heats of Formation ( $\Delta H_f$ ) :

From the  $\Delta H$  values of reactions calculated at the G3 theories in this study, it is possible to calculate heats of formation for some alkenes and dibromoalkanes. The  $\Delta H_f$  values obtained in this study are given in Table 3.10. From the G3MP2B3 enthalpy of reaction for  $\text{CH}_2=\text{CH}_2 + \text{Br}_2 \rightarrow \text{trans-CH}_2\text{Br-CH}_2\text{Br}$  ( $-125.7 \text{ kJ mol}^{-1}$ ) and the most recent and reliable experimental  $\Delta H_f(\text{CH}_2=\text{CH}_2)$  and  $\Delta H_f(\text{Br}_2)$  (given in Table 3.10),  $\Delta H_f$  (trans- $\text{CH}_2\text{Br-CH}_2\text{Br}$ ) is calculated to be  $-42.3 \text{ kJ mol}^{-1}$ , which is in good agreement with experiment ( $-37.52 \text{ kJ mol}^{-1}$ ). Similarly,  $\Delta H_f(\text{CH}_2=\text{CH}_2)$  is calculated from the same reaction enthalpy and by using the experimental  $\Delta H_f(\text{Br}_2)$  and  $\Delta H_f(\text{trans-CH}_2\text{Br-CH}_2\text{Br})$ . The resulting  $\Delta H_f(\text{CH}_2=\text{CH}_2)$  is  $57.3 \text{ kJ mol}^{-1}$ , the value being in excellent agreement with experiment. Following the same procedure, it was possible to calculate  $\Delta H_f$  for  $\text{CH}_3\text{-CH}_2=\text{CH}_2$ , trans- $\text{CH}_3\text{-CH}_2\text{Br-CH}_2\text{Br}$ ,  $(\text{CH}_3)_2\text{C}=\text{CH}_2$  and trans- $(\text{CH}_3)_2\text{CBr-CH}_2\text{Br}$  using the enthalpies of reaction for  $\text{CH}_3\text{-CH}_2=\text{CH}_2 + \text{Br}_2 \rightarrow \text{trans-CH}_3\text{-CH}_2\text{Br-CH}_2\text{Br}$  ( $-129.0 \text{ kJ mol}^{-1}$  at G3MP2B3) and  $(\text{CH}_3)_2\text{C}=\text{CH}_2 + \text{Br}_2 \rightarrow \text{trans-}(\text{CH}_3)_2\text{CBr-CH}_2\text{Br}$  ( $-126.0 \text{ kJ mol}^{-1}$  at G3MP2B3(BC)), along with experimental  $\Delta H_f$  for  $\text{Br}_2$ ,  $\text{CH}_3\text{-CH}_2=\text{CH}_2$ , trans- $\text{CH}_3\text{-CH}_2\text{Br-CH}_2\text{Br}$ ,  $(\text{CH}_3)_2\text{C}=\text{CH}_2$  and trans- $(\text{CH}_3)_2\text{CBr-CH}_2\text{Br}$  obtained from the literature. These  $\Delta H_f$  values are also in excellent agreement with the experimental values, all within  $6.6 \text{ kJ mol}^{-1}$ . No experimental or theoretical  $\Delta H_f$  have been reported for trans- $\text{CHFBr-CH}_2\text{Br}$ , trans- $\text{CHClBr-CH}_2\text{Br}$ , (E)- $\text{CHFBr=CHFBr}$  and (E)- $\text{CHClBr=CHClBr}$ . In this study,  $\Delta H$  for

$\text{CHF}=\text{CH}_2 + \text{Br}_2 \rightarrow \text{trans-CHFBr-CH}_2\text{Br}$  ( $-91.7 \text{ kJ mol}^{-1}$  at G3MP2B3(BC)),  $\text{CHCl}=\text{CH}_2 + \text{Br}_2 \rightarrow \text{trans-CHClBr-CH}_2\text{Br}$  ( $-123.3 \text{ kJ mol}^{-1}$  at G3MP2B3(BC)),  $(\text{E})\text{-CHF}=\text{CHF} + \text{Br}_2 \rightarrow \text{trans-CHFBr-CHFBr}$  ( $-121.0 \text{ kJ mol}^{-1}$  at G3MP2B3(BC)) and  $(\text{E})\text{-CHCl}=\text{CHCl} + \text{Br}_2 \rightarrow \text{trans-CHClBr-CHClBr}$  ( $-94.4 \text{ kJ mol}^{-1}$  at G3MP2B3(BC)) have been obtained. From this data and the experimental  $\Delta H_f$  of  $\text{CHF}=\text{CH}_2$ ,  $\text{CHCl}=\text{CH}_2$ ,  $(\text{E})\text{-CHF}=\text{CHF}$  and  $(\text{E})\text{-CHCl}=\text{CHCl}$ , the  $\Delta H_f$  values for  $\text{trans-CHFBr-CH}_2\text{Br}$ ,  $\text{trans-CHClBr-CH}_2\text{Br}$ ,  $\text{trans-CHFBr-CHFBr}$  and  $\text{trans-CHClBr-CHClBr}$  were calculated to be  $-214.8$ ,  $-63.4$ ,  $-400.1$  and  $-61.8 \text{ kJ mol}^{-1}$ , respectively.

### 3.4 Conclusions

A comprehensive investigation was conducted on the possible mechanisms involved in the reaction of alkenes with  $\text{Br}_2$  and  $2\text{Br}_2$ . It has been found that there are two possible mechanisms for the reaction of alkenes with one  $\text{Br}_2$ ; one involving a perpendicular attack on the  $\text{C}=\text{C}$  double bond producing a bromonium/ $\text{Br}^-$  ion pair. However, the mechanism does not lead to product. The other pathway is a sidewise attack by a  $\text{Br}_2$  on the  $\text{C}=\text{C}$  bond producing first a bromonium/ $\text{Br}^-$  ion pair followed by formation of the  $\text{trans-1,2-}$  dibromoalkane. Therefore, the only mechanism found for reaction with one  $\text{Br}_2$  molecule producing  $\text{trans-1,2-}$  dibromoalkane is through sidewise attack by  $\text{Br}_2$ . Reaction of ethene with  $2\text{Br}_2$  involves several different pathways all producing  $\text{trans-1,2-}$  dibromoalkane as the product. The overall reaction barrier is the lowest for the reaction of ethene +  $2\text{Br}_2$ . The

bromination reactions of alkenes in  $\text{CCl}_4$  predict mechanisms similar to that obtained in the gas phase. However, the solvent model predicts a lowering of free energies of activation for the rate-determining steps of all the reactions in  $\text{CCl}_4$  solution. The overall free energy of activation obtained from the most likely pathway (pathway F) involving  $2\text{Br}_2$  is in excellent agreement with experiment for the reaction in non polar aprotic solvents. For polar protic solvents, the calculated activation energies obtained from the reaction with a single  $\text{Br}_2$  mediated by a solvent molecule are in excellent agreement with experiment. The calculated free energies of activation decrease with the polarity of solvents, which is in agreement with the experimental observations (Table 3.8). All of the reactions are found to be exothermic and exergonic for the formation of the trans-1,2-dibromoalkane product.

### 3.5 References

- (1) Smith, M. B.; March, J. *March's Advanced Organic Chemistry: Reactions, Mechanisms, and Structure*, 6<sup>th</sup> ed.; Wiley-Interscience: Hoboken NJ, 2007.
- (2) de la Mare, P. B. D.; Bolton, R., *Electrophilic Additions to Unsaturated Systems*; 2nd ed.; Elsevier: New York, 1982.
- (3) Brown, R. S.; Slebocka-Tilk, H.; Bennet, A. J.; Bellucci, G.; Bianchini, R.; Ambrosetti, R., *J. Am. Chem. Soc.*, **1990**, *112*, 6310.
- (4) Schmid, G. H.; Garrat, D. G., In *The Chemistry of Double-Bonded Functional Groups*; Patai, S., Ed.; Wiley: New York, 1977; Suppl. A, Part 2, p 725.

- (5) Brown, R. S.; Gedye, R.; Slebocka-Tilk, H.; Buschek, J.; Kopecky, K., *J. Am. Chem. Soc.*, **1984**, *106*, 4515.
- (6) Bellucci, G.; Chiappe, C.; Marioni, F., *J. Am. Chem. Soc.*, **1987**, *109*, 515.
- (7) Bellucci, G.; Bianchini, R.; Chiappe, C.; Marioni, F.; Spagna, R., *J. Am. Chem. Soc.*, **1988**, *110*, 546.
- (8) Roberts, I.; Kimball, G. E., *J. Am. Chem. Soc.*, **1937**, *59*, 947.
- (9) Olah, G. A.; Bollinger, J. M., *J. Am. Chem. Soc.*, **1968**, *90*, 947.
- (10) Olah, G. A.; Bollinger, J. M.; Brinich, J., *J. Am. Chem. Soc.*, **1968**, *90*, 2587.
- (11) Berman, D. W.; Anicich, V.; Beauchamp, J. L., *J. Am. Chem. Soc.*, **1979**, *101*, 1239.
- (12) Wieting, R. D.; Staley, R. H.; Beauchamp, J. L., *J. Am. Chem. Soc.*, **1974**, *96*, 7552.
- (13) Staley, R. H.; Wieting, R. D.; Beauchamp, J. L., *J. Am. Chem. Soc.*, **1977**, *99*, 5964.
- (14) Kim, J. K.; Findlay, M. C.; Henderson, W. G.; Caserio, M. C., *J. Am. Chem. Soc.*, **1973**, *95*, 2184.
- (15) Angelini G.; Speranza M., *J. Am. Chem. Soc.*, **1981**, *103*, 3792.
- (16) Tsai, B. P.; Werner, A. S.; Baer, T., *J. Chem. Phys.*, **1975**, *63*, 4384.
- (17) McLafferty, F. W., *Anal. Chem.*, **1962**, *34*, 2.
- (18) Strating, J.; Wieringa, J. H.; Wynberg, H., *J. Chem. Soc. D: Chem. Commun.*, **1969**, 907.
- (19) Slebocka-Tilk H.; Ball R. G.; Brown R. S., *J. Am. Chem. Soc.*, **1985**, *107*, 4504.
- (20) Bellucci, G.; Chiappe, C.; Bianchini, R.; Lenoir, D.; Herges, R., *J. Am. Chem. Soc.*, **1995**, *117*, 12001.

- (21) Olah, G. A.; Prakash, G. K. S., *J. Org. Chem.* **1977**, *42*, 580.
- (22) Koerner, T.; Brown, R. S.; Gainsforth J. L.; Klobukowski, M., *J. Am. Chem. Soc.*, **1998**, *120*, 5628.
- (23) Chretien, J. R.; Coudert, J.; Ruasse, M., *J. Org. Chem.*, **1993**, *58*, 1917.
- (24) Olah, G. A., *Halonium Ions*; Wiley: New York, 1975.
- (25) Garnier, F.; Dubois, J. E., *Bull. Soc. Chim. Fr.*, **1968**, 3797.
- (26) Olah, G. A.; Hockswender Jr., T. R., *J. Am. Chem. Soc.*, **1974**, *96*, 3574.
- (27) Yamabe, S.; Minato, T.; Inagaki, S., *J. Chem. Soc., Chem. Commun.*, **1988**, 532.
- (28) Hamilton, T. P.; Schaefer, H. F., *J. Am. Chem. Soc.*, **1990**, *112*, 8260.
- (29) Cammi, R.; Mennucci, B.; Pomelli, C.; Cappelli, C.; Corni, S.; Frediani, L.; Trucks, G. W.; Frisch, M., *J. Theor. Chem. Acc.*, **2004**, *111*, 66.
- (30) Strnad, M.; Martins-Costa, M. T. C.; Millot, C.; Tunon, I.; Ruiz-Lopez, M. F.; Rivail, J. L.; *J. Chem. Phys.*, **1997**, *106*, 3643.
- (31) Hamilton, T. P.; Schaefer, H. F., *J. Am. Chem. Soc.*, **1991**, *113*, 7147.
- (32) Cossi, M.; Persico, M.; Tomas, J., *J. Am. Chem. Soc.*, **1994**, *116*, 5373.
- (33) Chiappe, C.; Lenoir, D.; Pomelli, C. S.; Bianchini, R., *Phys. Chem. Chem. Phys.*, **2004**, *6*, 3235.
- (34) Ruiz, E.; Salahub, D. R.; Vela, A., *J. Am. Chem. Soc.* **1995**, *117*, 1141.
- (35) Lenoir D.; Chiappe, C., *Chem. Eur. J.*, **2003**, *9*, 1036.
- (36) Curtiss L. A.; Redfern P.C.; Raghavachari K.; Rassolov V.; Pople J. A., *J. Chem. Phys.*, **1999**, *110*, 4703.

- (37) Baboul A. G.; Curtiss L. A.; Redfern P. C.; Raghavachari K., *J. Chem. Phys.*, **1999**, *110*, 7650.
- (38) Frisch, M. J.; Trucks, G. W.; Schlegel, H. B.; Scuseria, G. E.; Robb, M. A.; Cheeseman, J. R.; Montgomery, Jr., J. A.; Vreven, T.; Kudin, K. N.; Burant, J. C.; Millam, J. M.; Iyengar, S. S.; Tomasi, J.; Barone, V.; Mennucci, B.; Cossi, M.; Scalmani, G.; Rega, N.; Petersson, G. A.; Nakatsuji, H.; Hada, M.; Ehara, M.; Toyota, K.; Fukuda, R.; Hasegawa, J.; Ishida, M.; Nakajima, T.; Honda, Y.; Kitao, O.; Nakai, H.; Klene, M.; Li, X.; Knox, J. E.; Hratchian, H. P.; Cross, J. B.; Bakken, V.; Adamo, C.; Jaramillo, J.; Gomperts, R.; Stratmann, R. E.; Yazyev, O.; Austin, A. J.; Cammi, R.; Pomelli, C.; Ochterski, J. W.; Ayala, P. Y.; Morokuma, K.; Voth, G. A.; Salvador, P.; Dannenberg, J. J.; Zakrzewski, V. G.; Dapprich, S.; Daniels, A. D.; Strain, M. C.; Farkas, O.; Malick, D. K.; Rabuck, A. D.; Raghavachari, K.; Foresman, J. B.; Ortiz, J. V.; Cui, Q.; Baboul, A. G.; Clifford, S.; Cioslowski, J.; Stefanov, B. B.; Liu, G.; Liashenko, A.; Piskorz, P.; Komaromi, I.; Martin, R. L.; Fox, D. J.; Keith, T.; Al-Laham, M. A.; Peng, C. Y.; Nanayakkara, A.; Challacombe, M.; Gill, P. M. W.; Johnson, B.; Chen, W.; Wong, M. W.; Gonzalez, C.; Pople, J. A. Gaussian 03, Revision B.05, Gaussian, Inc., Wallingford CT, 2004.
- (39) Islam, S. M.; Hollett, J. W.; Poirier, R. A., *J. Phys. Chem. A.*, **2007**, *111*, 526.
- (40) Rassolov, V. A.; Ratner, M. A.; Pople, J. A.; Redfern, P. C.; Curtiss, L. A., *J. Computational Chemistry*, **2001**, *22*, 976.
- (41) Binning Jr, R. C.; Curtiss, L. A., *J. Comp. Chem.*, **1990**, *11*, 1206.
- (42) Curtiss, L. A.; Redfern, P. C.; Rassolov, V.; Kedziora, G. S.; Pople, J. A. *J. Chem. Phys.*, **2001**, *114*, 9287.

- (43) <http://chemistry.anl.gov/compmat/comptherm.htm>
- (44) Dubois, J. E.; Mouvier, G., *Tetrahedron Lett.*, **1963**, 1325.
- (45) Dubois, J. E.; Mouvier, G., *Bull. Soc. Chim. Fr.*, **1968**, 1426.
- (46) Modro, A.; Schmid, G. H.; Yates, K., *J. Org. Chem.*, **1977**, *42*, 3673.
- (47) Hanna, J. G.; Siggia, S., *Anal. Chem.*, **1965**, *37*, 690.
- (48) Chase, M. W., NIST-JANAF Thermochemical Tables, 4th ed., Monograph 9. *J. Phys. Chem. Ref. Data*, **1998**, 1-1951.
- (49) Wagman, D. D.; Evans, W. H.; Parker, V. B.; Shumm, R. H.; Halow, I.; Bailey, S.M.; Churney, K. L.; Nuttall, R. L., *J. Phys. Chem. Ref. Data.* **1982**, *11* (2).

**TABLE 3.1: Activation energies, free energies and enthalpies of activation (kJ mol<sup>-1</sup>) at 298.15K for the reaction of CH<sub>2</sub>=CH<sub>2</sub>, CH<sub>3</sub>-CH<sub>2</sub>=CH<sub>2</sub>, (CH<sub>3</sub>)<sub>2</sub>CH=CH<sub>2</sub>, CH<sub>2</sub>=CHF, CH<sub>2</sub>=CHCl, (E)-CHF=CHF and (E)-CHCl=CHCl with Br<sub>2</sub> (Pathway A).<sup>a,b</sup>**

Level/Basis Set	$\Delta E_{a,TS}^A$	$\Delta G_{TS}^\ddagger{}^A$	$\Delta H_{TS}^\ddagger{}^A$
		CH <sub>2</sub> =CH <sub>2</sub> + Br <sub>2</sub>	
MP2/6-31G(d)	238.4	229.8	235.2
MP2/BC6-31G(d)	256.4	251.7	250.6
MP2/6-31+G(d)	238.3	231.7	235.2
MP2(FULL)/6-31G(d)	240.9	231.1	237.6
MP2/G3MP2large //MP2(FULL)/6-31G(d)	268.5		
		CH <sub>3</sub> -CH <sub>2</sub> =CH <sub>2</sub> + Br <sub>2</sub>	
MP2/6-31G(d)	230.6	219.6	227.2
MP2/BC6-31G(d)	249.8	236.6	246.3
MP2(FULL)/6-31G(d)	233.5	221.8	230.1
MP2/G3MP2large //MP2(FULL)/6-31G(d)	262.6		
		(CH <sub>3</sub> ) <sub>2</sub> C=CH <sub>2</sub> + Br <sub>2</sub>	
MP2/6-31G(d)	224.1	211.7	220.7
MP2/BC6-31G(d)	244.8	230.7	241.1
MP2(FULL)/6-31G(d)	227.6	214.4	224.0
MP2/G3MP2large //MP2(FULL)/6-31G(d)	258.2		
		CHF=CH <sub>2</sub> + Br <sub>2</sub>	
MP2/6-31G(d)	230.2	224.7	227.6
MP2/BC6-31G(d)	247.6	241.3	244.8
MP2(FULL)/6-31G(d)	232.4	226.3	229.8
MP2/G3MP2large //MP2(FULL)/6-31G(d)	259.6		
		CHCl=CH <sub>2</sub> + Br <sub>2</sub>	
MP2/6-31G(d)	228.2	223.5	225.7
MP2/BC6-31G(d)	244.9	238.7	242.1
MP2(FULL)/6-31G(d)	230.4	224.9	227.9
MP2/G3MP2large //MP2(FULL)/6-31G(d)	255.9		
		(E)-CHF=CHF + Br <sub>2</sub>	

MP2/6-31G(d)	226.1	222.2	223.2
MP2/BC6-31G(d)	243.3	231.4	242.8
MP2(FULL)/6-31G(d)	228.0	222.9	225.1
MP2/G3MP2large	254.9		
//MP2(FULL)/6-31G(d)			
		(E)-CHCl	CHCl + Br <sub>2</sub>
MP2/6-31G(d)	232.6	226.5	229.4
MP2/BC6-31G(d)	249.3	241.2	246.0
MP2(FULL)/6-31G(d)	234.4	226.5	231.2
MP2/G3MP2large	256.1		
//MP2(FULL)/6-31G(d)			

<sup>a</sup> Barrier as defined in Figure 3.1.

<sup>b</sup> The products are all in trans conformation.

TABLE 3.2: Activation energies, free energies and enthalpies of activation ( $\text{kJ mol}^{-1}$ ) at 298.15K for the reaction of  $\text{CH}_2=\text{CH}_2$ ,  $\text{CH}_3-\text{CH}_2=\text{CH}_2$ ,  $(\text{CH}_3)_2\text{CH}=\text{CH}_2$ ,  $\text{CH}_2=\text{CHF}$  and  $\text{CH}_2=\text{CHCl}$  with  $\text{Br}_2$  (Pathway B).<sup>a,b,c,d</sup>

Level/Basis Set	$\Delta E_{a,\text{TS1}}^{\text{B}}$	$\Delta G_{\text{TS1}}^{\ddagger \text{B}}$	$\Delta H_{\text{TS1}}^{\ddagger \text{B}}$	$\Delta E_{a,\text{TS2}}^{\text{B}}$	$\Delta G_{\text{TS2}}^{\ddagger \text{B}}$	$\Delta H_{\text{TS2}}^{\ddagger \text{B}}$	$\Delta E_{a,\text{TS3}}^{\text{B}}$	$\Delta G_{\text{TS3}}^{\ddagger \text{B}}$	$\Delta H_{\text{TS3}}^{\ddagger \text{B}}$
$\text{CH}_2=\text{CH}_2 + \text{Br}_2 \rightarrow \text{CH}_2\text{Br}-\text{CH}_2\text{Br}$									
HF/6-31G(d)	303.0	335.3	301.5	42.7	38.6	37.4	11.4	15.5	9.5
HF/BC6-31G(d)	300.3	320.9	298.5	44.5	40.4	39.4	14.7	16.8	12.6
MP2/6-31G(d)	252.9	275.9	251.0	60.8	57.1	56.5	15.0	15.2	12.7
$\text{CCl}_4^{\text{e}}$		262.9			55.8			16.4	
MP2/BC6-31G(d)	247.3	263.5	245.1	58.3	54.8	54.2	18.3	20.0	16.1
B3LYP/6-31G(d)	186.7	212.9	184.7	(36.9)	(33.2)	(37.2)	10.7	11.2	8.5
$\text{CCl}_4^{\text{e}}$		191.0			(67.6)			12.3	
B3LYP/BC6-31G(d)	189.1	206.1	186.4	12.3 <sup>f</sup>	10.3 <sup>f</sup>	9.2 <sup>f</sup>	14.0	14.2	11.7
				(9.1)	(8.7)	(6.2)			
B3LYP/6-31+G(d)	193.7	225.7	191.8	(40.8)	(46.4)	(38.4)	10.8	11.2	8.5
B3LYP/BC6-31+G(d)	188.0	208.2	183.3	(14.2)	(13.5)	(11.2)	15.7	15.9	13.2
B3P86/BC6-31G(d)	188.5	199.1	185.9	21.7	18.5	18.4	15.6	15.7	13.3
B3PW91/6-31G(d)	195.1	220.5	195.5	(52.5)	(52.8)	(50.1)	11.6	12.1	9.4
B3PW91/BC6-31G(d)	193.5	214.4	190.7	21.4	18.0	18.1	15.1	15.2	12.9
MP2/G3MP2large	250.6	279.0	244.8	63.5	64.1	62.7	16.0	20.5	14.1
//MP2(FULL)/6- MP2/G3MP2large	262.0	285.2	256.9	-	-	-	15.6	16.6	13.8
//B3LYP/6-31G(d) G3MP2	-	-	-	-	-	-	14.4	18.9	12.6

G3MP2B3	-	-	-	-	-	-	13.9	14.9	12.1
	$\text{CH}_3\text{-CH}_2\text{=CH}_2 + \text{Br}_2 \rightarrow \text{CH}_3\text{-CH}_2\text{Br-CH}_2\text{Br}$								
HF/6-31G(d)	286.7	317.4	284.5	(17.7)	(13.5)	(12.7)	20.8	23.8	19.0
HF/BC6-31G(d)	283.3	302.2	280.8	22.3	18.5	17.3	23.3	26.1	21.5
MP2/6-31G(d)	201.1	213.2	193.4	45.7	38.8	40.2	23.6	26.3	21.7
$\text{CCl}_4^e$		233.5			42.6			26.6	
MP2/BC6-31G(d)	200.4	204.0	190.3	45.0	40.4	39.9	26.8	29.1	24.8
B3LYP/6-31G(d)	167.2	188.5	164.4	(-1.7)	(-3.2)	(-8.6)	17.9	20.9	16.0
B3LYP/BC6-31G(d)	168.1	176.3	167.5	(0.1)	(-1.5)	(-3.8)	20.6	23.1	18.6
$\text{CCl}_4^e$		165.9			(42.7)			21.6	
B3LYP/6-31+G(d)	173.4	203.4	170.8	(0.6)	(-0.9)	(-6.8)	18.1	21.2	16.2
B3LYP/BC6-31+G(d)	163.7	177.3	160.7	(8.8)	(6.1)	(4.8)	23.2	26.2	21.3
B3P86/6-31G(d)	167.1	191.3	164.1	-	-	-	19.0	21.9	17.1
B3P86/BC6-31G(d)	166.3	175.9	162.6	13.6	10.3	10.0	22.1	24.5	20.1
B3PW91/6-31G(d)	174.8	205.1	171.8	(6.1)	(0.0)	(4.7)	18.7	21.7	16.9
B3PW91/BC6-31G(d)	170.9	176.4	170.0	13.3	11.0	9.8	21.8	24.3	19.8
MP2/G3MP2large	230.7	252.6	228.7	48.9	43.3	48.6	23.9	26.0	23.1
//MP2(FULL)/6- MP2/G3MP2large	243.1	263.5	239.3	-	-	-	23.6	26.6	21.5
//B3LYP/6-31G(d)									
G3MP2	-	-	-	37.0	31.4	36.7	22.4	24.5	21.6
G3MP2B3	-	-	-	-	-	-	22.0	25.1	20.0
	$(\text{CH}_3)_2\text{C=CH}_2 + \text{Br}_2 \rightarrow (\text{CH}_3)_2\text{CBr-CH}_2\text{Br}$								
HF/BC6-31G(d)	276.2	289.0	272.3	56.1	58.1	52.2	24.6	27.6	22.7
MP2/BC6-31G(d)	189.3	189.7	178.4	54.2	53.0	50.6	28.3	30.8	26.1

B3LYP/BC6-31G(d)	150.7	158.8	145.4	(21.2)	(24.1)	(18.8)	21.3	24.5	19.3
B3LYP/BC6-31+G(d)	146.6	155.0	142.3	(21.3)	(24.3)	(18.8)	24.6	27.6	22.5
B3P86/BC6-31G(d)	147.2	155.1	141.6	(27.4)	(29.4)	(24.9)	23.1	26.2	21.1
B3PW91/BC6-31G(d)	152.2	161.5	146.7	(27.7)	(30.1)	(25.2)	22.9	26.0	20.8
MP2/G3MP2large	203.3	214.1	200.7	-	-	-	25.2	28.2	22.9
//B3LYP/BC6-31G(d)									
G3MP2B3(BC)	187.4	198.3	184.8	-	-	-	23.3	26.2	21.0
CHF=CH <sub>2</sub> + Br <sub>2</sub> → CHFBr-CH <sub>2</sub> Br (Syn addition of Br <sub>2</sub> )									
HF/BC6-31G(d)	327.0	340.5	324.8	13.5	18.4	13.1	15.0	17.3	12.7
MP2/BC6-31G(d)	224.2	234.5	222.4	33.6	37.2	33.4	18.3	20.2	15.8
B3LYP/BC6-31G(d)	190.3	202.5	187.9	7.2	4.9	2.8	13.4	15.5	10.8
B3P86/BC6-31G(d)	187.7	199.5	185.2	6.8	3.4	2.1	15.1	17.2	12.6
B3PW91/BC6-31G(d)	191.6	206.3	189.2	6.4	2.9	1.8	14.6	16.7	12.1
MP2/G3MP2large	263.8	275.9	260.3	-	-	-	15.7	17.0	13.6
//B3LYP/BC6-31G(d)									
G3MP2B3(BC)	255.6	267.7	252.1	-	-	-	13.8	15.0	11.7
CHF=CH <sub>2</sub> + Br <sub>2</sub> → CHFBr-CH <sub>2</sub> Br (Anti addition of Br <sub>2</sub> )									
HF/BC6-31G(d)	299.7	319.7	297.3	(5.1)	(3.6)	(1.8)	25.0	27.4	23.0
MP2/BC6-31G(d)	238.4	253.4	235.8	23.0	20.5	19.5	27.8	29.8	25.5
B3LYP/BC6-31G(d)	177.8	193.2	175.3	(-10.8)	(-13.8)	(-10.7)	29.6	32.4	27.0
MP2/G3MP2large//MP	250.6	279.0	244.8	63.5	64.1	62.7	16.0	20.5	14.1
2(FULL)/BC6-31G(d)									
MP2/G3MP2large	259.6	273.8	255.9	-	-	-	25.3	28.1	23.3
//B3LYP/BC6-31G(d)									
G3MP2B3(BC)	252.1	266.3	248.4	-	-	-	23.3	26.1	21.4

CHCl=CH <sub>2</sub> + Br <sub>2</sub> → CHClBr-CH <sub>2</sub> Br (Syn addition of Br <sub>2</sub> )									
HF/BC6-31G(d)	330.8	353.8	328.0	16.4	18.0	15.0	19.3	21.8	17.1
MP2/BC6-31G(d)	206.1	221.4	205.0	6.8	10.7	6.1	22.9	25.0	20.5
B3LYP/BC6-31G(d)	191.6	206.9	188.8	25.1	23.9	17.9	18.1	20.3	15.6
MP2/G3MP2large	236.5	251.2	233.0	60.3	64.3	58.3	19.8	22.5	17.7
//B3LYP/BC6-31G(d)									
G3MP2B3(BC)	217.6	232.3	214.2	34.1	38.1	32.1	17.7	20.4	15.6
CHCl=CH <sub>2</sub> + Br <sub>2</sub> → CHClBr-CH <sub>2</sub> Br (Anti addition of Br <sub>2</sub> )									
HF/BC6-31G(d)	309.6	329.9	307.1	(9.7)	(6.8)	(5.7)	32.3	34.4	30.2
MP2/BC6-31G(d)	240.1	255.6	237.4	27.2	23.6	23.2	34.2	36.0	31.9
B3LYP/BC6-31G(d)	180.7	195.9	178.0	(-)	(-14.7)	(-11.0)	27.7	30.0	25.5
MP2/G3MP2large//MP	238.1	266.5	232.3	28.5	29.1	27.7	30.2	34.7	28.4
2(FULL)/BC6-31G(d)									
MP2/G3MP2large	259.0	273.4	255.4	-	-	-	30.6	33.3	28.7
//B3LYP/BC6-31G(d)									
G3MP2B3(BC)	-	-	-	-	-	-	28.3	31.0	26.4

<sup>a</sup> Barriers as defined in Figure 3.2 and 3.3, respectively.

<sup>b</sup> The values in parentheses are single point values using optimized MP2 structures.

<sup>c</sup> (-) indicates missing values due to failure to optimize the bromonium/Br<sup>-</sup> ion pair or, in the QCISD(T) calculation for G3 theories.

<sup>d</sup> The products are all in trans conformation.

<sup>e</sup> The PCM-United Atom (UA0) model was used for optimized structures. In all cases  $\Delta G = \Delta\Delta G$  (thermal correction) +  $\Delta G_{\text{solv}}$ .

<sup>f</sup> Using MaxStep=1 for the optimization.

**TABLE 3.3: Activation energies, free energies and enthalpies of activation (kJ mol<sup>-1</sup>) at 298.15K for the reaction of (E)-CHF=CHF and (E)-CHCl=CHCl with Br<sub>2</sub> (Pathway B).<sup>a,b,c</sup>**

	HF/BC6-31G(d)	MP2/BC6-31G(d)	B3LYP/BC6-31G(d)	G3MP2B3(BC)
(E)-CHF=CHF + Br <sub>2</sub> → CHFBr-CHFBr				
$\Delta E_{a,TS1}^B$	331.8	220.1	197.3	286.4
$\Delta G_{TS1}^\ddagger$	344.5	231.2	206.1	296.0
$\Delta H_{TS1}^\ddagger$	328.2	217.5	193.5	283.4
$\Delta E_{a,TS2}^B$	-	53.5	9.6	69.0
$\Delta G_{TS2}^\ddagger$	-	55.8	10.0	71.9
$\Delta H_{TS2}^\ddagger$	-	50.6	5.5	67.3
$\Delta E_{a,TS3}^B$	30.4	29.8	25.7	25.8
$\Delta G_{TS3}^\ddagger$	31.2	30.5	26.7	29.4
$\Delta H_{TS3}^\ddagger$	27.6	26.9	22.7	23.6
$\Delta E_{a,TS4}^B$	35.4	35.6	27.8	30.7
$\Delta G_{TS4}^\ddagger$	38.5	40.0	31.0	34.2
$\Delta H_{TS4}^\ddagger$	33.1	32.9	25.3	28.4
(E)-CHCl=CHCl + Br <sub>2</sub> → CHClBr-CHClBr				
$\Delta E_{a,TS1}^B$	357.1	217.1	215.8	233.8
$\Delta G_{TS1}^\ddagger$	371.8	231.8	223.5	242.7
$\Delta H_{TS1}^\ddagger$	353.0	214.8	211.8	230.9
$\Delta E_{a,TS2}^B$	16.5	80.6	42.4	91.9
$\Delta G_{TS2}^\ddagger$	16.6	78.7	40.1	92.1
$\Delta H_{TS2}^\ddagger$	13.9	77.7	38.9	90.8
$\Delta E_{a,TS3}^B$	28.9	31.4	24.1	27.9
$\Delta G_{TS3}^\ddagger$	33.0	33.4	26.6	32.0
$\Delta H_{TS3}^\ddagger$	27.0	29.2	22.0	25.6
$\Delta E_{a,TS4}^B$	59.6	59.6	50.3	50.8
$\Delta G_{TS4}^\ddagger$	62.9	62.3	53.7	54.7
$\Delta H_{TS4}^\ddagger$	57.0	56.7	47.5	48.5

<sup>a</sup> Mechanistic pathway as defined in Figure 3.4.

<sup>b</sup> (-) indicates missing values due to failure to optimize the transition state.

<sup>c</sup> The products are all in trans conformation.

TABLE 3.4: Activation energies, free energies and enthalpies of activation ( $\text{kJ mol}^{-1}$ ) at 298.15K for the reaction of  $\text{CH}_2=\text{CH}_2$  and  $2\text{Br}_2$  (Pathway C).<sup>a,b</sup>

Level/Basis Set	$\Delta E_{a,\text{TS1}}^{\text{C}}$	$\Delta G_{\text{TS1}}^{\ddagger\text{C}}$	$\Delta H_{\text{TS1}}^{\ddagger\text{C}}$	$\Delta E_{a,\text{TS2}}^{\text{C}}$	$\Delta G_{\text{TS2}}^{\ddagger\text{C}}$	$\Delta H_{\text{TS2}}^{\ddagger\text{C}}$	$\Delta E_{a,\text{TS3}}^{\text{X}}$	$\Delta G_{\text{TS3}}^{\ddagger\text{X}}$	$\Delta H_{\text{TS3}}^{\ddagger\text{X}}$
HF/6-31G(d)	301.2	324.9	302.0	35.1	36.9	31.7	12.2	20.1	7.6
HF/BC6-31G(d)	284.4	304.3	282.6	34.5	30.8	30.0	16.1	17.8	13.9
MP2/6-31G(d)	232.8	260.8	230.7	55.1	52.6	51.2	17.1	18.2	14.8
CCl <sub>4</sub> <sup>c</sup>		252.9			64.3			18.4	
MP2/BC6-31G(d)	-	-	-	50.6	51.5	46.8	17.6	18.9	15.1
B3LYP/6-31G(d)	160.3	180.7	160.5	31.0	26.0	27.0	14.7	16.9	12.5
B3LYP/BC6-31G(d)	157.4	175.2	154.3	31.4	30.0	27.5	14.9	18.6	12.5
B3LYP/6-31+G(d)	167.8	207.5	165.7	31.3	23.8	27.2	14.7	15.9	12.5
B3LYP/BC6-31+G(d)	160.8	181.3	158.4	32.9	32.2	29.2	15.4	21.7	10.3
MP2/G3MP2large //B3LYP/6-31G(d)	232.1	249.8	229.5	69.7	68.6	69.5	17.7	20.5	16.0
G3MP2B3	207.3	224.9	204.7	50.7	49.6	50.5	15.6	18.4	13.9

<sup>a</sup> Barriers as defined in Figure 3.5 and 3.6.

<sup>b</sup> (-) indicates missing values due to failure to optimize the transition state.

<sup>c</sup> The PCM–United Atom (UA0) model was used for optimized structures. In all cases  $\Delta G = \Delta\Delta G$  (thermal correction) +  $\Delta G_{\text{solv}}$ .

TABLE 3.5: Activation energies, free energies and enthalpies of activation ( $\text{kJ mol}^{-1}$ ) at 298.15K for the reaction of  $\text{CH}_2=\text{CH}_2$  and  $2\text{Br}_2$  (Pathway D).<sup>a,b</sup>

Level/Basis Set	$\Delta E_{a,\text{TS1}}^{\text{D}}$	$\Delta G_{\text{TS1}}^{\ddagger \text{D}}$	$\Delta H_{\text{TS1}}^{\ddagger \text{D}}$	$\Delta E_{a,\text{TS2}}^{\text{D}}$	$\Delta G_{\text{TS2}}^{\ddagger \text{D}}$	$\Delta H_{\text{TS2}}^{\ddagger \text{D}}$
HF/6-31G(d)	302.0	325.5	302.8	113.0	90.4	103.2
HF/BC6-31G(d)	288.5	305.2	286.4	132.6	114.8	123.2
MP2/6-31G(d)	232.8	260.8	230.7	191.3	177.9	183.4
CCl <sub>4</sub> <sup>c</sup>		251.4			151.0	
MP2/BC6-31G(d)	225.6	222.8	238.0	-	-	-
B3LYP/6-31G(d)	160.5	176.3	160.6	148.6	137.1	139.8
CCl <sub>4</sub> <sup>c</sup>		160.9			112.1	
B3LYP/BC6-31G(d)	-	-	-	156.6	128.2	147.9
B3LYP/6-31+G(d)	167.8	203.1	165.7	147.1	136.6	138.4
B3LYP/BC6-31+G(d)	-	-	-	158.1	129.4	148.9
MP2/G3MP2large //B3LYP/6-31G(d)	242.6	248.6	232.9	214.2	212.6	215.3
G3MP2B3	204.3	210.3	194.6	180.2	178.5	181.2

<sup>a</sup> Barriers as defined in Figure 3.7 and 3.8.

<sup>b</sup> (-) indicates missing values due to failure to optimize the transition state.

<sup>c</sup> The PCM–United Atom (UA0) model was used for optimized structures. In all cases  $\Delta G = \Delta\Delta G$  (thermal correction) +  $\Delta G_{\text{solv}}$ .

**TABLE 3.6: Activation energies, free energies and enthalpies of activation (kJ mol<sup>-1</sup>) at 298.15K for the reaction of CH<sub>2</sub>=CH<sub>2</sub> and 2Br<sub>2</sub> (Pathway E).<sup>a,b</sup>**

Level/Basis Set	$\Delta E_{a,TS1}^E$	$\Delta G_{TS1}^{\ddagger E}$	$\Delta H_{TS1}^{\ddagger E}$	$\Delta E_{a,TS2}^{E1}$	$\Delta G_{TS2}^{\ddagger E1}$	$\Delta H_{TS2}^{\ddagger E1}$
HF/6-31G(d)	476.0	509.8	473.9	45.9	44.3	43.5
CCl <sub>4</sub> <sup>c</sup>		404.4 <sup>d</sup>			79.2	
HF/BC6-31G(d)	470.1	490.0	467.4	44.9	43.0	42.5
MP2/G3MP2large //HF/6-31G(d)	315.6	346.3	310.1	35.4	35.3	34.2
	$\Delta E_{a,TS2}^{E2}$	$\Delta G_{TS2}^{\ddagger E2}$	$\Delta H_{TS2}^{\ddagger E2}$	$\Delta E_{a,TS3}^{E2}$	$\Delta G_{TS3}^{\ddagger E2}$	$\Delta H_{TS3}^{\ddagger E2}$
HF/6-31G(d)	7.6	11.1	5.4	47.7	44.9	45.0
HF/BC6-31G(d)	10.1	13.5	8.1	46.3	43.7	43.8
MP2/BC6-31G(d)	10.8	14.0	8.2	10.9	9.7	9.2
B3LYP/BC6-31G(d)	8.7	11.9	6.3	20.4	20.5	18.0
B3LYP/BC6-31+G(d)	8.9	10.9	6.3	18.1	18.7	15.8
MP2/G3MP2large //HF/6-31G(d)	7.4	4.0	-2.0	38.9	38.0	37.9

<sup>a</sup> Barriers as defined in Figure 3.9 and 3.10.

<sup>b</sup> TS1<sup>E</sup> and TS2<sup>E1</sup> were only obtained at HF/6-31G(d) and HF/BC6-31G(d).

<sup>c</sup> The PCM–United Atom (UA0) model was used for optimized structures. In all cases  $\Delta G = \Delta\Delta G$  (thermal correction) +  $\Delta G_{solv}$ .

<sup>d</sup> Have two imaginary frequencies; the smallest one is 14.98 cm<sup>-1</sup>.

TABLE 3.7: Activation energies, free energies and enthalpies of activation ( $\text{kJ mol}^{-1}$ ) at 298.15K for the reaction of  $\text{CH}_2=\text{CH}_2$  and  $2\text{Br}_2$  (Pathway F).<sup>a,b</sup>

Level/Basis Set	$\Delta E_{a,\text{TS1}}^{\text{F}}$	$\Delta G_{\text{TS1}}^{\ddagger,\text{F}}$	$\Delta H_{\text{TS1}}^{\ddagger,\text{F}}$	$\Delta E_{a,\text{TS3}}^{\text{F}}$	$\Delta G_{\text{TS3}}^{\ddagger,\text{F}}$	$\Delta H_{\text{TS3}}^{\ddagger,\text{F}}$
HF/BC6-31G(d)	-	-	-	151.9	177.8	155.3
MP2/BC6-31G(d)	103.8	126.0	104.2	111.6	136.8	112.4
B3LYP/BC6-31G(d)	90.5	108.8	89.1	101.8	123.1	100.6
B3LYP/6-31G(d)	103.3	117.0	104.5	110.9	126.6	112.2
B3LYP/BC6-31+G(d)	83.6	99.3	82.2	100.7	119.3	99.7
G3MP2B3	119.0	129.1	116.5	122.7	134.3	119.8
G3MP2B3(BC)	117.5	132.3	112.5	125.6	142.6	119.9

<sup>a</sup> Mechanistic pathway and barriers as defined in Figure 3.11 and 3.12, respectively.

<sup>b</sup> (-) indicates missing values due to failure to optimize the transition state.

**TABLE 3.8: The calculated overall free energies of activation ( $\text{kJ mol}^{-1}$ ) at 298.15K for the reaction of  $\text{CH}_2=\text{CH}_2$  and  $2\text{Br}_2$  in solution at B3LYP/BC6-31G(d) (Pathway F) and experimental values.**

Solvent ( $\epsilon$ ) <sup>a</sup>	Calculated	Solvent ( $\epsilon$ ) <sup>a</sup>	Experimental
$\text{CCl}_4$ (2.23)	90.4 (87.1) <sup>b</sup>	$\text{CH}_3\text{COOH}$ (6.15)	76.8 <sup>c</sup>
$\text{CH}_2\text{Cl}_2$ (8.93)	64.6	$\text{CCl}_2\text{H}-\text{CCl}_2\text{H}$ (8.2)	66.4 <sup>c</sup>
$\text{CH}_2\text{Cl}-\text{CH}_2\text{Cl}$ (10.36)	52.7	$\text{CH}_3\text{OH}$ (32.63)	64.6 <sup>d</sup> (72.5) <sup>e</sup>
$\text{CH}_3\text{OH}$ (32.63)	39.2 (75.5) <sup>f</sup>		

<sup>a</sup> In order of increasing dielectric constants ( $\epsilon$ ).

<sup>b</sup> The value in parenthesis is obtained at MP2/BC6-31G(d) level of theory.

<sup>c</sup> Reference 46.

<sup>d</sup> Reference 45.

<sup>e</sup> Corrected for solvent concentration (See text for explanation).

<sup>f</sup> For the reaction of ethene +  $\text{Br}_2$  mediated by a  $\text{CH}_3\text{OH}$  molecule in  $\text{CH}_3\text{OH}$  solution.

TABLE 3.9: Thermodynamic properties (kJ mol<sup>-1</sup>) at 298.15K for the reaction of CH<sub>2</sub>=CH<sub>2</sub>, CH<sub>3</sub>-CH<sub>2</sub>=CH<sub>2</sub>, (CH<sub>3</sub>)<sub>2</sub>CH=CH<sub>2</sub>, CH<sub>2</sub>=CHF, CH<sub>2</sub>=CHCl, (E)-CHF=CHF and (E)-CHCl=CHCl with Br<sub>2</sub>.<sup>a</sup>

Level/Basis Set	$\Delta E$	$\Delta G$	$\Delta H$	$\Delta E$	$\Delta G$	$\Delta H$
	CH <sub>2</sub> =CH <sub>2</sub> + Br <sub>2</sub> → CH <sub>2</sub> Br-CH <sub>2</sub> Br			CH <sub>3</sub> -CH <sub>2</sub> =CH <sub>2</sub> + Br <sub>2</sub> → CH <sub>3</sub> -CH <sub>2</sub> Br-CH <sub>2</sub> Br		
HF/6-31G(d)	-133.2	-81.3	-121.7	-123.4	-66.5	-112.8
HF/BC6-31G(d)	-134.1	-80.8	-122.9	-130.8	-74.0	-120.4
MP2/6-31G(d)	-162.6	-110.5	-151.1	-164.2	-107.1	-153.8
	CCl <sub>4</sub> <sup>b</sup>	-111.1			-109.0	
MP2/BC6-31G(d)	-159.1	-106.0	-148.2	-166.3	-109.7	-156.4
B3LYP/6-31G(d)	-133.2	-81.3	-123.0	-123.5	-68.7	-114.2
	CCl <sub>4</sub> <sup>b</sup>	-92.2			-77.8	
B3LYP/BC6-31G(d)	-134.5	-82.8	-124.5	-131.0	-76.1	-121.8
B3LYP/6-31+G(d)	-123.1	-71.0	-112.7	-114.2	-59.2	-104.8
B3LYP/BC6-31+G(d)	-138.2	-85.1	-127.4	-147.2	-90.3	-136.9
B3P86/6-31G(d)	-	-	-	-147.1	-91.9	-137.6
B3P86/BC6-31G(d)	-156.9	-105.0	-146.7	-154.8	-99.8	-145.7
B3PW91/6-31G(d)	-148.3	-98.0	-138.0	-138.5	-83.3	-129.1
B3PW91/BC6-31G(d)	-149.7	-97.8	-139.5	-146.3	-91.2	-137.0
MP2/G3MP2large //MP2(FULL)/6-31G(d)	-159.6	-123.8	-163.4	-163.7	-106.3	-166.8
MP2/G3MP2large //B3LYP/6-31G(d)	-157.4	-119.8	-161.1	-160.3	-103.0	-163.2
G3MP2	-123.1	-87.3	-126.8	-127.6	-85.4	-130.8

G3MP2B3	-122.0	-84.3	-125.7	-126.0	-83.8	-129.0
Experimental			-120.9±1.3 <sup>c</sup>			-122.5±0.8 <sup>c</sup>
	(CH <sub>3</sub> ) <sub>2</sub> C=CH <sub>2</sub> + Br <sub>2</sub> → (CH <sub>3</sub> ) <sub>2</sub> CBr-CH <sub>2</sub> Br			CHF=CH <sub>2</sub> + Br <sub>2</sub> → CHFBr-CH <sub>2</sub> Br		
HF/BC6-31G(d)	-126.1	-69.0	-116.5	-117.5	-62.7	-108.1
MP2/BC6-31G(d)	-173.7	-116.7	-164.7	-146.2	-91.5	-136.9
B3LYP/BC6-31G(d)	-125.7	-71.1	-117.5	-119.2	-66.3	-111.0
B3LYP/BC6-31+G(d)	-152.5	-95.5	-142.9	-	-	-
B3P86/BC6-31G(d)	-151.7	-96.8	-143.6	-139.7	-86.6	-131.4
B3PW91/BC6-31G(d)	-141.9	-86.9	-133.7	-132.1	-78.9	-123.8
MP2/G3MP2large	-155.5	-112.0	-158.1	-138.3	-92.9	-141.1
//B3LYP/BC6-31G(d)						
G3MP2B3(BC)	-123.4	-79.9	-126.0	<b>-88.9</b>	-43.5	-91.7
Experimental			-126.3 <sup>c</sup>			
	CHCl=CH <sub>2</sub> + Br <sub>2</sub> → CHClBr-CH <sub>2</sub> Br			(E)-CHF=CHF + Br <sub>2</sub> → CHFBr-CHFBr		
HF/BC6-31G(d)	-98.4	-43.5	-89.4	-117.6	-60.7	-109.2
MP2/BC6-31G(d)	-136.0	-81.1	-127.0	-151.9	-95.4	-143.8
B3LYP/6-31G(d)	-96.3	-43.1	-88.2			
B3LYP/BC6-31G(d)	-103.1	-50.0	-95.1	-121.8	-67.3	-114.8
MP2/G3MP2large	-134.6	-92.3	-137.1	-146.6	-103.6	-149.1
//B3LYP/BC6-31G(d)						
G3MP2B3(BC)	-120.9	-78.8	-123.3	-118.6	-75.6	-121.0
	(E)-CHCl=CHCl + Br <sub>2</sub> → CHClBr-CHClBr					
HF/BC6-31G(d)	-66.4	-9.5	-59.2			
MP2/BC6-31G(d)	-117.5	-62.3	-110.3			
B3LYP/6-31G(d)	-63.7	-8.8	-57.5			
B3LYP/BC6-31G(d)	-75.4	-20.6	-69.4			
MP2/G3MP2large	-123.0	-78.6	-125.2			
//B3LYP/BC6-31G(d)						

G3MP2B3(BC)	-92.2	-47.8	-94.4
Experimental			-72.4 <sup>c</sup>

---

<sup>a</sup> The products are all in trans conformation.

<sup>b</sup> The PCM–United Atom (UA0) model was used for optimized structures. In all cases  $\Delta G = \Delta\Delta G$  (thermal correction) +  $\Delta G_{\text{solv}}$ .

<sup>c</sup> The values are obtained from reference 48.

TABLE 3.10: Heats of formation,  $\Delta H_f$ , (kJ mol<sup>-1</sup>) at 298.15K.<sup>a</sup>

Species	$\Delta H_f$		Species	$\Delta H_f$	
	Experimental <sup>b</sup>	Present work		Experimental	Present work
CH <sub>2</sub> =CH <sub>2</sub>	52.57	57.3	trans-CHFBr-CH <sub>2</sub> Br		-214.8
trans-CH <sub>2</sub> Br-CH <sub>2</sub> Br	-37.52	-42.3	CH <sub>2</sub> =CHCl	29.0 <sup>b</sup>	
CH <sub>3</sub> -CH <sub>2</sub> =CH <sub>2</sub>	20.41	26.9	trans-CHClBr-CH <sub>2</sub> Br		-63.4
trans-CH <sub>3</sub> -CH <sub>2</sub> Br-CH <sub>2</sub> Br	-71.18	-77.7	(E)-CHF=CHF	-310.0 <sup>c</sup>	
(CH <sub>3</sub> ) <sub>2</sub> CH=CH <sub>2</sub>	-17.9 ± 1.1	-18.2	trans-CHFBr-CHFBr		-400.1
trans-(CH <sub>3</sub> ) <sub>2</sub> CBr-CH <sub>2</sub> Br	-113.3 ± 1.0	-113.0	(E)-CHCl=CHCl	1.7 <sup>b</sup>	
Br <sub>2</sub>	30.91		trans-CHClBr-CHClBr		-61.8
CH <sub>2</sub> =CHF	-136.0				

<sup>a</sup> See text for explanation.

<sup>b</sup> Reference 48

<sup>c</sup> Reference 49.

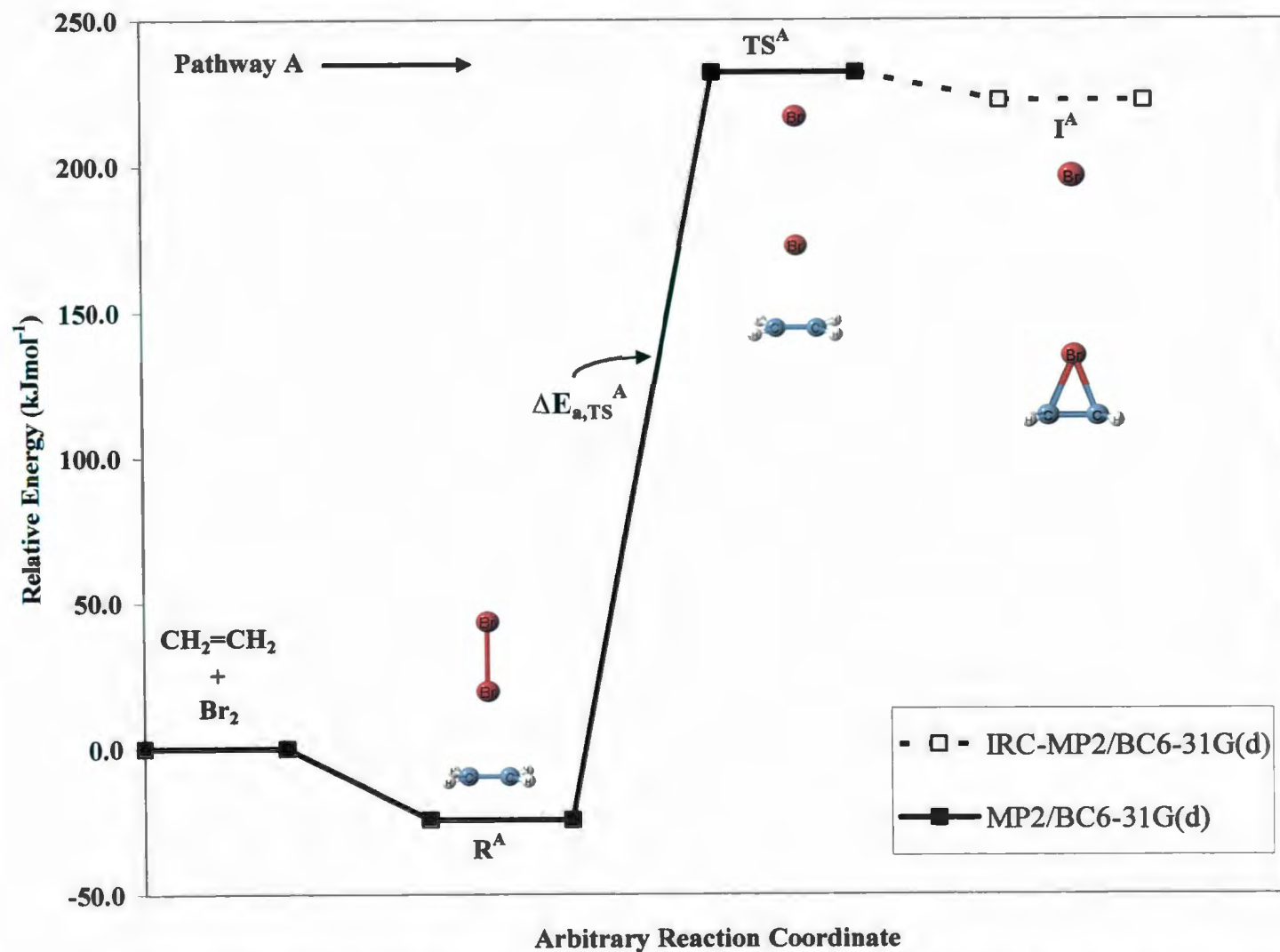


Figure 3.1. Pathway and barrier for the reaction of  $\text{CH}_2=\text{CH}_2 + \text{Br}_2$  (Pathway A) at MP2/BC6-31G(d) level of theory. Although the IRC leads to  $\text{I}^{\text{A}}$  no optimized structure was found.

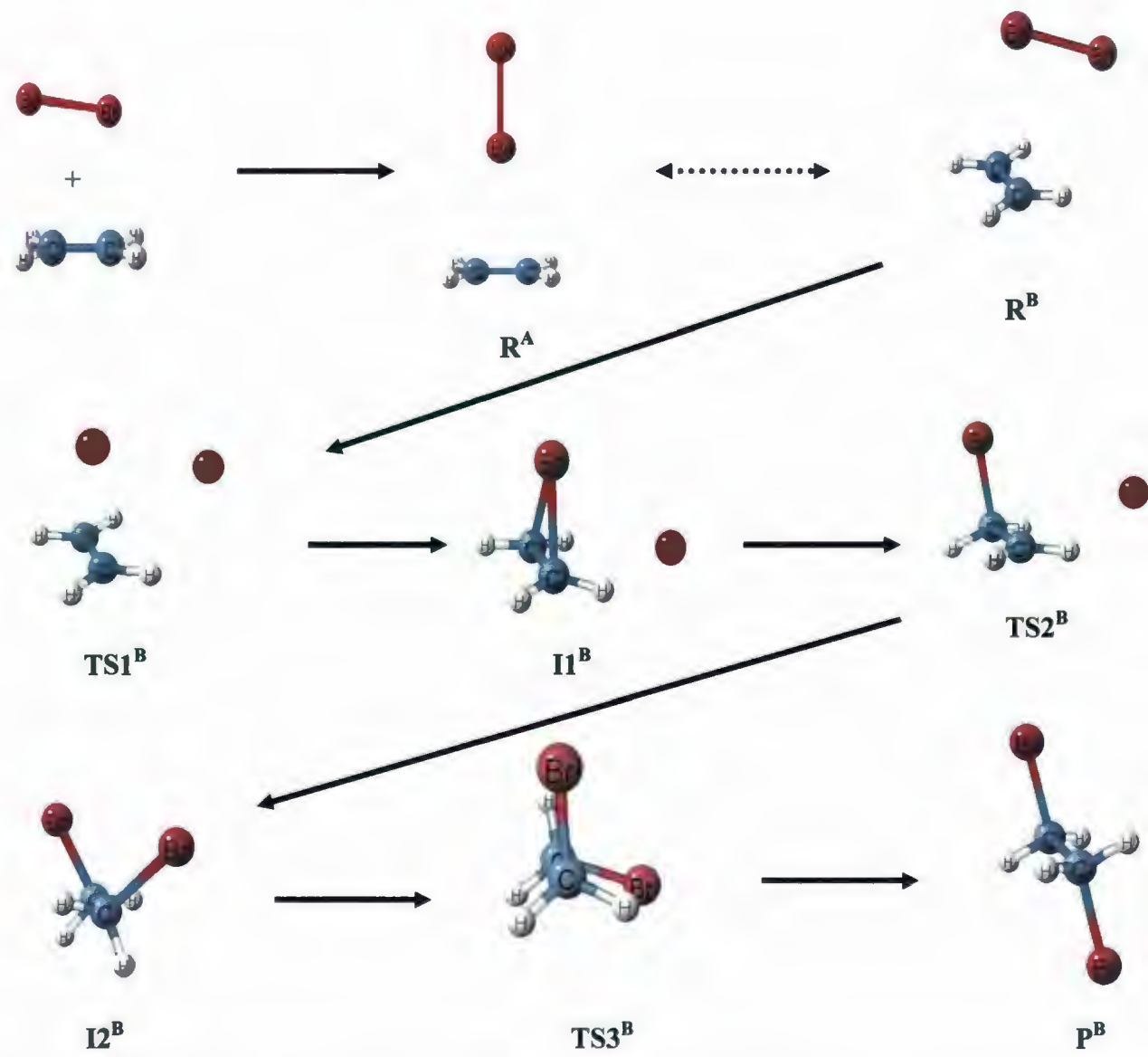


Figure 3.2. Mechanism for the reaction of CH<sub>2</sub>=CH<sub>2</sub> + Br<sub>2</sub> (Pathway B). Similar structures are found for the bromination of CH<sub>3</sub>-CH<sub>2</sub>=CH<sub>2</sub>, (CH<sub>3</sub>)<sub>2</sub>CH=CH<sub>2</sub>, CH<sub>2</sub>=CHF and CH<sub>2</sub>=CHCl.

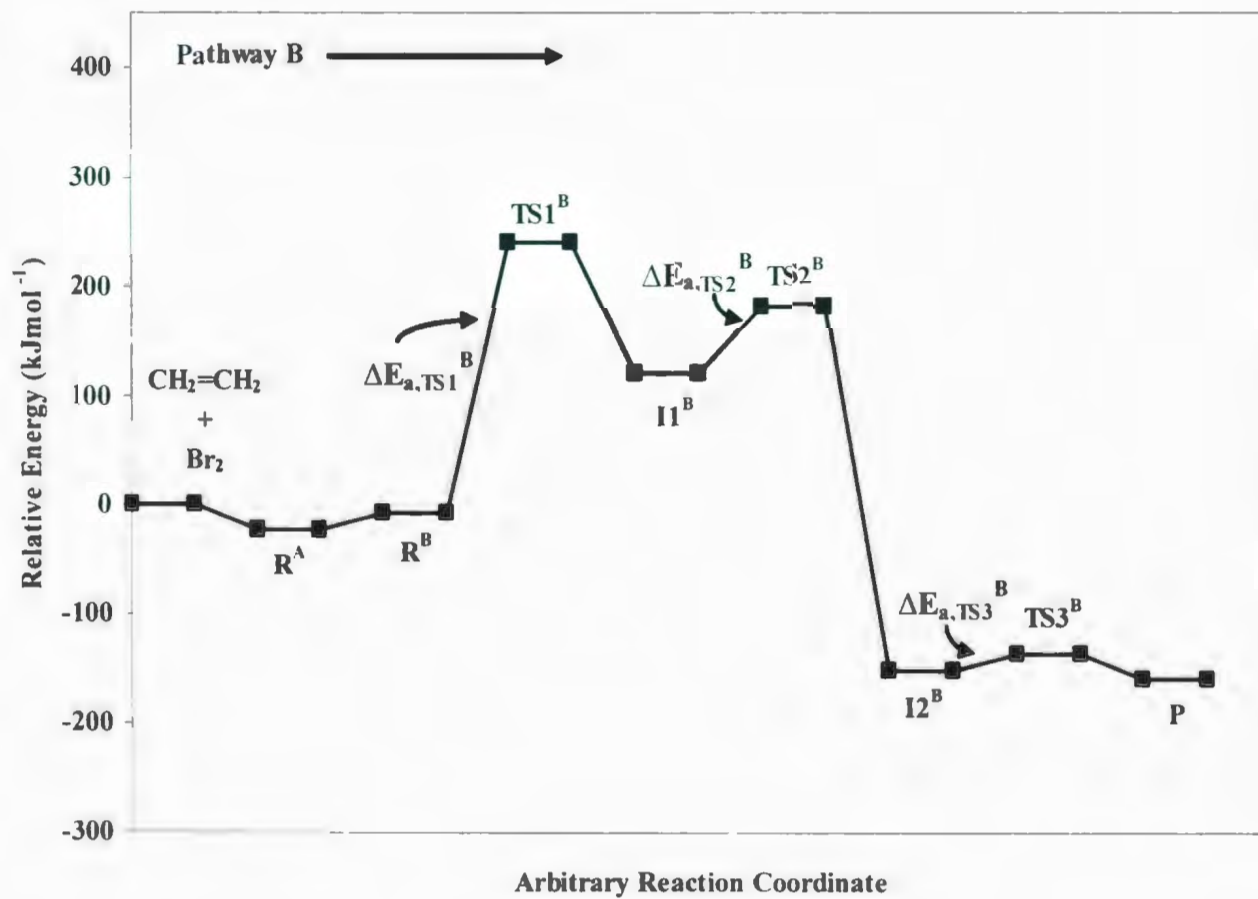


Figure 3.3. Pathway for the reaction of  $\text{CH}_2=\text{CH}_2 + \text{Br}_2$  (Pathway B) at MP2/BC6-31G(d) level of theory (see Figure 3.2 for structures).

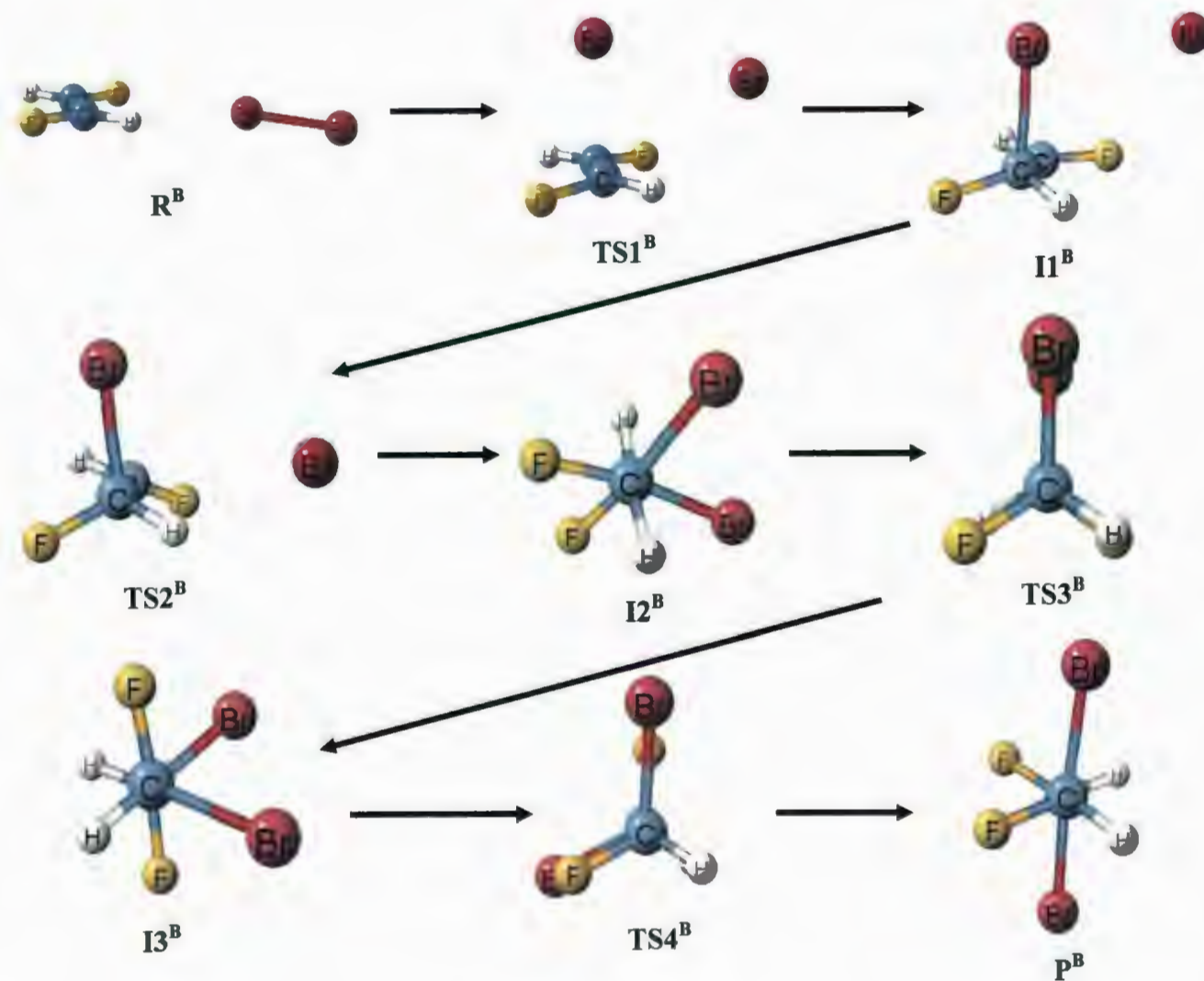


Figure 3.4. Mechanism for the reaction of (E)-CHF=CHF + Br<sub>2</sub> (Pathway B). Similar structures are found for the bromination of (E)-CHCl=CHCl.

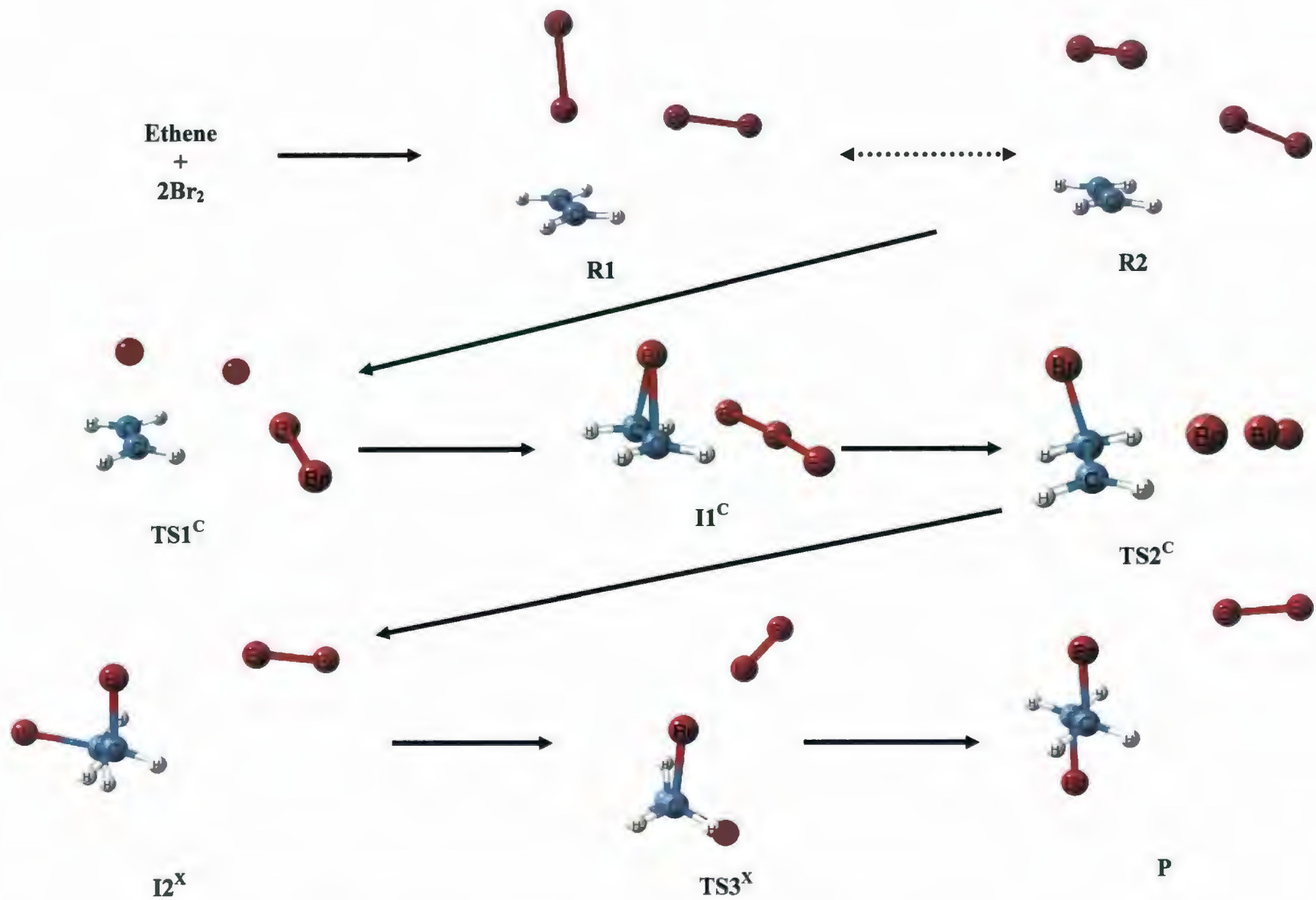


Figure 3.5. Mechanism for the reaction of  $\text{CH}_2=\text{CH}_2 + 2\text{Br}_2$  (Pathway C).

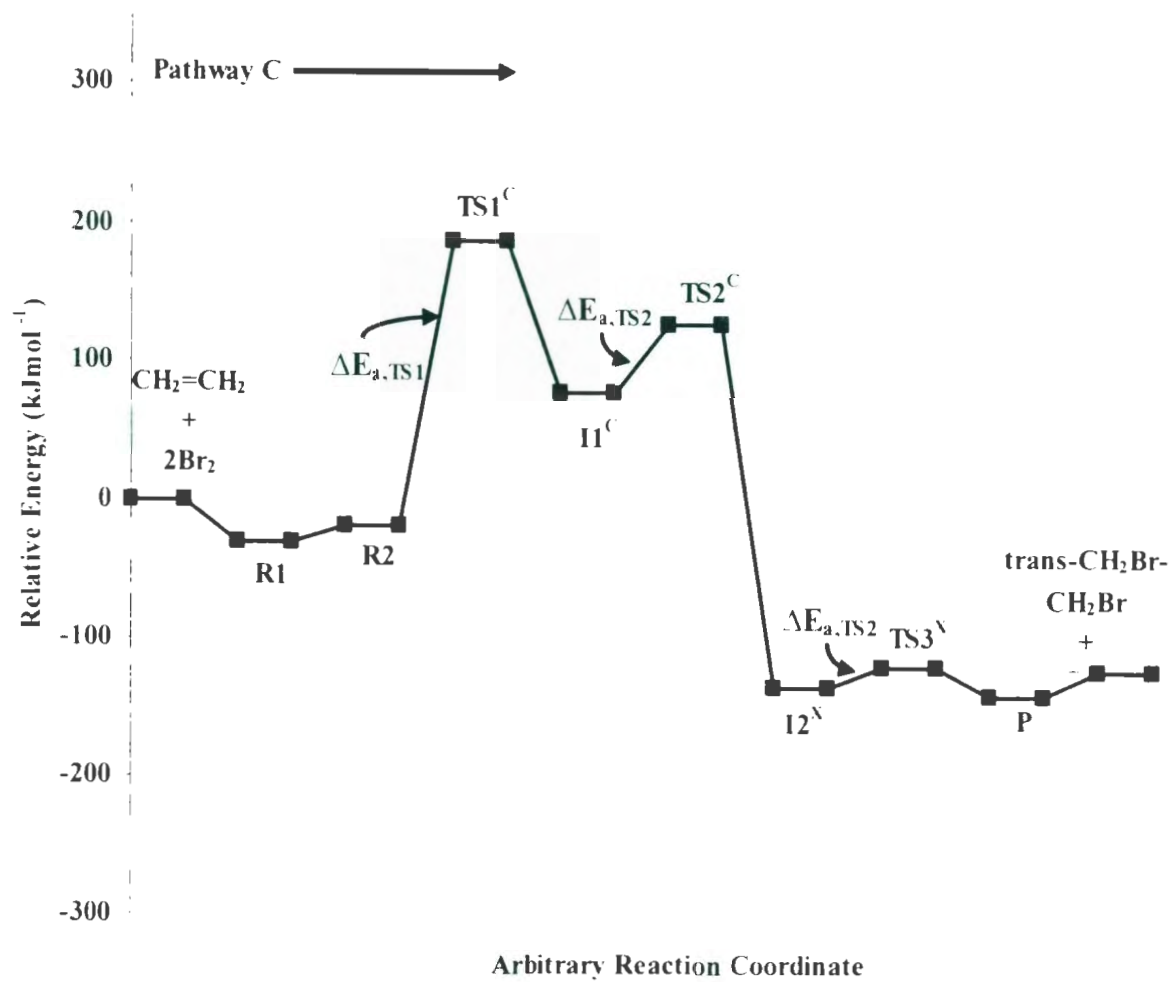


Figure 3.6. Pathway for the reaction of  $\text{CH}_2=\text{CH}_2 + 2\text{Br}_2$  (Pathway C) at G3MP2B3 level of theory (see Figure 3.5 for structures).

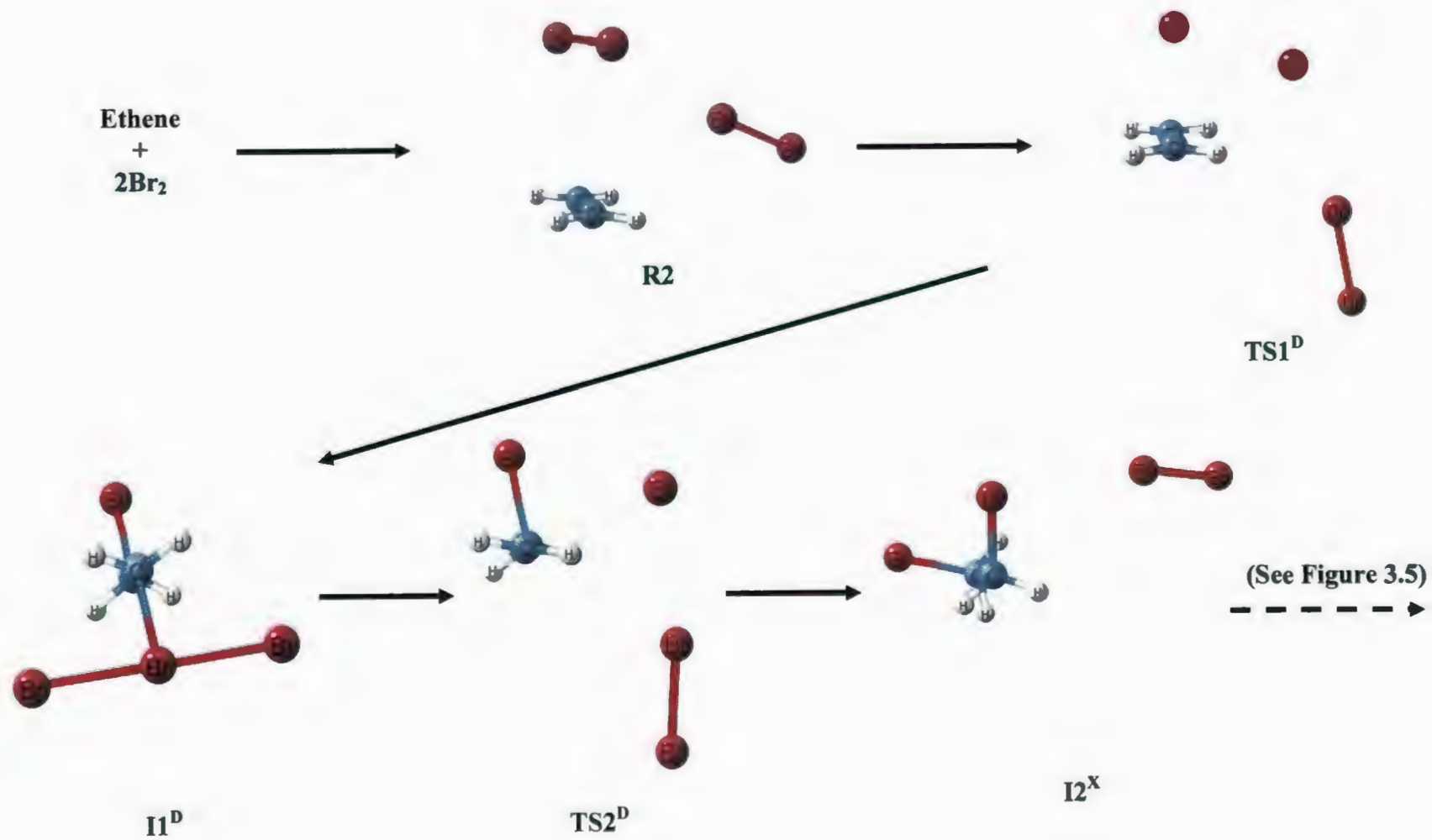


Figure 3.7. Mechanism for the reaction of  $\text{CH}_2=\text{CH}_2 + 2\text{Br}_2$  (Pathway D).

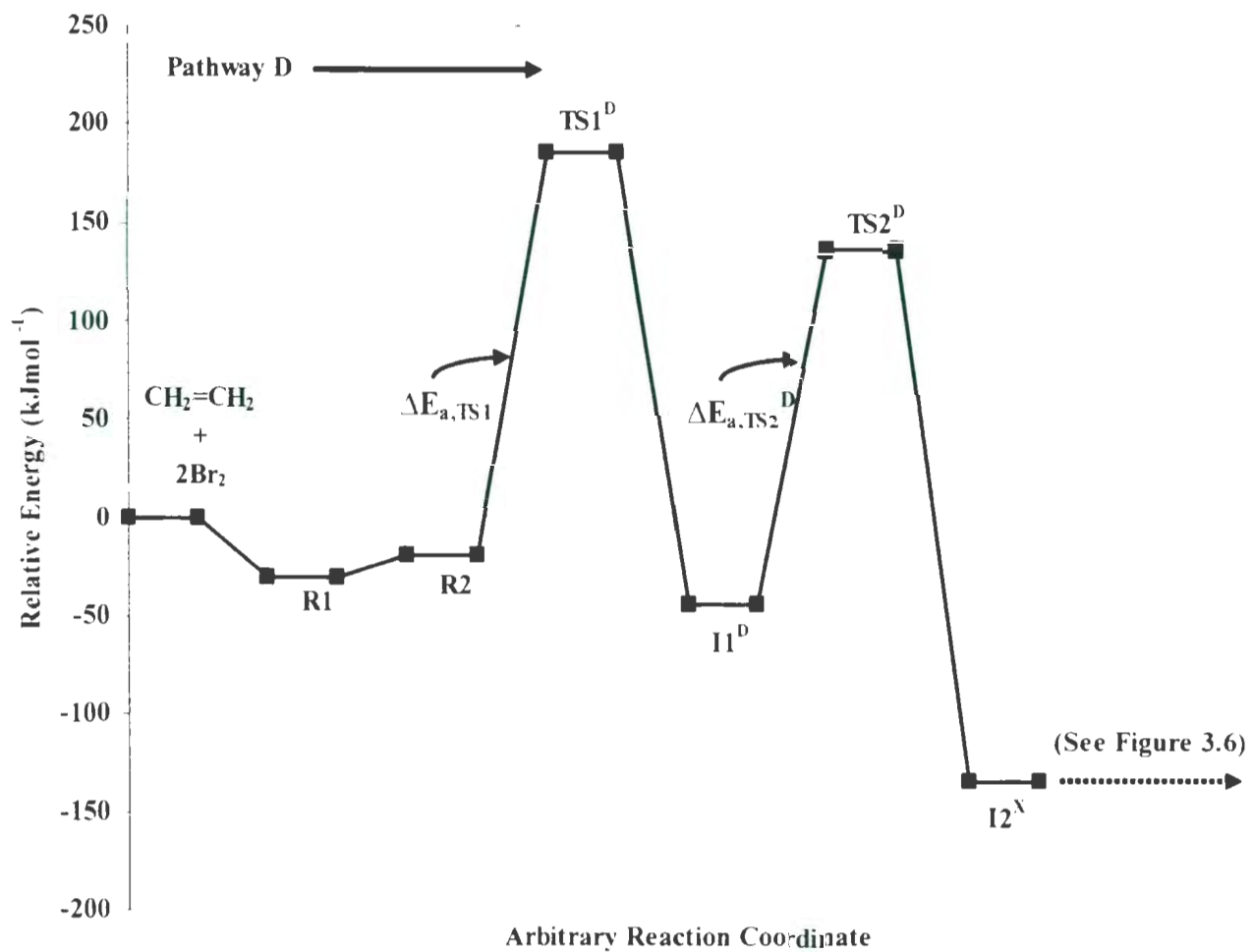


Figure 3.8. Pathway for the reaction of  $\text{CH}_2=\text{CH}_2 + 2\text{Br}_2$  (Pathway D) at G3MP2B3 level of theory (see Figure 3.7 for structures).

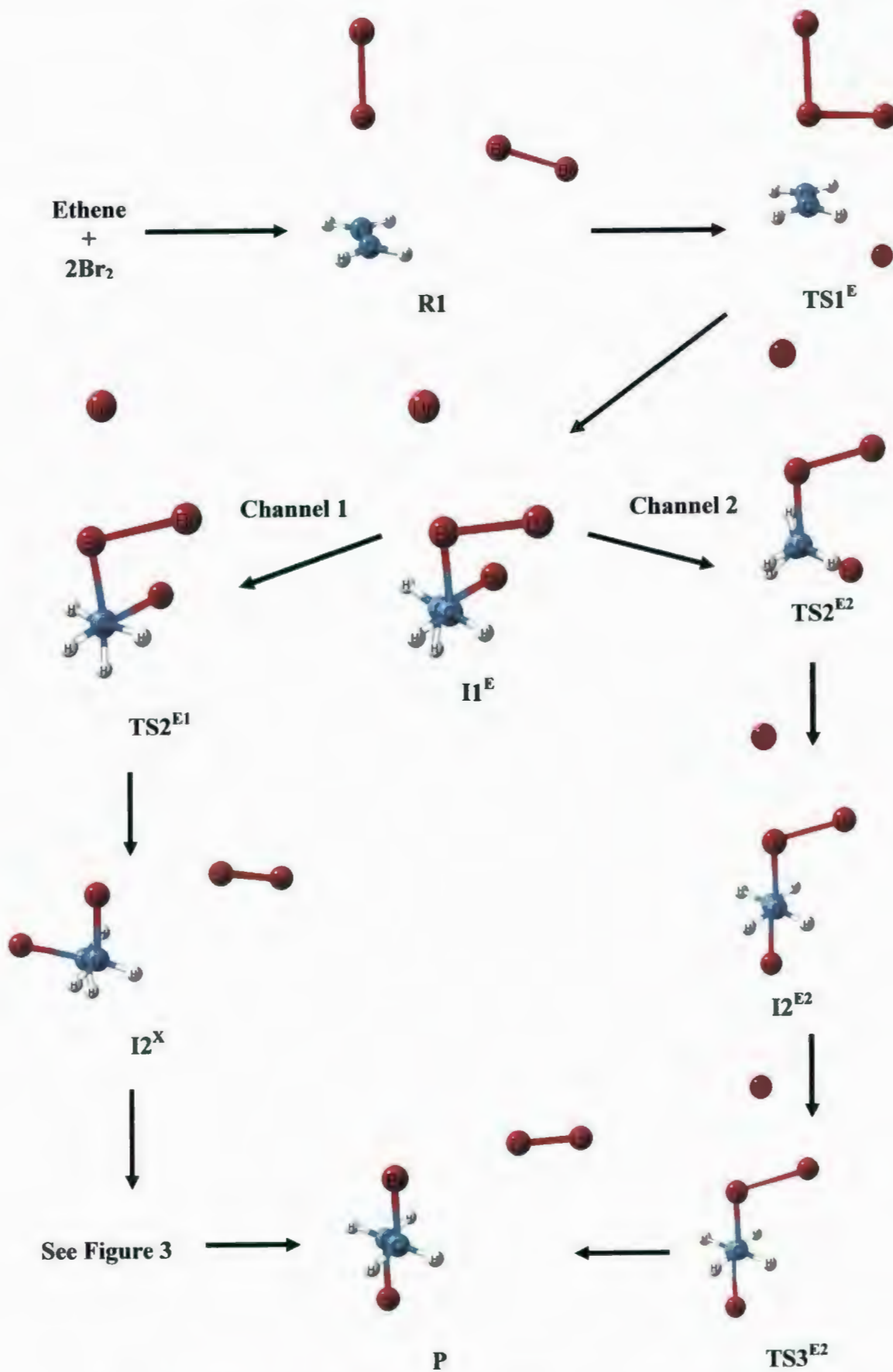


Figure 3.9. Mechanism for the reaction of CH<sub>2</sub>=CH<sub>2</sub> + 2Br<sub>2</sub> (Pathway E).

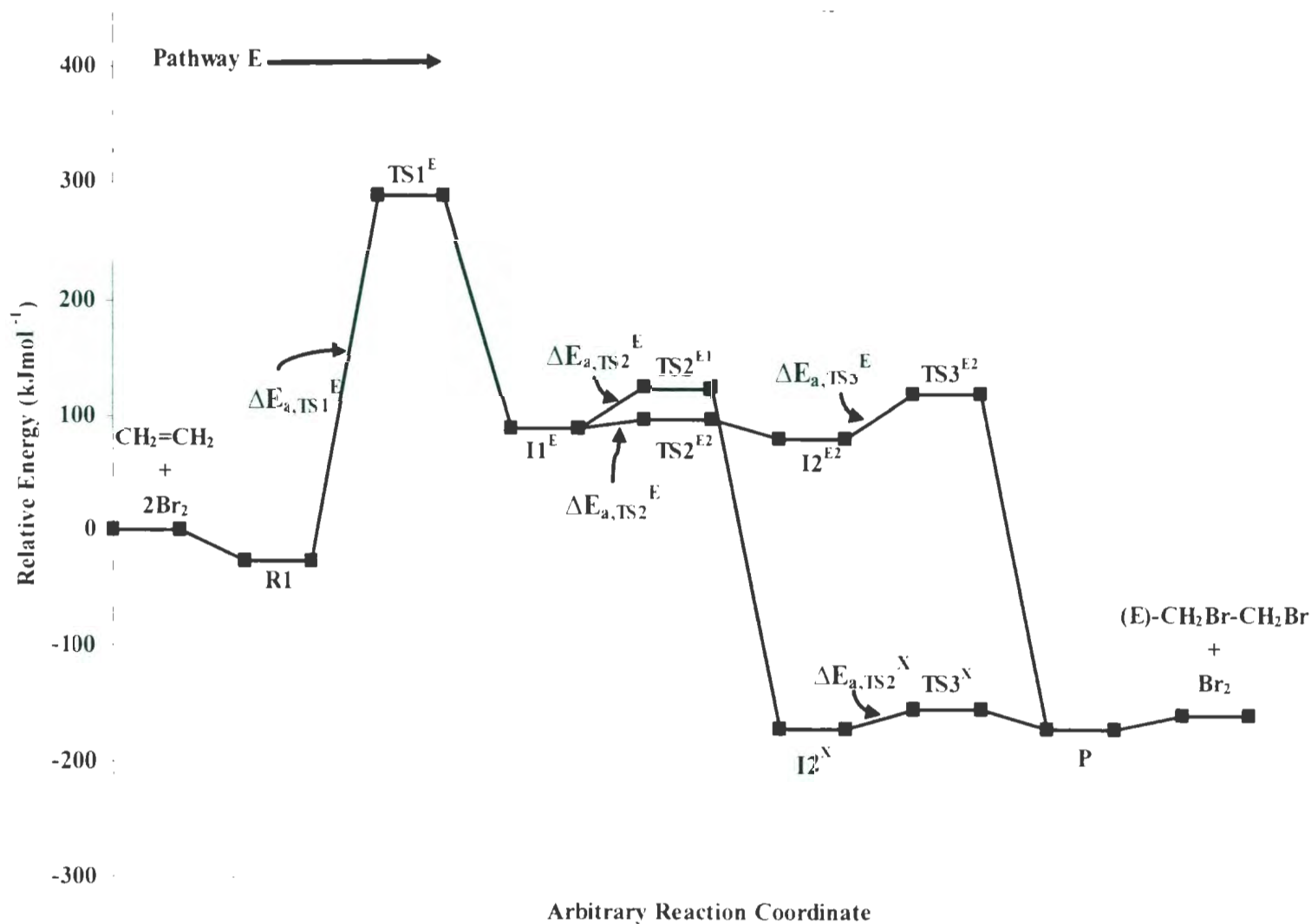


Figure 3.10. Pathway for the reaction of CH<sub>2</sub>=CH<sub>2</sub> + 2Br<sub>2</sub> (Pathway E) at MP2/G3MP2large//HF/6-31G(d) level of theory (see Figure 3.9 for structures).

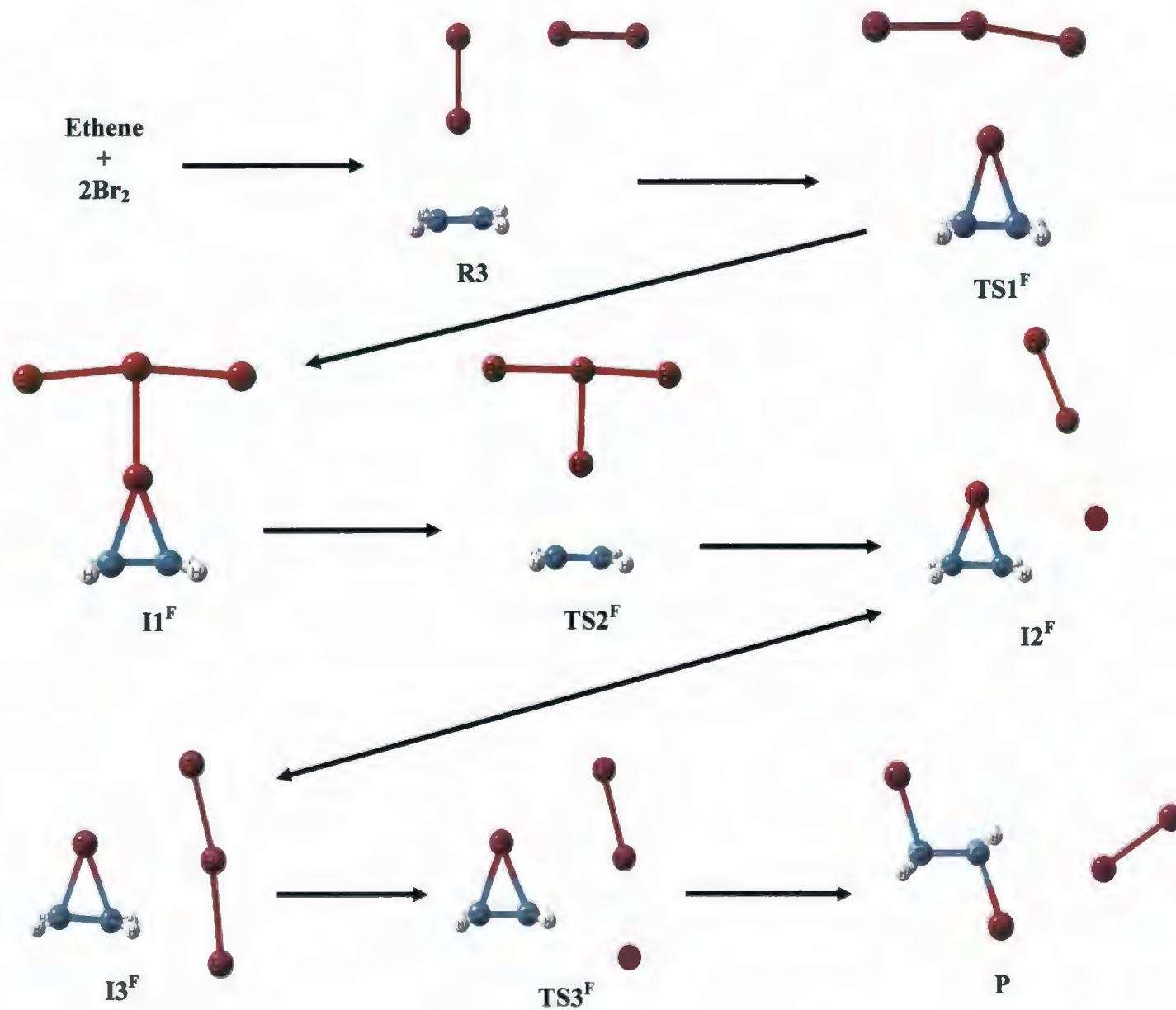


Figure 3.11. Mechanism for the reaction of  $\text{CH}_2=\text{CH}_2 + 2\text{Br}_2$  (Pathway F).

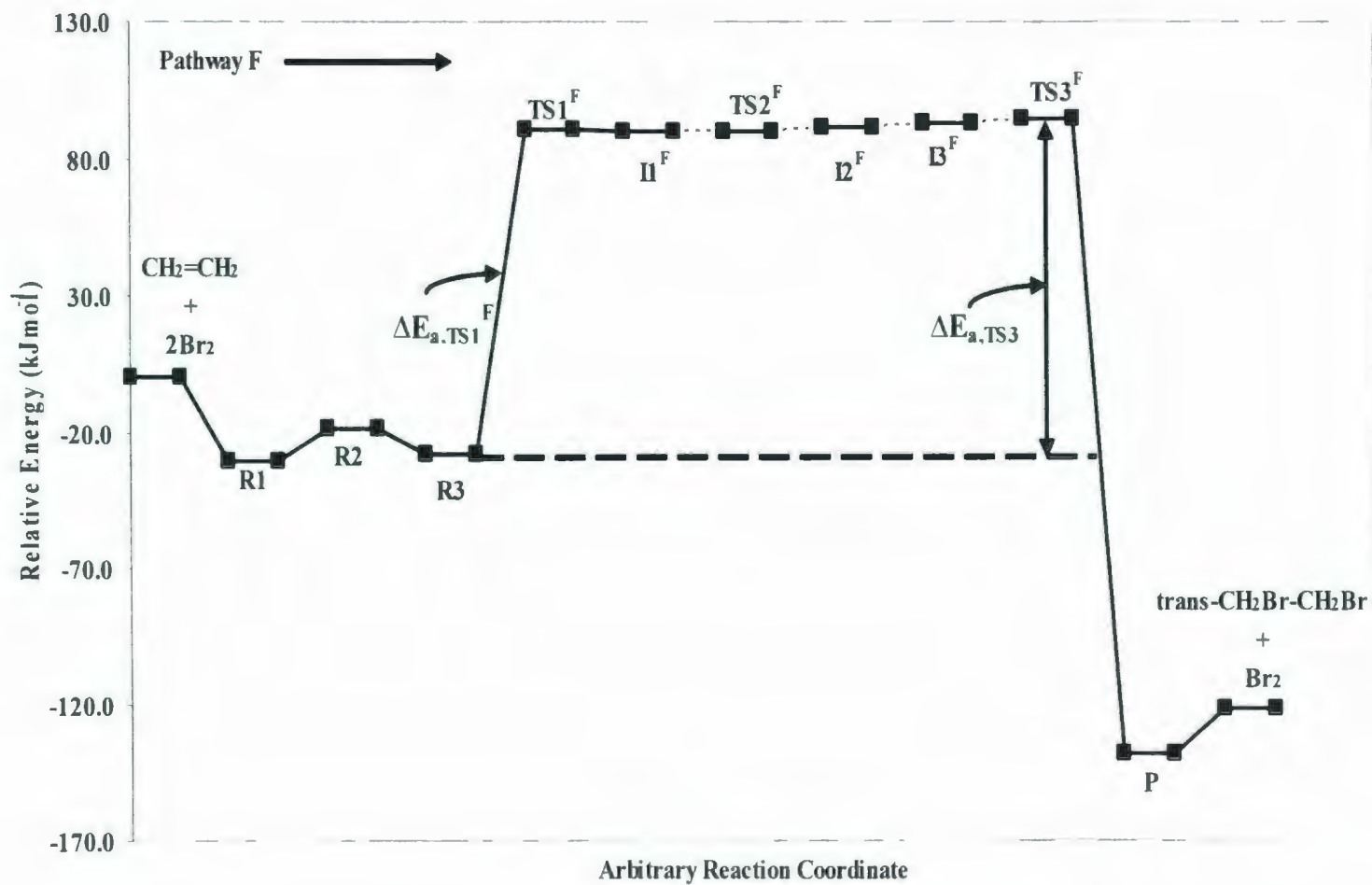


Figure 3.12. Pathway for the reaction of  $\text{CH}_2=\text{CH}_2 + 2\text{Br}_2$  (Pathway F) at G3MP2B3 level of theory (see Figure 3.11 for structures). For  $\text{TS2}^{\text{F}}$ ,  $\text{I2}^{\text{F}}$  and  $\text{I3}^{\text{F}}$  the G3MP2B3 energies are calculated using HF/6-31G(d) by optimized geometries.

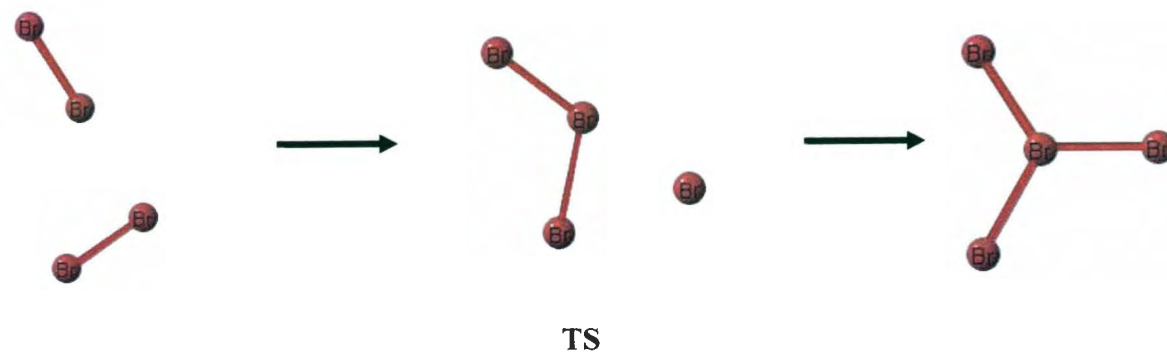


Figure 3.13. Mechanism for the reaction of  $\text{Br}_2 + \text{Br}_2 \rightarrow \text{Br}_4$ .

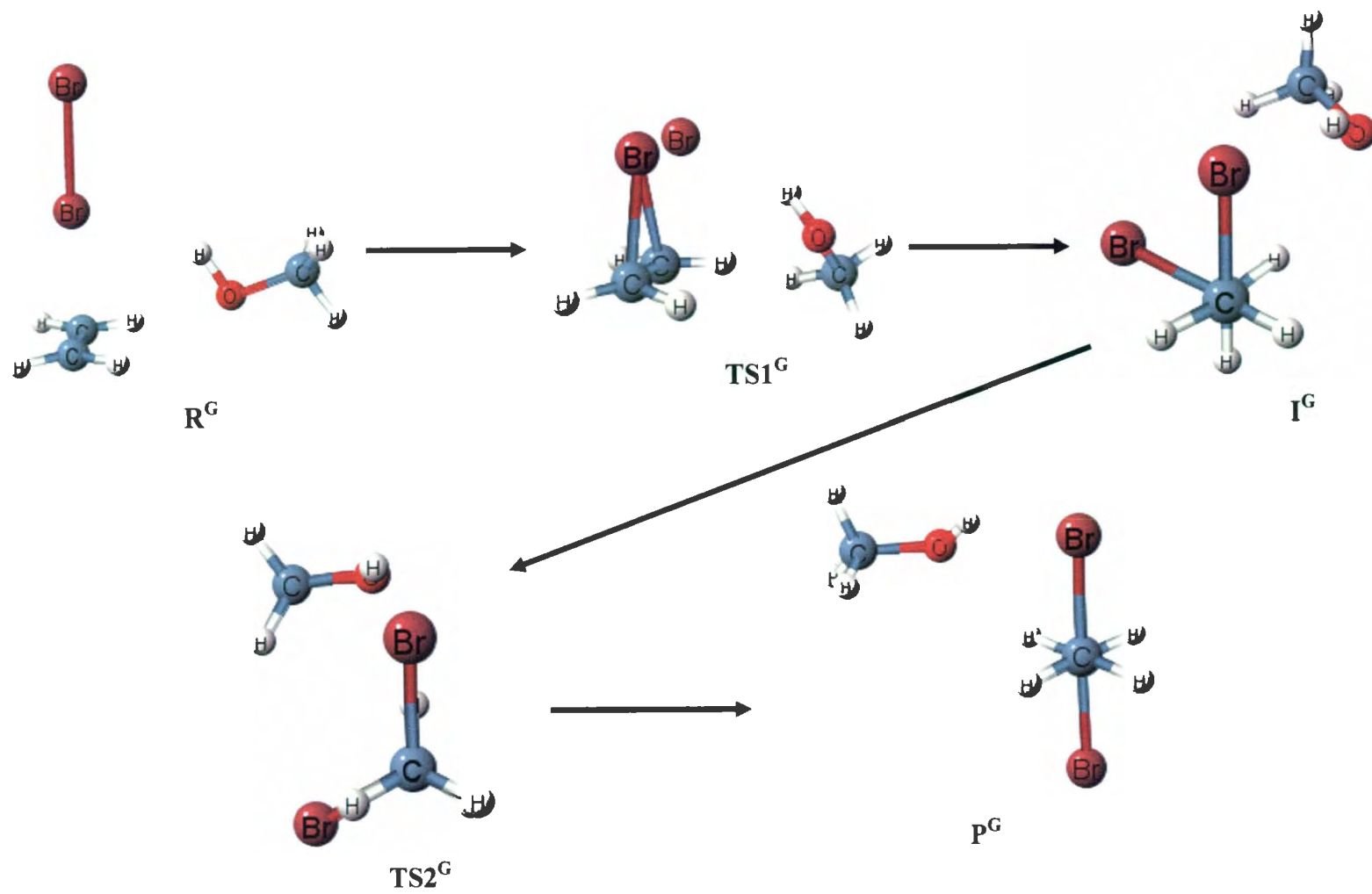


Figure 3.14. Mechanism for the reaction of  $\text{CH}_2=\text{CH}_2 + \text{Br}_2$  mediated by a  $\text{CH}_3\text{OH}$  molecule (Pathway G).

## CHAPTER 4

# The addition reaction of adamantylideneadamantane with $\text{Br}_2$ and $2\text{Br}_2$ - A Computational Study

### 4.1 Introduction

Bromination of alkenes is a well-known organic reaction.<sup>1-2</sup> Experimentally, the reaction mechanism is considered to have several steps, depending on the alkene and the solvent used.<sup>2-7</sup> A bromine/alkene charge-transfer complex (CTC) and the bromonium ion have been considered to be the main intermediates in the bromination of alkenes. The existence of a cyclic bromonium ion intermediate was first proposed by Roberts and Kimball.<sup>8</sup> However, no structural evidence of the occurrence of a cyclic bromonium ion was

reported despite the many experimental attempts by a variety of techniques.<sup>9-15</sup> Strating and co-workers<sup>16</sup> first produced a bromonium ion tribromide in the lab by reacting adamantylideneadamantane (1) with Br<sub>2</sub> in CCl<sub>4</sub>. Slebocka-Tilk et al.<sup>17</sup> for the first time obtained the X-ray structure of the adamantylideneadamantane bromonium ion with a Br<sub>3</sub><sup>-</sup> counterion (2) (Scheme 4.1). Later, Brown et al.<sup>18</sup> also reported the existence of another bromonium ion of bicycle [3.3.1]nonylidenebicyclo [3.3.1] nonane. (E)-2,2,5,5-Tetramethyl-3,4-diphenylhex-3-ene (3) is the first reported example of an olefin whose interaction with bromine is limited to π complex formation (Scheme 4.2).<sup>19</sup> Similarly, tetraneopentylethylene (4) does not react with bromine in CCl<sub>4</sub> solution and no π complex was formed between these two reagents on the basis of the <sup>13</sup>C NMR spectrum (Scheme 4.3).<sup>20</sup> Thus the reactivity of olefins toward bromine depends on their steric hindrance.

Theoretical studies of the bromination of alkenes are quite limited as compared to experiment. Yamabe et al.<sup>21</sup> studied the mechanism for the reactions, X<sub>2</sub> + C<sub>2</sub>H<sub>4</sub> → C<sub>2</sub>H<sub>4</sub>X<sub>2</sub> [X = F, Cl, and Br] at the MP3/3-21G//RHF/3-21G level of theory and found that the fluorination of ethene occurs via a four-centered transition state with an activation energy of 212.5 kJ mol<sup>-1</sup>, while chlorination and bromination give a zwitterionic three-center transition state with the activation barrier of 212.1, and 256.9 kJ mol<sup>-1</sup>, respectively. Hamilton and Schaefer<sup>22</sup> in their study on the structure and energetics of C<sub>2</sub>H<sub>4</sub>Br<sup>+</sup> isomers also proposed that the transition state is a three-membered bromonium ion with a nearby counter bromide ion. Recently, Cammi et al.<sup>23</sup> studied the bromination of ethene but only from the charge transfer complex (CTC) to the transition state (TS) at the MP2/CEP-121G(aug) level of

theory. The free energy barrier in going from the CTC to the TS was found to be 250.8 kJ mol<sup>-1</sup> in the gas phase and 34.2 kJ mol<sup>-1</sup> in water.

Recently,<sup>24</sup> we have investigated the bromination reaction for a series of simple alkenes, namely, ethene, propene, isobutene, flouroethene, chloroethene, (E)-1,2-difluoroethene and (E)-1,2-dichloroethene. It was found that Br<sub>2</sub> can react with alkenes via two different mechanisms. One involves a perpendicular attack by Br<sub>2</sub> to C-C bond by a one-step pathway producing the bromonium/bromide ion pair intermediate. The second mechanism consists of sidewise attack by Br<sub>2</sub> to the C-C bond producing first the bromonium/bromide ion pair intermediate which then produces the trans-1,2-dibromoalkane via multiple-steps. Ethene can react with 2Br<sub>2</sub> via several mechanisms all leading to the trans-1,2-dibromoethane product. It was found that in this case the bromination reaction in gas phase and in non-polar aprotic solvents was mediated by the second bromine molecule. The most likely pathway for the reaction of ethene and 2Br<sub>2</sub> was found to be a multiple-step process involving the formation of an ethane bromonium/Br<sub>3</sub><sup>-</sup> ion pair intermediate which then leads to the formation of the 1,2-dibromo product by trans addition of a Br atom from Br<sub>3</sub><sup>-</sup> to one of the bromonium ion carbons. The corresponding activation energy was 122.7 kJ mol<sup>-1</sup> at the G3MP2B3 level of theory. For non-polar aprotic solvents such as CH<sub>2</sub>Cl<sub>2</sub> and CH<sub>2</sub>ClCH<sub>2</sub>Cl, the overall activation energies for the ethene + 2Br<sub>2</sub> reaction are found to be 64.6 and 52.7 kJ mol<sup>-1</sup>, respectively at B3LYP/6-31G(d) level of theory. This is in excellent agreement with the experimental activation energy of 66.4 kJ mol<sup>-1</sup> for the reaction in CCl<sub>2</sub>H-CCl<sub>2</sub>H.<sup>25</sup> However, in polar protic solvents such as CH<sub>3</sub>OH, the calculated free energy agreed

very well with experiment<sup>26</sup> only when the reaction was mediated by a single CH<sub>3</sub>OH molecule. A kinetic expression was proposed that accounts for the difference between bromination of alkenes in protic and non-protic solvents.

In this study, we investigated the mechanism for the reaction of bromine with adamantylideneadamantane which is known to stop the reaction by producing a bromonium/tribromide ion pair.<sup>16, 17</sup> The typical bridged bromonium ion would be in this case Ad<sup>+</sup>Ad sterically hindered by four conformationally constrained axial hydrogen atoms of the cyclohexane moiety as illustrated in Figure 4.1. Therefore, no further reaction occurs to form the dibromo product. No reaction can occur even with small nucleophiles such as fluoride ions.<sup>27</sup> Although the reaction mechanism of Ad<sup>+</sup>Ad with Br<sub>2</sub> was extensively studied previously<sup>3, 16, 17, 27-31</sup>, no computational study was conducted to investigate the mechanism of the bromination of Ad<sup>+</sup>Ad. A potential energy surface for the bromination reaction of Ad<sup>+</sup>Ad that leads to the bromonium/tribromide ion pair will provide further insight into the bromination reaction of alkenes. It is difficult to extract conclusive information about the mechanistic pathways from experiments only. Thus, quantum chemical calculations provide the only source for a detailed characterization of the potential energy surface along the reaction path.

## 4.2 Method

All the electronic structure calculations were carried out with Gaussian03<sup>32</sup>. The

geometries of reactants, transition states, intermediates and products were fully optimized at the HF and B3LYP levels of theory using the 6-31G(d) basis set. Energies were also obtained using MP2/6-31G(d)//HF/6-31G(d), MP2/6-31G(d)//B3LYP/6-31G(d) and B3LYP/6-31G(d)//B3LYP/6-31G(d) single point calculations. Frequencies were calculated for all structures to ensure the absence of imaginary frequencies in the minima and for the presence of only one imaginary frequency in the transition states. The complete reaction pathways for all the mechanisms discussed in this study were verified using intrinsic reaction coordinate (IRC) analysis for all transition states. Structures at the last IRC points were optimized to positively identify the reactants and products to which each transition state is connected. Free energies of activation and relative stabilities of reactants and products in  $\text{CCl}_4$  and in  $\text{CH}_2\text{ClCH}_2\text{Cl}$  for the addition reaction of bromine to Ad-Ad were calculated with the polarizable continuum model (PCM) as implemented in Gaussian03. All free energy calculations involving solvation were performed using the solution-phase structures optimized at the HF/6-31G(d) and B3LYP/6-31G(d) levels of theory. By default, the PCM model builds up the cavity using the united atom (UA0) model.

## **4.3 Results and Discussion**

The results for the reaction of adamantylideneadamantane (Ad-Ad) with  $\text{Br}_2$  and  $2\text{Br}_2$  in the gas phase and in  $\text{CCl}_4$  are given in Tables 4.1-4.5.

### **4.3.1 Potential energy surface for the reaction of Ad=Ad + Br<sub>2</sub>: Pathway A**

Pathway A is the only pathway found for the reaction of Ad-Ad with one Br<sub>2</sub>. The structures involved in pathway A are shown in Figure 4.2. The relative energies of reactants, intermediates, transition states, and products are shown in Figure 4.3. Activation energies, free energies and enthalpies of activation for the reaction of Ad-Ad with Br<sub>2</sub> are given in Table 4.1. Ad-Ad can form two complexes with Br<sub>2</sub>. In one complex, R1<sup>Δ</sup>, Br<sub>2</sub> is coplanar and perpendicular to the C=C bond and in the other complex, R2<sup>Δ</sup>, Br-Br and C=C bonds are skewed to each other (Figure 4.2). All the levels except for HF, predict R1<sup>Δ</sup> to be more stable than R2<sup>Δ</sup>, by 21.2 kJ mol<sup>-1</sup> at B3LYP/6-31G(d) level of theory. Pathway A is a one-step mechanism in which adamantylideneadamantane bromonium Br<sup>+</sup> ion pair (I<sup>Δ</sup>) is formed via transition state TS<sup>Δ</sup> where one Br attacks the C=C bond of Ad=Ad. In the reactant complex R2<sup>Δ</sup>, the Br-Br and C=C bond distances are 2.316 and 1.349 Å, respectively at B3LYP/6-31G(d) level of theory, while in TS<sup>Δ</sup>, the distances increase to 3.058 and 1.419 Å, respectively. On the other hand, the Br-C bond distance in R2<sup>Δ</sup> decreases from 4.719 Å to 2.751 Å in TS<sup>Δ</sup>. Intrinsic reaction coordinate (IRC) analysis confirmed that TS<sup>Δ</sup> leads to R2<sup>Δ</sup> and I<sup>Δ</sup>. The activation energy (AE<sub>a,TS<sup>Δ</sup></sub>) for the reaction of Ad-Ad with Br<sub>2</sub> is 272.8 and 134.7 kJ mol<sup>-1</sup> at HF/6-31G(d) and B3LYP/6-31G(d) levels of theory, respectively. At MP2/6-31G(d)//HF/6-31G(d) the barrier is lowered to 111.4 kJ mol<sup>-1</sup>, while at MP2/6-31G(d)/B3LYP/6-31G(d) the barrier is increased to 145.3 kJ mol<sup>-1</sup>. The surprising lowering in the barrier by 161.4 kJ mol<sup>-1</sup> at MP2/6-31G(d)//HF/6-31G(d) suggests both the importance of electron correlation and different PES at MP2 and HF. The B3LYP/6-31G(d)/B3LYP/6-31G(d) calculation decreases the B3LYP/6-31G(d) barrier by 28.7 kJ mol<sup>-1</sup> to 106.0 kJ mol<sup>-1</sup>. The solvent model used in this study predicts a free energy of activation of

251.7 and 115.4 kJ mol<sup>-1</sup> in CCl<sub>4</sub> and 234.8 and 97.5 kJ mol<sup>-1</sup> in CH<sub>2</sub>ClCH<sub>2</sub>Cl at HF/6-31G(d) and B3LYP/6-31G(d), respectively. Although optimized structures for the trans-1,2-dibromo product (P) were obtained by all the levels of theory, no transition state leading from I<sup>A</sup> to P was obtained despite successive attempts. P was found to be more stable than I<sup>A</sup> by 26.4 and 64.2 kJ mol<sup>-1</sup> at the HF/6-31G(d) and B3LYP/6-31G(d) levels of theory, respectively. It is interesting to note that no optimized structures for the cis-1,2-dibromo product was found in this study despite successive attempts by different levels of theory.

### 4.3.2 Potential energy surfaces for the reaction of Ad=Ad with 2Br<sub>2</sub>

The results for the reaction of Ad=Ad and 2Br<sub>2</sub> will be discussed in the following order: 1) pathway B, 2) pathway C, and 3) pathway D.

#### 4.3.2.1 Pathway B:

The structures involving pathway B are shown in Figure 4.4. The relative energies of reactants, intermediates and transition states are shown in Figure 4.5. Activation energies, free energies and enthalpies of activation for pathway B are given in Table 4.2. Reactant complex (R<sup>B</sup>) of Ad=Ad + 2Br<sub>2</sub> is similar to R2<sup>A</sup>, except that the second Br<sub>2</sub> interacts sidewise. Pathway B is a one-step mechanism in which an ion pair of the bromonium ion and Br<sub>3</sub><sup>-</sup> ion is formed via a transition state TS<sup>B</sup> where one Br atom of Br<sub>2</sub> attacks the C-C bond of Ad=Ad, while the other Br atom transfers to the other Br<sub>2</sub>. In the reactant complex R<sup>B</sup>, the Br-Br bond distance for the Br<sub>2</sub> attacking the C-C is 2.329 Å at the B3LYP/6-31G(d) level

of theory, while in  $TS^B$ , the distance increases to 2.878 Å. The C-Br (Br attacking the C-C) and Br---Br<sub>2</sub> bond distances start at 4.699 and 3.172 Å in  $R^B$  and decrease to 2.904 and 2.723 Å in  $TS^B$  respectively at B3LYP/6-31G(d). IRC analysis confirmed that  $TS^B$  leads to  $R^B$  and  $I^B$ . The activation energy for the reaction of Ad-Ad with 2Br<sub>2</sub> in pathway B is 256.8 at HF/6-31G(d) and 94.1 kJ mol<sup>-1</sup> at B3LYP/6-31G(d). The activation energies at MP2/6-31G(d)/HF/6-31G(d) and MP2/6-31G(d)-B3LYP/6-31G(d) are 91.6 and 91.8 kJ mol<sup>-1</sup>, respectively, in excellent agreement with the B3LYP/6-31G(d) results. The barrier decreases to 64.4 kJ mol<sup>-1</sup> at the B3LYP/6-31+G(d)-B3LYP/6-31G(d) level of theory. Applying the solvent model yields a mechanism very similar to the gas phase one. The solvent model used in this study predicts that the free energy of activation for this reaction would be lowered in CCl<sub>4</sub> and CH<sub>2</sub>ClCH<sub>2</sub>Cl by 15.1 and 26.8 kJ mol<sup>-1</sup>, respectively at B3LYP/6-31G(d).

#### 4.3.2.2 Pathway C:

The structures of reactants, intermediates, transition states and products of pathway C are shown in Figure 4.6 for the reaction of Ad-Ad and 2Br<sub>2</sub>. The relative energies of reactants, intermediates, transition states and products are shown in Figure 4.7. Activation energies, free energies and enthalpies of activation for pathway C are given in Table 4.3.

In pathway C, intermediate  $I^C$  is formed via  $TS^C$ , which differs from  $TS^B$  in that, the Br<sub>2</sub> attacking the C-C bond of Ad-Ad is tilted from the perpendicular. This leads to a different bromonium/Br<sub>3</sub><sup>-</sup> ion pair ( $I^C$ ). In the reactant complex  $R^C$ , the Br-Br bond distance of Br<sub>2</sub> that attacks the C-C is 2.284 Å at HF/6-31G(d) level of theory, while in  $TS^C$ , the same Br-Br distance increases to 2.748 Å. The corresponding activation energy ( $\Delta E_{a,TS^C}^{\ddagger}$ ) is 61.3 kJ mol<sup>-1</sup>

at HF/6-31G(d). No transition state structure was found at B3LYP/6-31G(d) level of theory, however both  $R^C$  and  $I^C$  were obtained at this level. MP2/6-31G(d) /HF/6-31G(d) and B3LYP/6-31G(d) /HF/6-31G(d) single point calculations predict a negative barrier (Table 4.3 and Figure 4.7). The B3LYP results therefore suggest that the reaction would be barrierless and occur spontaneously in the gas phase. This pathway was only found in the gas phase. Optimization of  $TS^C$  in solution leads to a slightly different transition state which corresponds to a different pathway, pathway D. Since  $R^B$  and  $R^C$  differ by only 3.1 kJ mol<sup>-1</sup> at B3LYP/6-31G(d), a simple  $R^B \rightarrow R^C$  conversion is more likely to occur.

#### 4.3.2.3 Pathway D:

The structures involved in pathway D are shown in Figure 4.8. The relative energies of reactants, intermediates and transition states are shown in Figure 4.9. Activation energies, free energies and enthalpies of activation for pathway D are given in Table 4.4. In addition to the two bromonium/ $Br_3^-$  ion pairs ( $I^B$  and  $I^C$ ), a third bromonium/ $Br_3^-$  ion pair ( $I^D$ ) is formed via  $TS^D$  in pathway D, with an activation energy ( $\Delta E_{a,TS^D}$ ) of only 54.8 kJ mol<sup>-1</sup> at HF/6-31G(d). The structure of  $TS^D$  involves a perpendicular attack by a  $Br_2$  on the C-C bond while the other  $Br_2$  is coplanar with the C-C bond and the attacking  $Br_2$ . In the reactant complex  $R^D$ , the  $Br_2$  that attacks the C-C has a Br-Br bond distance of 2.285 Å at HF/6-31G(d), while in  $TS^D$ , it increases to 2.805 Å. This bromonium/ $Br_3^-$  ion pair ( $I^D$ ) is very similar to that observed experimentally.<sup>17</sup> No reactant complex ( $R^D$ ) or transition state ( $TS^D$ ) was found at the B3LYP/6-31G(d) level of theory. The MP2/6-31G(d) /HF/6-31G(d) and B3LYP/6-31G(d) /HF/6-31G(d) single point calculations predict, as for pathway C, that the

reaction is barrierless in the gas phase. This mechanism is also observed in  $\text{CCl}_4$  and  $\text{CH}_2\text{ClCH}_2\text{Cl}$ . The free energies of activation in  $\text{CCl}_4$  and  $\text{CH}_2\text{ClCH}_2\text{Cl}$  decrease by 45.1 and 74.5  $\text{kJ mol}^{-1}$  at HF/6-31G(d), suggesting that the reaction is most likely barrierless in solution as well. This is in accordance with experiment<sup>31</sup> where an equilibrium mixture of  $\text{Ad}=\text{Ad} + 2\text{Br}_2 \rightleftharpoons \text{adamantylideneadamantane bromonium}/\text{Br}_3^-$  was reported with no evidence of any  $\text{Ad}=\text{Ad}/2\text{Br}_2$  complex formation. Furthermore, the reaction is also highly favoured with a  $\Delta E = -135.7 \text{ kJ mol}^{-1}$  at B3LYP/6-31+G(d)//B3LYP/6-31G(d) and  $-144.1 \text{ kJ mol}^{-1}$  at MP2/6-31G(d)// B3LYP/6-31G(d).

### 3.3.3 Relative Stabilities:

The relative energies of the trans-1,2-dibromo product (P), bromonium/ $\text{Br}^-$  ion pair ( $\text{I}^{\text{A}}$ ) and the three bromonium/ $\text{Br}_3^-$  ion pairs ( $\text{I}^{\text{B}}$ ,  $\text{I}^{\text{C}}$  and  $\text{I}^{\text{D}}$ ) are given in Table 4.5. All the levels of theory predict P to be more stable than  $\text{I}^{\text{A}}$  with  $\Delta E = -26.4$  at HF/6-31G(d) and  $\Delta E = -64.2 \text{ kJ mol}^{-1}$  at B3LYP/6-31G(d). There is excellent agreement between the MP2/6-31G(d)//HF/6-31G(d) and MP2/6-31G(d)//B3LYP/6-31G(d) values of  $-93.2$  and  $-90.8 \text{ kJ mol}^{-1}$ , respectively, which are in reasonable agreement with the B3LYP/6-31G(d) value of  $-64.2 \text{ kJ mol}^{-1}$ . All the levels of theory also predict  $\Delta G (\text{I}^{\text{A}} \rightarrow \text{P})$  to be negative in the gas phase (Table 4.5). However, in  $\text{CH}_2\text{ClCH}_2\text{Cl}$   $\Delta G (\text{I}^{\text{A}} \rightarrow \text{P})$  becomes positive with values of 102.4 and 38.4  $\text{kJ mol}^{-1}$  at HF/6-31G(d) and B3LYP/6-31G(d), respectively. Therefore, the bromonium/ $\text{Br}^-$  ( $\text{I}^{\text{A}}$ ) is favored over the 1,2-dibromo product (P) in  $\text{CH}_2\text{ClCH}_2\text{Cl}$ . In  $\text{CCl}_4$ , according to HF/6-31G(d)  $\text{I}^{\text{A}}$  is favored ( $\Delta G = 40.4 \text{ kJ mol}^{-1}$ ), while according to B3LYP/6-31G(d) level of theory the dibromo product (P) is slightly favored ( $\Delta G = -12.7 \text{ kJ mol}^{-1}$ ).

Comparing the three bromonium/ $\text{Br}_3^-$  ion pairs ( $\text{I}^{\text{B}}$ ,  $\text{I}^{\text{C}}$  and  $\text{I}^{\text{D}}$ ),  $\text{I}^{\text{D}}$  is predicted (except HF) to be the most stable in both gas phase and solution.  $\text{I}^{\text{D}}$  is more stable than  $\text{I}^{\text{B}}$  with  $\Delta\text{E}(\text{I}^{\text{B}} \rightarrow \text{I}^{\text{D}})$  of  $-49.1 \text{ kJ mol}^{-1}$  at B3LYP/6-31G(d). Single point calculations at MP2/6-31G(d)/HF/6-31G(d) and MP2/6-31G(d)/B3LYP/6-31G(d) also predict  $\text{I}^{\text{D}}$  to be more stable than  $\text{I}^{\text{B}}$  by  $-15.2$  and  $-41.8 \text{ kJ mol}^{-1}$ , respectively. At the B3LYP/6-31G(d) level of theory  $\Delta\text{G}$  is  $-51.5 \text{ kJ mol}^{-1}$ .  $\text{I}^{\text{D}}$  is also predicted to be more stable in  $\text{CCl}_4$  and  $\text{CH}_2\text{ClCH}_2\text{Cl}$  solutions with  $\Delta\text{G}$  values of  $-31.0$  and  $-24.5 \text{ kJ mol}^{-1}$ , respectively. For  $\text{I}^{\text{C}} \rightarrow \text{I}^{\text{D}}$ ,  $\text{I}^{\text{C}}$  is found to be more stable than  $\text{I}^{\text{D}}$  at HF/6-31G(d) ( $\Delta\text{E} = 9.8 \text{ kJ mol}^{-1}$ ) and  $\text{I}^{\text{D}}$  is found to be more stable at B3LYP/6-31G(d) ( $\Delta\text{E} = -10.4 \text{ kJ mol}^{-1}$ ).  $\Delta\text{G}(\text{I}^{\text{C}} \rightarrow \text{I}^{\text{D}})$  is found to be negative with a value of  $-15.9 \text{ kJ mol}^{-1}$  at B3LYP/6-31G(d) in the gas phase. All the levels of theory also predict  $\Delta\text{G}$  to be negative in  $\text{CCl}_4$  and in  $\text{CH}_2\text{ClCH}_2\text{Cl}$  with values of  $-0.2$  and  $-4.6 \text{ kJ mol}^{-1}$  respectively at HF/6-31G(d) and  $-10.2$  and  $-8.2 \text{ kJ mol}^{-1}$ , respectively at B3LYP/6-31G(d). For  $\text{I}^{\text{D}} \rightarrow \text{trans-1,2-dibromo product (P)} + \text{Br}_2$ ,  $\Delta\text{E}$  is  $40.5 \text{ kJ mol}^{-1}$  at HF/6-31G(d) and  $110.6 \text{ kJ mol}^{-1}$  at B3LYP/6-31G(d). All the levels of theory also predict  $\Delta\text{G}(\text{I}^{\text{D}} \rightarrow \text{P} + \text{Br}_2)$  to be positive with  $\Delta\text{E}$  values of  $17.6$  and  $108.4 \text{ kJ mol}^{-1}$  at HF/6-31G(d) and B3LYP/6-31G(d), respectively. This again suggests that  $\text{I}^{\text{D}}$  is a very stable structure. Similar results were also obtained in  $\text{CCl}_4$  and  $\text{CH}_2\text{ClCH}_2\text{Cl}$  solution (Table 4.5). Therefore, bromination of adamantylideneadamantane will undoubtedly favor the formation of  $\text{I}^{\text{D}}$  in  $\text{CCl}_4$  and  $\text{CH}_2\text{ClCH}_2\text{Cl}$  which is in excellent agreement with the X-ray structure.<sup>17</sup> To investigate if  $\text{I}^{\text{D}}$  dissociates into the adamantylideneadamantane bromonium ion ( $\text{Ad-Ad-Br}^+$ ) and the  $\text{Br}_3^-$ , we have tried to optimize the dissociated products. It is interesting to see that despite successive

attempts with both HF and B3LYP levels of theory, an optimized structure for Ad-Ad-Br<sup>+</sup> (Figure 4.1) was not found in the gas phase or in solution (CCl<sub>4</sub> and CH<sub>2</sub>ClCH<sub>2</sub>Cl).

#### 4.4. Conclusions

A comprehensive investigation was conducted to obtain all possible mechanisms involved in the reaction of Ad=Ad with Br<sub>2</sub> and 2Br<sub>2</sub>. Only one pathway, pathway A, was found for the reaction of Ad=Ad with one Br<sub>2</sub> producing a bromonium/Br<sup>-</sup> ion pair (I<sup>A</sup>). For the reaction of Ad=Ad with 2Br<sub>2</sub> three different pathways, pathways B, C and D, all producing bromonium/Br<sup>-</sup> ion pairs (I<sup>B</sup>, I<sup>C</sup> and I<sup>D</sup>) were found. Structures for pathways A and B were obtained at both the HF and B3LYP levels of theory, while for pathways C and D all structures were only obtained at the HF level. According to the HF/6-31G(d) level, both pathways C and D are the most favored pathways with very low activation energies as compared to pathways A and B (Tables 4.1, 4.2, 4.3 and 4.4). The HF/6-31G(d) activation energies were lowered by 138.1 and 162.7 kJ mol<sup>-1</sup> at B3LYP/6-31G(d) for pathways A and B, respectively. Since the activation energy is significantly lower for the reaction of Ad=Ad with 2Br<sub>2</sub> as compared to the reaction with a single Br<sub>2</sub>, the addition of bromine to Ad=Ad is indeed mediated by a second Br<sub>2</sub> molecule where the second Br<sub>2</sub> assists in the ionization of the reactant complex to form a bromonium/Br<sup>-</sup> ion pair. This is in agreement with our previous study on the bromination reaction of ethene.<sup>24</sup> According to B3LYP/6-31G(d) the reaction would occur spontaneously in the gas phase as well as in some solvents without a barrier to yield I<sup>C</sup> and I<sup>D</sup> via pathways C and D respectively. Single point calculations at

MP2/6-31G(d)//HF/6-31G(d) and MP2/6-31G(d)//B3LYP/6-31G(d) also predict no barrier for pathways C and D. This is certainly worth investigating and we hope that gas-phase experimentalist will test this prediction. No transition state leading from the bromonium/Br<sup>-</sup> or bromonium/Br<sub>3</sub><sup>-</sup> ion pair to the trans-1,2-dibromo product (P) was obtained for the pathways investigated despite successive attempts. The most stable bromonium/Br<sub>3</sub><sup>-</sup> ion pair (I<sup>D</sup>) corresponds to the observed X-ray structure.<sup>17</sup> I<sup>D</sup> was also predicted to be the most stable structure in CCl<sub>4</sub> and CH<sub>2</sub>ClCH<sub>2</sub>Cl and would form spontaneously via pathway D.

Barriers and relative stabilities calculated using the MP2 level of theory were generally in better agreement with B3LYP than HF. Because of the size of the system, only optimization at HF/6-31G(d) and B3LYP/6-31G(d) and, MP2/6-31G(d)//HF/6-31G(d), MP2/6-31G(d)//B3LYP/6-31G(d) and B3LYP/6-31+G(d)//HF/6-31G(d) single point calculations were possible. Our previous work on the bromination of alkenes<sup>24</sup> suggests that these are reliable levels of theory for this system.

## 4.5 References

- (1) Smith, M. B.; March, J. *March's advanced organic chemistry: reactions, mechanisms, and structure*, 6<sup>th</sup> ed.; John Wiley & sons, Inc.: New Jersey, 2007.
- (2) Mare, P. B. D.; Bolton, R. *Electrophilic Additions to Unsaturated Systems*; Elsevier: New York, 1982.

- (3) Brown, R. S.; Slebocka-Tilk, H.; Bennet, A. J.; Bellucci, G.; Bianchini, R.; Ambrosetti, R. *J. Am. Chem. Soc.*, **1990**, *112*, 6310.
- (4) Schmid, G. H.; Garrat, D. G. *The Chemistry of Double-Bonded Functional Groups*; Patai, S., Ed.; Wiley: New York, 1977; Suppl. A, Part 2, p 725.
- (5) Brown, R. S.; Gedye, R.; Slebocka-Tilk, H.; Buschek, J.; Kopecky, K. *J. Am. Chem. Soc.*, **1984**, *106*, 4515.
- (6) Bellucci, G.; Chiappe, C.; Marioni, F. *J. Am. Chem. Soc.*, **1987**, *109*, 515
- (7) Bellucci, G.; Bianchini, R.; Chiappe, C.; Marioni, F.; Spagna, R. *J. Am. Chem. Soc.*, **1988**, *110*, 546.
- (8) Roberts, I.; Kimball, G.E. *J. Am. Chem. Soc.*, **1937**, *59*, 947.
- (9) Berman, D. W.; Anicich, V.; Beauchamp, J. L. *J. Am. Chem. Soc.*, **1979**, *101*, 1239.
- (10) Wieting, R. D.; Staley, R. H.; Beauchamp, J. L. *J. Am. Chem. Soc.*, **1974**, *96*, 7552.
- (11) Staley, R. H.; Wieting, R. D.; Beauchamp, J. L. *J. Am. Chem. Soc.*, **1977**, *99*, 5964.
- (12) Kim, J. K.; Findlay, M. C.; Henderson, W. G.; Caserio, M. C. *J. Am. Chem. Soc.*, **1973**, *95*, 2184.
- (13) Angelini G.; Speranza M. *J. Am. Chem. Soc.*, **1981**, *103*, 3792.
- (14) Tsai, B. P.; Werner, A. S.; Baer, T. *J. Chem. Phys.*, **1975**, *63*, 4384.
- (15) McLafferty, F. W. *Anal. Chem.*, **1962**, *34*, 2.
- (16) Strating, J.; Wieringa, J. H.; Wynberg, H. *J. Chem. Soc. D: Chem. Commun.*, **1969**, 907.
- (17) Slebocka-Tilk H.; Ball R. G.; Brown R. S. *J. Am. Chem. Soc.*, **1985**, *107*, 4504.
- (18) Brown, R. S.; Nagorski, R. W.; Bennet, A. J., McClung, R. E. D.; Aarts, G. H. M.; Klobukowski, M.; McDonald, R.; Santarsiero, B. D. *J. Am. Chem. Soc.*, **1994**, *116*, 2448.

- (19) Bellucci, G.; Chiappe, C.; Bianchini, R.; Lenoir, D.; Herges, R. *J. Am. Chem. Soc.*, **1995**, *117*, 12001.
- (20) Olah, G. A.; Prakash, G. K. S. *J. Org. Chem.* **1977**, *42*, 580.
- (21) Yamabe, S.; Minato, T.; Inagaki, S. *J. Chem. Soc., Chem. Commun.*, **1988**, 532.
- (22) Hamilton, T. P.; Schaefer, H. F. *J. Am. Chem. Soc.*, **1990**, *112*, 8260.
- (23) Cammi, R.; Mennucci, B.; Pomelli, C.; Cappelli, C.; Corni, S.; Frediani, L.; Trucks, G. W.; Frisch, M. J. *Theor. Chem. Acc.* **2004**, *111*, 66.
- (24) Islam, S. M.; Poirier, R. A. *J. Phys. Chem. A*, **2007**, *111*, 13218.
- (25) Modro, A.; Schmid, G. H.; Yates, K. *J. Org. Chem.*, **1977**, *42*, 3673.
- (26) Dubois, J. E.; Mouvier, G. *Bull. Soc. Chim. Fr.*, **1968**, 1426.
- (27) Lenoir, D.; Chiappe, C. *Chem. Eur. J.*, **2003**, *9*, 1036.
- (28) Chiappe, C.; Rubertis, A. D.; Lemmen, P.; Lenoir, D. *J. Org. Chem.*, **2000**, *65*, 1273.
- (29) Bellucci, G.; Bianchini, R.; Chiappe, C.; Ambrosetti, R.; Catalano, D.; Bennet, A. J.; Slebocka-Tilk, H.; Aarts, G. H. M.; Brown, R. S. *J. Org. Chem.*, **1993**, *58*, 3401-3406.
- (30) Brown, R. S. *Acc. Chem. Res.*, **1997**, *30*, 131.
- (31) Bellucci, G.; Bianchini, R.; Chiappe, C.; Marioni, F.; Ambrosetti, R.; Brown, R. S.; Slebocka-Tilk, H. *J. Am. Chem. Soc.* **1989**, *111*, 2640.
- (32) Frisch, M. J.; Trucks, G. W.; Schlegel, H. B.; Scuseria, G. E.; Robb, M. A.; Cheeseman, J. R.; Montgomery, Jr., J. A.; Vreven, T.; Kudin, K. N.; Burant, J. C.; Millam, J. M.; Iyengar, S. S.; Tomasi, J.; Barone, V.; Mennucci, B.; Cossi, M.; Scalmani, G.; Rega, N.; Petersson, G. A.; Nakatsuji, H.; Hada, M.; Ehara, M.; Toyota, K.; Fukuda, R.; Hasegawa, J.; Ishida, M.; Nakajima, T.; Honda, Y.; Kitao, O.; Nakai, H.; Klene, M.; Li, X.; Knox, J. E.; Hratchian, H.

P.; Cross, J. B.; Bakken, V.; Adamo, C.; Jaramillo, J.; Gomperts, R.; Stratmann, R. E.; Yazyev, O.; Austin, A. J.; Cammi, R.; Pomelli, C.; Ochterski, J. W.; Ayala, P. Y.; Morokuma, K.; Voth, G. A.; Salvador, P.; Dannenberg, J. J.; Zakrzewski, V. G.; Dapprich, S.; Daniels, A. D.; Strain, M. C.; Farkas, O.; Malick, D. K.; Rabuck, A. D.; Raghavachari, K.; Foresman, J. B.; Ortiz, J. V.; Cui, Q.; Baboul, A. G.; Clifford, S.; Cioslowski, J.; Stefanov, B. B.; Liu, G.; Liashenko, A.; Piskorz, P.; Komaromi, I.; Martin, R. L.; Fox, D. J.; Keith, T.; Al-Laham, M. A.; Peng, C. Y.; Nanayakkara, A.; Challacombe, M.; Gill, P. M. W.; Johnson, B.; Chen, W.; Wong, M. W.; Gonzalez, C.; Pople, J. A. Gaussian 03, Revision B.05, Gaussian, Inc., Wallingford CT, 2004.

**TABLE 4.1: Activation energies, free energies and enthalpies of activation (kJ mol<sup>-1</sup>) at 298.15K for the reaction of adamantalydineadamantane with Br<sub>2</sub> (Pathway A).<sup>a</sup>**

Level/Basis Set	$\Delta E_{a,TS}^A$	$\Delta H_{TS}^\ddagger{}^A$	$\Delta G_{TS}^\ddagger{}^A$
HF/6-31G(d)			
Gas Phase	272.8	269.4	281.8
CCl <sub>4</sub> <sup>b</sup>			251.7
CH <sub>2</sub> ClCH <sub>2</sub> Cl <sup>b</sup>			234.8
MP2/6-31G(d)//HF/6-31G(d)			
Gas Phase	111.4		
B3LYP/6-31G(d)			
Gas Phase	134.7	131.0	141.4
CCl <sub>4</sub> <sup>b</sup>			115.4
CH <sub>2</sub> ClCH <sub>2</sub> Cl <sup>b</sup>			97.5
MP2/6-31G(d)//B3LYP/6-31G(d)	145.3		
B3LYP/6-31+G(d)// B3LYP/6-31G(d)	106.0		

<sup>a</sup> Barriers are calculated from the Ad=Ad/Br<sub>2</sub> complex as defined in Figure 4.2 and 4.3.

<sup>b</sup> The PCM-United Atom model was used for optimized structures. In all cases  $\Delta G = \Delta\Delta G$  (thermal correction) +  $\Delta G_{solv}$ .

**TABLE 4.2: Activation energies, free energies and enthalpies of activation (kJ mol<sup>-1</sup>) at 298.15K for the reaction of adamantalydineadamantane with 2Br<sub>2</sub> (Pathway B).<sup>a</sup>**

Level/Basis Set	$\Delta E_{a,TS}^B$	$\Delta H_{TS}^\ddagger{}^B$	$\Delta G_{TS}^\ddagger{}^B$
HF/6-31G(d)			
Gas Phase	256.8	255.7	263.1
CCl <sub>4</sub> <sup>b</sup>			240.8
CH <sub>2</sub> ClCH <sub>2</sub> Cl <sup>b</sup>			217.4
MP2/6-31G(d)//HF/6-31G(d)			
Gas Phase	91.6		
B3LYP/6-31G(d)			
Gas Phase	94.1	90.0	97.5
CCl <sub>4</sub> <sup>b</sup>			82.4
CH <sub>2</sub> ClCH <sub>2</sub> Cl <sup>b</sup>			70.7
MP2/6-31G(d)//B3LYP/6-31G(d)	91.8		
B3LYP/6-31+G(d)// B3LYP/6-31G(d)	64.4		

<sup>a</sup> Barriers are calculated from the Ad=Ad/2Br<sub>2</sub> complex as defined in Figure 4.4 and 4.5.

<sup>b</sup> The PCM-United Atom model was used for optimized structures. In all cases  $\Delta G = \Delta\Delta G$  (thermal correction) +  $\Delta G_{solv}$ .

**TABLE 4.3: Activation energies, free energies and enthalpies of activation (kJ mol<sup>-1</sup>) at 298.15K for the reaction of adamantyldineadamantane with 2Br<sub>2</sub> (Pathway C) in the gas phase.<sup>a</sup>**

<b>Level/Basis Set</b>	<b><math>\Delta E_{a,TS}^c</math></b>	<b><math>\Delta H_{TS}^{\ddagger c}</math></b>	<b><math>\Delta G_{TS}^{\ddagger c}</math></b>
HF/6-31G(d)	61.3	60.5	80.2
MP2/6-31G(d)//HF/6-31G(d)	-46.0		
B3LYP/6-31G(d)// HF/6-31G(d)	-30.2		
B3LYP/6-31+G(d)// HF/6-31G(d)	-44.7		

<sup>a</sup> Barrier are calculated from the Ad=Ad/2Br<sub>2</sub> complex as defined in Figure 4.6 and 4.7.

**TABLE 4.4: Activation energies, free energies and enthalpies of activation (kJ mol<sup>-1</sup>) at 298.15K for the reaction of adamantyldineadamantane with 2Br<sub>2</sub> (Pathway D).<sup>a</sup>**

Level/Basis Set	$\Delta E_{a,TS}^D$	$\Delta H_{TS}^\ddagger^D$	$\Delta G_{TS}^\ddagger^D$
HF/6-31G(d)			
Gas Phase	54.8	54.2	81.3
CCl <sub>4</sub> <sup>b</sup>			36.2
CH <sub>2</sub> ClCH <sub>2</sub> Cl <sup>b</sup>			6.8 <sup>c</sup>
MP2/6-31G(d)//HF/6-31G(d)	-52.3		
B3LYP/6-31G(d)// HF/6-31G(d)	-32.2		
B3LYP/6-31+G(d)// HF/6-31G(d)	-55.6		

<sup>a</sup> Barriers are calculated from the Ad=Ad/2Br<sub>2</sub> complex as defined in Figure 4.8 and 4.9, respectively.

<sup>b</sup> The PCM-United Atom model was used for optimized structures. In all cases  $\Delta G = \Delta\Delta G$  (thermal correction) +  $\Delta G_{solv}$ .

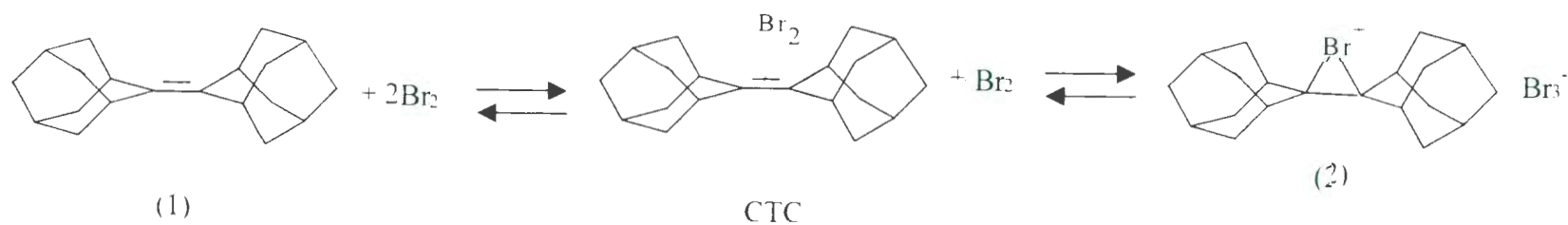
<sup>c</sup> Single point calculation using the HF/6-31G(d) optimized gas phase structure.

TABLE 4.5: Relative Stabilities ( $\text{kJ mol}^{-1}$ ) at 298.15 K.

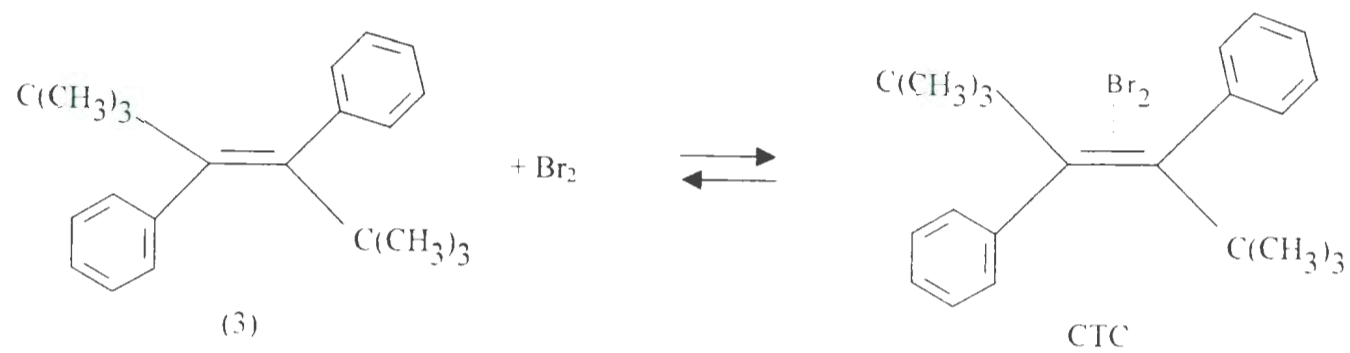
Level/Basis Set	$\text{I}^{\text{A}} \rightarrow \text{P}$			$\text{I}^{\text{B}} \rightarrow \text{I}^{\text{D}}$			$\text{I}^{\text{C}} \rightarrow \text{I}^{\text{D}}$			$\text{I}^{\text{D}} \rightarrow \text{P} + \text{Br}_2^{\text{b}}$		
	$\Delta\text{E}$	$\Delta\text{H}$	$\Delta\text{G}$	$\Delta\text{E}$	$\Delta\text{H}$	$\Delta\text{G}$	$\Delta\text{E}$	$\Delta\text{H}$	$\Delta\text{G}$	$\Delta\text{E}$	$\Delta\text{H}$	$\Delta\text{G}$
HF/6-31G(d)												
Gas Phase	-26.4	-21.9	-9.9	2.1	2.7	2.0	9.8	10.2	7.6	40.5	40.2	17.6
$\text{CCl}_4^{\text{a}}$			40.4			-3.1			-0.2			-48.6
$\text{CH}_2\text{ClCH}_2\text{Cl}^{\text{a}}$			102.4			-8.5			-4.6			93.8
MP2/6-31G(d)//HF/6-31G(d)												
Gas Phase	-93.2			-15.2			8.0			47.8		
B3LYP/6-31G(d)												
Gas Phase	-64.2	-59.8	-47.9	-49.1	-45.3	-51.5	-10.4	-7.4	-15.9	110.6	108.2	84.1
$\text{CCl}_4^{\text{a}}$			-12.7			-31.0			-10.2			83.4
$\text{CH}_2\text{ClCH}_2\text{Cl}^{\text{a}}$			38.4			-24.5			-8.2			108.4
MP2/6-31G(d)/ B3LYP/6-31G(d)												
Gas Phase	90.8			-41.8			-6.0			80.5		

<sup>a</sup> The PCM-United Atom model was used for optimized structures. In all cases  $\Delta G = \Delta\Delta G$  (thermal correction) +  $\Delta G_{\text{solv}}$ .

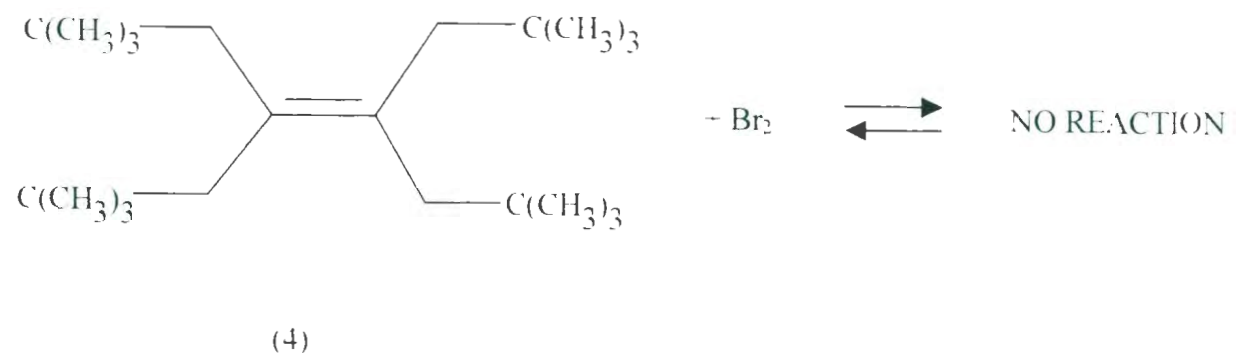
<sup>b</sup> Since the values are relatively large, we have neglected BSSE correction.



Scheme 4.1 Reaction of Adamantylideneadamantane (1) with bromine in  $\text{CCl}_4$  forms adamantylideneadamantane bromonium ion with a  $\text{Br}_3^-$  counterion (2).



Scheme 4.2 Reaction of (E)-2,2,5,5-tetramethyl-3,4-diphenylhex-3-ene (3) with bromine forms a CTC complex only.



Scheme 4.3 Tetra-tert-butylethylene (4) does not react with bromine in  $\text{CCl}_4$  solution.

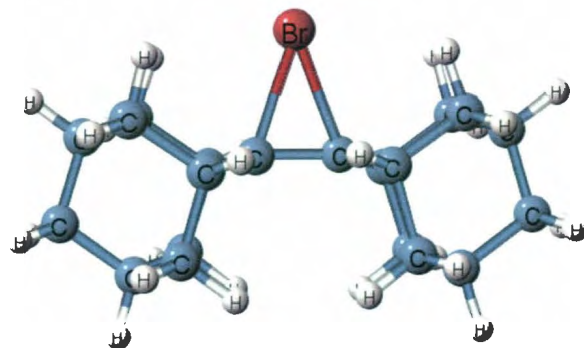


Figure 4.1. Expected structure of the adamantylideneadamantane bromonium ion.

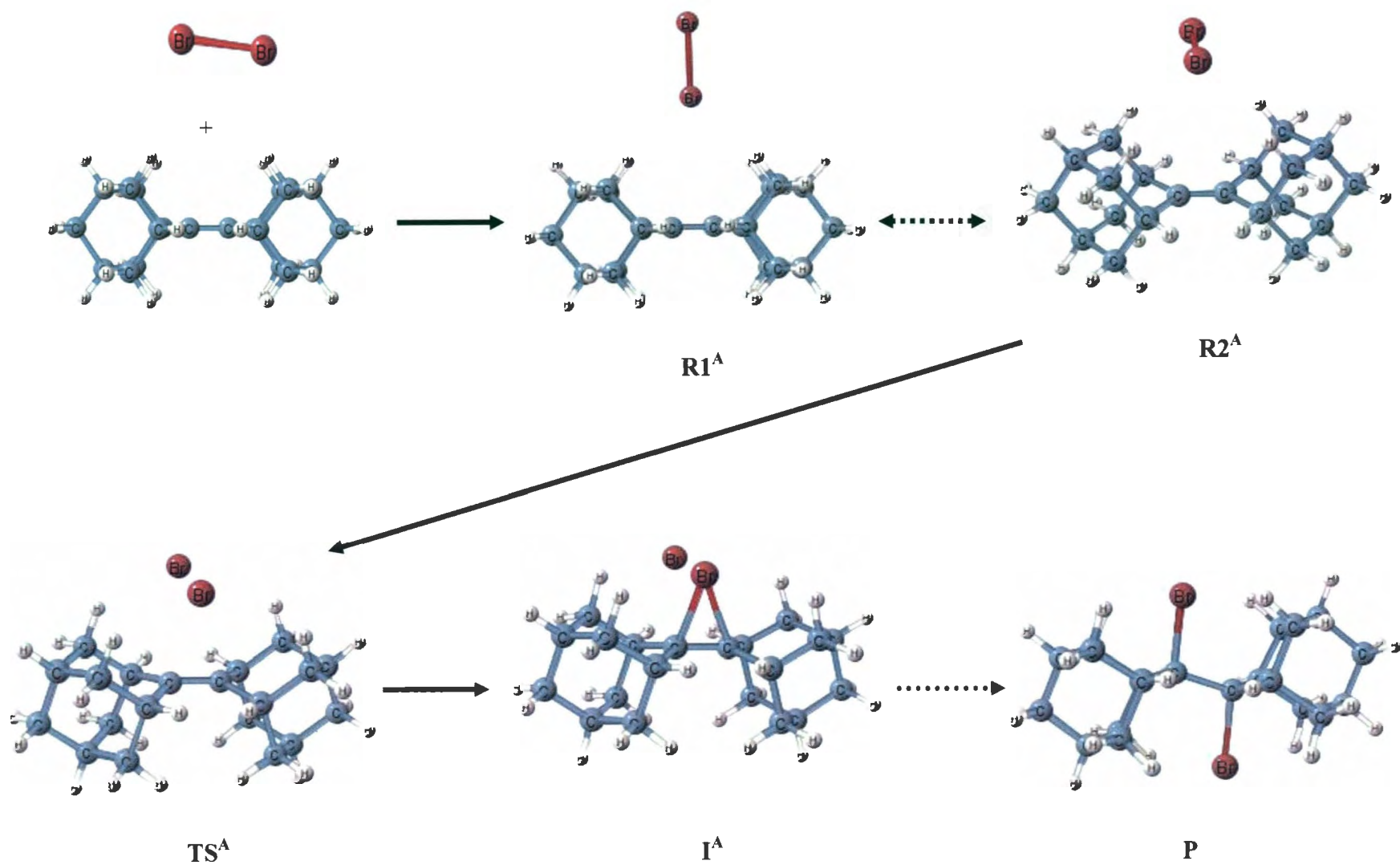


Figure 4.2. Mechanism for the reaction of Ad=Ad + Br<sub>2</sub> (Pathway A).

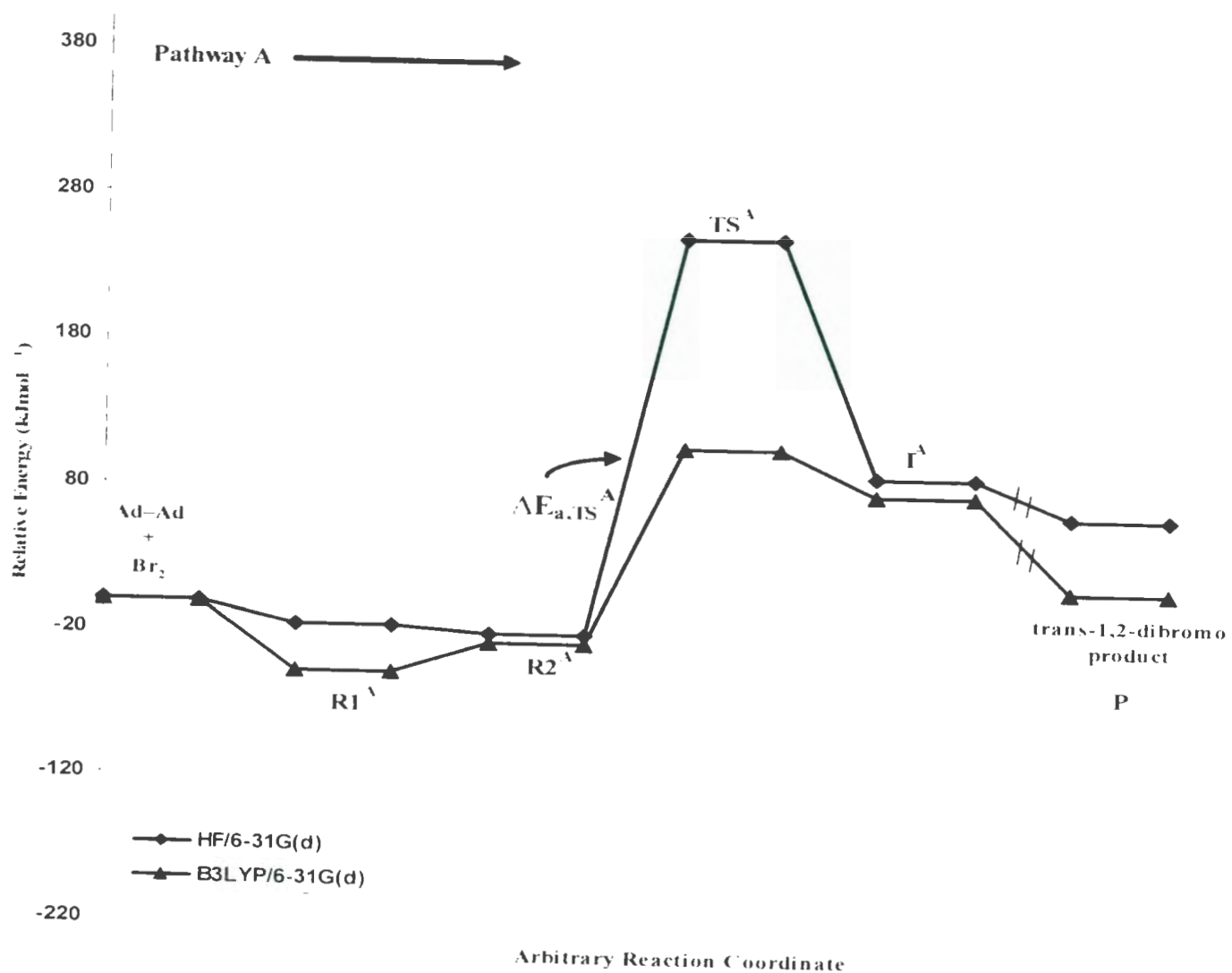


Figure 4.3. Reaction pathway for the reaction of Ad=Ad + Br<sub>2</sub> (Pathway A) at HF/6-31G(d) and B3LYP/6-31G(d) level of theory (see Figure 4.2 for structures).

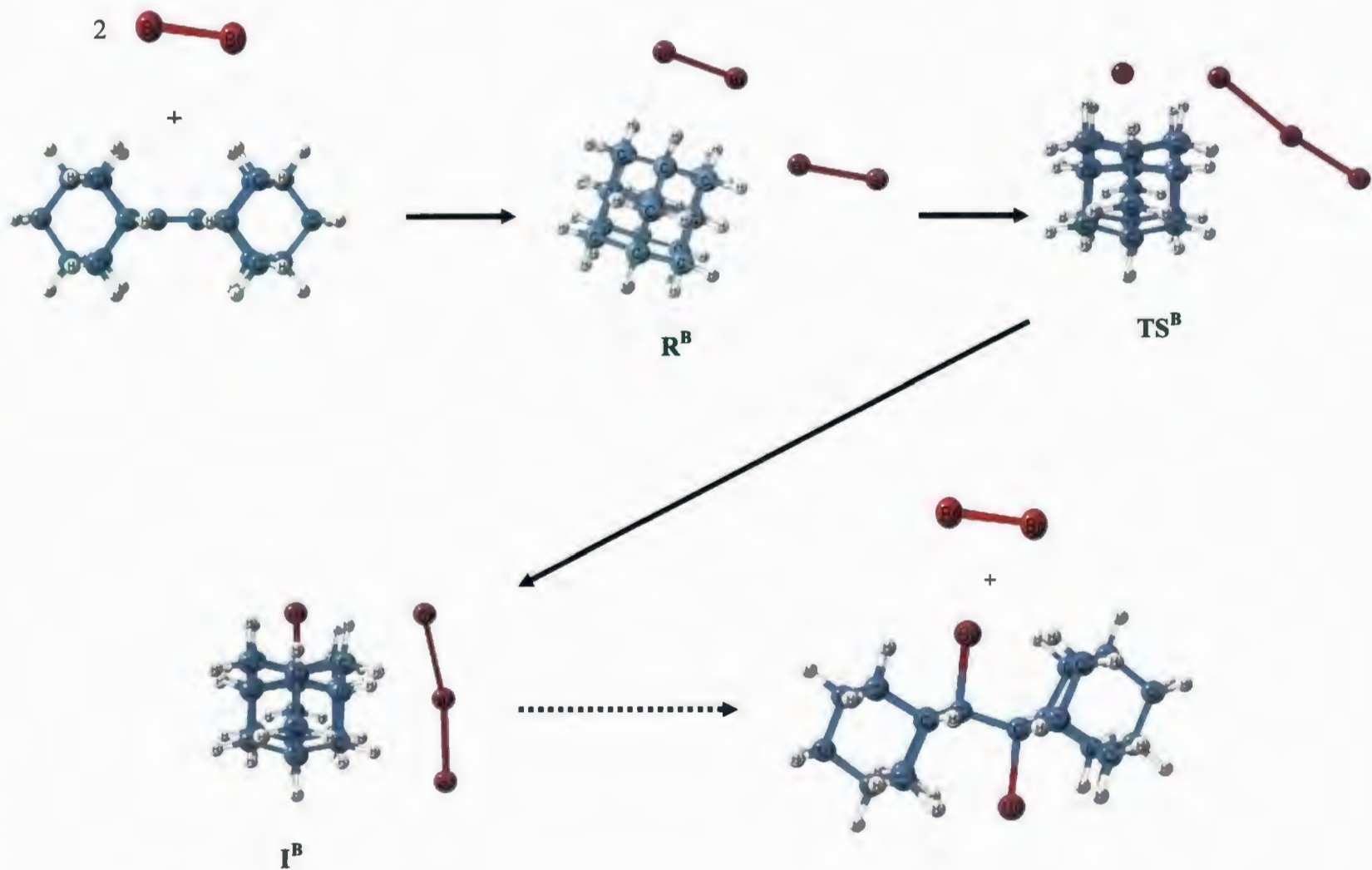


Figure 4.4. Mechanism for the reaction of Ad=Ad + 2Br<sub>2</sub> (Pathway B).

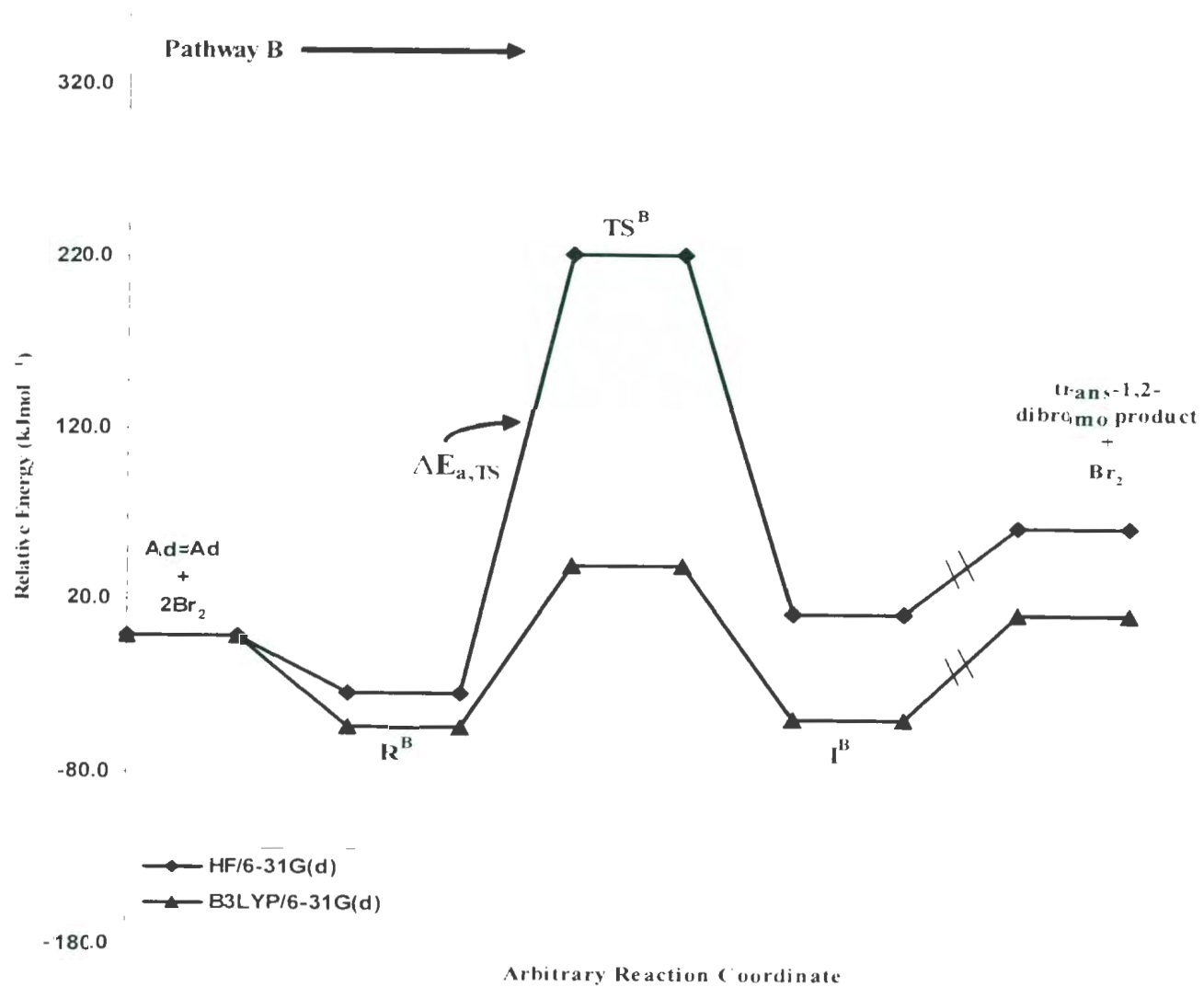


Figure 4.5. Reaction pathway for the reaction of Ad=Ad + 2Br<sub>2</sub> (Pathway B) at HF/6-31G(d) and B3LYP/6-31G(d) level of theory (see Figure 4.4 for structures).

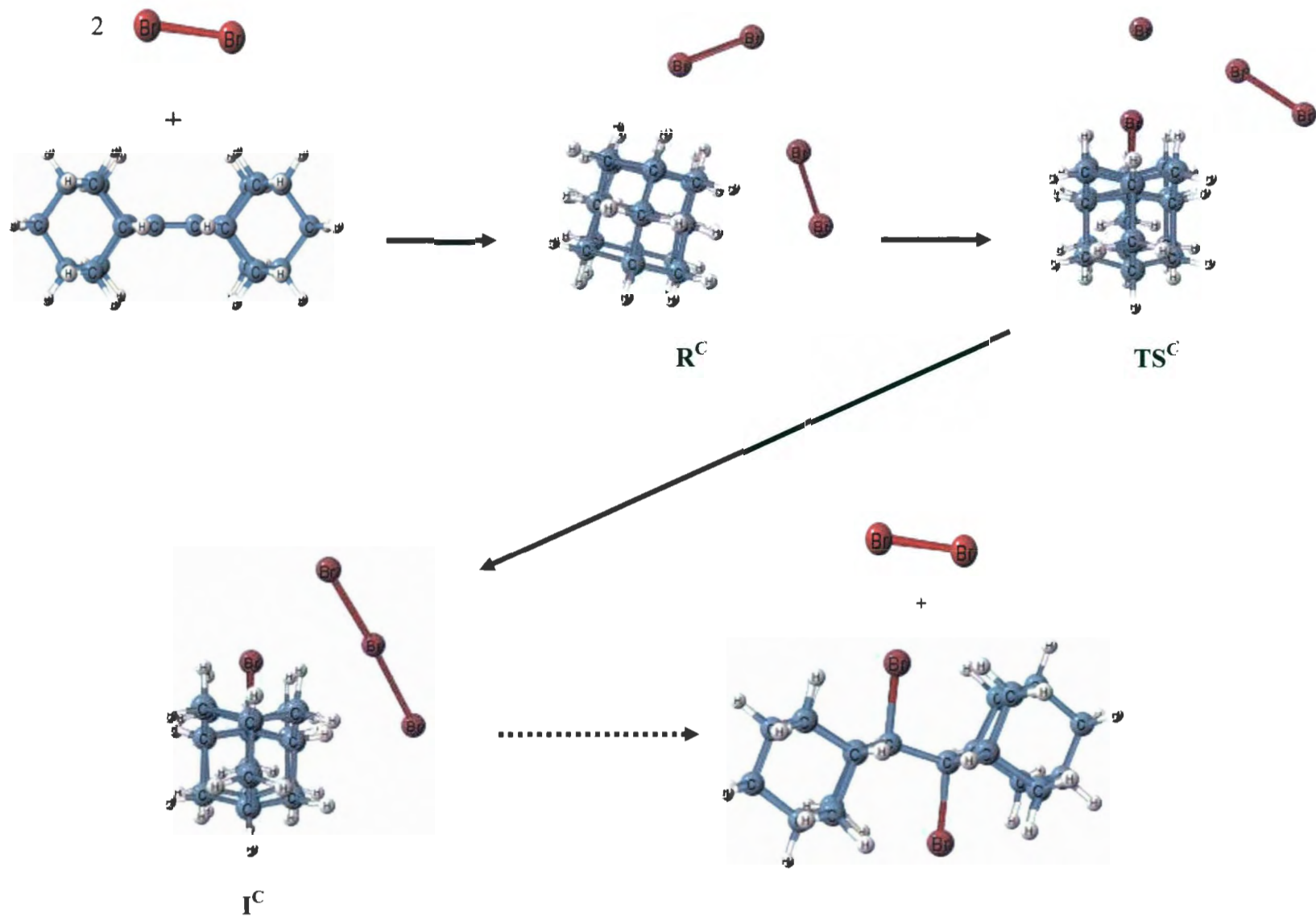


Figure 4.6. Mechanism for the reaction of Ad=Ad + 2Br<sub>2</sub> (Pathway C).

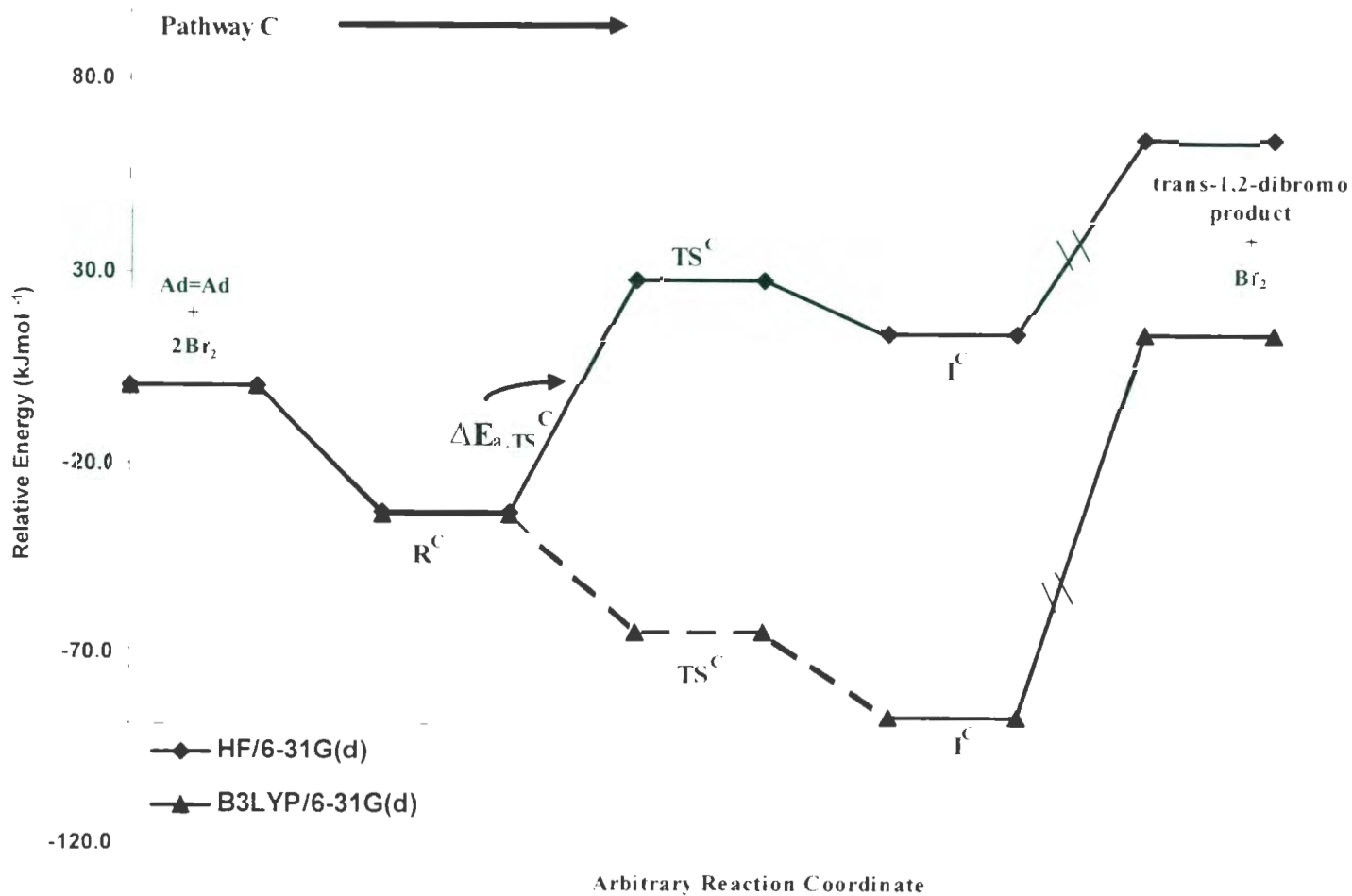


Figure 4.7. Reaction pathway for the reaction of Ad=Ad + 2Br<sub>2</sub> (Pathway C) at HF/6-31G(d) level of theory. For R<sup>C</sup> and TS<sup>C</sup> B3LYP/6-31G(d) / HF 6-31G(d) single point energies are indicated by dashed lines (see Figure 4.6 for structures).

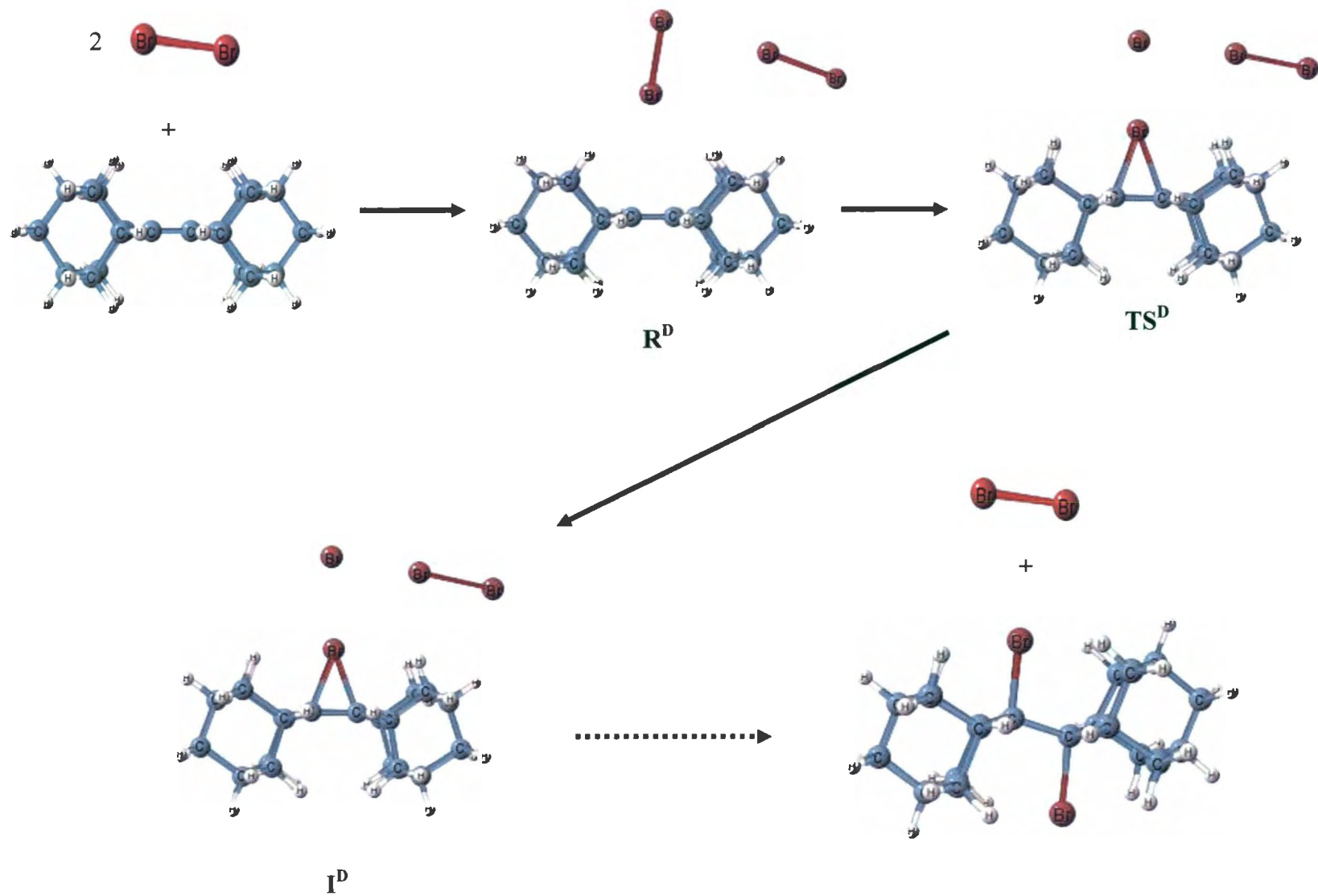


Figure 4.8. Mechanism for the reaction of Ad=Ad +  $2\text{Br}_2$  (Pathway D).

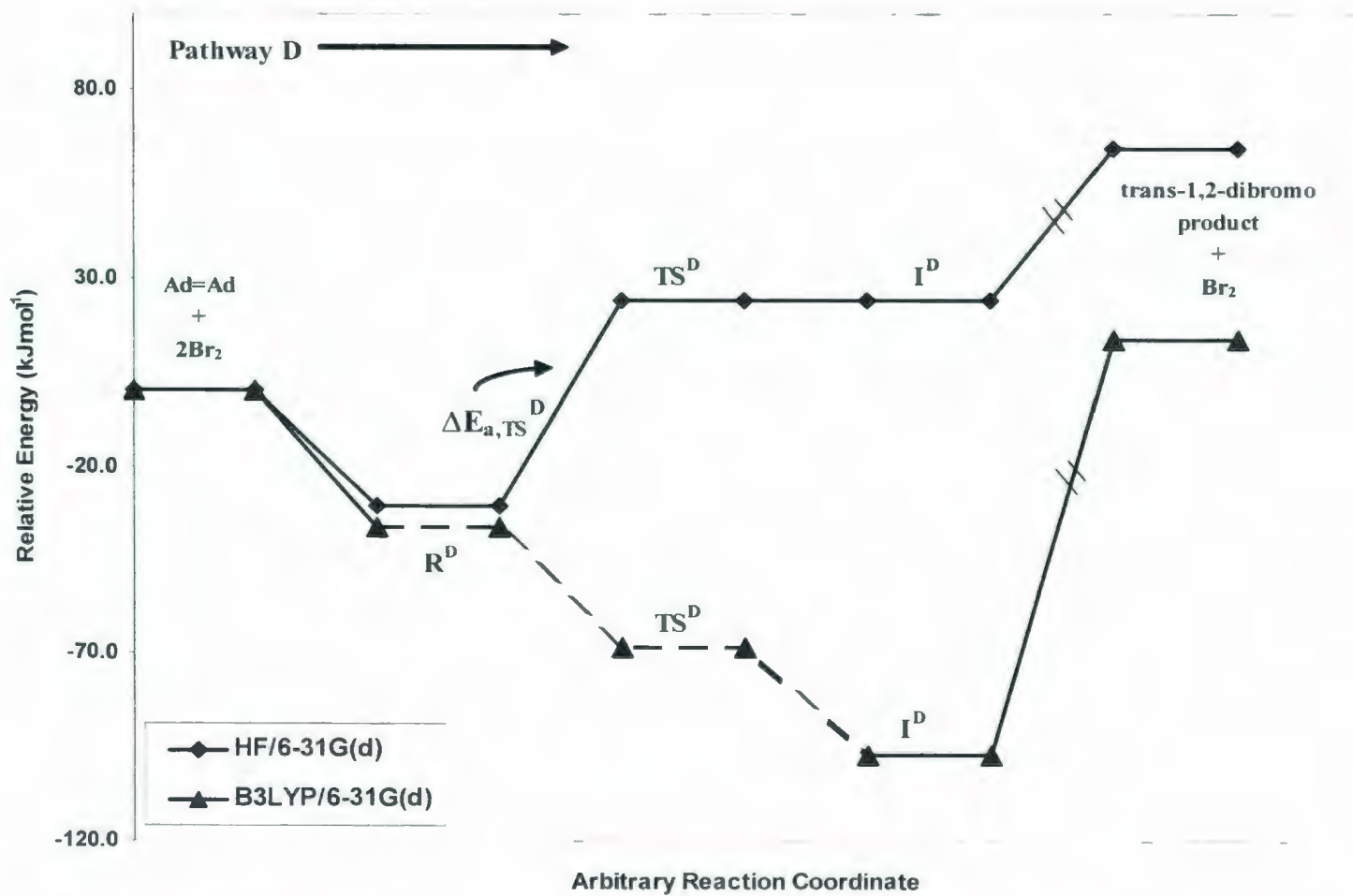


Figure 4.9. Reaction pathway for the reaction of Ad=Ad + 2Br<sub>2</sub> (Pathway D) at HF/6-31G(d) level of theory. For R<sup>D</sup> and TS<sup>D</sup> B3LYP/6-31G(d)//HF/6-31G(d) single point energies are indicated by dashed lines (see Figure 4.8 for structures).

## CHAPTER 5

# A comparison of the Standard 6-31G and Binning-Curtiss Basis Sets for Third Row Elements

### 5.1 Introduction

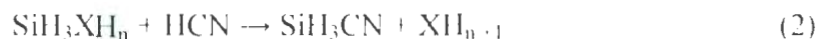
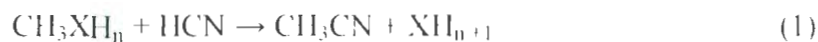
Calculations for compounds containing 1<sup>st</sup> and 2<sup>nd</sup> row elements are now very common. However, fewer calculations have been performed for compounds containing 3<sup>rd</sup> row main group elements. Such computations require basis sets that are consistent with those used for the 1<sup>st</sup> and 2<sup>nd</sup> row elements in order to obtain accurate and reliable results.<sup>1</sup> For 3<sup>rd</sup> row elements the Binning-Curtiss (BC6-31G) basis set<sup>2</sup> has been used in combination with the standard 6-31G basis set in most electronic structure packages (for example, Gaussian<sup>3</sup> and GAMESS<sup>4</sup>). However, this basis set does not actually meet the

definition of the standard 6-31G basis set, but it is constructed from a contraction of the Dunning basis set.<sup>2</sup> The core functions are highly contracted with respect to those which represent the valence region which are kept uncontracted in order to maintain flexibility. For example, for the BC6-31G basis set, the s, p and d shells consists of six (821111), four (6311), and one (5) contracted functions, respectively which gives a total of 24 basis functions. Rassolov et al.<sup>5</sup> have developed a standard 6-31G basis set for the third row elements to use in G3 theories<sup>6</sup>, where the 3d orbitals are included in the valence space of the third row elements, resulting in a total of 29 basis functions. However, very little has been reported<sup>7, 8</sup> on the use of the standard 6-31G basis set vs. the BC6-31G basis set for lower levels of theory (e.g., HF, MP2 and B3LYP) for compounds containing 3<sup>rd</sup> row elements. No detailed investigation of geometries and frequencies for compounds containing 3<sup>rd</sup> row elements have been performed using the standard 6-31G basis set. From our previous study<sup>7</sup>, thermodynamic properties for  $\text{SiH}_3\text{Br} + \text{HCN} \rightarrow \text{SiH}_3\text{CN} + \text{HBr}$  and  $\text{SiHBr} + \text{H}_2 \rightarrow \text{SiH}_2 + \text{HBr}$ , calculated at HF, MP2 and B3LYP levels using the standard 6-31G basis set, were found to be in better agreement with Gaussian-n theories compared to values obtained using the BC6-31G basis set for bromine with the same levels of theory. However, in a later study<sup>8</sup> on the reaction of alkenes with bromine, the thermodynamic properties obtained with the standard 6-31G basis set were found to agree very well with the values obtained with the BC6-31G basis set. In this study, we have extended the study to encompass other third row main group elements. G3MP2 theory<sup>9</sup> and experimental results where available are used in this study in evaluating the performance of the standard 6-31G and the BC6-31G basis sets for compounds

containing first row and second row elements in combination with the third row elements Ga, Ge, As, Se and Br. The results are compared, contrasted, and evaluated at the HF, MP2 and B3LYP levels of theory.

## 5.2 Method

In this study, the performance of the third row basis sets is evaluated by comparing the thermodynamic properties for the following isogyric reactions:



where, X = Ga, Ge, As, Se, and Br and  $n = 2, 3, 2, 1, 0$ , respectively, and for,



The geometries and frequencies for molecules containing third row atoms are also investigated. All the electronic structure calculations were carried out with Gaussian03.<sup>3</sup> The geometries of all reactants and products were fully optimized at the HF, MP2 and B3LYP levels of theory using both the 6-31G(d) and 6-31G(d,p) basis sets. For 3<sup>rd</sup> row elements, Ga, Ge, As, Se, and Br, both the standard 6-31G<sup>5</sup> and BC6-31G<sup>2</sup> basis sets are used throughout. Geometries of all the compounds were optimized ensuring all had their expected symmetries. In our previous work,<sup>7, 8</sup> it was found that the enthalpies of reaction calculated by using G3MP2<sup>9</sup>, G3B3<sup>10</sup> and G3MP2B3<sup>10</sup> levels of theory all agreed to

within 5.3 kJ mol<sup>-1</sup>. Therefore, the G3MP2 level of theory is used in this study which is expected to adequately reproduce the experimental data. G3MP2 theory is based on geometry optimizations performed at the MP2(full) level of theory using the standard 6-31G(d) basis set for 1<sup>st</sup>, 2<sup>nd</sup> and 3<sup>rd</sup> row elements. In some cases G3MP2 calculations were also performed using the BC6-31G(d) basis set for 3<sup>rd</sup> row elements. For the standard 6-31G(d) basis set, the G3MP2 energy is the summation of the following single point energies:

$$E[\text{QCISD(T)/6-31G(d)}] + \Delta E_{\text{MP2}} + \Delta E(\text{SO}) + E(\text{HLC}) + E(\text{ZPE}), \text{ where } (\Delta E_{\text{MP2}})$$

$[E(\text{MP2/G3MP2Large})] - [E(\text{MP2/6-31G(d)})]$ . While, the G3MP2 energy calculated using the BC6-31G(d) basis set is given by

$$E[\text{QCISD(T)/BC6-31G(d)}] + \Delta E_{\text{MP2}} + \Delta E(\text{SO}) + E(\text{HLC}) + E(\text{ZPE}), \text{ where } (\Delta E_{\text{MP2}})$$

$$[E(\text{MP2/G3MP2Large})] - [E(\text{MP2/BC6-31G(d)})]$$

For all the 3<sup>rd</sup> row elements the G3MP2large basis set,<sup>1-11</sup> which is not yet incorporated in Gaussian03, was used for G3MP2 calculations. Frequencies were calculated for all structures to ensure the absence of imaginary frequencies in the minima.

### 5.3 Results and Discussion

The optimized geometries, frequencies, the thermodynamic properties of the isogyric reactions and heats of formation of some energetically stable compounds containing 3<sup>rd</sup> row elements are presented in Tables 5.1-5.9.

### 5.3.1 Geometries of molecules containing 3<sup>rd</sup> row elements:

Bond lengths and angles calculated at MP2 and B3LYP levels of theory using the standard 6-31G(d,p) and BC6-31G(d,p) basis sets for all the structures containing 3<sup>rd</sup> row elements are listed in Table 5.1 along with the experimental data where available. The geometric parameters calculated with the standard 6-31G(d,p) and BC6-31G(d,p) basis sets are quite different. The MP2 bond lengths are always shorter than the B3LYP bond lengths and with a few exceptions ( $\angle\text{H-C-H}$  in  $\text{CH}_3\text{Br}$ ,  $\text{CH}_3\text{SeH}$ ,  $\text{CH}_3\text{AsH}_2$  and  $\text{CH}_3\text{GaH}_2$  and  $\angle\text{H-Si-X}$  (X = Br, Ga) in  $\text{SiH}_3\text{Br}$  and  $\text{SiH}_3\text{GaH}_2$ ) MP2 bond angles are larger or almost equal to B3LYP angles. However, for all the levels of theory the agreement with experiment is similar to that found for compounds containing 1<sup>st</sup> and 2<sup>nd</sup> row elements. Table 5.2 lists the mean absolute deviations (MAD) in bond lengths and angles from experiment and calculations. A total of 25 experimental bond lengths and 18 experimental bond angles were used to calculate the mean absolute deviations from experiment. A total of 36 bond lengths and 36 bond angles were used to calculate the mean absolute deviations between the values calculated at MP2 and B3LYP level of theory using the standard 6-31G(d,p) and BC6-31G(d,p) basis sets. For bond lengths the MAD is  $\sim 0.012\text{\AA}$  except for B3LYP/6-31G(d,p) which has a MAD of  $0.019\text{\AA}$ . The lowest MAD ( $0.0118\text{\AA}$ ) is given by MP2/6-31G(d). For bond angles the MAD (18 of bond angles) is 0.5-0.6. Changes in bond lengths with change in basis set are generally larger at B3LYP ( $0.0078\text{\AA}$ ) than at MP2 (MAD= $0.0057\text{\AA}$ ). For example in HBr, the difference in bond lengths calculated at B3LYP/6-31G(d,p) and B3LYP/BC6-31G(d,p) is  $0.0098\text{\AA}$ , while the difference at MP2/6-31G(d,p) and MP2/BC6-31G(d,p) is  $0.0018\text{\AA}$ .

However, the difference due to change of basis set at the MP2 level for X-H bond distances in GaH<sub>3</sub>, CH<sub>3</sub>SeH, SiH<sub>3</sub>SeH, SiH<sub>3</sub>GeH<sub>3</sub>, CH<sub>3</sub>GaG<sub>2</sub> and SiH<sub>3</sub>GaH<sub>2</sub> and C-X bond distances in CH<sub>3</sub>Br and CH<sub>3</sub>AsH<sub>2</sub> are larger than the respective B3LYP values.

### 5.3. 2 Frequencies of molecules containing 3<sup>rd</sup> row elements:

Frequencies for the molecules containing 3<sup>rd</sup> row elements at MP2/6-31G(d,p), MP2/BC6-31G(d,p), B3LYP/6-31G(d,p) and B3LYP/BC6-31G(d,p) are listed in Table 5.3 along with the experimental frequencies where available. MAD values for the frequencies are given in Table 5.4. A total of 145 frequencies of compounds containing 3<sup>rd</sup> row elements were used to calculate the MAD between calculated frequencies and 73 to calculate the MAD between experimental and calculated frequencies. In most cases the B3LYP/6-31G(d,p) frequencies are in better agreement with experimental frequencies (Table 5.3 and 5.4), with a MAD of 40.1 cm<sup>-1</sup> compared to 57.8 cm<sup>-1</sup> for B3LYP/BC6-31G(d,p) and, 94.2 cm<sup>-1</sup> and 105.4 cm<sup>-1</sup> for MP2/6-31G(d,p) and MP2/BC6-31G(d,p), respectively. Therefore, for both MP2 and B3LYP the standard 6-31G basis set gives the best agreement and overall the B3LYP with the standard 6-31G(d,p) basis set performs the best in calculating frequencies for molecules containing 3<sup>rd</sup> row elements. B3LYP frequencies are found to be slightly more sensitive to basis set than MP2 frequencies, i.e. the differences between the frequencies calculated at B3LYP/6-31G(d,p) and B3LYP/BC6-31G(d,p),  $\Delta\nu(\text{B3LYP})$ , are generally larger than the differences between the frequencies calculated at MP2/6-31G(d,p) and MP2/BC6-31G(d,p),  $\Delta\nu(\text{MP2})$  (Table 5.3). For unscaled frequencies the MAD between MP2/6-31G(d,p) and MP2/BC6-

31G(d,p) is  $16.4 \text{ cm}^{-1}$ , while between B3LYP/6-31G(d,p) and B3LYP/BC6-31G(d,p) the MAD is  $20.3 \text{ cm}^{-1}$ . The MAD between the MP2/6-31G(d,p) and B3LYP/6-31G(d,p) is  $58.9 \text{ cm}^{-1}$ , while the MAD between the MP2/BC6-31G(d,p) and B3LYP/BC6-31G(d,p) is  $51.8 \text{ cm}^{-1}$ , when unsealed frequencies are used. Standard frequency scaling factors for compounds containing 1<sup>st</sup> and 2<sup>nd</sup> row elements are available in the literature.<sup>12,13</sup> The MAD for scaled frequencies using the standard scale factors are also given in Table 5.4. Scaling improves the frequencies significantly at all levels of theory and basis sets. After scaling MP2/6-31G(d,p) now has the lowest MAD ( $24.4 \text{ cm}^{-1}$ ) from experiment. For B3LYP/6-31G(d,p) and B3LYP/BC6-31G(d,p) the MAD are lowered to 29.6 and 29.3  $\text{kJ mol}^{-1}$ , respectively when frequencies are scaled. The MAD between B3LYP/6-31G(d,p) and B3LYP/BC6-31G(d,p) is  $19.5 \text{ cm}^{-1}$ , while MP2/6-31G(d,p) and MP2/BC6-31G(d,p) is  $15.3 \text{ cm}^{-1}$ . It is interesting to note that after scaling the MAD are now similar for all levels of theory and basis sets.

The frequency scaling factors for 1<sup>st</sup> and 2<sup>nd</sup> row elements are 0.9608 and 0.9370 at B3LYP/6-31G(d,p) and MP2/6-31G(d,p), respectively.<sup>12,13</sup> Using the 73 experimental frequencies available for compounds containing 3<sup>rd</sup> row elements scaling factors were calculated by dividing the experimental frequencies with the corresponding calculated frequencies and then taking their average. The scale factors were found to be 0.9408, 0.9246 at B3LYP/6-31G(d,p) and B3LYP/BC6-31G(d,p), respectively and 0.8982 and 0.8926 at MP2/6-31G(d,p) and MP2/BC6-31G(d,p), respectively. These scaling factors indicate that in general frequencies calculated for compounds involving 3<sup>rd</sup> row elements

tend to be generally higher than those calculated for compounds containing 1<sup>st</sup> and 2<sup>nd</sup> row elements.

### **5.3.3 Thermodynamic properties for the isogyric reactions involving 3<sup>rd</sup> row elements:**

The thermodynamic properties for reactions (1) and (2) are listed in Table 5.5. For all X, X= Ga, Ge, As, Se, and Br, reaction (1) is exothermic with G3MP2 enthalpies of -2.3, -9.2, -29.6, -46.7, and -56.0 kJ mol<sup>-1</sup>, respectively. From Figure 5.1, it is interesting to note that all levels predict that the enthalpy of reaction becomes more exothermic in going from Ga to Br. The G3MP2 free energies of reaction for X= Ge, As, Se and Br are exergonic with values of -9.2, -29.9, -44.5, and -54.3 kJ mol<sup>-1</sup>, while for X=Ga the reaction is slightly endergonic with a G3MP2 free energy of 5.0 kJ mol<sup>-1</sup>. For X= Ga, Ge and As, reaction (2) is exothermic with G3MP2 enthalpies of -23.8, -25.3 and -14.2 kJ mol<sup>-1</sup>, respectively, while for X= Se and Br, reaction (2) is endothermic with  $\Delta H$  of 13.0 and 43.6 kJ mol<sup>-1</sup>, respectively. From Figure 5.2, we see that in this case the enthalpy of reaction becomes more endothermic in going from Ga to Br for all levels of theory. Similarly, the free energies are exergonic for X= Ga, Ge and As, with values of -19.3, -27.5 and -17.3 kJ mol<sup>-1</sup>, respectively and endergonic for X= Se and Br, with values of 11.7 and 43.8 kJ mol<sup>-1</sup> at G3MP2. For the reactions with CH<sub>3</sub>Br and SiH<sub>3</sub>Br, the G3MP2 enthalpies and free energies are calculated using both the standard 6-31G(d) and BC6-31G(d) basis sets. The G3MP2 energies calculated using the standard 6-31G(d) and the BC6-31G(d) basis set differ by only 0.2 kJ mol<sup>-1</sup> for the reaction with CH<sub>3</sub>Br and 1.6 kJ

mol<sup>-1</sup> with SiH<sub>3</sub>Br (Table 5.5). Experimental enthalpies of reaction estimated from the heats of formation of the individual species (Table 5.9, to be discussed) are only available for the reaction with CH<sub>3</sub>Br and SiH<sub>3</sub>Br. The G3MP2 enthalpies for both these two reactions agree reasonably well with experiment deviating by 7 kJ mol<sup>-1</sup> and 14 kJ mol<sup>-1</sup>, respectively. Although in some reactions addition of p-polarization functions to hydrogen give better thermodynamic values, overall polarization functions have little effect on the thermodynamics. Figure 5.3 (reaction (1)) and Figure 5.4 (reaction (2)) represent the differences between the G3MP2 enthalpies from the enthalpies calculated at MP2 and B3LYP levels of theory using both the standard 6-31G(d,p) and BC6-31G(d,p) basis sets. From Figure 5.3, it is clear that when X = Br, the error in the enthalpies calculated at MP2 and B3LYP levels of theory is small for both the basis sets. This is similar to our previous investigation on the bromination of alkenes.<sup>8</sup> However, the errors in enthalpies calculated at B3LYP/6-31G(d,p) are slightly larger for X = Ga, Ge, As and Se. For all X in reaction (2), the enthalpies of reaction calculated at both MP2 and B3LYP levels of theory using the standard 6-31G(d,p) basis set are in excellent agreement with the G3MP2 enthalpies (all within 5 kJ mol<sup>-1</sup>), while the BC6-31G(d) basis set performs especially poorly for X = Ge, As, Se, and Br. It is important to mention here that for the reaction of HCN with SiH<sub>3</sub>AsH<sub>2</sub> the enthalpy calculated by the BC6-31G basis set is found to be endothermic, while with standard 6-31G, it is found to be exothermic in agreement with the G3MP2 level of theory (Table 5.5).

Both reactions (1) and (2) involved HCN as one of the reactants. To see the effect of 2<sup>nd</sup> row elements on reaction thermodynamics, two more reactions, reaction (3) ( $\text{CH}_3\text{Br} + \text{HCl} \rightarrow \text{CH}_3\text{Cl} + \text{HBr}$ ) and reaction (4) ( $\text{SiH}_3\text{Br} + \text{HCl} \rightarrow \text{SiH}_3\text{Cl} + \text{HBr}$ ) are considered. The thermodynamic properties for reaction (3) and (4) are listed in Table 5.6 and the plot of reaction enthalpies vs. theory/basis set are given in Figure 5.5 for reaction (3) and Figure 5.6 for reaction (4). G3MP2 enthalpies calculated with the standard 6-31G(d) basis set are in excellent agreement with the G3MP2 enthalpies calculated with the BC6-31G(d) basis set, differing by only 0.1 kJ mol<sup>-1</sup> for reaction (3) and 1.6 kJ mol<sup>-1</sup> for reaction (4). The G3MP2 enthalpies were also found to agree well with experiment differing by no more than 5 kJ mol<sup>-1</sup>. The G3MP2 enthalpies calculated with both the standard 6-31G(d) and BC6-31G(d) basis set are found to be endothermic for reaction (3) and exothermic for reaction (4). For reaction (3), the HF, MP2 and B3LYP enthalpies calculated using the standard 6-31G and the BC6-31G basis set are in excellent agreement, differing by no more than 4.3 kJ mol<sup>-1</sup>. In this case, all enthalpies of reaction are in good agreement with both the G3MP2 and experimental values. However, for reaction (4), the differences between the enthalpies of reaction calculated with the standard 6-31G and the BC6-31G basis set are large, ranging from 17.5 to 23.4 kJ mol<sup>-1</sup>. The reaction enthalpies calculated with the standard 6-31G basis set are found to be exothermic (except for MP2/6-31G(d,p)), while the reaction enthalpies obtained by BC6-31G are endothermic for all levels of theory and basis sets investigated (Table 5.6 and Figure 5.6). In this case, the enthalpies calculated with the BC6-31G basis set are in poor agreement with both the G3MP2 and the experimental values. Therefore, the choice of

basis set is extremely important for reactions involving both 2<sup>nd</sup> and 3<sup>rd</sup> row elements. For reactions (2) and (4), both involving Si, the standard 6-31G basis set predicts better reaction enthalpies and free energies than the BC6-31G basis set. It would be interesting to see if the same result is found for other 2<sup>nd</sup> row elements. Therefore, thermodynamic properties for reaction (5),  $\text{PH}_2\text{Br} + \text{HCN} \rightarrow \text{PH}_2\text{CN} + \text{HBr}$ , are calculated using both the standard 6-31G and the BC6-31G basis sets and the values are given in Table 5.7. The plot of reaction enthalpies vs. level of theory/basis set is shown in Figure 5.7. Differences in enthalpies calculated with the standard 6-31G and the BC6-31G basis set range from 9.3 to 15.4 kJ mol<sup>-1</sup> depending on the level of theory. Like reaction (4),  $\text{SiH}_3\text{Br}$ , the reaction enthalpies and free energies calculated with the standard 6-31G basis set is in better agreement with G3MP2 values (Table 5.7 and Figure 5.7).

#### **Mean Absolute Deviations (MAD) of the reaction enthalpies:**

The mean absolute deviations for the reaction enthalpies involving 1<sup>st</sup> and 3<sup>rd</sup> row elements, reaction (1), and for reactions involving 1<sup>st</sup>, 2<sup>nd</sup> and 3<sup>rd</sup> row elements, reactions (2) and (5), are calculated at different levels of theory and basis sets from G3MP2 enthalpies and the values are given in Table 5.8. The MAD for enthalpies of reactions involving 1<sup>st</sup> and 3<sup>rd</sup> row elements are not significantly affected by the change of basis set, ranging from 2.6 to 13.5 kJ mol<sup>-1</sup> for the standard 6-31G basis set and 1.8 to 5.8 kJ mol<sup>-1</sup> for BC6-31G basis set. The MAD are slightly higher at B3LYP/6-31G(d,p) and HF/6-31G(d). On the other hand, the MAD for the reaction enthalpies involving 1<sup>st</sup>, 2<sup>nd</sup> and 3<sup>rd</sup> row elements (reaction (2) and (5)) are significantly larger for the BC6-31G basis set at

all levels of theory investigated, ranging from 10.1 to 18.4 kJ mol<sup>-1</sup>. The MAD for the standard 6-31G basis set range from only 2.3 to 8.5 kJ mol<sup>-1</sup> depending on the level of theory. Therefore, although the Binning-Curtiss and standard basis sets perform almost identically for reactions involving only 1<sup>st</sup> and 3<sup>rd</sup> row elements, the standard basis set performs much better for reactions involving 1<sup>st</sup>, 2<sup>nd</sup> and 3<sup>rd</sup> row elements. These results indicate that the BC6-31G basis set for 3<sup>rd</sup> row elements is improperly balanced relative to the standard 6-31G basis set used for 1<sup>st</sup> and 2<sup>nd</sup> row elements. The imbalance would result in basis set superposition error and basis set incompleteness error. The extra basis functions (3d) for the standard basis set are evidently playing a significant role, especially when bonding between 2<sup>nd</sup> and 3<sup>rd</sup> row elements is present.

#### 5.3.4 Exploring Heats of Formation ( $\Delta H_f$ ) :

No experimental or theoretical heats of formation ( $\Delta H_f$ ) have been reported for CH<sub>3</sub>SeH, SiH<sub>3</sub>SeH, CH<sub>3</sub>AsH<sub>2</sub>, SiH<sub>3</sub>AsH<sub>2</sub>, CH<sub>3</sub>GeH<sub>3</sub> and SiH<sub>3</sub>GeH<sub>3</sub>. In this study, the enthalpies for reaction (1) and reaction (2) for all X, X = Ga, Ge, As, Se, and Br, have been obtained. The  $\Delta H_f$  values obtained in this study are given in Table 5.9. From the G3MP2 enthalpies of reaction and the most recent and reliable experimental heats of formation for CH<sub>3</sub>CN, SiH<sub>3</sub>CN, SeH<sub>2</sub>, AsH<sub>3</sub>, GeH<sub>4</sub>, HCN,  $\Delta H_f$  for CH<sub>3</sub>SeH, SiH<sub>3</sub>SeH, CH<sub>3</sub>AsH<sub>2</sub>, SiH<sub>3</sub>AsH<sub>2</sub>, CH<sub>3</sub>GeH<sub>3</sub> and SiH<sub>3</sub>GeH<sub>3</sub> are calculated to be 18.3, 18.0, 38.4, 82.4, 41.9 and 117.4 kJ mol<sup>-1</sup>, respectively. Heats of formation were also calculated for HCN, CH<sub>3</sub>CN, SiH<sub>3</sub>CN, HBr, CH<sub>3</sub>Br, SiH<sub>3</sub>Br, CH<sub>3</sub>Cl, HCl and SiH<sub>3</sub>Cl, for which reliable  $\Delta H_f$  values are available for comparison. The  $\Delta H_f$  for CH<sub>3</sub>Br, HCN, CH<sub>3</sub>CN and HBr are

calculated using the G3MP2 enthalpy of reaction for  $\text{CH}_3\text{Br} + \text{HCN} \rightarrow \text{CH}_3\text{CN} + \text{HBr}$  ( $\Delta H$  -56.0 kJ mol<sup>-1</sup> at G3MP2) and most recent experimental heats of formation for  $\text{CH}_3\text{Br}$ ,  $\text{HCN}$ ,  $\text{CH}_3\text{CN}$  and  $\text{HBr}$  (given in Table 5.9). The resulting  $\Delta H_f$  values are -37.8, 131.8, 73.9 and -36.4 kJ mol<sup>-1</sup> respectively, all values being in excellent agreement with experiment. Similarly, heats of formation for  $\text{HCN}$ ,  $\text{SiH}_3\text{Br}$ ,  $\text{SiH}_3\text{CN}$  and  $\text{HBr}$  are calculated using the enthalpy of reaction for  $\text{SiH}_3\text{Br} + \text{HCN} \rightarrow \text{SiH}_3\text{CN} + \text{HBr}$  (43.6 kJ mol<sup>-1</sup> at G3MP2), along with experimental heats of formation for  $\text{HCN}$ ,  $\text{SiH}_3\text{Br}$ ,  $\text{HBr}$  and  $\text{SiH}_3\text{CN}$ . The  $\Delta H_f$  values are again in excellent agreement with experiment. Heats of formation of  $\text{CH}_3\text{Br}$ ,  $\text{HBr}$ ,  $\text{SiH}_3\text{Br}$ ,  $\text{CH}_3\text{Cl}$ ,  $\text{HCl}$  and  $\text{SiH}_3\text{Cl}$  are also calculated using the enthalpy of reaction (3),  $\text{CH}_3\text{Br} + \text{HCl} \rightarrow \text{CH}_3\text{Cl} + \text{HBr}$  (11.1 kJ mol<sup>-1</sup> at G3MP2) and reaction (4),  $\text{SiH}_3\text{Br} + \text{HCl} \rightarrow \text{SiH}_3\text{Cl} + \text{HBr}$  (-2.7 kJ mol<sup>-1</sup> at G3MP2) and by using the experimental heats of formation of  $\text{CH}_3\text{Br}$ ,  $\text{HCl}$ ,  $\text{CH}_3\text{Cl}$ ,  $\text{HBr}$ ,  $\text{SiH}_3\text{Br}$  and  $\text{SiH}_3\text{Cl}$ . The  $\Delta H_f$  values obtained by reaction (3) is in excellent agreement with experiment, while the values obtained by using reaction (4) is also in reasonable agreement with experiment differing by no more than 4.8 kJ mol<sup>-1</sup> from experiment. Therefore, these results provide further evidence that the G3MP2 enthalpies are very reliable for the reactions studied and proved to be useful in predicting the performance of the standard 6-31G and BC6-31G basis sets.

## 5.4 Conclusions

Computations were carried out in order to compare the standard and BC6-31G basis sets for thermodynamic properties, geometries and frequencies. The performance of

the standard 6-31G basis set compared to the BC6-31G basis set for a series of isogyric reactions containing third row elements, Ga, Ge, As, Se and Br, was evaluated using G3MP2 theory. A comparison of the thermodynamic properties calculated with the standard 6-31G and the BC6-31G basis set with the G3MP2 energies revealed that for compounds with 1<sup>st</sup> row elements and 3<sup>rd</sup> row elements, both basis sets perform equally well, while compounds with 2<sup>nd</sup> and 3<sup>rd</sup> row elements or with 1<sup>st</sup>, 2<sup>nd</sup> and 3<sup>rd</sup> row elements, the standard 6-31G basis set showed the best performance. Optimized geometries were also tabulated and compared for the standard 6-31G(d,p) and BC6-31G(d,p) basis sets. Geometric parameters calculated with both the basis sets were found to agree well with experiment, with errors similar to those found for compounds containing 1<sup>st</sup> and 2<sup>nd</sup> row elements. Frequencies were also compared to experiment and the unscaled B3LYP 6-31G(d,p) frequencies were found to be in better agreement with experiment (Table 5.4). MP2/6-31G(d,p) were also found to predict better frequencies than MP2/BC6-31G(d,p). Scaling the frequencies with standard scale factors lowers the MAD for all levels and basis sets studied suggesting that the standard scale factors for 1<sup>st</sup> and 2<sup>nd</sup> row elements may also be used for 3<sup>rd</sup> row elements. Calculations using G3MP2 theory proved useful in determining accuracy of level of theory and basis set. When studying reactions involving heavy atoms, the choice of basis set is crucial. As illustrated in this study, enthalpies of reaction can vary up to 30.4 kJ mol<sup>-1</sup> at the B3LYP and MP2 levels of theory which in several cases may lead to predicting a reaction is endothermic when it is actually exothermic and vice versa. Since the standard 6-31G basis set performs very well with all the reactions, we recommend that the standard 6-31G basis

set be used for calculations involving 3<sup>rd</sup> row elements. It has also been shown that reaction enthalpies calculated at G3MP2, along with existing experimental data can be used to calculate reliable heats of formation.

## 5.5 References

- (1) Curtiss, L.A.; Redfern, P.C. *J. Chem. Phys.*, **2001**, *114*, 9287.
- (2) Binning, Jr., R. C.; Curtiss, L. A. *J. Comput. Chem.*, **1990**, *11*, 1206.
- (3) Frisch, M. J.; Trucks, G. W.; Schlegel, H. B.; Scuseria, G. E.; Robb, M. A.; Cheeseman, J. R.; Montgomery, Jr., J. A.; Vreven, T.; Kudin, K. N.; Burant, J. C.; Millam, J. M.; Iyengar, S. S.; Tomasi, J.; Barone, V.; Mennucci, B.; Cossi, M.; Scalmani, G.; Rega, N.; Petersson, G. A.; Nakatsuji, H.; Hada, M.; Ehara, M.; Toyota, K.; Fukuda, R.; Hasegawa, J.; Ishida, M.; Nakajima, T.; Honda, Y.; Kitao, O.; Nakai, H.; Klene, M.; Li, X.; Knox, J. E.; Hratchian, H. P.; Cross, J. B.; Bakken, V.; Adamo, C.; Jaramillo, J.; Gomperts, R.; Stratmann, R. E.; Yazyev, O.; Austin, A. J.; Cammi, R.; Pomelli, C.; Ochterski, J. W.; Ayala, P. Y.; Morokuma, K.; Voth, G. A.; Salvador, P.; Dannenberg, J. J.; Zakrzewski, V. G.; Dapprich, S.; Daniels, A. D.; Strain, M. C.; Farkas, O.; Malick, D. K.; Rabuck, A. D.; Raghavachari, K.; Foresman, J. B.; Ortiz, J. V.; Cui, Q.; Baboul, A. G.; Clifford, S.; Cioslowski, J.; Stefanov, B. B.; Liu, G.; Liashenko, A.; Piskorz, P.; Komaromi, I.; Martin, R. L.; Fox, D. J.; Keith, T.; Al-Laham, M. A.; Peng, C. Y.; Nanayakkara, A.; Challacombe, M.; Gill, P. M. W.; Johnson, B.; Chen, W.; Wong, M. W.; Gonzalez, C.; Pople, J. A. Gaussian 03, Revision B.05, Gaussian, Inc., Wallingford CT, 2004.

- (4) Schmidt, M. W.; Baldrige, K. K.; Boatz, J. A.; Elbert, S. T.; Gordon, M. S.; Jensen, J. J.; Koseki, S.; Matsunaga, N.; Nguyen, K. A.; Su, S.; Windus, T. L.; Dupuis, M.; Montgomery, J. A. *J. Comput. Chem.*, **1993**, *14*, 1347. GAMESS Version 22 Feb 2006 (R5) from Iowa State University.
- (5) Rassolov, V. A.; Ratner, M. A.; Pople, J. A.; Redfern, P. C.; Curtiss, L. A. *J. Comput. Chem.*, **2001**, *22*, 976.
- (6) Curtiss, L. A.; Raghavachari, K.; Redfern, P. C.; Rassolov, V.; Pople, J. A. *J. Chem. Phys.*, **1998**, *109*, 7764.
- (7) Islam, S. M.; Hollett, J. W.; Poirier, R. A., *J. Phys. Chem. A.*, **2007**, *111*, 526.
- (8) Islam, S. M.; Poirier, R. A., *J. Phys. Chem. A.* **2007**, *111*, 13218.
- (9) Curtiss, L. A.; Redfern, P. C.; Raghavachari, K.; Rassolov, V.; Pople, J. A., *J. Chem. Phys.*, **1999**, *110*, 4703.
- (10) Baboul, A. G.; Curtiss, L. A.; Redfern, P. C.; Raghavachari, K. *J. Chem. Phys.*, **1999**, *110*, 7650.
- (11) Curtiss, L. *Computational Thermochemistry on the web*.  
<http://chemistry.anl.gov/compmat/comptherm.htm> (accessed Sept 24, 2007).
- (12) National Institute of Standards and Technology, *Vibrational frequency scaling factors on the web*. <http://srdata.nist.gov/eccbdf/vsf.asp> (accessed Sept 24, 2007).
- (13) Scott, A. P.; Radom, L. *J. Phys. Chem.* **1996**, *100*, 16502.
- (14) Bartmess, J. E.; Finkle, R. J. *Can. J. Chem.* **2005**, *83*, 2005.

- (15) Inorganic (non carbon-containing) compounds. In *Tables of Interatomic Distances and Configuration in Molecules and Ions*, Spec. Publ. 18; Sutton, L. E., Ed.; The Chemical Society: London, UK, 1956-1959, pp M 1s-M 58s.
- (16) Stevenson, D. P. *J. Chem. Phys.*, **1940**, *8*, 285-287.
- (17) Ohno, K.; Matsumura, H.; Endo, Y.; Hirota, E. *J. Mol. Spectrosc.*, **1986**, *118*, 1.
- (18) Stevenson, P. E.; Lipscomb, W. N. *J. Chem. Phys.*, **1970**, *52*, 5343.
- (19) Breidung, J.; Thiel, W.; Demaison, J. *Chem. Phys. Lett.* **1997**, *266*, 515.
- (20) Harjanto, H.; Harper, W. W.; Clouthier, D. J. *J. Chem. Phys.*, **1996**, *105*, 10189.
- (21) Herzberg, G.; Verma, R. D. *Can. J. Phys.*, **1964**, *42*, 395.
- (22) Herzberg, G. *Molecular Spectra and Molecular Structure. III. Electronic Spectra and Electronic Structure of Polyatomic Molecules*; D. Van Nostrand: Princeton, NJ, 1967.
- (23) Graner, G. *J. Mol. Spectrosc.*, **1981**, *90*, 394.
- (24) Duncan, J. L. *J. Mol. Struct.*, **1970**, *6*, 447.
- (25) Duncan, J. L.; Harvie, J. L.; McKean, D. C.; Cradock, S. *J. Mol. Struct.*, **1986**, *145*, 225.
- (26) Chadwick, D.; Millen, D. J. *J. Mol. Struct.*, **1975**, *25*, 216.
- (27) Harvey, A. B.; Wilson, M. K. *J. Chem. Phys.*, **1966**, *45*, 678.
- (28) Harvey, A. B.; Wilson, M. K. *J. Chem. Phys.*, **1966**, *44*, 3535.
- (29) Mathews, S.; Duncan, J. L.; McKean, D. C.; Smart, B. A. *J. Mol. Struct.*, **1997**, *413*, 553.
- (30) Laurie, V. W. *J. Chem. Phys.*, **1959**, *30*, 1210.

- (31) (a) Obenhammer, H.; Lobreyer, T.; Sundermeyer, W. *J. Mol. Struct.*, **1994**, 323, 125-128. (b) Jensen, J. O. *Spectrochim. Acta. Part A* **2003**, 59, 3093.
- (32) Huber, K. P.; Herzberg, G. *Molecular Spectra and Molecular Structure. IV. Constants of Diatomic Molecules*; Van Nostrand Reinhold: New York, 1979.
- (33) Shimanouchi, T. Molecular Vibrational Frequencies. In *NIST Chemistry WebBook, NIST Standard Reference Database Number 69*, Eds. P.J. Linstrom and W.G. Mallard, June 2005, National Institute of Standards and Technology, Gaithersburg MD, 20899 (<http://webbook.nist.gov>).
- (34) Straley, J. W.; Tindal, C. H.; Nielsen, H. H. *Phys. Rev.*, **1942**, 62, 161.
- (35) Pullumbi, P.; Bouteiller, Y.; Manceron, L.; Mijoule, C. *Chem. Phys.*, **1994**, 185, 25.
- (36) Wang, X.; Andrews, L. *J. Phys. Chem. A*, **2003**, 107, 11371.
- (37) Muller, J.; Sternkicker, H.; Bergmann, U.; Atakan, B. *J. Phys. Chem. A*, **2000**, 104, 3627.
- (38) Papelewski, P.; Beckers, H.; Burger, H. *J. Mol. Spectrosc.*, **2002**, 213, 69.
- (39) Duncan, J. L.; Allan, A.; McKean, D. C. *Mol. Phys.*, **1970**, 18, 289.
- (40) Lannon, J. A.; Weiss, G. S.; Nixon, E. R. *Spectrochimica Acta Part A* **1970**, 26, 221.
- (41) Adams, G. P.; Carson, A. S.; Laye, P.G. *Trans. Faraday Soc.*, **1966**, 62, 1447.
- (42) Hansel, A.; Scheiring, C.; Glantschnig, M.; Lindinger, W.; Ferguson, E. E. *J. Chem. Phys.*, **1998**, 109, 1748.
- (43) An, X.; Mansson, M. *J. Chem. Thermodyn.*, **1983**, 15, 287.

- (44) *CRC Handbook of Chemistry and Physics*; CRC: Boca Raton, FL, 1977-1978; Vol. 58, pp D69.
- (45) McBride, B. J.; Zsche, M. J.; Gordon, S. *NASA Glenn Coefficients for Calculating Thermodynamic Properties of Individual Species*; Glenn Research Center: Cleveland, OH, 2002; pp 20.
- (46) Chase, M. W. *NIST-JANAF Thermochemical Tables*, 4th ed., Monograph 9. *J. Phys. Chem. Ref. Data*, 1998; pp 1-1951.
- (47) Gibson, S. T.; Greene, J. P.; Berkowitz, J. *J. Chem. Phys.*, **1986**, 85, 4815.
- (48) Berkowitz, J. *J. Chem. Phys.*, **1988**, 89, 7065.
- (49) Gunn, S. R.; Jolly, W. L.; Green, L. G. *J. Phys. Chem.*, **1960**, 64, 1334.
- (50) Ruscic, B.; Schwarz, M.; Berkowitz, J. *J. Chem. Phys.*, **1990**, 92, 1865.
- (51) Gunn, S. R.; Green, L. G. *J. Phys. Chem.*, **1961**, 65, 779.

TABLE 5.1: Optimized and experimental structural parameters for compounds containing 3<sup>rd</sup> row elements (bond lengths in Å and angles in degrees).

Molecules	Point Group	Geometric parameter	MP2			B3LYP			Exptl.
			/6-31G(d,p)	/BC6-31G(d,p)	$\Delta^s$	/6-31G(d,p)	/BC6-31G(d,p)	$\Delta^s$	
HBr	C <sub>∞v</sub>	H-Br	1.4075	1.4057	0.0018	1.4269	1.4171	0.0098	1.4144 <sup>a</sup>
			1.4129 <sup>b</sup>						
SeH <sub>2</sub>	C <sub>2v</sub>	Se-H	1.4527	1.4480	0.0047	1.4738	1.4614	0.0124	1.4600 <sup>a</sup>
		∠H-Se-H	91.6	91.5	0.1	91.2	91.0	0.2	1.4605 <sup>b</sup> 90 <sup>c</sup>
AsH <sub>3</sub>	C <sub>3v</sub>	As-H	1.5042	1.5043	-0.0001	1.5271	1.5181	0.009	1.5108 <sup>a</sup>
		∠H-As-H	93.0	92.2	0.8	91.9	91.2	0.7	1.5187 <sup>b</sup> 90 <sup>c</sup>
GeH <sub>4</sub>	T <sub>d</sub>	Ge-H	1.5219	1.5285	-0.0066	1.5369	1.5306	0.0063	1.5151 <sup>a</sup>
		∠H-Ge-H	109.5	109.5	0.0	109.5	109.5	0.0	1.5293 <sup>b</sup> 1.514 <sup>d</sup> 109.5 <sup>c</sup>
GaH <sub>3</sub>	D <sub>3h</sub>	Ga-H	1.5579	1.5785	-0.0206	1.5700	1.5733	-0.0033	1.560 <sup>a</sup>
		∠H-Ga-H	120.0	120.0	0.0	120.0	120.0	0.0	1.5505 <sup>e</sup>
PH <sub>2</sub> Br	C <sub>s</sub>	P-Br	2.2474	2.2440	0.0034	2.2775	2.2612	0.0163	2.234 <sup>f</sup>
		P-H	1.4067	1.4063	0.0004	1.4248	1.4242	0.0006	2.230 <sup>f</sup> 1.425 <sup>f</sup>
		Br-H	2.7894	2.7847	0.0047	2.8183	2.8106	0.0077	1.412 <sup>f</sup>

SiHBr	Cs	$\angle$ H-P-Br	96.8	96.7	0.1	96.4	96.8	-0.4	96.1 <sup>f</sup>
		$\angle$ H-P-H	93.5	93.4	0.1	92.2	92.1	0.1	92.4 <sup>f</sup>
		Si-Br	2.2529	2.2470	0.0059	2.2809	2.2601	0.0208	2.237 <sup>g</sup>
		Si-H	1.5086	1.5082	0.0004	1.5308	1.5309	-0.0001	2.231 <sup>h</sup>
		$\angle$ H-Si-Br	94.5	94.6	-0.1	94.2	94.6	-0.4	1.518 <sup>g</sup>
CH <sub>3</sub> Br	C <sub>3v</sub>	C-Br	1.9424	1.9480	-0.0056	1.9658	1.9625	0.0033	1.561 <sup>h</sup>
		C-H	1.0832	1.0834	-0.0002	1.0879	1.0878	0.0001	93.4 <sup>g</sup>
		$\angle$ H-C-Br	108.1	107.8	0.3	107.7	107.7	0.0	1.939 <sup>i</sup>
		$\angle$ H-C-H	110.8	111.1	-0.3	111.2	111.2	0.0	1.934 <sup>j</sup>
		Si-Br	2.2294	2.2249	0.0045	2.2484	2.2299	0.0185	1.933 <sup>k</sup>
SiH <sub>3</sub> Br	C <sub>3v</sub>	Si-H	1.4690	1.4686	0.0004	1.4808	1.4808	0.0	1.113 <sup>i</sup>
		$\angle$ H-Si-Br	108.4	108.4	0.0	108.5	108.7	-0.2	1.082 <sup>j</sup>
		$\angle$ H-Si-H	110.5	110.5	0.0	110.4	110.2	0.2	1.086 <sup>k</sup>
		C-Se	1.9610	1.9503	0.0107	1.9812	1.9633	0.0179	107.7 <sup>j</sup>
		C-H	1.0896	1.0899	-0.0003	1.0909	1.0912	-0.0003	111.2 <sup>j</sup>
CH <sub>3</sub> SeH	Cs	Se-H	1.4730	1.4799	-0.0069	1.4827	1.4848	-0.0021	111.17 <sup>k</sup>
		$\angle$ H-C-H	110.7	110.9	-0.2	110.9	110.9	0.0	2.212 <sup>l</sup>
		$\angle$ C-Se-H	95.0	95.8	-0.8	94.9	95.6	-0.7	2.210 <sup>m</sup>
		C-H	1.0896	1.0899	-0.0003	1.0909	1.0912	-0.0003	1.474 <sup>l</sup>
		Se-H	1.4730	1.4799	-0.0069	1.4827	1.4848	-0.0021	1.487 <sup>m</sup>
								108.2 <sup>l</sup>	

SiH <sub>3</sub> SeH	Cs	Si-Se	2.2909	2.2895	0.0014	2.3086	2.2963	0.0123	
		Si-H	1.4816	1.4810	0.0006	1.4851	1.4846	0.0005	
		Se-H	1.4741	1.4812	-0.0071	1.4829	1.4849	-0.0020	
		∠H-Si-H	110.2	110.3	-0.1	109.9	109.9	0.0	
		∠Si-Se-H	93.9	94.5	-0.6	93.6	94.2	-0.6	
CH <sub>3</sub> AsH <sub>2</sub>	Cs	C-As	1.9798	1.9607	0.0191	1.999	1.983	0.016	1.92 <sup>o</sup>
		C-H	1.0924	1.0928	-0.0004	1.0920	1.0916	0.0004	1.09 <sup>o</sup>
		As-H	1.5248	1.5354	-0.0106	1.5300	1.5205	0.0095	
		∠H-C-H	109.4	109.2	0.2	109.6	109.9	-0.3	
		∠C-As-H	96.0	96.5	-0.5	95.6	95.1	0.5	
SiH <sub>3</sub> AsH <sub>2</sub>	Cs	Si-As	2.3705	2.3672	0.0033	2.3949	2.3698	0.0251	
		Si-H	1.4838	1.4836	0.0002	1.4873	1.4857	0.0016	
		As-H	1.5243	1.5357	-0.0114	1.5347	1.5186	0.0161	1.52 <sup>o</sup>
		∠H-Si-H	109.1	109.2	-0.1	108.8	108.8	0.0	109.28 <sup>o</sup>
		∠Si-As-H	93.6	93.8	-0.2	92.8	93.5	-0.7	94 <sup>o</sup>
CH <sub>3</sub> GeH <sub>3</sub>	C <sub>3v</sub>	C-Ge	1.9540	1.9474	0.0066	1.9692	1.9515	0.0177	1.9490 <sup>p</sup>
		C-H	1.0873	1.0874	-0.0001	1.0924	1.0924	0.0	1.9453 <sup>q</sup>
		Ge-H	1.5264	1.5324	-0.0060	1.5414	1.5361	0.0053	1.0921 <sup>p</sup>
		∠H-C-H	108.7	108.8	-0.1	108.7	108.7	0.0	1.083 <sup>q</sup>
		∠C-Ge-H	110.3	110.6	-0.3	110.2	110.6	-0.4	1.5285 <sup>p</sup>
		∠H-Ge-H	108.5	108.3	0.2	108.4	108.3	0.1	1.529 <sup>q</sup>
									108.841 <sup>p</sup>
							108.4 <sup>q</sup>		
							109.3 <sup>q</sup>		
							108.776 <sup>p</sup>		
SiH <sub>3</sub> GeH <sub>3</sub>	C <sub>3v</sub>	Si-Ge	2.3838	2.3828	0.0010	2.3987	2.3795	0.0192	2.36 <sup>r</sup>
		Si-H	1.4761	1.4758	0.0003	1.4872	1.4868	0.0004	1.49 <sup>r</sup>

CH <sub>3</sub> GaH <sub>2</sub>	Cs	Ge-H	1.5252	1.5337	-0.0085	1.5400	1.5372	0.0028	1.53 <sup>r</sup>
		∠Si-Ge-H	110.7	110.7	0.0	110.8	110.8	0.0	
		∠H-Si-H	108.8	108.9	-0.1	108.6	108.6	0.0	108.8 <sup>r</sup>
		∠H-Ge-H	108.2	108.2	0.0	108.1	108.1	0.0	108.8 <sup>r</sup>
		C-Ga	1.9686	1.9874	-0.0188	1.9796	1.9771	0.0025	
		Ga-H	1.5636	1.5840	-0.0204	1.5769	1.5800	-0.0031	
		C-H	1.0919	1.0928	-0.0009	1.0974	1.0980	-0.0006	
		∠C-Ga-H	120.6	120.9	-0.3	120.6	121.0	-0.4	
		∠H-Ga-H	118.8	118.2	0.6	118.7	118.0	0.7	
		∠Ga-C-H	108.6	109.1	-0.5	108.6	108.9	-0.3	
SiH <sub>3</sub> GaH <sub>2</sub>	Cs	∠Ga-C-H	111.9	112.2	-0.3	111.8	112.1	-0.3	
		∠H-C-H	107.5	107.1	0.4	107.5	107.2	0.3	
		∠H-C-H	109.3	108.9	0.4	109.5	109.1	0.4	
		Si-Ga	2.4212	2.4199	0.0013	2.4315	2.4004	0.0311	
		Ga-H	1.5626	1.5830	-0.0204	1.5762	1.5789	-0.0027	
		Si-H	1.4808	1.4816	-0.0008	1.4922	1.4929	-0.0007	
		∠Si-Ga-H	121.0	121.5	-0.5	121.0	121.6	-0.6	
		∠H-Ga-H	118.1	116.9	1.2	117.9	116.7	1.2	
		∠Ga-Si-H	108.8	108.8	0.0	108.7	108.6	0.1	
		∠Ga-Si-H	112.0	112.1	-0.1	112.4	112.6	-0.2	
∠H-Si-H	107.8	107.7	0.1	107.5	107.4	0.1			
∠H-Si-H	108.3	108.3	0.0	108.2	108.1	0.1			

<sup>a</sup> Reference 14; <sup>b</sup> Reference 15; <sup>c</sup> Reference 16; <sup>d</sup> Reference 17; <sup>e</sup> Reference 18; <sup>f</sup> Reference 19; <sup>g</sup> Reference 20; <sup>h</sup> Reference 21; <sup>i</sup> Reference 22; <sup>j</sup> Reference 23; <sup>k</sup> Reference 24; <sup>l</sup> Reference 25; <sup>m</sup> Reference 26; <sup>n</sup> Reference 27; <sup>o</sup> Reference 28; <sup>p</sup> Reference 29; <sup>q</sup> Reference 30; <sup>r</sup> Reference 31.

<sup>s</sup> Δ represents the difference between parameters calculated with the standard 6-31G(d,p) and the BC6-31G(d,p) basis sets.

**TABLE 5.2: Mean Absolute Deviations for bond lengths and angles (bond lengths in Å and angles in degrees).<sup>a</sup>**

<b>Comparison</b>	<b>MAD (bond lengths)</b>	<b>MAD (Angles)</b>
Experiment vs.		
MP2/6-31G(d,p)	0.0118	0.6
MP2/BC6-31G(d,p)	0.0124	0.6
B3LYP/6-31G(d,p)	0.0187	0.5
B3LYP/BC6-31G(d,p)	0.0124	0.5
MP2/6-31G(d,p) vs.		
MP2/BC6-31G(d,p)	0.0057	0.3
B3LYP/BC6-31G(d,p) vs.		
B3LYP/6-31G(d,p)	0.0078	0.3

<sup>a</sup> Mean absolute deviations from experiment were calculated from 25 bond lengths and 18 bond angles, while 36 bond lengths and 36 bond angles were used to calculate the MAD between the calculated bond lengths and angles.

TABLE 5.3: Calculated and experimental frequencies (in  $\text{cm}^{-1}$ ) for compounds containing 3<sup>rd</sup> row elements. <sup>a</sup>

Molecules	Point Group	Freq.	MP2			B3LYP			Experiment
			/6-31G(d,p)	/BC6-31G(d,p)	$\Delta v^m$	/6-31G(d,p)	/BC6-31G(d,p)	$\Delta v^m$	
HBr	$C_{\infty v}$	$\nu_1$	2759.3	2765.6	-6.3	2622.9	2663.3	-40.4	2558.5 <sup>b</sup>
SeH <sub>2</sub>	$C_{2v}$	$\nu_1$	1125.1	1162.3	-37.2	1074.5	1131.5	-57.0	1034.2 <sup>c</sup>
		$\nu_2$	2544.3	2595.3	-51.0	2395.5	2449.6	-54.1	2344.5 <sup>c</sup>
		$\nu_3$	2564.0	2611.8	-47.8	2412.3	2466.2	-53.9	2357.8 <sup>c</sup>
AsH <sub>3</sub>	$C_{3v}$	$\nu_1$	980.8	986.7	-5.9	946.3	968.7	-22.4	906.0 <sup>c</sup>
		$\nu_2(e)$	1079.2	1116.0	-36.8	1031.1	1071.7	-40.6	1003 <sup>c</sup>
		$\nu_3$	2315.1	2380.0	-64.9	2182.4	2261.6	-79.2	2116.1 <sup>c</sup>
		$\nu_4(e)$	2332.4	2395.0	-62.6	2200.7	2282.3	-81.6	2123.0 <sup>c</sup>
GeH <sub>4</sub>	$T_d$	$\nu_1(t_2)$	861.3	851.3	10.0	823.6	820.1	3.5	819 <sup>d</sup>
		$\nu_2(e)$	965.1	956.3	8.8	928.9	935.3	-6.4	931 <sup>d</sup>
		$\nu_3$	2245.8	2332.0	-86.2	2138.3	2252.0	-113.7	2114 <sup>d</sup>
		$\nu_4(t_2)$	2247.4	2340.1	-92.7	2148.7	2273.6	-124.9	
GaH <sub>3</sub>	$D_{3h}$	$\nu_1$	750.4	730.1	20.3	718.4	711.3	7.1	717.4 <sup>e,f</sup>
		$\nu_2(e)$	792.5	784.3	8.2	762.5	776.5	-14.0	758.7 <sup>e,g</sup>
		$\nu_3(e)$	2033.8	2039.8	-6.0	1966.6	2018.2	-51.6	1923.2 <sup>e,g</sup>
		$\nu_4$	2038.2	2049.9	-11.7	1961.3	2012.2	-50.9	
PH <sub>2</sub> Br	$C_s$	$\nu_1$	412.8	423.9	-11.1	383.0	398.7	-15.7	399.79 <sup>h</sup>
		$\nu_2$	818.7	821.4	-2.7	784.9	794.2	-9.3	794.90 <sup>h</sup>
		$\nu_3$	863.9	869.8	-5.9	819.1	831.1	-12.0	812.46 <sup>h</sup>
		$\nu_4$	1165.6	1165.8	-0.2	1135.5	1138.1	-2.6	
		$\nu_5$	2524.0	2522.6	1.4	2389.0	2387.2	1.8	

SiHBr	Cs	$\nu_6$	2537.7	2537.2	0.5	2401.9	2400.9	1.0	
		$\nu_1$	422.7	432.4	-9.6	394.9	410.1	-15.2	424.3 <sup>i</sup>
		$\nu_2$	815.7	820.7	-5.0	774.7	785.3	-10.6	553.6 <sup>i</sup>
		$\nu_3$	2164.4	2164.8	-0.4	2039.7	2038.1	1.6	1970.9 <sup>i</sup>
CH <sub>3</sub> Br	C <sub>3v</sub>	$\nu_1$	639.0	632.0	7.0	588.4	592.8	-4.4	617 <sup>j</sup> , 611 <sup>k,c</sup>
		$\nu_2(e)$	1009.3	1003.9	5.4	968.1	967.6	0.5	974 <sup>j</sup>
		$\nu_3$	1405.2	1394.9	10.3	1345.8	1343.2	2.6	1333 <sup>j</sup>
		$\nu_4(e)$	1536.5	1540.4	-3.9	1487.7	1490.5	-2.8	1472 <sup>j</sup>
		$\nu_5$	3177.4	3173.9	3.5	3097.2	3096.1	1.1	3082 <sup>j</sup> , 2972 <sup>k</sup>
		$\nu_6(e)$	3304.2	3302.5	1.7	3211.4	3210.0	1.4	3184 <sup>j</sup>
SiH <sub>3</sub> Br	C <sub>3v</sub>	$\nu_1$	441.9	448.1	-6.2	414.9	429.2	-14.3	430 <sup>c</sup>
		$\nu_2(e)$	655.4	668.4	-13	628.9	643.8	-14.9	633 <sup>c</sup>
		$\nu_3$	991.4	1000.1	-8.7	944.5	957.9	-13.4	930 <sup>c</sup>
		$\nu_4(e)$	999.0	1001.4	-2.4	954.9	955.2	-0.3	950 <sup>c</sup>
		$\nu_5$	2356.2	2360.1	-3.9	2253.3	2254.7	-1.4	2200 <sup>c</sup>
		$\nu_6(e)$	2374.5	2378.1	-3.6	2271.7	2271.8	-0.1	2196 <sup>c</sup>
CH <sub>3</sub> SeH	C <sub>s</sub>	$\nu_1$	212.0	229.3	-17.3	198.3	181.2	17.1	145 <sup>i</sup>
		$\nu_2$	614.0	606.1	7.9	572.8	571.1	1.7	584 <sup>i</sup>
		$\nu_3$	744.9	764.2	-19.3	715.1	744.3	-29.2	712 <sup>i</sup>
		$\nu_4$	961.1	950.2	10.9	919.5	914.7	4.8	921 <sup>i</sup>
		$\nu_5$	1046.8	1052.0	-5.2	1009.7	1022.8	-13.1	980 <sup>i</sup>
		$\nu_6$	1386.1	1379.2	6.9	1329.8	1329.7	0.1	1288 <sup>i</sup>
		$\nu_7$	1530.0	1536.9	-6.9	1485.1	1490.4	-5.3	1433 <sup>i</sup>
		$\nu_8$	1543.0	1548.0	-5.0	1494.6	1498.5	-3.9	1447 <sup>i</sup>
		$\nu_9$	2535.1	2582.3	-47.2	2378.9	2425.4	-46.5	2330 <sup>i</sup>
		$\nu_{10}$	3163.0	3162.5	0.5	3083.6	3082.4	1.2	2955 <sup>i</sup>
		$\nu_{11}$	3277.1	3277.2	-0.1	3182.4	3181.0	1.4	3027 <sup>i</sup>
		$\nu_{12}$	3284.0	3286.7	-2.7	3190.6	3190.6	0.0	3032 <sup>i</sup>

SiH <sub>3</sub> SeH	Cs	$\nu_1$	184.4	175.2	9.2	175.9	102.1	73.8
		$\nu_2$	412.3	420.6	-8.3	386.7	399.8	-13.1
		$\nu_3$	529.2	554.5	-25.3	507.6	537.4	-29.8
		$\nu_4$	626.4	641.3	-14.9	598.2	615.0	-16.8
		$\nu_5$	779.1	802.4	-23.3	754.6	784.4	-29.8
		$\nu_6$	972.9	981.9	-9.0	924.4	937.2	-12.8
		$\nu_7$	982.0	983.2	-1.2	939.5	938.2	1.3
		$\nu_8$	1014.8	1020.1	-5.3	970.9	976.5	-5.6
		$\nu_9$	2336.4	2337.6	-1.2	2235.1	2235.3	-0.2
		$\nu_{10}$	2346.3	2347.0	-0.7	2244.5	2243.6	0.9
		$\nu_{11}$	2361.3	2365.0	-3.7	2260.4	2262.6	-2.2
		$\nu_{12}$	2527.4	2561.9	-34.5	2378.8	2409.5	-30.7
CH <sub>3</sub> AsH <sub>2</sub>	Cs	$\nu_1$	206.2	238.4	-32.2	195.4	224.1	-28.7
		$\nu_2$	589.7	590.0	-0.3	554.1	555.5	-1.4
		$\nu_3$	667.2	699.3	-32.1	651.3	680.6	-29.3
		$\nu_4$	703.5	726.0	-22.5	678.6	701.7	-23.1
		$\nu_5$	966.8	959.3	7.5	932.3	930.3	2.0
		$\nu_6$	999.6	1015.4	-15.8	964.8	985.2	-20.4
		$\nu_7$	1057.8	1097.6	-39.8	1009.9	1050.9	-41.0
		$\nu_8$	1356.8	1351.4	5.4	1305.4	1305.9	-0.5
		$\nu_9$	1530.6	1542.1	-11.5	1488.4	1497.6	-9.2
		$\nu_{10}$	1534.9	1544.3	-9.4	1490.2	1498.4	-8.2
		$\nu_{11}$	2297.1	2365.1	-68.0	2157.8	2227.9	-70.1
		$\nu_{12}$	2309.7	2374.2	-64.5	2172.4	2241.9	-69.5
		$\nu_{13}$	3152.3	3154.0	-1.7	3070.9	3071.2	-0.3
$\nu_{12}$	3259.2	3262.0	-2.8	3157.7	3160.3	-2.6		
$\nu_{13}$	3272.0	3278.0	-6.0	3178.2	3179.4	-1.2		
SiH <sub>3</sub> AsH <sub>2</sub>	Cs	$\nu_1$	162.4	143.9	18.5	135.7	128.6	7.1
		$\nu_2$	376.6	379.7	-3.1	350.0	357.1	-7.1

		$\nu_3$	462.5	500.8	-38.3	444.1	485.8	-41.7	
		$\nu_4$	481.2	515.3	-34.1	458.9	497.9	-39	
		$\nu_5$	704.6	748.5	-43.9	681.4	732.1	-50.7	
		$\nu_6$	758.9	805.7	-46.8	726.0	778.3	-52.3	
		$\nu^-$	950.3	956.1	-5.8	902.7	912.6	-9.9	
		$\nu_8$	990.0	992.7	-2.7	950.0	951.6	-1.6	
		$\nu_9$	1000.3	1002.2	-1.9	958.4	959.8	-1.4	
		$\nu_{10}$	1046.4	1084.8	-38.4	996.8	1046.5	-49.7	
		$\nu_{11}$	2298.1	2324.2	-26.1	2173.2	2225.7	-52.5	
		$\nu_{12}$	2312.1	2338.8	-26.7	2187.5	2238.3	-50.8	
		$\nu_{13}$	2322.5	2341.8	-19.3	2223.6	2240.6	-17.0	
		$\nu_{12}$	2337.6	2368.8	-31.2	2239.1	2250.8	-11.7	
		$\nu_{13}$	2341.3	2376.5	-35.2	2241.1	2261.6	-20.5	
CH <sub>3</sub> GeH <sub>3</sub>	C <sub>3v</sub>	$\nu_1$	177.9	193.0	-15.1	158.3	183.0	-24.7	157 <sup>c</sup>
		$\nu_2(e)$	506.9	496.3	10.6	493.4	490.1	3.3	506 <sup>c</sup>
		$\nu_3$	616.0	637.3	-21.3	586.0	613.9	-27.9	602 <sup>c m</sup>
		$\nu_4$	882.4	872.4	10.0	848.1	845.4	2.7	843 <sup>c m</sup>
		$\nu_5(e)$	886.7	876.8	9.9	857.4	857.5	-0.1	848 <sup>c</sup>
		$\nu_6(e)$	942.0	934.0	8.0	905.1	913.7	-8.6	900 <sup>c</sup>
		$\nu^-$	1340.7	1332.6	8.1	1297.0	1295.4	1.6	1254 <sup>c m</sup>
		$\nu_8(e)$	1525.5	1528.4	-2.9	1484.0	1486.7	-2.7	1428 <sup>c</sup>
		$\nu_9(e)$	2222.4	2312.4	-90	2126.0	2244.6	-118.6	2085 <sup>c m</sup>
		$\nu_{10}$	2223.9	2317.3	-93.4	2129.3	2259.2	-129.9	2084 <sup>c</sup>
		$\nu_{11}$	3147.0	3147.2	-0.2	3063.8	3065.2	-1.4	2938 <sup>c m</sup>
		$\nu_{12}(e)$	3255.7	3257.0	-1.3	3153.4	3154.9	-1.5	2997 <sup>c</sup>
SiH <sub>3</sub> GeH <sub>3</sub>	C <sub>3v</sub>	$\nu_1$	122.2	122.3	-0.1	109.2	131.5	-22.3	144 <sup>n</sup>
		$\nu_2$	370.1	356.6	13.5	348.4	340.1	8.3	312 <sup>n</sup> , 318 <sup>m</sup>
		$\nu_3(e)$	376.7	369.5	7.2	370.2	371.0	-0.8	371 <sup>n</sup>
		$\nu_4(e)$	627.1	619.5	7.6	600.1	602.5	-2.4	550 <sup>n</sup>

CH <sub>3</sub> GaH <sub>2</sub>	Cs	$\nu_5$	825.3	818.1	7.2	794.2	796.2	-2.0	780 <sup>n</sup> , 785.2 <sup>m</sup>
		$\nu_6(e)$	926.6	916.0	10.6	889.3	899.1	-9.8	881 <sup>n</sup>
		$\nu_7$	948.9	943.9	5.0	904.6	905.9	-1.3	890 <sup>n</sup> , 890.3 <sup>m</sup>
		$\nu_8(e)$	997.6	997.2	0.4	955.5	955.4	0.1	930 <sup>n</sup>
		$\nu_9$	2218.7	2294.8	-76.1	2124.5	2221.3	-96.8	2052 <sup>n</sup> ,
		$\nu_{10}(e)$	2223.9	2305.7	-81.8	2134.1	2235.2	-101.1	2076.6 <sup>m</sup>
		$\nu_{11}$	2319.3	2319.2	0.1	2222.5	2235.7	-13.2	2069 <sup>n</sup>
		$\nu_{12}(e)$	2334.0	2334.5	-0.5	2236.9	2254.8	-17.9	2151 <sup>n</sup> ,
		$\nu_1$	10.5	36.4	-25.9	37.3	30.2	7.1	2163.1 <sup>m</sup>
		$\nu_2$	430.2	417.5	12.7	418.2	419.2	-1.0	2160 <sup>n</sup>
		$\nu_3$	519.2	514.1	5.1	501.8	498.7	3.1	
		$\nu_4$	586.4	597.3	-10.9	560.0	578.9	-18.9	
		$\nu_5$	769.1	758.1	11.0	750.4	748.9	1.5	
		$\nu_6$	805.2	792.5	12.7	773.9	781.2	-7.3	
		$\nu_7$	821.1	806.0	15.1	800.0	792.4	7.6	
$\nu_8$	1299.5	1293.8	5.7	1256.1	1254.0	2.1			
$\nu_9$	1510.7	1510.3	0.4	1470.2	1468.6	1.6			
$\nu_{10}$	1520.7	1518.9	1.8	1477.0	1475.4	1.6			
$\nu_{11}$	2004.7	2019.9	-15.2	1933.4	1993.3	-59.9	1892.0 <sup>g</sup>		
$\nu_{12}$	2012.1	2030.1	-18.0	1935.6	1994.3	-58.7	1898.0 <sup>g</sup>		
$\nu_{13}$	3127.6	3123.8	3.8	3039.5	3038.6	0.9			
$\nu_{14}$	3221.7	3214.6	7.1	3115.0	3111.7	3.3			
$\nu_{15}$	3253.5	3245.4	8.1	3148.2	3144.9	3.3			
SiH <sub>3</sub> GaH <sub>2</sub>	Cs	$\nu_1$	6.6	13.0	-6.4	29.5	35.6	-6.1	
		$\nu_2$	336.7	326.1	10.6	318.6	323.9	-5.3	
		$\nu_3$	339.8	334.8	5.0	325.9	332.5	-6.6	
		$\nu_4$	407.3	394.2	13.1	379.8	381.0	-1.2	
		$\nu_5$	573.2	562.7	10.5	544.7	549.4	-4.7	

$\nu_6$	618.5	604.9	13.6	591.3	591.5	-0.2
$\nu_7$	781.7	772.5	9.2	753.0	769.5	-16.5
$\nu_8$	933.1	929.5	3.6	884.3	888.8	-4.5
$\nu_9$	991.1	990.0	1.1	947.7	946.1	1.6
$\nu_{10}$	999.3	998.7	0.6	956.5	956.1	0.4
$\nu_{11}$	2006.3	2023.9	-17.6	1932.6	1994.8	-62.2
$\nu_{12}$	2009.2	2026.2	-17	1940.7	2001.5	-60.8
$\nu_{13}$	2297.2	2293.0	4.2	2198.4	2195.5	2.9
$\nu_{14}$	2314.2	2311.0	3.2	2216.5	2215.2	1.3
$\nu_{15}$	2321.0	2318.3	2.7	2224.2	2222.9	1.3

<sup>a</sup> Calculated frequencies are not scaled.

<sup>b</sup> Reference 32; <sup>c</sup> Reference 33; <sup>d</sup> Reference 34; <sup>e</sup> Reference 35; <sup>f</sup> Reference 36; <sup>g</sup> Reference 37; <sup>h</sup> Reference 38; <sup>i</sup> Reference 20; <sup>j</sup> Reference 39; <sup>k</sup> Reference 22; <sup>l</sup> Reference 27; <sup>m</sup> Reference 40; <sup>n</sup> Reference 31(b).

<sup>m</sup> $\Delta$  represents the difference between frequencies calculated with the standard 6-31G(d,p) and the BC6-31G(d,p) basis sets.

**TABLE 5.4: Mean Absolute Deviations for frequencies (in  $\text{cm}^{-1}$ ).<sup>a</sup>**

<b>Comparison (Unscaled Frequencies)</b>	<b>MAD</b>	<b>Comparison (Scaled Frequencies)</b>	<b>MAD</b>
Experiment vs.		Experiment vs.	
MP2/6-31G(d,p)	94.2	MP2/6-31G(d,p)	24.4
MP2/BC6-31G(d,p)	105.4	MP2/BC6-31G(d,p)	35.4
B3LYP/6-31G(d,p)	40.1	B3LYP/6-31G(d,p)	29.6
B3LYP/BC6-31G(d,p)	57.8	B3LYP/BC6-31G(d,p)	29.3
MP2/6-31G(d,p) vs.		MP2/6-31G(d,p) vs.	
MP2/BC6-31G(d,p)	16.4	MP2/BC6-31G(d,p)	15.3
B3LYP/6-31G(d,p)	58.9	B3LYP/6-31G(d,p)	22.7
B3LYP/BC6-31G(d,p) vs.		B3LYP/BC6-31G(d,p) vs.	
B3LYP/6-31G(d,p)	20.3	B3LYP/6-31G(d,p)	19.5
MP2/BC6-31G(d,p)	51.8	MP2/BC6-31G(d,p)	18.9

<sup>a</sup> A total of 73 frequencies were used to calculate the MAD between experimental and calculated frequencies and 145 frequencies were used to calculate the MAD between the calculated frequencies.

TABLE 5.5: Thermodynamic properties for the reactions (1) and (2) (in kJ mol<sup>-1</sup>) at 298.15K.

Level	$\Delta E$	$\Delta H$	$\Delta G$	$\Delta E$	$\Delta H$	$\Delta G$	$\Delta(\Delta H)^a$	$\Delta E$	$\Delta H$	$\Delta G$	$\Delta E$	$\Delta H$	$\Delta G$	$\Delta(\Delta H)^a$
	6-31G(d)			BC6-31G(d)				6-31G(d)			BC6-31G(d)			
	$\text{CH}_3\text{GaH}_2 + \text{HCN} \rightarrow \text{CH}_3\text{CN} + \text{GaH}_3$							$\text{SiH}_3\text{GaH}_2 + \text{HCN} \rightarrow \text{SiH}_3\text{CN} + \text{GaH}_3$						
HF	-22.0	-25.5	-18.6	-11.5	-14.7	-8.3	-10.8	-29.0	-36.4	-29.5	-24.4	-31.6	-24.6	-4.8
MP2(P) <sup>b</sup>	-4.1	-6.8	-0.9	0.2	-2.3	2.7	-4.5	-22.6	-28.4	-21.5	-22.4	-25.6	-28.4	-2.8
B3LYP(P) <sup>b</sup>	-14.5	-17.9	-11.8	-8.1	-8.7	-11.1	-9.2	-17.9	-24.3	-18.9	-16.1	-22.3	-17.5	-2.0
G3MP2	-0.8	-2.3	5.0					-22.3	-23.8	-19.3				
	$\text{CH}_3\text{GeH}_3 + \text{HCN} \rightarrow \text{CH}_3\text{CN} + \text{GeH}_4$							$\text{SiH}_3\text{GeH}_3 + \text{HCN} \rightarrow \text{SiH}_3\text{CN} + \text{GeH}_4$						
HF	-24.3	-27.4	-27.8	-5.3	-8.7	-9.3	-18.7	-31.1	-36.5	-36.4	-14.7	-19.7	-19.6	-16.8
MP2(P) <sup>b</sup>	-11.1	-13.4	-14.1	1.4	-0.4	-1.3	-13.0	-24.6	-28.5	-28.6	-16.7	-19.7	-19.7	-8.8
B3LYP(P) <sup>b</sup>	-22.2	-25.6	-25.6	-10.2	-13.0	-13.5	-12.6	-21.6	-26.4	-26.0	-14.1	-18.0	-17.7	-8.4
G3MP2	-8.6	-9.2	-9.2					-24.4	-25.3	-27.5				
	$\text{CH}_3\text{AsH}_2 + \text{HCN} \rightarrow \text{CH}_3\text{CN} + \text{AsH}_3$							$\text{SiH}_3\text{AsH}_2 + \text{HCN} \rightarrow \text{SiH}_3\text{CN} + \text{AsH}_3$						
HF	-41.2	-45.4	-46.0	-25.5	-30.3	-31.3	-15.1	-19.4	-24.9	-25.6	12.0	5.2	4.3	-30.1
HF(P) <sup>b</sup>	-40.6	-44.6	-45.2	-30.8	-34.7	-35.7	-9.9	-37.7	-24.8	-25.4	3.7	-1.8	-2.4	-23.0
MP2	-29.8	-33.2	-34.0	-15.9	-19.9	-21.1	-13.3	-9.7	-14.0	-14.9	19.2	13.7	12.5	-27.7
MP2(P) <sup>b</sup>	-29.2	-32.3	-33.0	-20.0	-23.0	-24.2	-9.3	-11.8	-15.8	-16.7	10.0	5.8	4.9	-21.6
B3LYP	-41.8	-45.7	-46.1	-27.0	-31.4	-32.2	-14.3	-14.3	-19.2	-19.3	14.1	7.9	7.3	-27.1
B3LYP(P) <sup>b</sup>	-39.1	-43.2	-43.6	-30.0	-33.8	-34.6	-9.4	-12.3	-17.3	-17.3	8.3	3.1	2.7	-20.4

G3MP2	-29.6	-29.6	-29.9					-14.1	-14.2	-17.3				
	<b>CH<sub>3</sub>SeH + HCN → CH<sub>3</sub>CN + SeH<sub>2</sub></b>							<b>SiH<sub>3</sub>SeH + HCN → SiH<sub>3</sub>CN + SeH<sub>2</sub></b>						
HF	-50.9	-56.6	-54.5	-41.5	-47.3	-45.4	-9.3	15.9	8.8	10.1	46.9	39.2	40.3	-30.4
HF(P) <sup>b</sup>	-53.5	-59.0	-56.9	-49.1	-54.2	-52.3	-4.8	12.9	6.0	7.3	37.1	30.4	31.6	-24.4
MP2	-39.8	-44.5	-42.7	-33.1	-37.7	-36.0	-6.8	22.7	16.8	17.7	50.7	44.2	45.0	-27.4
MP2(P) <sup>b</sup>	-42.9	-47.3	-45.4	-39.9	-43.9	-42.2	-3.4	17.8	12.2	13.1	40.4	34.9	35.9	-22.7
B3LYP	-49.4	-54.6	-52.4	-40.6	-45.5	-43.3	-9.1	15.6	9.1	10.5	43.4	36.7	38.2	-27.6
B3LYP(P) <sup>b</sup>	-49.6	-55.0	-52.7	-45.6	-50.5	-47.9	-4.5	14.9	8.3	9.8	36.3	30.2	32.7	-21.9
G3MP2	-47.1	-46.7	-44.5					12.3	13.0	11.7				
	<b>CH<sub>3</sub>Br + HCN → CH<sub>3</sub>CN + HBr</b>							<b>SiH<sub>3</sub>Br + HCN → SiH<sub>3</sub>CN + HBr<sup>e</sup></b>						
HF	-49.3	-55.4	-53.6	-45.2	-51.4	-49.6	-4.0	58.2	50.1	50.6	82.0	73.5	73.9	-23.4
HF(P) <sup>b</sup>	-56.2	-62.0	-60.1	-55.6	-61.2	-59.3	-0.8	51.0	43.3	43.9	71.0	63.2	63.6	-19.9
MP2	-42.4	-47.3	-45.8	-41.0	-45.8	-44.3	-1.5	58.4	51.8	51.9	79.6	72.6	72.6	-20.8
MP2(P) <sup>b</sup>	-50.5	-55.1	-53.5	-51.0	-55.4	-53.8	0.3	49.5	43.1	43.3	68.7	62.1	62.2	-19.0
B3LYP	-48.8	-54.1	-52.2	-44.5	-49.9	-48.0	-4.2	50.7	43.6	44.1	72.1	64.6	64.9	-21.0
B3LYP(P) <sup>b</sup>	-52.9	-58.1	-56.2	-52.2	-57.2	-55.3	-0.9	46.2	39.3	39.8	63.8	56.8	57.2	-17.5
G3MP2	-56.9	-56.0	-54.3	-57.1	-56.1	-54.5	0.1	42.0	43.6	43.8	40.4	42.0	42.1	1.6
Experimental		-63.2 <sup>c</sup>												29.6 <sup>d</sup>

<sup>a</sup>Δ(ΔH) represents the difference between enthalpies of reaction calculated with the standard 6-31G and the BC6-31G basis sets.

<sup>b</sup>Represents 6-31G(d,p) basis set.

<sup>c</sup>The value is calculated from experimental ΔH<sub>f</sub> of CH<sub>3</sub>Br, HCN, CH<sub>3</sub>CN and HBr given in Table 5.9.

<sup>d</sup>The value is calculated from experimental ΔH<sub>f</sub> of SiH<sub>3</sub>Br, HCN, SiH<sub>3</sub>CN and HBr given in Table 5.9.

<sup>c</sup> The thermodynamic properties are taken from reference 7.

TABLE 5.6: Thermodynamic properties for the reactions (3) and (4) (in kJ mol<sup>-1</sup>) at 298.15K.

Level	$\Delta E$	$\Delta H$	$\Delta G$	$\Delta E$	$\Delta H$	$\Delta G$	$\Delta(\Delta H)^a$	$\Delta E$	$\Delta H$	$\Delta G$	$\Delta E$	$\Delta H$	$\Delta G$	$\Delta(\Delta H)^a$
	6-31G(d)			BC6-31G(d)				6-31G(d)			BC6-31G(d)			
	CH <sub>3</sub> Br + HCl → CH <sub>3</sub> Cl + HBr							SiH <sub>3</sub> Br + HCl → SiH <sub>3</sub> Cl + HBr						
HF	1.0	0.5	-2.4	5.1	4.5	1.7	-4.0	-5.4	-6.7	-6.8	18.4	16.7	16.5	-23.4
HF(P) <sup>b</sup>	6.0	5.4	2.6	6.6	6.2	3.4	-0.8	-1.2	-2.4	-2.4	18.7	17.5	17.4	-19.9
MP2	2.5	2.1	-0.7	3.9	3.6	0.8	-1.5	-1.7	-2.9	-2.9	19.5	17.9	17.8	-20.8
MP2(P) <sup>b</sup>	8.9	8.4	5.6	8.4	8.1	5.3	0.3	4.0	2.9	2.9	23.2	21.8	21.8	-18.9
B3LYP	2.3	1.9	-0.9	6.6	6.2	3.3	-4.3	-5.2	-6.1	-6.1	16.2	14.9	14.7	-21.0
B3LYP(P) <sup>b</sup>	7.0	6.5	3.7	7.7	7.4	4.7	-0.9	-1.3	-2.3	-2.3	16.3	15.2	15.1	-17.5
G3MP2	11.3	11.1	8.3	11.2	11.0	8.2	0.1	-2.4	-2.7	-2.7	-4.0	-4.3	-1.7	-1.6
Experimental		6.5 <sup>c</sup>												-7.7 <sup>d</sup>

<sup>a</sup> $\Delta(\Delta H)$  represents the difference between enthalpies of reaction calculated with the standard 6-31G and the BC6-31G basis sets.

<sup>b</sup> Represents 6-31G(d,p) basis set.

<sup>c</sup> The value is calculated from the experimental  $\Delta H_f$  of CH<sub>3</sub>Br, HCl, CH<sub>3</sub>Cl and HBr given in Table 5.9.

<sup>d</sup> The value is calculated from the experimental  $\Delta H_f$  of SiH<sub>3</sub>Br, HCl, SiH<sub>3</sub>Cl and HBr given in Table 5.9.

**TABLE 5.7: Thermodynamic properties for the reaction (5) (in kJ mol<sup>-1</sup>) at 298.15K.**

Level	$\Delta E$	$\Delta H$	$\Delta G$	$\Delta E$	$\Delta H$	$\Delta G$	$\Delta(\Delta H)^a$
	6-31G(d)			BC6-31G(d)			
HF	18.8	11.4	12.8	34.4	26.8	28.0	-15.4
HF(P) <sup>b</sup>	11.9	4.9	6.3	23.7	16.7	18.0	-11.8
MP2	15.0	9.0	10.0	29.4	23.1	24.0	-14.1
MP2(P) <sup>b</sup>	6.3	0.6	1.6	18.6	12.8	13.8	-12.2
B3LYP	17.1	10.7	12.0	30.2	23.5	24.7	-12.8
B3LYP(P) <sup>b</sup>	12.9	6.5	7.9	22.1	15.8	17.1	-9.3
G3MP2	4.5	5.6	6.8				

<sup>a</sup> $\Delta(\Delta H)$  represents the difference between enthalpies of reaction calculated with the standard 6-31G and the BC6-31G basis sets.

<sup>b</sup>Represents 6-31G(d,p) basis set.

**TABLE 5.8: Mean Absolute deviations for the enthalpies of reaction involving 1<sup>st</sup> and 3<sup>rd</sup> row elements, reaction (1), and 1<sup>st</sup>, 2<sup>nd</sup> and 3<sup>rd</sup> row elements, reaction (2) and (5), (in kJ mol<sup>-1</sup>).**

Theory	Reaction (1)		Reactions (2) and (5)	
	6-31G(d)	BC6-31G(d)	6-31G(d)	BC6-31G(d)
HF	13.5	3.8	8.5	18.4
HF(P) <sup>b</sup>	6.7	3.6	3.1	10.1
MP2	2.9	5.8	2.6	17.6
MP2(P) <sup>b</sup>	2.6	3.8	2.6	12.5
B3LYP	5.2	1.8	2.3	14.1
B3LYP(P) <sup>b</sup>	11.2	3.9	2.4	11.1

<sup>a</sup> MAD is calculated from G3MP2 enthalpies.

<sup>b</sup> Represents 6-31G(d,p) basis set.

**TABLE 5.9: Heats of formation ( $\Delta H_f$ ) (in  $\text{kJ mol}^{-1}$ ) at 298.15K.<sup>a</sup>**

Molecules	Experiment	Present work	Molecules	Present work <sup>a</sup>
CH <sub>3</sub> Br	-38.0±1.3 <sup>b</sup>	-37.8 <sup>n</sup> , -38.7 <sup>p</sup>	CH <sub>3</sub> SeH	18.3
HCN	131.67 <sup>c</sup>	131.8 <sup>n</sup> , 131.9 <sup>o</sup>	SiH <sub>3</sub> SeH	18.0
CH <sub>3</sub> CN	74.04±0.37 <sup>d</sup>	73.9 <sup>n</sup>	CH <sub>3</sub> AsH <sub>2</sub>	38.4
HBr	-36.2 <sup>e,f</sup>	-36.4 <sup>n</sup> , -36.5 <sup>o</sup> , -35.5 <sup>p</sup> , -31.4 <sup>q</sup>	SiH <sub>3</sub> AsH <sub>2</sub>	82.4
SiH <sub>3</sub> Br	-78.24 <sup>g</sup>	-78.0 <sup>o</sup> , -83.0 <sup>q</sup>	CH <sub>3</sub> GeH <sub>3</sub>	41.9
SiH <sub>3</sub> CN	133.5 <sup>h</sup>	130.1 <sup>o</sup>	SiH <sub>3</sub> GeH <sub>3</sub>	117.4
SeH <sub>2</sub>	29.2±0.8 <sup>i</sup>			
AsH <sub>3</sub>	66.4±1 <sup>j,k</sup>			
GeH <sub>4</sub>	90.3±2 <sup>l,m</sup>			
CH <sub>3</sub> Cl	-83.68 <sup>g</sup>	-83.01 <sup>p</sup>		
HCl	-92.31 <sup>g</sup>	-93.0 <sup>o</sup> , -97.1 <sup>q</sup>		
SiH <sub>3</sub> Cl	-141.84 <sup>g</sup>	-137.1 <sup>q</sup>		

<sup>a</sup> See text for explanation.

<sup>b</sup> Reference 41; <sup>c</sup> Reference 42; <sup>d</sup> Reference 43; <sup>e</sup> Reference 44; <sup>f</sup> Reference 45; <sup>g</sup> Reference 46; <sup>h</sup> Reference 7 (obtained from experimental heats of formation and calculated heat of reaction); <sup>i</sup> Reference 47; <sup>j</sup> Reference 48; <sup>k</sup> Reference 49; <sup>l</sup> Reference 50; <sup>m</sup> Reference 51.

<sup>n</sup> Calculated using the enthalpy of reaction for  $\text{CH}_3\text{Br} + \text{HCN} \rightarrow \text{CH}_3\text{CN} + \text{HBr}$  and experimental  $\Delta H_f$  values for CH<sub>3</sub>Br, HCN, CH<sub>3</sub>CN and HBr.

<sup>o</sup> Calculated using the enthalpy of reaction for  $\text{SiH}_3\text{Br} + \text{HCN} \rightarrow \text{SiH}_3\text{CN} + \text{HBr}$  and experimental  $\Delta H_f$  values for SiH<sub>3</sub>Br, HCN, HBr and SiH<sub>3</sub>CN.

<sup>p</sup> Calculated using the enthalpy of reaction for  $\text{CH}_3\text{Br} + \text{HCl} \rightarrow \text{CH}_3\text{Cl} + \text{HBr}$  and experimental  $\Delta H_f$  values for CH<sub>3</sub>Br, HCl, CH<sub>3</sub>Cl and HBr.

<sup>q</sup> Calculated using the enthalpy of reaction for  $\text{SiH}_3\text{Br} + \text{HCl} \rightarrow \text{SiH}_3\text{Cl} + \text{HBr}$  and experimental  $\Delta H_f$  values for SiH<sub>3</sub>Br, HCl, SiH<sub>3</sub>Cl and HBr.

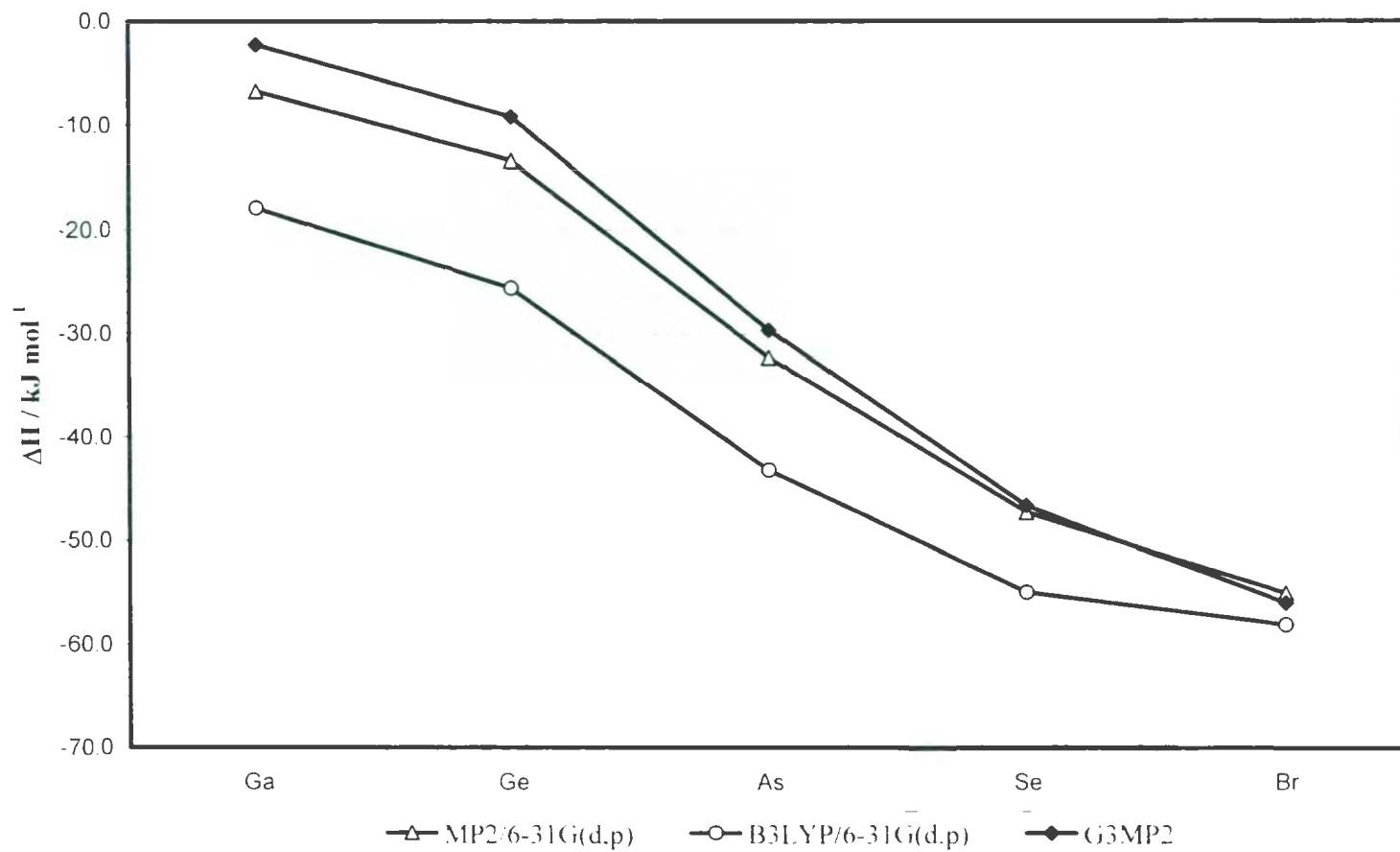


Figure 5.1. Enthalpies of reaction (1) calculated at different levels of theory with the standard 6-31G(d,p) basis set.

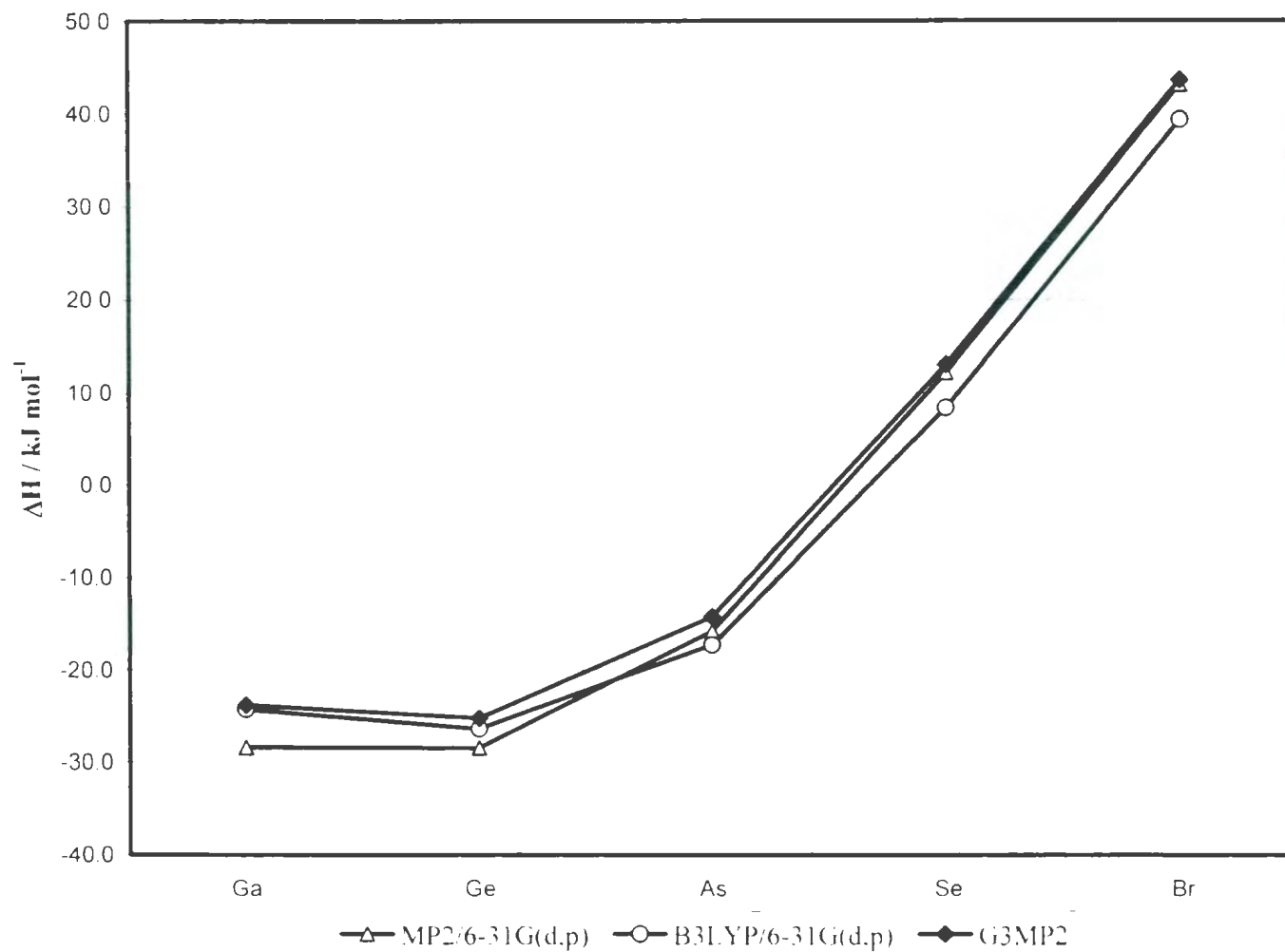


Figure 5.2. Enthalpies of reaction (2) calculated at different levels of theory with the standard 6-31G(d,p) basis set.

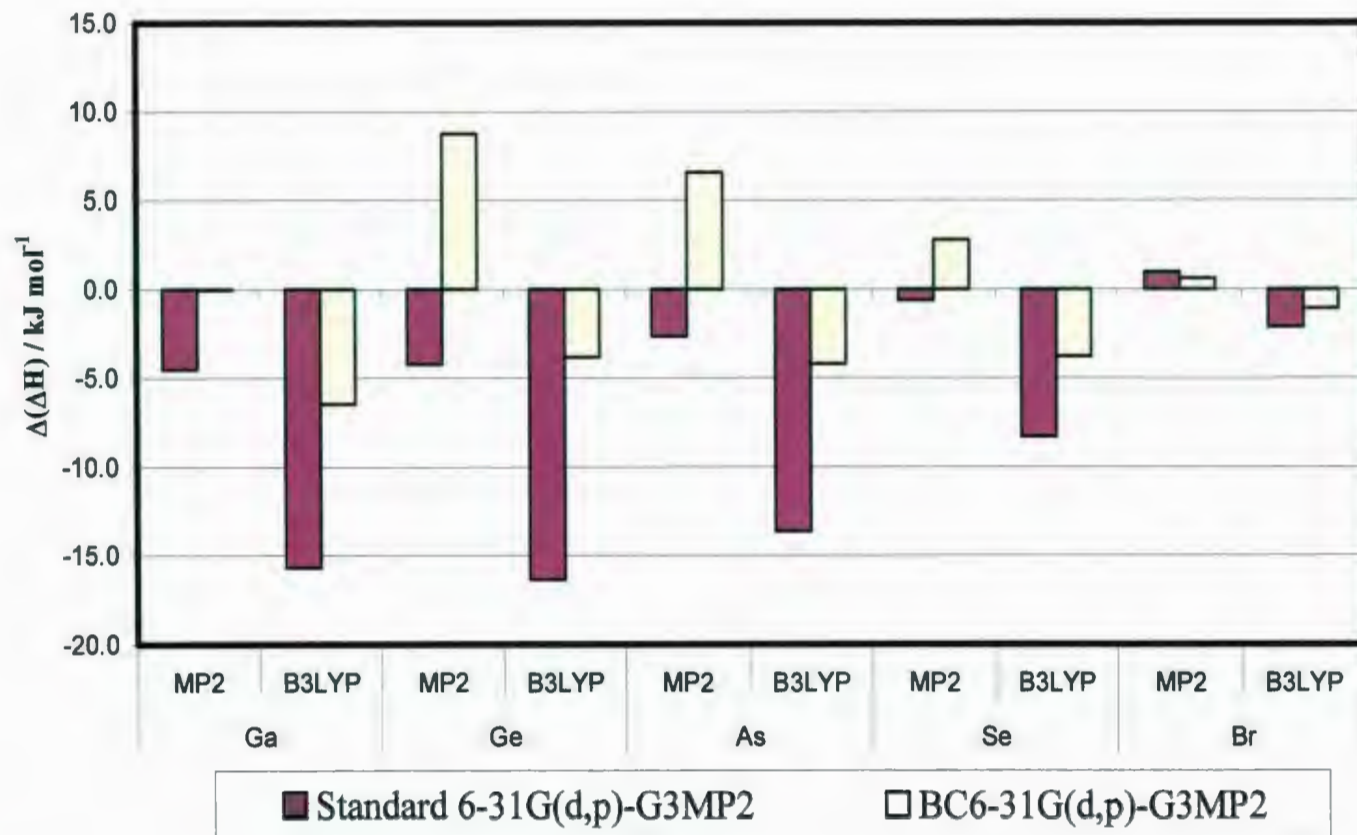


Figure 5.3. Difference between enthalpies of reaction (1) calculated at MP2 and B3LYP levels of theory with G3MP2.

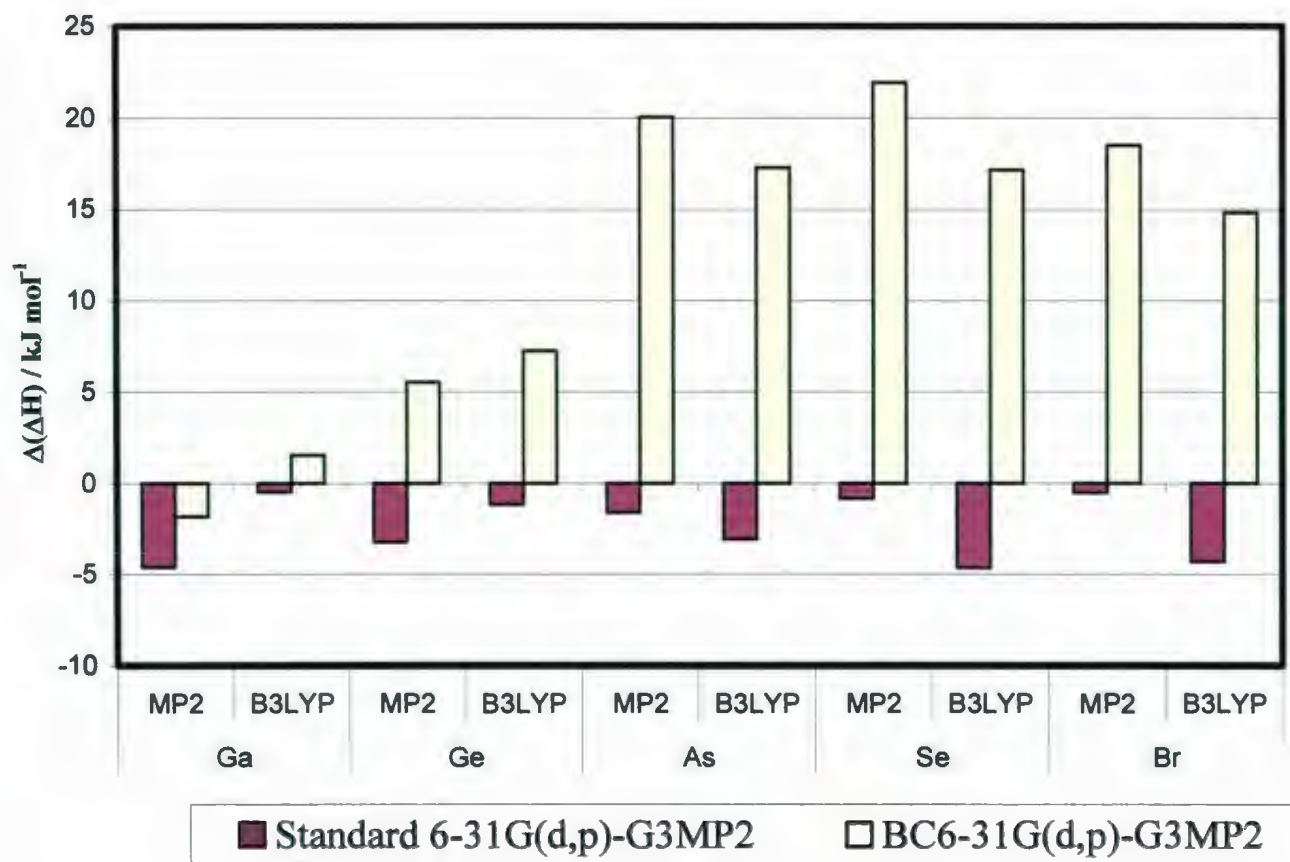


Figure 5.4. Difference between enthalpies of reaction (2) calculated at MP2 and B3LYP levels of theory with G3MP2.

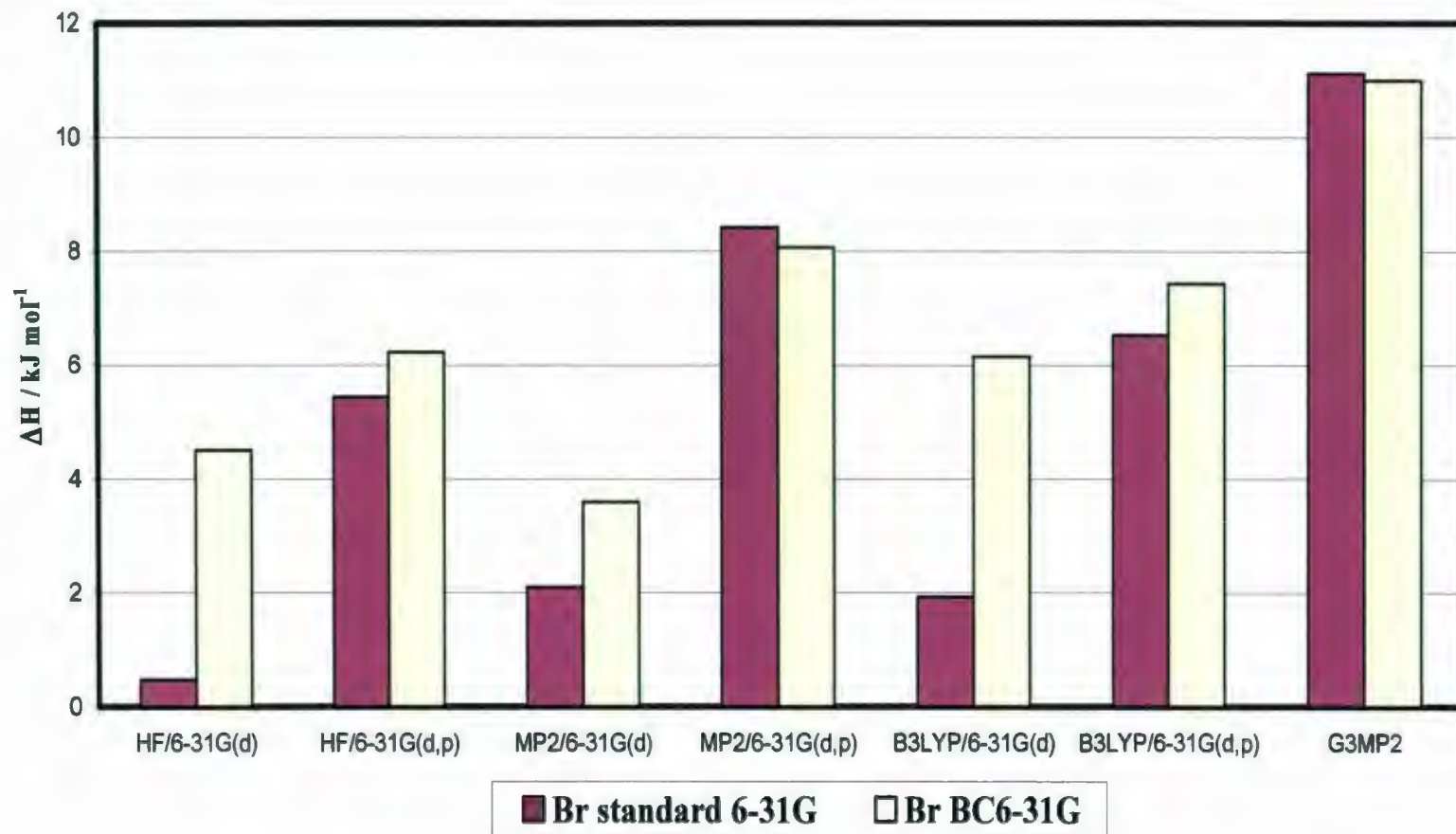


Figure 5.5. Enthalpy of reaction for  $\text{CH}_3\text{Br} + \text{HCl} \rightarrow \text{CH}_3\text{Cl} + \text{HBr}$  calculated at different levels of theory and basis sets.

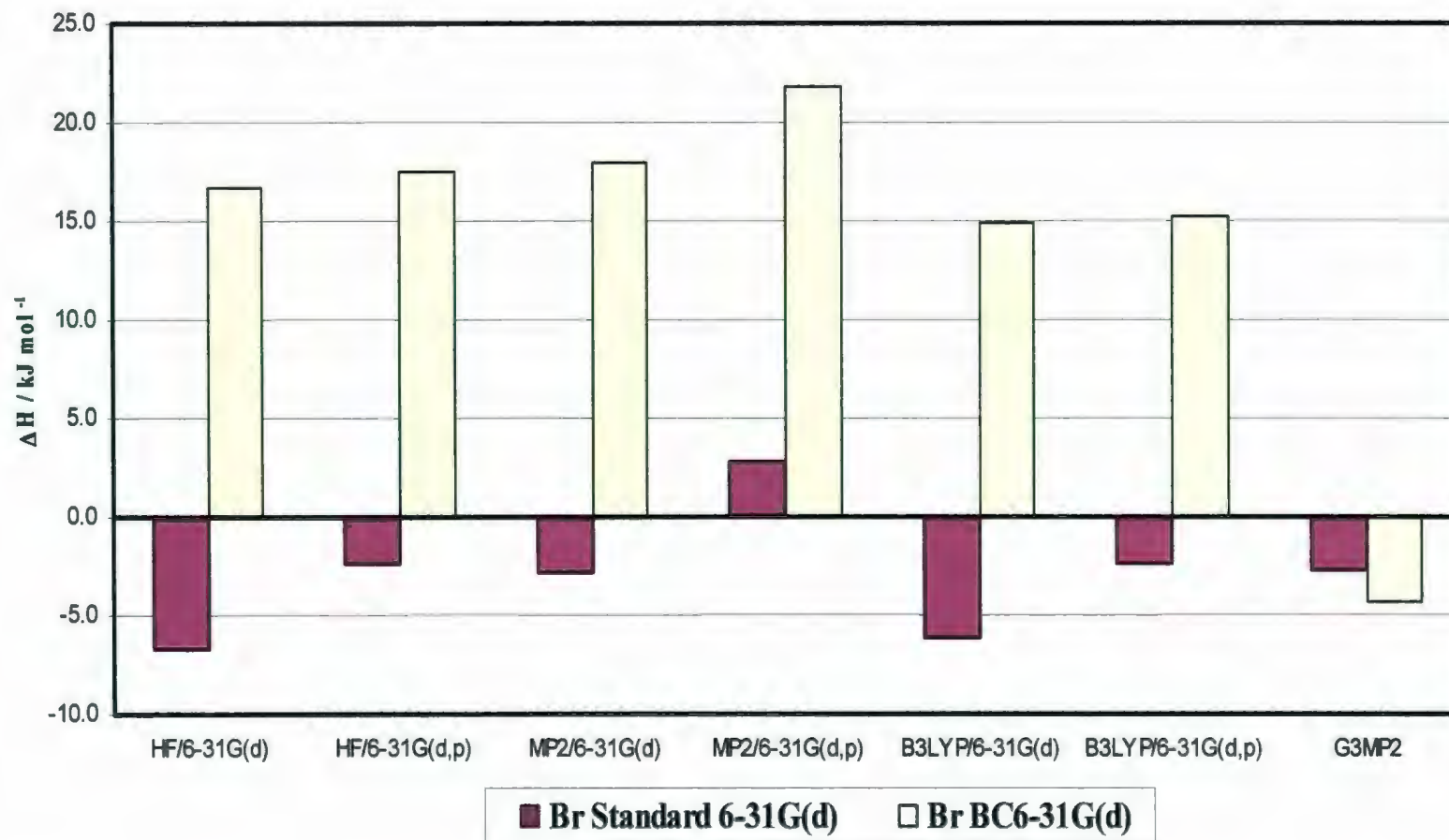


Figure 5.6. Enthalpy of reaction for  $\text{SiH}_3\text{Br} + \text{HCl} \rightarrow \text{SiH}_3\text{Cl} + \text{HBr}$  calculated at different levels of theory and basis sets.

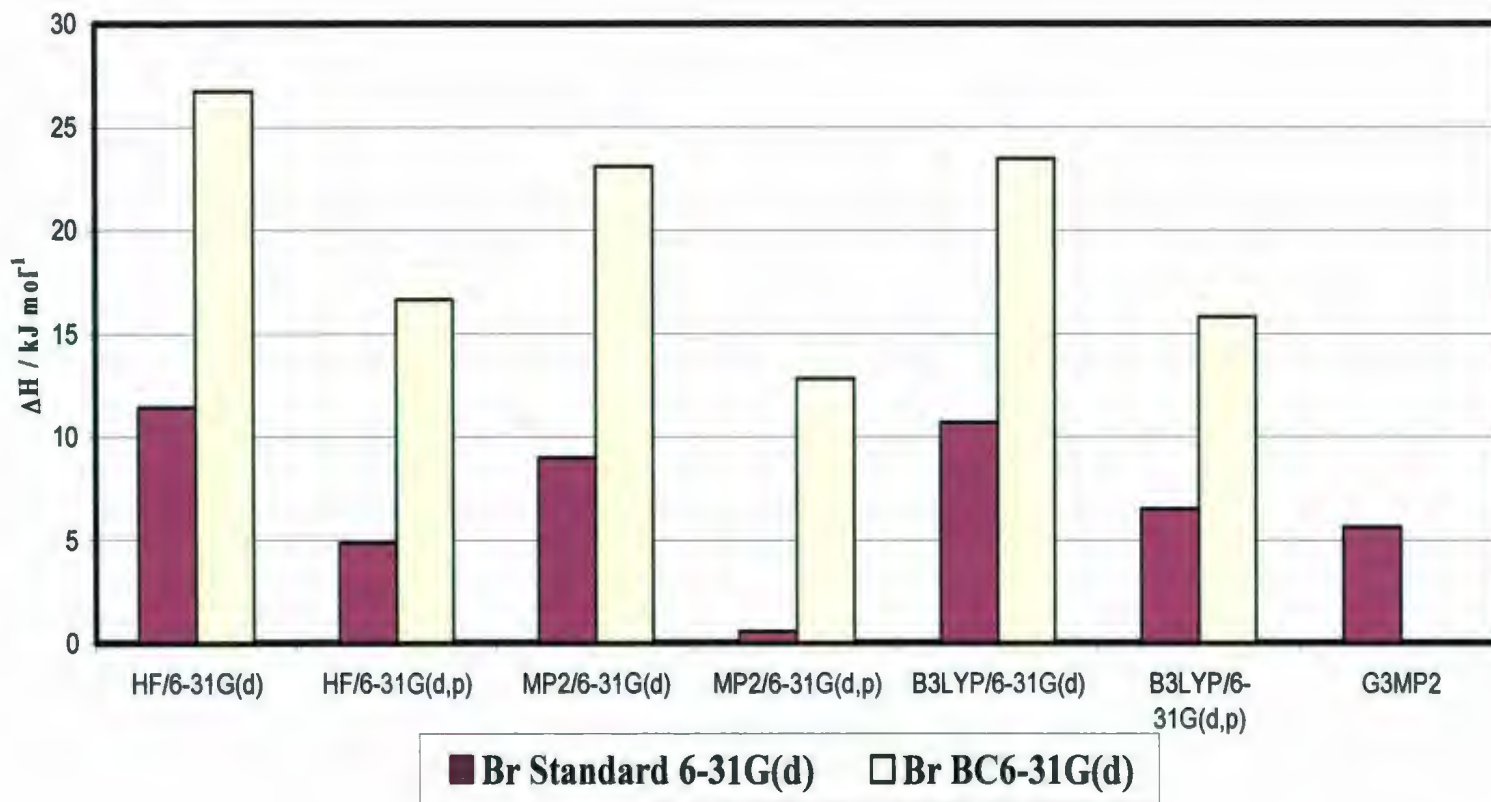


Figure 5.7. Enthalpy of reaction for  $\text{PH}_2\text{Br} + \text{HCN} \rightarrow \text{PH}_2\text{CN} + \text{HBr}$  calculated at different levels of theory and basis sets.

## CHAPTER 6

# **A new insight into using chlorine leaving group and nucleophile carbon kinetic isotope effects to determine substituent effects on the structure of S<sub>N</sub>2 transition states**

### **6.1 Introduction**

The effect of substituents on the structure of the S<sub>N</sub>2 transition state has been of major interest for several decades.<sup>1-12</sup> The major experimental tool used to determine the substituent effect on transition state structure has been a kinetic isotope effect (KIE). Although many different types of KIEs have been used to probe the transition states of S<sub>N</sub>2 reactions,<sup>4,6 - 9,13 - 17</sup> most of the studies have used leaving group KIEs to determine

the relative lengths of C<sub>α</sub>-LG transition-state bond.<sup>1,4,9,15,18</sup> Until recently, the interpretation of these KIEs was thought to be straightforward, i.e., it was believed that a larger leaving group KIE was indicative of greater C<sub>α</sub>-LG bond rupture in the TS. However, a recent theoretical investigation of chlorine leaving group KIEs<sup>19</sup> indicated that the interpretation of these KIEs was not as straightforward as had been previously thought. In fact, this study showed that all the chlorine leaving group KIEs for 26 S<sub>N</sub>2 reactions with methyl chloride fell in a very narrow range of values and that there was no relationship between the magnitude of the KIE and the C<sub>α</sub>-Cl bond length in the transition state! The total KIE (k<sup>35</sup>/k<sup>37</sup>) is the product of the tunneling KIE, (KIE<sub>T</sub>) the imaginary frequency ratio or temperature independent factor, (TIF) and the temperature dependent factor, (TDF) that represents the isotope effect on the vibrational contribution to the KIE,<sup>20,21</sup> equation 1,

$$\frac{k^{35}}{k^{37}} = \underbrace{\left(\frac{k^{35}}{k^{37}}\right)_{\text{Tunnel}}}_{\text{KIE}_T} \times \underbrace{\left(\frac{\nu^{\ddagger 35}}{\nu^{\ddagger 37}}\right)}_{\text{TIF}} \times \underbrace{\prod_i^{3N-6} \frac{\mu_{i37}^R \sinh(\mu_{i35}^R / 2)}{\mu_{i35}^R \sinh(\mu_{i37}^R / 2)}}_{\text{TDF}} \times \prod_i^{3N^{\ddagger}-7} \frac{\mu_{i35}^{\ddagger} \sinh(\mu_{i37}^{\ddagger} / 2)}{\mu_{i37}^{\ddagger} \sinh(\mu_{i35}^{\ddagger} / 2)} \quad (1)$$

where R represents the isotopically substituted reactant, ‡ indicates the transition state,  $\mu_i = h\nu_i/k_B T$  and the  $\nu_i$ 's are the vibrational frequencies. The relationship between the magnitude of the KIE and the C<sub>α</sub>-Cl bond length in the transition state failed because the product of KIE<sub>T</sub> and TIF accounted for a significant portion of the total KIE and was not related to transition state structure in any discernable way. This meant that one could not use the magnitude of the total KIE to estimate the C<sub>α</sub>-Cl transition-state bond length even

though the TDF term of the KIE was related to the length of the  $C_{\alpha}$ -Cl bond in the transition state.<sup>19</sup> A subsequent study by Matsson, Paneth and Westaway and coworkers<sup>22</sup> has demonstrated that one can still use a leaving group chlorine KIE to determine the length of the  $C_{\alpha}$ -Cl bond in a reaction where the solvent has been varied, i.e., to determine the solvent effect on the length of the  $C_{\alpha}$ -Cl bond in an  $S_N2$  TS. The next question was whether one could use chlorine leaving group KIEs to determine the substituent effects on transition state structure in a series of  $S_N2$  reactions of *para*-substituted benzyl chlorides where both the  $KIE_T$  and the TIF were expected to be almost identical for each reaction in the series. An additional question was whether the nucleophile carbon KIE could be used to determine the relative length of the NC- $C_{\alpha}$  transition-state bond in these reactions.

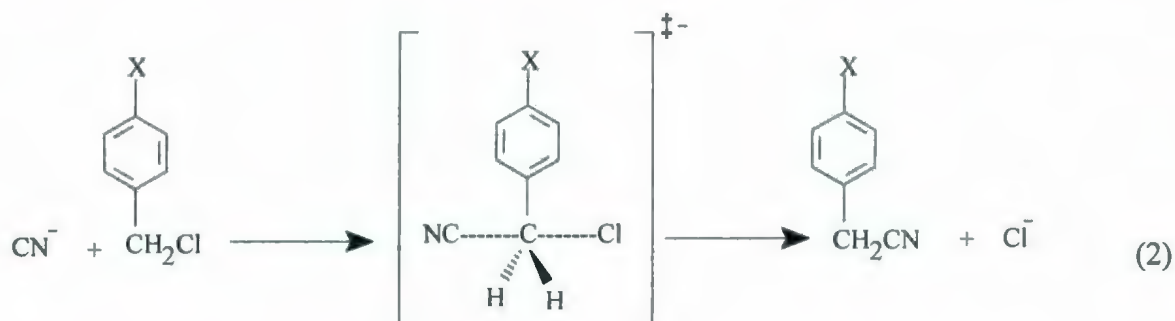
## 6.2 Method

The calculations were done at the RHF/6-31+G(d), the B3LYP/6-31+G(d) and the B3LYP/aug-cc-pVDZ level of theory. The last method was chosen because it gave the closest KIEs to the experimental values in a thorough examination of the available methods for calculating transition state structure and the KIEs in the ethyl chloride - cyanide ion  $S_N2$  reaction.<sup>23</sup> Un-scaled frequencies and no solvent were used for the calculations. All calculations were performed with Gaussian03 using default convergence criteria.<sup>24</sup> Each transition structure had one imaginary frequency that corresponds to the transfer of the alpha carbon from the chlorine of the leaving group to the carbon of the cyanide ion nucleophile. The effect of tunneling on the calculations was done using the

Wigner approximation.<sup>25</sup> All the KIEs were calculated with the program ISOEFF98.<sup>26</sup> The procedure for measuring the experimental KIEs is available in Appendix B.

### 6.3 Results and Discussion

The substituent effect on the structure of the S<sub>N</sub>2 transition state has been determined by measuring the secondary α-deuterium- ( $k_H/k_D$ )<sub>α</sub>, the chlorine leaving group- ( $k^{35}/k^{37}$ ) and the nucleophile carbon  $k^{11}/k^{14}$  KIEs for the reactions between cyanide ion and *para*-substituted benzyl chlorides, equation 2, in THF at 20°C.



where, X = CH<sub>3</sub>, H, F, Cl and NO<sub>2</sub>.

The solvent for this study was chosen because of its very low dielectric constant of 7.3.<sup>27</sup> Although a recent study<sup>22</sup> showed that a significant change in solvent does not change the structure of a Type I (where the nucleophilic atoms in the transition state have the same charge) S<sub>N</sub>2 transition state significantly, the lowest dielectric solvent possible was used for this study to investigate whether the lack of solvent in the theoretical calculations of the transition structures and the KIEs for the cyanide ion – *para*-substituted benzyl chloride S<sub>N</sub>2 reactions, had a significant effect on the results.

**Secondary  $\alpha$ -Deuterium KIEs:** The secondary  $\alpha$ -deuterium  $[(k_H/k_D)_\alpha]$  KIEs were measured for only the *para*-hydrogen- and *para*-chlorobenzyl chlorides to determine the symmetry of the  $S_N2$  transition states. Westaway et al.<sup>28</sup> found that the change in the magnitude of the  $(k_H/k_D)_\alpha$  with substituent was small (by  $\leq 1\%$ ) for  $S_N2$  reactions with unsymmetric transition states and much larger (3 – 12%) for  $S_N2$  reactions with symmetric (central) transition states. The  $(k_H/k_D)_\alpha$ s were measured at 0°C rather than the 20°C that was used for the other KIEs, to slow the reactions enough so that the rate constants and KIEs could be determined. This temperature difference does not affect the conclusion about the symmetry of the transition states for these reactions because these KIEs only decrease by approximately 0.008 when the temperature decreases by 20°C<sup>11, 29, 30</sup> and, more importantly, it is the difference in the KIEs for the reactions with different substituents, not the absolute magnitude of the KIEs, that is important in assessing the symmetry of  $S_N2$  transition states. The change in the experimental  $(k_H/k_D)_\alpha$ s with substituent, Table 6.1, is very small, i.e., approximately 0.6% for these reactions, indicating that the transition states are unsymmetric, i.e., either reactant-like or product-like. The calculations, Table 6.2, confirm that these reactions proceed via unsymmetric transition states. Although the calculated KIEs are slightly (about 1-2%) smaller than the experimental values, the change in the KIE with substituent is very small, e.g., the KIE at the B3LYP/aug-cc-pVDZ level of theory, the method that best reproduces the experimental KIEs<sup>23</sup>, only changes by 1.2% when the *para*-substituent is changed from methyl to nitro. Finally, it is important to note that the calculated transition states for this

system of reactions are all reactant-like with long NC-C<sub>α</sub> and relatively short C<sub>α</sub>-Cl bonds, i.e., the percent extension of the NC-C<sub>α</sub> and C<sub>α</sub>-Cl bonds on going to the transition state at the B3LYP/aug-cc pVDZ level of theory (see Table 6.5), equation 3, is 61 ± 1 and 22 ± 1 percent, respectively.

$$\% \text{ extension on going to the transition state} = \frac{[\text{bond length in the TS} - \text{bond length in the reactant (product)}] \times 100}{\text{bond length in the reactant (product)}} \quad (3)$$

It is also important to note that the calculated KIEs indicate that the (k<sub>H</sub>/k<sub>D</sub>)<sub>α</sub> decreases when a more electron-withdrawing substituent is on the benzene ring of the substrate. This substituent effect on the KIE has been found in almost every investigation of the (k<sub>H</sub>/k<sub>D</sub>)<sub>α</sub>s for the reactions of *para*-substituted benzyl compounds.<sup>28, 31</sup> It is also important to note that the substituent effect on these calculated KIEs was checked by plotting the calculated KIEs in Table 6.2 against the Hammett σ value for each substituent.<sup>32</sup> The correlation coefficient for each plot was very high, ranging from 0.954 to 0.980. It is interesting that the worst fit with the Hammett σ values is found with the calculations using the largest basis set and that the best fit is with the RHF/6-31+G(d) calculations. However, the correlation coefficients in all the Hammett σ plots are very high giving one great confidence that the trends predicted by the calculations are correct.

**Chlorine Leaving Group KIEs:** The chlorine leaving group (k<sup>35</sup>/k<sup>37</sup>) KIEs were measured for the S<sub>N</sub>2 reactions between cyanide ion and four *para*-substituted benzyl

chlorides in THF at 20°C, Table 6.3. The values from the original set of experiments measuring these KIEs are in column 2 of Table 6.3. The surprising observation is that the KIEs do not follow a single trend, i.e., the KIE becomes smaller when a more electron-withdrawing substituent is present for the *para*-methyl- through the *para*-chloro- but then increases for the *para*-nitro substituent. The KIEs for the *para*-chloro- and *para*-nitrobenzyl chlorides were re-measured to ensure that the KIE for the *para*-nitrobenzyl chloride was really greater than that found for the *para*-chlorobenzyl chloride. The results and the averages show that the KIEs for these two reactions are reproducible and that the KIE for the *para*-nitrobenzyl chloride is indeed, greater than that for the *para*-chlorobenzyl chloride. This means there is no clean trend in these KIEs when a more electron-withdrawing substituent is on the benzene ring of the substrate.

The C<sub>α</sub>-Cl ground state and transition-state bond lengths and the  $k^{35}/k^{37}$ s for these reactions were calculated at several levels of theory, Tables 6.4 – 6.6, to demonstrate that the results were not restricted to a particular level of theory. Although there are differences in the C<sub>α</sub>-Cl bond lengths in the ground state and transition state and in the KIEs predicted by the different levels of theory, the general trend is that the ground state and transition state C<sub>α</sub>-Cl bond lengths and the chlorine KIEs in Tables 6.4 – 6.6 decrease when a more electron-withdrawing substituent is present. It is worth noting that the B3LYP/aug-cc-pVDZ calculations gave the best agreement with the experimental KIEs. This is in agreement with the study by Fang et al.<sup>23</sup> It is also worth noting that although scaling the frequencies in the calculations alters the magnitude of the chlorine KIEs, it

does not affect the trend (substituent effect) in the KIEs. Finally, adding solvent to the calculation using a solvent continuum model, does not affect the trend in the chlorine KIEs either.

The substituent effect on the calculated parameters was again checked by plotting the calculated parameter in Tables 6.4 – 6.6 against the Hammett  $\sigma$  value for each substituent.<sup>32</sup> All the calculated parameters behaved as one would expect, i.e., the correlation coefficient for each plot was very high, ranging from 0.926 to 0.997 for the ground state C $_{\alpha}$ -Cl bond lengths, from 0.990 to 0.994 for the transition state C $_{\alpha}$ -Cl bond lengths and from 0.942 to 0.991 for the chlorine KIEs. It is interesting that again the worst fit with the Hammett  $\sigma$  values is found with the calculations using the largest basis set and that the best fit is with the RHF/6-31+G(d) calculations. However, the correlation coefficients in all the Hammett  $\sigma$  plots are very high giving one great confidence that the trends predicted by the calculations are correct.

The calculated KIEs, Table 6.6, decrease as a more electron-withdrawing substituent is added to the substrate whereas the experimental KIEs, Table 6.3, only decrease from the *para*-methylbenzyl chloride to the *para*-chlorobenzyl chloride and the KIE found for the *para*-nitrobenzyl chloride reaction is larger than the KIE for the *para*-chlorobenzyl chloride reaction. It is worth noting that this same inconsistency arose in Grimsrud's study,<sup>33</sup> of the chlorine KIEs for a series of S $_N$ 2 reactions of *para*-substituted benzyl chlorides and several different nucleophiles, Table 6.7, i.e., the chlorine KIE for

the *para*-nitrobenzyl chloride reaction was larger than the KIE for the *para*-chlorobenzyl chloride reaction when the nucleophile was iodide ion. Because 1) the chlorine leaving group KIE for the *para*-nitrobenzyl chloride reaction was smaller than the KIE for the *para*-chlorobenzyl chloride reaction when the nucleophile was thiophenoxide ion, *n*-butyl thiolate anion or methoxide ion as expected, and 2) the calculations indicate that the KIE for the *para*-nitrobenzyl chloride reaction should be smaller than the KIE for the *para*-chlorobenzyl chloride reaction, the *para*-nitrobenzyl chloride reactions with cyanide ion and iodide ion were re-examined. HPLC analyses showed that both reactions yielded several products. In particular, the *para*-nitrobenzyl chloride – cyanide ion reaction gave several products with the main product being a trimer possibly formed by the mechanism shown in Scheme 6.1.<sup>34, 35</sup> Also, since significant amounts of the trimer were found before all the substrate was consumed, the chlorine is removed from the *para*-nitrobenzyl chloride in several different reactions and the observed chlorine KIE is not due to the simple S<sub>N</sub>2 reaction with cyanide ion. Another indication that the reaction is not clean is that spin trap reagents and EPR spectroscopy<sup>36</sup> showed that the reactions between *para*-nitrobenzyl chloride and both iodide ion and cyanide ion contained radicals. Thus, neither of these reactions are the simple S<sub>N</sub>2 reactions that had been supposed. This means the chlorine leaving group KIE for the *para*-nitrobenzyl chloride reaction should not be considered in determining if chlorine KIEs can be used to determine the relative amount of C<sub>α</sub>-Cl bond rupture in the transition states of the cyanide ion – *para*-substituted benzyl chloride S<sub>N</sub>2 reactions. In fact, it is important to note that the plot of the chlorine KIEs versus the Hammett  $\sigma$  values for the *para*-methyl- to the *para*-chloro- substituents in

these *para*-substituted benzyl chloride - cyanide ion S<sub>N</sub>2 reactions, has a correlation coefficient of 0.982. Thus, both the calculated and the experimental chlorine KIEs indicate that one should be able to use the chlorine leaving group KIE to determine the substituent effect (the relative amount of C<sub>α</sub>-Cl bond rupture) on the transition states of S<sub>N</sub>2 reactions. Finally, it is worth noting that this trend in chlorine leaving group KIEs with substituent has been observed experimentally in several S<sub>N</sub>2 reactions.<sup>2, 8, 12</sup>

**The nucleophile carbon k<sup>11</sup>/k<sup>14</sup> KIEs:** The nucleophile carbon k<sup>11</sup>/k<sup>14</sup> KIEs, Table 6.8, were measured to learn whether these KIEs could be used to determine the substituent effect on the NC-C<sub>α</sub> transition-state bond for the cyanide ion - *para*-substituted benzyl chloride S<sub>N</sub>2 reactions. An analysis of these nucleophile carbon KIEs and their errors suggests that there is no measurable trend in the KIE with a change in substituent.

All three levels of theory suggest that the NC-C<sub>α</sub> transition-state bond becomes shorter, Table 6.5, and the nucleophile carbon KIE, Table 6.9, becomes more inverse (NC-C<sub>α</sub> bond formation is more complete) in the transition state when a more electron-withdrawing substituent is on the benzene ring of the substrate. It is important to note that the changes in the NC-C<sub>α</sub> transition-state bond and the KIEs predicted by all three levels of theory correlate extremely well with the Hammett σ values of the *para*-substituent. The correlation coefficients for the plots relating the length of the NC-C<sub>α</sub> transition-state bond and the Hammett σ constant for the *para*-substituent are 0.997 for all three levels of theory and the correlation coefficients for the KIE versus the Hammett σ values for the

substituent range from 0.995 to 0.999. It is also important to note that the substituent effect on the length of the NC-C $\alpha$  transition-state bond predicted by theory is consistent with the results of several experimental studies that have used KIEs and Hammett  $\sigma$  values to determine the substituent effect on the lengths of the Nu-C $\alpha$  transition-state bonds in S $_N$ 2 reactions.<sup>5, 8, 10, 12, 31</sup>

Although all three levels of theory suggest the NC-C $\alpha$  transition-state bond shortens when a more electron-withdrawing substituent is present, this change was not detected experimentally. However, two of the three theoretical methods, Table 6.5, showed that the change in the NC-C $\alpha$  transition-state bond with substituent was smaller than the corresponding change in the C $\alpha$ -Cl transition-state bond with substituent, i.e., the (change in the C $\alpha$ -Cl/change in the NC-C $\alpha$ ) transition-state bond with substituent is 1.53 for the B3LYP/aug-cc-pVDZ level of theory, 1.33 for the B3LYP/6-31+G(d) level of theory and 1.00 for the RHF/6-31+G(d) level of theory. This much smaller change in the NC-C $\alpha$  transition-state bond with substituent is probably why the change in the nucleophile carbon KIE was too small to detect experimentally.

Finally, it is interesting that the difference in the nucleophile KIEs with level of theory, Table 6.9, is much smaller than for the difference in the chlorine leaving group KIEs, Table 6.6, with level of theory. For example, the difference in the nucleophile KIE with level of theory is  $\leq 1\%$  whereas the difference in the chlorine leaving group KIE with level of theory is approximately 40%. Another observation is that the nucleophile

KIE was not as close to the experimental value as the chlorine KIEs. The calculated chlorine KIEs at the B3LYP/aug-cc-pVDZ level differ from the experimental values by only approximately 0.0012 whereas the calculated nucleophile carbon KIEs differ from the experimental values by approximately 0.020. This difference between the theoretical and the experimental values is even clearer if one considers the percent difference between the experimental and theoretical values of the KIEs. The average percent difference in the chlorine KIEs is approximately  $0.0012/0.0058 \times 100 = 21 \%$  while that for the nucleophile carbon KIEs is approximately  $0.0192/0.0019 \times 100 = 1011 \%$ . This same problem, i.e., that the difference between the calculated and experimental KIE was larger for the nucleophile carbon KIEs than for the leaving group KIEs, was observed in a previous study.<sup>23</sup>

**The substituent effect on transition state structure:** Both the experimental and theoretical substituent effect on the  $C_{\alpha}$ -Cl transition-state bond, Tables 6.5 and 6.6, is that it becomes shorter when a more electron-withdrawing substituent is on the benzene ring. The calculated transition state structures and nucleophile carbon KIEs, Tables 6.5 and 6.9, indicate that the NC- $C_{\alpha}$  transition-state bond also shortens, but by a smaller amount, when a more electron-withdrawing substituent is present. Thus, the calculations suggest that the transition state becomes tighter when a more electron-withdrawing substituent is present but that the greatest change in structure is in the  $C_{\alpha}$ -Cl transition-state bond. It is worth noting that this result is predicted by Westaway's "Bond Strength Hypothesis"<sup>37</sup> which states that the greatest change in structure with substituent will be in the weaker

reacting bond, i.e., in this case, the C<sub>α</sub>-Cl bond. It is also important to note that the experimental KIEs, as far as is possible, confirm this trend in the transition state structure with substituent. It is also important to note that these changes in transition state structure with substituent have been found in other studies of the substituent effect on transition state structure of S<sub>N</sub>2 reactions.<sup>2,5,8,10,12,31</sup> The important conclusion of this study is that with some reservations, (*vide infra*), both leaving group- and nucleophile KIEs should be able to determine the substituent effects on transition state structure as had been previously believed.

**The implications of the theoretical study on using leaving group chlorine KIEs to determine the substituent effect on the transition states of S<sub>N</sub>2 reactions:** The chlorine leaving group KIE can be expressed as

$$\text{KIE} = \text{TDF}_R \times \text{KIE}_T \times \text{TIF}^\ddagger \times \text{TDF}^\ddagger = \text{TDF}_R \times \text{KIE}^\ddagger \quad (4)$$

where the transition state contribution to the total KIE, (KIE<sup>‡</sup>), is the product of the tunneling KIE, KIE<sub>T</sub>, the imaginary frequency ratio for the reactions with the <sup>35</sup>Cl and <sup>37</sup>Cl isotopes, (TIF<sup>‡</sup>), and the isotope effect on the vibrational energy of the transition state, (TDF<sup>‡</sup>). TDF<sub>R</sub> represents the isotope effect on the vibrational energy of the reactants. The TDF<sub>R</sub> and TDF<sup>‡</sup> can be calculated<sup>21</sup> from

$$\text{TDF}_R = \prod_i^{3N-6} [(\mu_i^R_{37} \sinh(\mu_i^R_{35}/2))/(\mu_i^R_{35} \sinh(\mu_i^R_{37}/2))] \quad (5)$$

and

$$\text{TDF}^\ddagger = \prod_i^{3N^\ddagger-7} [(\mu_i^\ddagger_{35} \sinh(\mu_i^\ddagger_{37}/2))/(\mu_i^\ddagger_{37} \sinh(\mu_i^\ddagger_{35}/2))] \quad (6)$$

respectively, where R represents the substrate,  $\ddagger$  indicates the transition state,  $\mu_i = hv_i/k_B T$  and the  $v_i$ 's are the frequencies.  $\text{KIE}_T$  was calculated using the Wigner approximation.<sup>25</sup>

**The magnitude of the KIE versus the percent  $C_\alpha$ -Cl bond rupture in the transition state:** The individual contributions to the total chlorine leaving group KIEs, Table 6.10, shed light on the origin of these KIEs and have significant implications for those using these KIEs to determine the substituent effect on transition state structure. The first important observation is that the  $\text{KIE}^\ddagger$  contribution to the total KIE is very close to unity for all the reactions, i.e.,  $\text{KIE}^\ddagger$  ranges from 1.00002 to 0.99919. This means the  $\text{KIE}^\ddagger$  only accounts for approximately 10% of the total KIE and that the total KIE is mainly determined by  $\text{TDF}_R$ ! The  $\text{KIE}^\ddagger$  contribution is smaller than the  $\text{TDF}_R$  contribution to the total KIE because the  $\text{TDF}^\ddagger$  contributions to the KIE are only 36 - 38 % of the contributions due to  $\text{TDF}_R$ . This is reasonable because the vibrational energy of the  $C_\alpha$ -Cl bond in the transition state is smaller than that in the substrate. In fact,  $\text{TDF}^\ddagger$  will make a smaller and smaller contribution (the  $\text{TDF}^\ddagger$  will approach 1.00000) to the total KIE as the amount of  $C_\alpha$ -Cl bond rupture in the transition state increases. Both the  $\text{KIE}_T$  and the  $\text{TIF}^\ddagger$  also approach 1.00000 as the amount of  $C_\alpha$ -Cl bond rupture in the transition state increases. This means the KIE will increase with the amount of  $C_\alpha$ -Cl bond rupture in the

transition state for a particular reaction. This is undoubtedly why Paneth and co-workers<sup>19</sup> found the KIEs in their methyl chloride S<sub>N</sub>2 reactions did not approach the expected maximum value of 1.019 but were bunched between 1.006 and 1.009 regardless of the amount of C<sub>α</sub>-Cl bond rupture in the transition state. It is worth noting that the product {KIE<sub>T</sub> x TIF<sup>‡</sup>} makes a significant contribution to the total KIE, i.e., the {KIE<sub>T</sub> x TIF<sup>‡</sup>} represents between 34 and 38% of the total chlorine KIEs in Table 6.10. This is in agreement with the earlier study<sup>19</sup> of 26 methyl chloride S<sub>N</sub>2 reactions where the KIE<sub>T</sub> and TIF<sup>‡</sup> terms represented a significant contribution to the total KIE. Finally, it is interesting that the KIE<sub>T</sub> is less than 10% of the TIF<sup>‡</sup> contribution to the KIE.

**Substituent effects on the chlorine leaving group KIEs:** A detailed examination of the substituent effect on each of the terms in the calculated chlorine leaving group KIE, Table 6.10, shows that the substituent effect (KIE contribution for the *para*-methylbenzyl chloride reaction – KIE contribution for the *para*-nitrobenzyl chloride reaction) on the TDF<sub>R</sub> and TDF<sup>‡</sup> terms are of almost identical magnitude, i.e., they are -0.00044 and +0.00038, respectively, even though the absolute magnitude of the TDF<sub>R</sub> term is approximately 2.7 times greater than the TDF<sup>‡</sup> term. This is interesting because it suggests that changing a substituent changes the vibrational energy of the full C<sub>α</sub>-Cl and partial (C<sub>α</sub>-Cl) transition-state bond by the same relative amount.

Another important observation is that the substituent effect on KIE<sup>‡</sup> is greater (+0.00083) than the substituent effect on the TDF<sub>R</sub> contribution (-0.00044) to the KIE

and that this greater change in the  $KIE^\ddagger$  contribution to the total KIE is responsible for the decrease in the total KIE with the electron-withdrawing ability of the substituent. This is important because the  $TDF_R$  term increases with the electron-withdrawing ability of the substituent, i.e., increases in the opposite direction. The surprising finding is that the substituent effect on the  $KIE^\ddagger$  term is only greater than the substituent effect on the  $TDF_R$  term because the substituent effect on the  $TDF^\ddagger$ , the  $TIF^\ddagger$  and the  $KIE_T$  are all in the same direction, i.e., they each decrease with a more electron-withdrawing *para*-substituent. In fact, without the effect of the  $TIF^\ddagger$  and  $KIE_T$  the change in the total KIE with substituent would be very small and in the opposite (wrong, i.e., the  $C_\alpha$ -Cl transition state bond is shorter when a more electron-withdrawing substituent is present in every reaction investigated, Table 6.11) direction.

An analysis of the data in Table 6.10 led to the important conclusion that the substituent effect on the KIE is dependent on transition state structure. Three different substituent effects are possible. For instance, the contribution by  $TDF^\ddagger$  to the total KIE will be effectively zero (the  $TDF^\ddagger = 1.00000$  for all substituents) for a series of reactions with a very product-like transition state so little or no substituent effect will be found on this term. Also, since the imaginary frequency also decreases as the amount of  $C_\alpha$ -Cl bond rupture in the transition state increases, both the  $TIF^\ddagger$  and the  $KIE_T$  which depend on the imaginary frequency, will also decrease to 1.00000 for a very product-like transition state and the KIE will be given by the  $TDF_R$  term alone. In these cases, the substituent effect on the KIE will be opposite that expected from the calculated transition

state structures for the reactions, i.e., the substituent effect on the KIE will be opposite that found for the benzyl chloride – cyanide ion reactions in this study. A second possibility is when the amount of C<sub>α</sub>-Cl bond rupture in the transition state is small, i.e., the transition state is very reactant-like. In these cases, the TDF<sup>‡</sup>, the TIF<sup>‡</sup> and the KIE<sub>T</sub> will all be >1.00000 and near a maximum for the reaction, the substituent effect will be given by the larger KIE<sup>‡</sup> contribution to the KIE and the expected substituent effect on the reactions will be found, i.e., a smaller KIE will be found for the *para*-nitrobenzyl chloride than for the *para*-methyl benzyl chloride reaction. The third possibility will occur at some intermediate amount of C<sub>α</sub>-Cl bond rupture in the transition state where the magnitude of the KIE<sup>‡</sup> and the TDF<sub>R</sub> contributions to the KIE are approximately equal, i.e., where the (TDF<sub>R</sub> × TDF<sup>‡</sup>) equals 1.00000. In this case, no substituent effect will be found.

The proposal that variable substituent effects on the chlorine leaving group KIEs could be observed, was tested by calculating the transition structures and chlorine KIEs for four other S<sub>N</sub>2 reactions of *para*-substituted benzyl chlorides at the B3LYP/aug-cc-pVDZ level of theory. The reactions, which had Cl<sup>-</sup>, Br<sup>-</sup>, 4-nitropyridine and NH<sub>3</sub> as the nucleophiles, were chosen for this investigation because the percent extension of the C<sub>α</sub>-Cl transition-state bond in the reaction with methyl chloride<sup>19</sup> increased from 22% when the nucleophile was CN<sup>-</sup>, to 31% when the nucleophile was Cl<sup>-</sup>, to 34% when the nucleophile was Br<sup>-</sup> to 36.5% when the nucleophile was 4-nitropyridine to 40% when the

nucleophile was  $\text{NH}_3$  and would represent a change from the reactant-like transition state for the  $\text{CN}^-$  reaction to a product-like transition state for the  $\text{NH}_3$  reaction, i.e., the product-like  $\text{NH}_3$  transition state has a N- $\text{C}_\alpha$  and  $\text{C}_\alpha$ -Cl percent extensions, equation 3, of 15 and 42%, respectively. The results, Table 6.11, show that the normal (predicted by the transition structures for the reactions) substituent effect on the KIE is found when the nucleophile is  $\text{CN}^-$ ,  $\text{Cl}^-$  and  $\text{Br}^-$  and the percent extension of the  $\text{C}_\alpha$ -Cl transition-state bond is approximately 22%, 32%, and 36%, respectively, but that no substituent effect is found when the nucleophile is 4-nitropyridine and the percent extension of the  $\text{C}_\alpha$ -Cl transition-state bond is approximately 42%, and that the substituent effect is inverse when the nucleophile is  $\text{NH}_3$  and the percent extension of the  $\text{C}_\alpha$ -Cl transition-state bond is approximately 43%. It is important to note that these different substituent effects on the chlorine KIE are found even though the substituent effect on transition state-structure (the change in the percent extension of the  $\text{C}_\alpha$ -Cl transition state bond with substituent) is in the same direction for all four reactions, i.e., the  $\text{C}_\alpha$ -Cl transition state bond shortens when the *para*-substituent is more electron-withdrawing in all five reactions. This change in the substituent effect on the chlorine KIE as the amount of  $\text{C}_\alpha$ -Cl bond rupture in the transition state increases is exactly what is predicted above. Finally, it is interesting that although the percent extension of the  $\text{C}_\alpha$ -Cl transition state bond in the *para*-substituted benzyl chloride series of reactions is slightly larger than those for the methyl chloride reactions, they are not very different, i.e., the percent extension of the  $\text{C}_\alpha$ -Cl transition state bond in the (benzyl chloride/methyl chloride) reactions is  $22.6/21.6 = 1.046$ ,

$32.1/30.6 = 1.049$ ,  $36.6/34.1 = 1.073$ ,  $42.3/36.5 = 1.16$  and  $43.5/39.6 = 1.098$  for the  $\text{CN}^-$ , the  $\text{Cl}^-$ , the  $\text{Br}^-$ , 4-nitropyridine and  $\text{NH}_3$  nucleophiles, respectively. This is consistent with a slightly looser  $\text{S}_{\text{N}}2$  transition state for the benzyl chloride series of reactions as is expected. It is also interesting that the increased looseness of the transition states for the benzyl chloride reaction relative to the methyl chloride reaction increases when poor nucleophiles are used in the reaction.

**Substituent effects on nucleophile KIEs:** An analysis of the data in Table 6.12 also suggests that different substituent effects will also be found on the nucleophile KIE. First, the substituent effect (KIE contribution for the *para*-methylbenzyl chloride reaction – KIE contribution for the *para*-nitrobenzyl chloride reaction) on  $\text{TDF}^\ddagger$  is significantly larger than the substituent effect on any other factor. For instance, it is 17 times larger than that on the  $\text{TIF}^\ddagger$  and even 5 times larger than that on the product  $\{\text{TIF} \times \text{KIE}_{\text{T}}\}$ . Again, the substituent effect on the  $\text{KIE}_{\text{T}}$  is very small at approximately 20% of the substituent effect on the  $\text{TIF}^\ddagger$ . Of course, there is no substituent effect on the  $\text{TDF}_{\text{R}}$  because there is no bonding between the isotope and  $\text{C}_{\alpha}$  in the ground state. Both the  $\text{TDF}_{\text{R}}$  and  $\text{TDF}^\ddagger$  are large because of the strong  $\text{C}\equiv\text{N}$  bond in both the ground and transition state. However, it is important to note that the inverse  $\text{TDF}^\ddagger$  is larger than the normal  $\text{TDF}_{\text{R}}$ . This is because the new  $\text{C}-\text{C}_{\alpha}$  bond being formed in the transition state increases the vibrational energy of the carbon isotope in the  $\text{C}\equiv\text{N}^-$ .<sup>38</sup> This means the

substituent effect on  $TDF^\ddagger$  is major factor in determining the substituent effect on the nucleophile KIE.

Again, there will be a varying substituent effect on these KIEs. For a very reactant-like transition state with a long Nu-C $_{\alpha}$  bond, the ( $TDF_R \times TDF^\ddagger$ ) contribution to the total KIE will be to all intents and purposes = 1.00000 because the bonding to the isotope in the reactant and the transition state will be virtually the same. The  $KIE_T$  and  $TIF^\ddagger$  will also be very close to 1.00000 for a very reactant-like transition state. Therefore, all the KIEs will be equal to or very close to 1.00000 and no discernable substituent effect will be observed. If, on the other hand, the transition state is product-like with a short Nu-C $_{\alpha}$  bond, the  $TDF^\ddagger$  will be more inverse (larger) than the  $TDF_R$  and since both the  $KIE_T$  and the  $TIF^\ddagger$  increase with the amount of bond formation in the transition state, the KIE will decrease with the amount of Nu-C $_{\alpha}$  bond formation in the transition state. Also, since the substituent effect on the product of the  $KIE_T$  and  $TIF^\ddagger$  is smaller than the substituent effect on  $TDF^\ddagger$ , a measurable substituent effect on the KIE will be observed. The important discovery is that a larger and larger substituent effect on the nucleophile KIE will be found as the amount of Nu-C $_{\alpha}$  bond formation in the transition state increases.

The nitrogen ( $k^{14}/k^{15}$ ) KIEs for the reactions between  $NH_3$  and the *para*-substituted benzyl chlorides were calculated to test this suggestion. The carbon ( $k^{11}/k^{14}$ ) and nitrogen ( $k^{14}/k^{15}$ ) KIEs for the reactions with  $CN^-$  and  $NH_3$ , Table 6.13, show that the

substituent effect on the KIEs for these two reactions is effectively identical. However, considering that the maximum observed carbon KIE is approximately five times larger than the maximum nitrogen KIE, (1.22 versus 1.044)<sup>39,40</sup> the substituent effect on the nitrogen KIEs represents a much greater change in the nitrogen KIEs than in the carbon KIEs (6.4% for the <sup>14</sup>N/<sup>15</sup>N KIEs versus 1.3% for the <sup>11</sup>C/<sup>14</sup>C KIEs) as the above analysis suggests.

## 6.4 Conclusions

The important discovery from this study is that the substituent effect on both leaving group and nucleophile KIEs in S<sub>N</sub>2 reactions vary with transition state structure, i.e., one will only be able to observe a correct and measurable substituent effect on a C<sub>α</sub>-LG bond using leaving group KIEs if C<sub>α</sub>-LG bond rupture is significant but not well advanced in the transition state. Similarly, one will only be able to determine the substituent effect on the Nu-C<sub>α</sub> transition-state bond using nucleophile KIEs when Nu-C<sub>α</sub> bond formation is well advanced in the transition state, i.e., in a product-like S<sub>N</sub>2 transition state. Thus, although the leaving group KIEs and nucleophile KIEs can, in principle, be used to determine substituent effects on transition state structure, they will only be able to detect the correct substituent effect when the bond to the isotopic atom is short in the transition state. This is undoubtedly why different substituent effects on transition state structure have been reported for S<sub>N</sub>2 reactions. For example, in this study, the transition states have long NC-C<sub>α</sub> (the average percent bond extension in these transition states is 61%) and relatively short C<sub>α</sub>-Cl (the average bond extension in these

transition states is 22%) bonds. Therefore, a measurable, expected, substituent effect for the chlorine leaving group KIEs and a very small or no measurable substituent effect on the nucleophile carbon KIEs is expected and this is in fact, what is observed both experimentally and computationally. Unlike this study where the nucleophile KIEs do not change significantly with substituent, the nucleophile  $k^{11}/k^{14}$  carbon KIEs decreased when a more electron-withdrawing substituent was on the benzene ring of the leaving group in the  $S_N2$  reactions between cyanide ion and *m*-chlorobenzyl-*para*-substituted benzenesulfonates which were thought to react via product-like transition states with short NC-C $_{\alpha}$  bonds.<sup>10</sup> Paneth and co-workers<sup>9</sup> also found a measurable substituent effect on the nucleophile nitrogen KIEs when a more electron-withdrawing substituent was on the benzene ring of the nucleophile in the  $S_N2$  reactions between *para*-substituted N,N-dimethylanilines and methyl iodide. This clearly suggests these reactions proceed via product-like transition states.

Different substituent effects on chlorine leaving group KIEs have also been observed in the  $S_N2$  reactions of *para*-substituted benzyl chlorides. For instance, the chlorine leaving group KIEs for the  $S_N2$  reactions between thiophenoxide ion, iodide ion and *n*-butyl thiolate ion and methoxide ion and *para*-substituted benzyl chlorides, Table 6.7, show no consistent trend in the chlorine KIEs with the electron-withdrawing ability of the substituent.<sup>5,13</sup> In fact, the KIEs for 6 of the 11 possible comparisons increase, not decrease, when a more electron-withdrawing substituent is on the benzene ring of the substrate. However, in the  $S_N2$  reactions between *para*-substituted benzyl chlorides and

borohydride ion,<sup>12, 13</sup> the chlorine leaving group KIEs decrease significantly from 1.0076 to 1.0036 as the electron-withdrawing ability of the substituent increases. It has been suggested that the reactions in Table 6.7 have product-like transition states while the borohydride reactions have reactant-like transition states.

Finally, while this investigation of the leaving group and nucleophile KIEs suggests the usefulness of these KIEs for determining the substituent effects on transition state structure is limited, all is not lost. The failure to see a measurable substituent effect on a leaving group or nucleophile KIE indicates that the bond to the isotope is long in the transition state of the S<sub>N</sub>2 reaction. Thus, as well as being able to determine the substituent effect on transition state structure in some S<sub>N</sub>2 reactions, these KIEs can indicate whether an S<sub>N</sub>2 reaction has a reactant-like, a product-like, or a central transition state.

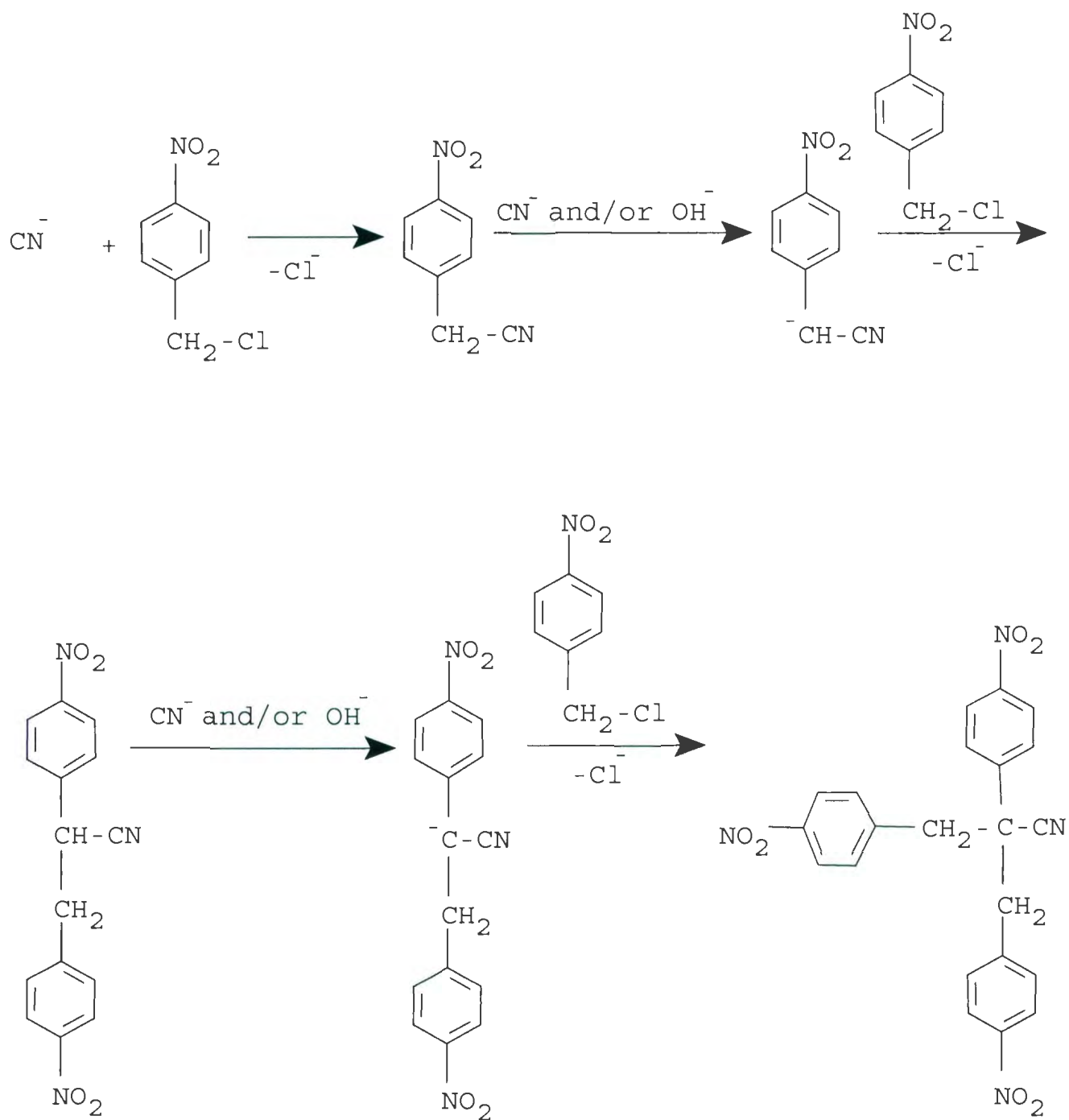
## 6.5 References

- (1) Hudson, R. F.; Klopman, G., *J. Chem. Soc.*, **1962**, 1062.
- (2) Hill, J. W.; Fry, A., *J. Amer. Chem. Soc.*, **1962**, 84, 2763.
- (3) Ballistreri, F. P.; Maccarone, E.; Mamo, A., *J. Org. Chem.*, **1976**, 41, 3364.
- (4) Westaway, K. C.; Ali, S. F., *Can. J. Chem.*, **1979**, 57, 1354.
- (5) Westaway, K. C.; Waszczylo, Z., *Can. J. Chem.*, **1982**, 60, 2500.
- (6) Ando, T.; Tanabe, H.; Yamataka, H., *J. Am. Chem. Soc.* **1984**, 106, 2084.

- (7) Lee, I.; Koh, H. J.; Lee, B.-S.; Sohn, D. S.; Lere, B. C., *J. Chem. Soc, Perkin Trans, 2*, **1991**, 174.
- (8) Matsson, O.; Persson, J.; Axelsson, B. S.; Langstrom, B.; Fang, Y.; Westaway, K.C., *J. Amer. Chem. Soc*, **1996**, 118, 6350.
- (9) Szyllabel-Godala, A.; Madhavan, S.; Rudzinski, J., O'Leary, M. H.; Paneth, P., *J. Phys. Org. Chem.*, **1996**, 9, 35.
- (10) Westaway, K. C.; Fang, Y-r.; Persson, J.; Matsson, O., *J. Amer. Chem. Soc*, **1998**, 120, 3340.
- (11) Westaway, K. C.; Jiang, W., *Can. J. Chem*, **1999**, 77, 879.
- (12) Koerner, T.; Fang, Y-r.; Westaway, K. C., *J. Amer. Chem. Soc.*, **2000**, 122, 7342.
- (13) Westaway, K. C., in *Advances in Physical Organic Chemistry*, Vo. 41, J. Richards, Editor, Elsevier, 2006, pp. 257.
- (14) Kato, S.; Davico, G. E.; Lee, H. S.; DePuy, C. H.; Bierbaum, V. M., *Int. J. Mass Spectrom*, **2001**, 210/211, 223.
- (15) Hargreaves, R. T.; Katz, A. M.; Saunders, W. H. Jr., *J. Amer. Chem. Soc.* **1976**, 98, 2614.
- (16) Lynn, K. R.; Yankwich, P. E., *J. Amer. Chem. Soc.*, **1961**, 83, 3220.
- (17) Koerner, T.; Fang, Y-r.; Westaway, K. C., *J. Amer. Chem. Soc.*, **2000**, 122, 7342.
- (18) Shiner, V. J.; Wilgis, F. P., in *Isotopes in Organic Chemistry*, Buncl, E. Saunders, W. H. Jr., Eds., Vol. 8, Elsevier, New York, 1992, p. 239.
- (19) Dybala-Defratyka, A.; Rostkowski, M.; Matsson, O.; Westaway, K. C.; Paneth, P., *J. Org. Chem.*, **2004**, 69, 4900.

- (20) Melander, L., in *Isotope Effects on Reaction Rates*, The Ronald Press, New York, N. Y., **1960**, pp 15 and 34.
- (21) Paneth, P., *Computers Chem.*, **1995**, 19, 231.
- (22) Fang, Y.; S. MacMillar, S.; Eriksson, J.; Kołodziejska-Huben, M.; Dybała-Defratyka, A.; Paneth, P.; Matsson, O.; Westaway, K. C., *J. Org. Chem.*, **2006**, 71, 4742.
- (23) Fang, Y.; Gao, Y.; Ryberg, P.; Eriksson, J.; Kolodziejska-Huben, M.; Dybala-Defratyka, A.; Madhavan, S.; Danielsson, R.; Paneth, P.; Matsson, O.; Westaway, K. C., *Chem. Eur. J.*, **2003**, 9, 2696.
- (24) Frisch, M. J.; et al. *Gaussian 03*, Revision B.05; Gaussian, Inc., Wallingford CT, 2004.
- (25) Wigner, E., *Z. Phys. Chem.*, B, **1932**, 19, 203.
- (26) Anisimov, V; Paneth, P., *J. Math. Chem.*, **1999**, 26, 75.
- (27) A. J. Gordon, R. A. Ford in *The Chemist's Companion*, John Wiley and Sons, New York, **1972**, pp. 6, 7. *Molecules*, John Wiley & Sons, New York, **1980**, p. 130.
- (28) Westaway, K. C.; Pham, T. V.; Fang, Y-r., *J. Am. Chem. Soc.*, **1997**, 119, 3670.
- (29) Koshy, K. M.; Robertson, R. E., *J. Amer. Chem. Soc.*, **1974**, 96, 914.
- (30) Shiner, V. J. Jr.; Dowd, W.; Fisher, R. D.; Hartshorn, S. R.; Kessik, M. A.; Milakofsky, L.; Rapp, M. W., *J. Amer. Chem. Soc.*, **1969**, 91, 4838.
- (31) Westaway, K. C. in *Isotopes in Organic Chemistry*, Buncl, E. Lee, C. C., Eds., Vol. 7, Elsevier, New York, **1987**, p. 336 – 342.
- (32) Gilliom, R. D., in *Introduction to Physical Organic Chemistry*, Addison-Wesley Publishing Company, Inc., Philippines, 1970, pp 146-147.

- (33) E. Grimsrud, PhD. Dissertation, University of Wisconsin, Madison, WI, 1971.
- (34) The tetrabutylammonium cyanide used in this study was only 95% pure. When tetrabutylammonium cyanide was dissolved in water, the solution had a pH greater than 11 suggesting that the contaminant was tetrabutylammonium hydroxide. However, it is not known whether the base in scheme 6.1 is cyanide ion and/or hydroxide ion.
- (35) Both the trimer and the dimer proceeding it in Scheme 6.1, have been isolated from the reaction and identified by NMR spectroscopy.
- (36) Crozet, M. P.; Flesia, E.; Surzur, J. M.; Boyer, M.; Tordo, P., *Tet. Lett.*, **1975**, 4563.
- (37) Westaway, K. C.; *Can. J. Chem.*, **1993**, 71, 2084.
- (38) Jobe, D. J.; Westaway, K. C., *Can. J. Chem.*, **1993**, 71, 1353.
- (39) Persson, J.; Berg, U.; Matsson, O., *J Org. Chem.*, **1995.**, 60, 5037.
- (40) W. E. Buddenbaum, V. J. Jr. Shiner, in *Isotope Effects on Enzyme-Catalyzed Reactions*, (Eds.: W. W. Cleland, M. H. O'Leary, D. B. Northrop), University Park Press, London, **1977**, p. 18.
- (41) Shiner, R. L.; Fuson, R. L.; Curtin, D. Y. In *The Systematic Identification of Organic Compounds*; 4 ed.; Wiley & Sons: New York, 1959, p 149.
- (42) Perrin, D. D.; Armarego, W. L. F. In *Purifications of Laboratory Chemicals*; 3 ed.; Pergamon Press: Oxford, 1988, p 60-61, 367.
- (43) Iwata, R.; Ido, T.; Takahashi, T.; Nakanishi, H.; Iida, S. *Applied Radiation And Isotopes* **1987**, 38, 97.
- (44) Christman, D. R.; Finn, R. D.; Karlstrom, K. I.; Wolf, A. P. *International Journal of Applied Radiation and Isotopes* **1975**, 26, 435.



Scheme 6.1. A possible mechanism for the reaction forming the largest side product from the reaction between tetrabutylammonium cyanide and *para*-nitrobenzyl chloride in THF at 20°C.

**TABLE 6.1** The experimental secondary  $\alpha$ -deuterium KIE for the  $S_N2$  reactions between cyanide ion and benzyl- and *para*-chlorobenzyl chloride at 0°C in THF.

<i>Para</i> -substituent	$k_H \times 10^3$ <sup>a</sup> (M <sup>-1</sup> .s <sup>-1</sup> )	$k_D \times 10^3$ <sup>a</sup> (M <sup>-1</sup> .s <sup>-1</sup> )	$(k_H/k_D)_{\alpha-D2}$
H	2.399 ± 0.002 <sup>b</sup>	2.385 ± 0.001 <sup>b</sup>	1.006 ± 0.001 <sup>c</sup>
Cl	9.713 ± 0.002	9.597 ± 0.001	1.012 ± 0.001

<sup>a</sup> The rate constant quoted is the average of the rate constants found in at least three different experiments.

<sup>b</sup> Standard deviation.

<sup>c</sup> The error in the KIE is  $1/k_D[(\Delta k_H)^2 + (k_H/k_D)^2 \times (\Delta k_D)^2]^{1/2}$ , where  $\Delta k_H$  and  $\Delta k_D$  are the standard deviations for the average rate constants for the reactions of the undeuterated and deuterated substrates, respectively.<sup>5</sup>

**TABLE 6.2** The secondary  $\alpha$ -deuterium  $(k_H/k_D)_\alpha$  KIEs for the  $S_N2$  reactions between cyanide ion and five *para*-substituted benzyl chlorides at 25°C using three different levels of theory.

<i>Para</i> - substituent	$(k_H/k_D)_\alpha$		
	RHF/6-31+G(d)	B3LYP/6-31+G(d)	B3LYP/aug-cc-pVDZ
CH <sub>3</sub>	0.9677	0.9837	0.9851
H	0.9606	0.9812	0.9812
F	0.9630	0.9824	0.9827
Cl	0.9521	0.9776	0.9788
NO <sub>2</sub>	0.9334	0.9695	0.9733
Substituent effect (CH <sub>3</sub> – NO <sub>2</sub> )	0.0342	0.01415	0.0118
$r^2$ <sup>a</sup>	0.980	0.973	0.954

<sup>a</sup> KIEs versus the Hammett  $\sigma$  constants.

**TABLE 6.3** The experimental chlorine leaving group KIEs for the S<sub>N</sub>2 reactions between cyanide ion and four *para*-substituted benzyl chlorides at 20°C in THF.

<i>Para</i> -substituent	Trial I	Trial II	Trial III	Average
CH <sub>3</sub>	1.00609 ± 0.00014 <sup>a</sup>			
H	1.00591 ± 0.00004			
Cl	1.00546 ± 0.00016	1.00527 ± 0.00009 <sup>a</sup>	1.00540 ± 0.00037 <sup>a</sup>	1.00537 ± 0.00024 <sup>b</sup>
NO <sub>2</sub>	1.00556 ± 0.00013	1.00568 ± 0.00009		1.00562 ± 0.00013 <sup>c</sup>

<sup>a</sup> Standard deviation for five separate experiments measuring the KIE.

<sup>b</sup> Standard deviation for 14 separate experiments measuring the KIE.

<sup>c</sup> Standard deviation for 9 separate experiments measuring the KIE.

**TABLE 6.4** The calculated  $C_{\alpha}$ -Cl bond length in five *para*-substituted benzyl chlorides at 25°C using three different levels of theory.

Para-substituent	$C_{\alpha}$ -Cl bond length (Å)		
	RHF/6-31+G(d)	B3LYP/6-31+G(d)	B3LYP/aug-cc-pVDZ
CH <sub>3</sub>	1.8107	1.8442	1.8490
H	1.8086	1.8413	1.8451
F	1.8085	1.8400	1.8449
Cl	1.8063	1.8400	1.8455
NO <sub>2</sub>	1.8005	1.8314	1.8364
Substituent effect (CH <sub>3</sub> – NO <sub>2</sub> )	0.0102	0.0128	0.0126
$r^2$ <sup>a</sup>	0.997	0.970	0.926

<sup>a</sup>  $C_{\alpha}$ -Cl bond lengths versus the Hammett  $\sigma$  constants.

**TABLE 6.5** The calculated  $C_{\alpha}$ -Cl and NC- $C_{\alpha}$  transition-state bond lengths for the  $S_N2$  reactions between cyanide ion and five *para*-substituted benzyl chlorides at 25°C using three different levels of theory.

<i>Para</i> - substituent	$(C_{\alpha}\text{-Cl})^{\ddagger}$ bond length (Å)			$(\text{NC-}C_{\alpha})^{\ddagger}$ bond length (Å)		
	RHF/6-31+G(d)	B3LYP/6-31+G(d)	B3LYP/aug-cc-pVDZ	RHF/6-31+G(d)	B3LYP/6-31+G(d)	B3LYP/aug-cc-pVDZ
CH <sub>3</sub>	2.3592	2.2844	2.2705	2.3984	2.3941	2.3836
H	2.3466	2.2757	2.2619	2.3857	2.3884	2.3778
F	2.3474	2.2746	2.2621	2.3858	2.3857	2.3771
Cl	2.3292	2.2633	2.2505	2.3670	2.3786	2.3697
NO <sub>2</sub>	2.2872	2.2267	2.2145	2.3247	2.3508	2.3469
Substituent effect (CH <sub>3</sub> – NO <sub>2</sub> )	0.0720	0.0557	0.0560	0.0737	0.0433	0.0367
$r^2$ <sup>a</sup>	0.993	0.994	0.990	0.995	0.999	0.999

<sup>a</sup> Transition state bond lengths versus the Hammett  $\sigma$  constants.

**TABLE 6.6** The chlorine ( $k^{35}/k^{37}$ ) leaving group KIEs for the  $S_N2$  reactions between cyanide ion and five *para*-substituted benzyl chlorides at 25°C using four different levels of theory and un-scaled frequencies.

<i>Para</i> - substituent	$k^{35}/k^{37}$		
	RHF/6-31+G(d)	B3LYP/6-31+G(d)	B3LYP/aug-cc-pVDZ
CH <sub>3</sub>	1.01012	1.00742	1.00717
H	1.01004	1.00743	1.00717
F	1.01003	1.00741	1.00716
Cl	1.00987	1.00728	1.00699
NO <sub>2</sub>	1.00950	1.00703	1.00676
Substituent effect (CH <sub>3</sub> – NO <sub>2</sub> )	0.00062	0.00039	0.00041
$r^2$ <sup>a</sup>	0.991	0.949	0.942

<sup>a</sup> KIEs versus the Hammett  $\sigma$  constants.

**TABLE 6.7** The experimental chlorine ( $k^{35}/k^{37}$ ) leaving group KIEs<sup>a, b</sup> for the  $S_N2$  reactions of *para*-substituted benzyl chlorides with various nucleophiles at 20°C.

Para-Substituent	$k^{35}/k^{37}$ Nucleophile			
	$C_6H_5S^-$	$I^-$	$C_4H_9S^-$	$CH_3O^-$
CH <sub>3</sub>	1.00931	1.00996	1.00894	1.00780
H	1.00948	-	1.00920	1.00800
Cl	1.00990	1.00973	1.00915	1.00806
NO <sub>2</sub>	1.00918	1.00976	1.00871	1.00768
Average	1.00947	1.00982	1.00900	1.00789
Standard deviation	0.00031	0.00013	0.00022	1.00018

<sup>a</sup> The error on each KIE was reported as 0.00010.

<sup>b</sup> The data is taken from reference 33.

**TABLE 6.8** The experimental nucleophile carbon  $k^{11}/k^{14}$  KIEs for the  $S_N2$  reactions between cyanide ion and three *para*-substituted benzyl chlorides at 20°C.

$k^{11}/k^{14}$	<i>Para</i> -substituent
CH <sub>3</sub>	$0.99951 \pm 0.0013^a$ (8) <sup>b</sup>
H	$1.00467 \pm 0.0009$ (6)
Cl	$1.00158 \pm 0.0025$ (9)

<sup>a</sup> Standard deviation.

<sup>b</sup> The number of separate evaluations of the KIE used to calculate the average KIE.

**TABLE 6.9** The nucleophile carbon  $k^{11}/k^{14}$  KIEs for the  $S_N2$  reactions between cyanide ion and five *para*-substituted benzyl chlorides at 25°C using three different levels of theory.

<i>Para</i> - substituent	$k^{11}/k^{14}$		
	RHF/6-31+G(d)	B3LYP/6-31+G(d)	B3LYP/aug-cc-pVDZ
CH <sub>3</sub>	0.97604	0.98259	0.98381
H	0.97476	0.98202	0.98329
F	0.97470	0.98173	0.98311
Cl	0.97292	0.98105	0.98248
NO <sub>2</sub>	0.96874	0.97873	0.98079
Substituent effect (CH <sub>3</sub> – NO <sub>2</sub> )	0.00730	0.00386	0.00302
$r^2$ <sup>a</sup>	0.995	0.999	0.999

<sup>a</sup> KIEs versus the Hammett  $\sigma$  constants.

**TABLE 6.10** The individual contributions to the chlorine leaving group KIEs for the S<sub>N</sub>2 reactions between cyanide ion and five *para*-substituted benzyl chlorides at 25°C in the gas phase at the B3LYP/aug-cc-pVDZ level of theory.

<i>Para</i> -substituent	TDF <sub>R</sub>	KIE <sub>T</sub>	TIF <sup>‡</sup>	TDF <sup>‡</sup>	KIE <sup>‡</sup> = {KIE <sub>T</sub> .TIF <sup>‡</sup> .TDF <sup>‡</sup> }	Total k <sup>35</sup> /k <sup>37</sup>
CH <sub>3</sub>	1.00714	1.00043	1.00215	0.997441	1.00002	1.00717
H	1.00725	1.00043	1.00210	0.99738	0.99991	1.00717
Cl	1.00725	1.00043	1.00201	0.99730	0.99973	1.00699
NO <sub>2</sub>	1.00758	1.00040	1.00174	0.99706	0.99919	1.00676
Substituent effect (CH <sub>3</sub> – NO <sub>2</sub> )	-0.00044	0.00003	0.00041	0.00038	0.00083	0.00041

**TABLE 6.11** Substituent effects on the transition structures and chlorine leaving group KIEs for different S<sub>N</sub>2 reactions with a series of *para*-substituted benzyl chlorides at 25°C using the B3LYP/aug-cc-pVDZ level of theory.

Nucleophile/ <i>Para</i> - substituent	CN <sup>-</sup>		Cl <sup>-</sup>		Br <sup>-</sup>		p-O <sub>2</sub> N-C <sub>6</sub> H <sub>4</sub> N		NH <sub>3</sub>	
	(% bond extension) <sup>‡</sup>	k <sup>35</sup> /k <sup>37</sup>	(% bond extension) <sup>‡</sup>	k <sup>35</sup> /k <sup>37</sup>	(% bond extension) <sup>‡</sup>	k <sup>35</sup> /k <sup>37</sup>	(% bond extension) <sup>‡</sup>	k <sup>35</sup> /k <sup>37</sup>	(% bond extension) <sup>‡</sup>	k <sup>35</sup> /k <sup>37</sup>
CH <sub>3</sub>	22.8	1.00717	32.2	1.00864	36.9	1.00884	42.5	1.00617	43.8	1.00650
H	22.6	1.00717	32.1	1.00858	36.6	1.00871	42.3	1.00625	43.5	1.00665
Cl	21.9	1.00699	31.4	1.00834	35.8	1.00860	41.8	1.00632	43.6	1.00666
NO <sub>2</sub>	20.6	1.00676	30.3	1.00792	34.3	1.00814	41.1	1.00620	42.6	1.00680
Substituent effect (CH <sub>3</sub> – NO <sub>2</sub> )	2.2	0.00041	1.9	0.00072	2.6	0.00070	1.4	0.00003	0.6	-0.00030

TABLE 6.12 The individual contributions to the calculated nucleophile carbon ( $k^{11}/k^{14}$ ) KIEs for the  $S_N2$  reactions between cyanide ion and five *para*-substituted benzyl chlorides at 25°C in the gas phase at the B3LYP/aug-cc-pVDZ level of theory.

<i>Para</i> -substituent	TDF <sub>R</sub>	KIE <sub>T</sub>	TIF <sup>‡</sup>	TDF <sup>‡</sup>	KIE <sup>‡</sup> = {KIE <sub>T</sub> .TIF <sup>‡</sup> .TDF <sup>‡</sup> }	Total $k^{11}/k^{14}$
CH <sub>3</sub>	1.29637	1.00182	1.00905	0.75076	0.75893	0.98381
H	1.29637	1.00184	1.00898	0.75040	0.75853	0.98329
F	1.29637	1.00183	1.00886	0.75036	0.75839	0.98311
Cl	1.29637	1.00185	1.00876	0.74994	0.75791	0.98248
NO <sub>2</sub>	1.29637	1.00194	1.00854	0.74874	0.75660	0.98079
Substituent effect (CH <sub>3</sub> – NO <sub>2</sub> )	0.00000	-0.00012	0.00051	0.00202	0.00233	0.00302

**TABLE 6.13** Substituent effects on the transition structures and nucleophile carbon  $k^{11}/k^{14}$  and nitrogen  $k^{14}/k^{15}$  KIEs for the SN2 reactions between cyanide ion and ammonia with a series of *para*-substituted benzyl chlorides, respectively, at 25°C using the B3LYP/aug-cc-pVDZ level of theory.

Nucleophile/ <i>Para</i> -substituent	CN <sup>-</sup>		NH <sub>3</sub>	
	(% bond extension) <sup>‡</sup>	$k^{11}/k^{14}$	(% bond extension) <sup>‡</sup>	$k^{14}/k^{15}$
CH <sub>3</sub>	62.06	0.9838	15.67	0.9913
H	61.71	0.9833	15.58	0.9908
Cl	61.17	0.9831	14.74	0.9904
NO <sub>2</sub>	59.66	0.9808	14.21	0.9885
Substituent effect (CH <sub>3</sub> – NO <sub>2</sub> )	2.40	0.0030	1.46	0.0028

## CHAPTER 7

# **Can incoming nucleophile carbon kinetic isotope effects be used to determine the transition state structure for different $S_N2$ reactions?**

### **7.1 Introduction**

Although many different types of kinetic isotope effects (KIEs) have been used to probe the structure of  $S_N2$  transition states,<sup>1-10</sup> most of the studies have used leaving group KIEs to estimate the relative lengths of the  $C_\alpha$ -LG bond in the transition state.<sup>2,5,8,11,12</sup> Until recently, the interpretation of these KIEs was thought to be straightforward, i.e., it was believed that a larger leaving group KIE was indicative of

greater C<sub>α</sub>-LG bond rupture in the transition state. However, a recent theoretical investigation of chlorine leaving group KIEs<sup>13</sup> indicated that the interpretation of these KIEs was not as straightforward as had been previously thought. This study showed that the chlorine leaving group KIEs for 26 S<sub>N</sub>2 reactions with methyl chloride fell in a very narrow range of values and that there was no relationship between the magnitude of the KIE and the C<sub>α</sub>-Cl bond length in the transition state!

The KIE is the product of the tunneling KIE, (KIE<sub>T</sub>) the imaginary frequency ratio or temperature independent factor, (TIF<sup>‡</sup>) and the temperature dependent factor, (TDF) that represents the isotope effect on the vibrations in the reactant (TDF<sub>R</sub>) and transition state (TDF<sup>‡</sup>), respectively.<sup>14,15</sup> equation 1,

$$\frac{k_L}{k_H} = \underbrace{\left(\frac{k_L}{k_H}\right)_T}_{\text{KIE}_T} \times \underbrace{\left(\frac{\nu_L^*}{\nu_H^*}\right)}_{\text{TIF}^{\ddagger}} \times \underbrace{\prod_i^{3N-6} \frac{\mu_{iH}^R \sinh(\mu_{iL}^R / 2)}{\mu_{iL}^R \sinh(\mu_{iH}^R / 2)}}_{\text{TDF}_R} \times \underbrace{\prod_i^{3N^{\ddagger}-7} \frac{\mu_{iL}^{\ddagger} \sinh(\mu_{iH}^{\ddagger} / 2)}{\mu_{iH}^{\ddagger} \sinh(\mu_{iL}^{\ddagger} / 2)}}_{\text{TDF}^{\ddagger}} \quad (1)$$

where R represents the reactant, ‡ indicates the transition state,  $\mu_i = h\nu_i/k_B T$  and the  $\nu_i$ 's are the vibrational frequencies and L and H represent species with the light and heavy isotopes, respectively. Dybala-Defratyka et al.<sup>13</sup> found that the relationship between the magnitude of the experimental KIE and the C<sub>α</sub>-Cl bond length in the transition state fails because the (KIE<sub>T</sub> × TIF<sup>‡</sup>) portion of the KIE accounted for a significant portion of the total KIE and is not related to transition state structure in any discernable way. However, although the TDF<sup>‡</sup> was related to the length of the C<sub>α</sub>-Cl bond in the transition state, one

cannot use the magnitude of the KIE to estimate the length of the  $C_{\alpha}$ -Cl transition state bond. This then led one to question whether one could use the magnitude of a nucleophile KIEs to estimate the relative lengths of the Nu- $C_{\alpha}$  transition state bond in different reactions or whether they would suffer from the same problem as the leaving group KIEs. This latter possibility seemed likely because the basic equation is the same and the nucleophile KIE measures the reverse of the leaving group KIEs, i.e., the amount of Nu- $C_{\alpha}$  bond formation rather than the amount of  $C_{\alpha}$ -LG bond rupture in the transition state. This experimental and theoretical study of the nucleophile KIEs for several  $S_N2$  reactions with different leaving groups and presumably very different transition states, examines whether the magnitude of the nucleophile KIEs from different reactions can be used to determine the relative lengths of the Nu- $C_{\alpha}$  transition state bond in  $S_N2$  reactions.

## 7.2 Method

The calculations were done at the RHF/6-31+G(d), the B3LYP/6-31+G(d) and the B3LYP/aug-cc-pVDZ level of theory. The last method was chosen because it gave the closest KIEs to the experimental values in a thorough examination of the readily available methods for calculating transition state structure and the KIEs in the ethyl chloride - cyanide ion  $S_N2$  reaction.<sup>16</sup> All calculations were performed with Gaussian03 using default convergence criteria.<sup>17</sup> For 3<sup>rd</sup> row elements, the standard 6-31G basis set<sup>18</sup> was found to be more reliable than the Binning-Curtiss basis set<sup>19</sup> (BC6-31G) available in Gaussian03.<sup>20</sup> Therefore, for bromine both the 6-31G and BC6-31G basis sets were used. Un-scaled frequencies were used for all the calculations. Each transition structure had

one imaginary frequency that corresponds to the transfer of the alpha carbon from the leaving group to the carbon of the cyanide ion nucleophile. The effect of tunneling ( $KIE_T$ ) was calculated using the Wigner approximation.<sup>21</sup> Calculations were also done in solvent (DMSO) using the polarizable continuum model (PCM) as implemented in Gaussian03. All the KIEs were calculated with the ISOEFF98 program.<sup>22</sup> The procedure for measuring the experimental KIEs is available in Appendix C.

### 7.3 Results and Discussion

The nucleophile carbon  $k^{11}/k^{14}$  KIEs for the  $S_N2$  reactions between cyanide ion and ethyl chloride, bromide, iodide and tosylate, were measured in anhydrous DMSO at 20°C to determine whether these KIEs could be used to estimate the relative lengths of the NC-C $_{\alpha}$  transition state bonds in these reactions. The secondary  $\alpha$ -deuterium KIEs were also measured for these reactions to try to define the transition state structure for these reactions in more detail. A recent study<sup>15</sup> showed that a significant change in solvent does not change the structure of a Type I (where the nucleophilic atoms in the transition state have the same charge)  $S_N2$  transition state significantly. This is tested by optimizing the transition state structures and the KIEs in both the gas phase and in solution.

The rate constants and experimental nucleophile carbon  $k^{11}/k^{14}$  KIEs and secondary  $\alpha$ -deuterium KIEs for the  $S_N2$  reactions between cyanide ion and ethyl chloride, bromide, iodide and tosylate in anhydrous DMSO at 20°C, are given in Tables

7.1 and 7.2, respectively. The transition structures obtained at the RHF/6-31+G(d), the B3LYP/6-31+G(d) and the B3LYP/aug-cc-pVDZ level of theory are presented in Table 7.3 and the corresponding nucleophile carbon  $k^{11}/k^{14}$  and secondary  $\alpha$ -deuterium KIEs are given in Tables 7.4 and 7.5 respectively.

Calculated and experimental free energies of activation are given in Table 7.6. The free energies of activation calculated from structures optimized in DMSO are in very good agreement with the values determined from the experimental rate constants for the halogens, differing by no more than 10 kJ mol<sup>-1</sup>. However, for ethyl tosylate the difference is significantly larger, where the calculated free energy of activation is too high by 45 kJmol<sup>-1</sup>. It is interesting to note that the computed free energy of activation increases with poorer leaving group, whereas, the experimental free energy of activation for ethyl tosylate appears to be too low for its leaving group ability.

### 7.3.1 Experimental Nucleophile Carbon $k^{11}/k^{14}$ KIEs

With the exception of the KIE for the ethyl chloride reaction, the nucleophile carbon  $k^{11}/k^{14}$  KIEs for the S<sub>N</sub>2 reactions between cyanide ion and ethyl chloride, bromide, iodide and tosylate in anhydrous DMSO at 20°C, Table 7.1, are smaller when a poorer leaving group is present. However, it is worth noting that the very small nucleophile carbon  $k^{11}/k^{14}$  for the ethyl chloride reaction has been estimated<sup>23</sup> from a <sup>12</sup>C/<sup>13</sup>C KIE measured in an earlier study<sup>16</sup> so comparing it with the KIEs from this study is problematic. Even so, it is interesting that the  $k^{11}/k^{14}$  decreases when a poorer *halogen*

leaving group is present in the substrate. Since a smaller nucleophile  $k^{11}/k^{14}$  is indicative of a shorter Nu-C $_{\alpha}$  transition state bond,<sup>4,24</sup> the nucleophile carbon  $k^{11}/k^{14}$  KIEs found in this investigation suggest that NC-C $_{\alpha}$  bond formation is more complete, i.e., the NC-C $_{\alpha}$  transition state bond is shorter, in the reactions with a poorer leaving group.

### 7.3.2 Experimental Secondary $\alpha$ -Deuterium KIEs

The secondary  $\alpha$ -deuterium KIEs were also measured for the S<sub>N</sub>2 reactions between ethyl chloride, bromide, iodide and tosylate in an effort to determine the structure of the S<sub>N</sub>2 transition states in more detail. The results, Table 7.2, show that the  $(k_H/k_D)_{\alpha}$  decreases with leaving group ability within the *halogen* series of leaving groups but that the  $(k_H/k_D)_{\alpha}$  for the ethyl tosylate reaction is much larger than expected based on leaving group ability.

The usual relationship between the magnitude of a secondary  $\alpha$ -deuterium KIE and transition state structure in S<sub>N</sub>2 reactions is that a larger KIE is found when the nucleophile – leaving group distance in the transition state is greater, at least for S<sub>N</sub>2 reactions with the same leaving group.<sup>28, 29</sup> If the same relationship holds for the ethyl halide S<sub>N</sub>2 reactions in this study even though they have different leaving groups, one would conclude that the transition state is tighter with shorter NC-C $_{\alpha}$  and/or C $_{\alpha}$ -LG bonds when a poorer *halogen* leaving group is present. In this regard, it is important to note that the plot of the experimental  $(k_H/k_D)_{\alpha}$  versus R<sub>TS</sub> (the nucleophile – leaving

group distance in the transition state, Table 7.3) for the ethyl halide reactions, is linear with a correlation coefficient of 0.991. This clearly suggests that the magnitude of the secondary  $\alpha$ -deuterium KIE is related to  $R_{TS}$  for a family of similar leaving groups.<sup>30</sup>

The problem, then, is how to interpret the much larger than expected  $(k_H/k_D)_\alpha$  of 1.062 found for the ethyl tosylate reaction. The plot of the experimental  $(k_H/k_D)_\alpha$  versus the nucleophile – leaving group distance in the transition state suggests the  $(k_H/k_D)_\alpha$  should be 0.95 whereas it is 1.062. Unfortunately, the interpretation of these KIEs is not straightforward. Much larger than expected secondary  $\alpha$ -deuterium KIEs are observed when the leaving group is large because the steric hindrance to the  $C_\alpha$ -H(D) bending vibrations in the tetrahedral reactant (with a short bond to the bulky leaving group) is greater than the steric hindrance to these vibrations in the pentacoordinate transition state where the bond to the leaving group is longer.<sup>31,32</sup> Support for this idea has been provided by Abraham and McLennan<sup>33</sup> who suggested that the lone pairs of electrons on the oxygens of arenesulfonate leaving groups cause a larger than expected  $(k_H/k_D)_\alpha$ . Thus, it appears the larger than expected  $(k_H/k_D)_\alpha$  of 1.062, as suggested  $R_{TS}$ , for the tosylate reaction is due to the bulky (sterically hindered) leaving group in the reaction. This is reasonable for the following reasons. 1) The cyanide ion nucleophile is small and will not sterically hinder the bending vibrations of the  $C_\alpha$ -H(D) bonds in the transition state. 2) Theoretical calculations of the transition structure at the B3LYP/aug-cc-pVDZ level of

theory, Table 7.3 indicate that the transition state is reactant-like with a long NC-C<sub>α</sub> and significant, but not extensive, C<sub>α</sub>-O bond rupture, i.e., the percent extension, equation 2,

$$\% \text{ extension on going to the transition state} = \frac{\text{TS bond length} - \text{reactant (product) bond length}}{\text{reactant (product) bond length}} \times 100\% \quad (3)$$

of the NC-C<sub>α</sub> and C<sub>α</sub>-O bonds on going to the transition state, is 64.8% and 28.3%, respectively. 3) Since the NC-C<sub>α</sub> and particularly, the C<sub>α</sub>-O % extension are greater than those found for the halide reaction transition states, the steric explanation for the much larger α-deuterium KIE is reasonable. Finally, since this steric effect of the bulky leaving group is not present in the halide reactions, their (k<sub>H</sub>/k<sub>D</sub>)<sub>α</sub>'s show a clean trend with the smaller KIE and tighter transition state, for the reactions with a poorer leaving group.

### **7.3.3 The effect of changing the leaving group on the structure of the S<sub>N</sub>2 transition state**

The nucleophile carbon KIEs suggest that the NC-C<sub>α</sub> bonds are shorter in the transition states with a poorer leaving group. The secondary α-deuterium KIEs indicate that the transition states with a poorer leaving group have a shorter R<sub>TS</sub> and shorter NC-C<sub>α</sub> and/or C<sub>α</sub>-LG transition state bonds. Unfortunately, the secondary α-deuterium KIEs do not enable one to determine the change in transition state structure with leaving group ability in any more detail because the change in the NC-C<sub>α</sub> transition state bond would also lead to the smaller secondary α-deuterium KIE that is observed with the poorer

leaving group. It is important to note that the transition states for all these reactions are reactant-like with long NC-C $_{\alpha}$  and significant, but not extensive, C $_{\alpha}$ -LG bond rupture, i.e., the percent extension, equation 2, of the NC-C $_{\alpha}$  and C $_{\alpha}$ -LG bonds on going to the transition state at the B3LYP/aug-cc-pVDZ level of theory, Table 7.3, is  $63 \pm 3\%$  and  $24 \pm 5\%$ , respectively. With one exception, the transition structures calculated at three different levels of theory show that the NC-C $_{\alpha}$  transition state bond shortens as one goes from a better to a poorer *halogen* leaving group. This is in agreement with the conclusion based on interpreting the experimental  $k^{11}/k^{14}$  carbon KIEs. The calculations at three levels of theory also suggest that both the C $_{\alpha}$ -LG transition state bond and R $_{TS}$  shorten when a poorer *halogen* leaving group is used. This agrees with the predictions based on the magnitude of the experimental  $(k_H/k_D)_{\alpha}$ s. Thus, the agreement between the transition state structures predicted by interpreting the experimental KIEs and those predicted by theory for the reactions with a *halogen* leaving group is excellent for both the nucleophile carbon and the secondary  $\alpha$ -deuterium KIEs.

Another important observation is that the calculations indicate that the change in the C $_{\alpha}$ -LG transition state bond with leaving group is much larger than the change in the NC-C $_{\alpha}$  transition state bond when a poorer *halogen* leaving group is used, i.e., the change in the NC-C $_{\alpha}$  transition state bonds in going from I $^{-}$  (best leaving group) to Cl $^{-}$  (poorest leaving group) is only 0.08 Å at the B3LYP/aug-cc-pVDZ level of theory whereas, the corresponding change in the C $_{\alpha}$ -LG transition state bond is four times larger at 0.31Å. The corresponding changes in the percent extension of these bonds are 5.2% for

the NC-C $\alpha$  and 6.4% for the C $\alpha$ -LG bonds with a change in the halogen leaving group. This is consistent with interpretation of the secondary  $\alpha$ -deuterium KIEs and the “Bond Strength Hypothesis”,<sup>34</sup> which predicts that the greatest change in the transition state structure with a change in leaving group will occur at the weakest reacting bond.

It is worth noting that the change in the C $\alpha$ -LG bond length with leaving group increases markedly from 0.31Å to 0.73Å when the tosylate leaving group result is included. This significant increase in this value for the tosylate leaving group again suggests that the tosylate reaction is very different and should not be compared to the results for the halogen leaving groups. Thus, again, the transition state for the ethyl tosylate reaction does not fit the trends found for the reactions with the halogen leaving groups, i.e., the ethyl tosylate transition state is looser with a longer NC-C $\alpha$  and longer C $\alpha$ -LG bonds than expected given its leaving group ability. Obviously, changing from a halogen to a tosylate leaving group alters the transition state structure too much to hope the reaction fits the trends found for the halogen family of leaving groups.

The important conclusions however, are 1) that one can use the nucleophile carbon KIEs to estimate the relative length of the NC-C $\alpha$  transition state bonds in a closely related series of S<sub>N</sub>2 reactions, i.e., those with a halogen leaving group, and 2) that the calculated transition structures results clearly support the R<sub>TS</sub> method (the nucleophile – leaving group distance) of interpreting the (k<sub>H</sub>/k<sub>D</sub>) $\alpha$ s in the S<sub>N</sub>2 transition state.<sup>28,29</sup>

### 7.3.4 Experimental vs calculated nucleophile $k^{11}/k^{14}$ carbon KIE

The next consideration was to compare the calculated KIEs with the experimental values. The nucleophile  $k^{11}/k^{14}$  carbon KIE calculated at three different levels of theory are presented along with the experimental values in Table 7.4. The results show that the  $k^{11}/k^{14}$  are only affected slightly by the level of theory, i.e., the nucleophile carbon KIEs only vary by 1.5%. The agreement between the experimental and the calculated KIEs is satisfying although theory predicts nucleophile carbon KIEs smaller than the experimental KIEs by approximately 2% at the B3LYP/aug-cc-pVDZ level of theory. However, at this level of theory the change in the calculated  $k^{11}/k^{14}$  with leaving group is smaller than the change in the experimental KIEs, i.e., 0.34% by theory and 0.39% experimentally. The trends in the calculated  $k^{11}/k^{14}$  do not consistently mirror those in the experimental KIEs. At the B3LYP/aug-cc-pVDZ level, the calculated  $k^{11}/k^{14}$  for the ethyl iodide reaction is slightly smaller than that for the ethyl bromide reaction, otherwise the trend follows experiment. This may arise from using the Huzinaga basis set<sup>35</sup> for iodine and the aug-cc-pVDZ basis set for the other atoms. This is reasonable because the ethyl iodide  $k^{11}/k^{14}$  is larger than the ethyl bromide  $k^{11}/k^{14}$  using the other three levels of theory.

Both the calculated and experimental  $k^{11}/k^{14}$  and calculated transition structures indicate the NC-C<sub>α</sub> transition state bond is shorter when a poorer *halogen* leaving group is present. Thus, both the transition structures and the KIEs predicted by theory agree

with the change in the NC-C<sub>α</sub> transition state bond predicted by interpreting the experimental  $k^{11}/k^{14}$ , i.e., that changing to a poorer leaving group leads to a shorter NC-C<sub>α</sub> bond length in transition state. The calculated  $k^{11}/k^{14}$  for the tosylate reaction are however smaller than expected based on their leaving group ability, with a substantially longer than expected NC-C<sub>α</sub> transition state bond length.

### 7.3.5 Experimental vs calculated $(k_H/k_D)_\alpha$ KIEs

The agreement between the experimental and the calculated secondary  $\alpha$ -deuterium KIEs, Table 7.5, is less satisfying. Although the  $(k_H/k_D)_\alpha$ s only change by  $\leq 3.0\%$  using different levels of theory, the difference between the B3LYP/aug-cc-pVDZ and experimental  $(k_H/k_D)_\alpha$ s is larger, i.e., they differ by 3.0 % for the ethyl bromide reaction and by 6.0 % and 6.1 % for the ethyl iodide and tosylate reactions, respectively. In fact, the difference between the calculated and experimental  $(k_H/k_D)_\alpha$  is only small (0.00%) for the ethyl chloride reaction. More importantly, the trend in the calculated  $(k_H/k_D)_\alpha$  for the reactions with the *halogen* leaving groups, is opposite to that found using the experimental values. The experimental values decrease with leaving group ability suggesting the transition state becomes tighter, whereas the calculated  $(k_H/k_D)_\alpha$  increase very slightly when a poorer leaving group is present. Since the change in the C<sub>α</sub>-LG bond is greater than the change in the NC-C<sub>α</sub> bond when a poorer leaving group is used, (*vide supra*) the increase in the calculated  $(k_H/k_D)_\alpha$  with a poorer leaving group suggests the transition state C<sub>α</sub>-LG bond lengthens when a poorer leaving group is present. This is

clearly opposite the change in transition structure with leaving group predicted by interpreting the experimental  $(k_H/k_D)_\alpha$  and the change in the transition structures calculated for these reactions!

Although the change in the experimental nucleophile carbon KIEs for the reactions with the *halogen* leaving groups is slightly larger than the change found theoretically, the change in the experimental  $\alpha$ -deuterium KIEs with leaving group is reversed (+4.2 % versus -1.8 %) compared to that found theoretically at the B3LYP/aug-cc-pVDZ level of theory. Finally, it is interesting that both the calculated and experimental  $(k_H/k_D)_\alpha$  for the ethyl tosylate reaction are larger than those for the ethyl halide reactions as would be expected for a reaction with a bulky leaving group.<sup>33</sup>

### 7.3.6 Effect of Solvent

In an attempt to estimate the effect of solvent (DMSO) on the transition structures and KIEs of these reactions, calculations were also performed using a continuum model. A comparison of the results in Tables 7.3 and 7.7 shows that adding solvent leads to a slightly more product-like transition state, i.e., with a slightly shorter NC-C $_\alpha$  and a slightly longer C $_\alpha$ -LG bond. More important however, is that in DMSO the trends in either  $R_{TS}$  or in transition structures with leaving group ability are not affected. It is interesting that the NC-C $_\alpha$  transition state bond for the ethyl bromide reaction at the B3LYP/aug-cc-pVDZ level is longer than that for the ethyl iodide reaction. Since this is

not true for the other two levels of theory, this problem may again be due to the use of two different basis sets for the calculation for the ethyl iodide reaction.

A comparison of the nucleophile carbon KIEs in Tables 7.4 and 7.8 shows that adding solvent to the calculation leads to a slightly smaller KIE in agreement with the change in transition state structure. More important, the B3LYP/aug-cc-pVDZ  $k^{11}/k^{14}$  decreases with a poorer leaving group just as the theory and the experimental KIEs suggest. It is interesting that the change in the experimental nucleophile carbon KIE with leaving group is larger than the change in the calculated B3LYP/aug-cc-pVDZ KIEs in DMSO with leaving group just as it was for the gas phase reactions, i.e., the change in the KIE with leaving group is 0.0034 in the gas phase and 0.0027 (Br-Cl) in DMSO whereas it is 0.0039 experimentally. The comparison of the B3LYP/aug-cc-pVDZ  $(k_H/k_D)_\alpha$ s in the gas phase and in solution, Tables 7.5 and 7.9, respectively, shows that two of the three KIEs for the halogen leaving group reactions are smaller in solution suggesting the transition structures are tighter in solution. However, Tables 7.3 and 7.7 indicate that except for the ethyl iodide, the calculated transition state structures are looser in solution based on  $R_{TS}$ . Also, the agreement between experiment and theory is not good. The experimental  $(k_H/k_D)_\alpha$  decrease, (the transition structures for these reactions become tighter) when a poorer leaving group is used whereas the calculated KIEs in Table 7.9 increase when a poorer leaving group is used. It is worth noting that this trend in the calculated KIE does not agree with the change in the calculated transition state structure for these reactions. Finally, the change in the experimental KIEs with leaving group

(4.2%) is effectively equal to the change calculated in solution (-4.0%) but larger than that found for the calculated KIEs (-1.8 %) in the gas phase.

### 7.3.7 The implications of the theoretical study on using nucleophile carbon KIEs to determine the transition states of S<sub>N</sub>2 reactions

The nucleophile carbon KIE can be expressed as

$$\text{KIE} = \text{TDF}_R \times \text{KIE}_T \times \text{TIF}^\ddagger \times \text{TDF}^\ddagger = \text{TDF}_R \times \text{KIE}^\ddagger \quad (3)$$

where the transition state contribution to the total KIE, (KIE<sup>‡</sup>), is the product of the tunneling, KIE<sub>T</sub>, the imaginary frequency ratio for the reactions with the <sup>11</sup>C and <sup>14</sup>C isotopes, (TIF<sup>‡</sup>), and the isotope effect on the vibrational energy of the transition state, (TDF<sup>‡</sup>). TDF<sub>R</sub> represents the isotope effect on the vibrational energy of the cyanide ion (reactant). The TDF<sub>R</sub> and TDF<sup>‡</sup> can be calculated<sup>36</sup> from

$$\text{TDF}_R = \prod_i^{3N-6} \left[ \frac{\mu_i^R \sinh(\mu_{iL}^R/2)}{\mu_{iL}^R \sinh(\mu_{iH}^R/2)} \right] \quad (4)$$

$$\text{TDF}^\ddagger = \prod_i^{3N^\ddagger-7} \left[ \frac{\mu_{iL}^\ddagger \sinh(\mu_{iH}^\ddagger/2)}{\mu_{iH}^\ddagger \sinh(\mu_{iL}^\ddagger/2)} \right] \quad (5)$$

respectively, where R represents the substrate, ‡ indicates the transition state, μ<sub>i</sub>=hv<sub>i</sub>/k<sub>B</sub>T and the v<sub>i</sub>'s are the vibrational frequencies and, L and H represent the <sup>11</sup>C and <sup>14</sup>C isotopes, respectively. KIE<sub>T</sub> was calculated using the Wigner approximation.<sup>21</sup>

The individual contributions to the nucleophile carbon KIEs calculated at the B3LYP/aug-cc-pVDZ level of theory, Table 7.10, helps shed light on the origin of these KIEs. All the terms except for  $TDF_R$  vary with leaving group.  $TDF_R$  is constant because there is no bonding between the carbon isotope in the cyanide ion and  $C_\alpha$  in the reactant. The  $TDF_R$  is large because of the strong  $C\equiv N$  bond in the ground state. Since the strong  $C\equiv N$  bond is also present in the transition state, the  $TDF^\ddagger$  terms are also large. However, the inverse  $TDF^\ddagger$  is larger than the normal  $TDF_R$  because the new  $NC-C_\alpha$  bond being formed in the transition state increases the vibrational energy of the carbon isotope in the  $C\equiv N^-$ .<sup>37</sup> This means the  $TDF^\ddagger$  is the major factor in determining the leaving group effect on the nucleophile KIE. Both  $KIE_T$  and  $TIF^\ddagger$  are small because there is very little bonding between the cyanide carbon and  $C_\alpha$  in the reactant-like transition states of all the reactions in this study, Table 7.3. The  $KIE_T$  and  $TIF^\ddagger$  vary in opposite directions with the change in leaving group, i.e., the  $KIE_T$  increases while the  $TIF^\ddagger$  decreases when a poorer leaving group is used in the ethyl halide reactions. However, since  $KIE_T$  is only about 1/3 the magnitude of the  $TIF^\ddagger$ , the  $[KIE_T \times TIF^\ddagger]$  decreases with a poorer leaving group. Since the  $TDF^\ddagger$  also decreases when a poorer leaving group is used, and changes more with leaving group than the other terms,  $KIE^\ddagger$  decreases with the leaving group ability. As a result, the total KIE decreases when the length of the  $NC-C_\alpha$  transition state bond shortens in the transition state.

The last column of Table 7.10, which gives  $[\text{KIE}_T \times \text{TIF}]$  as a percentage of the nucleophile carbon KIEs, shows that  $[\text{KIE}_T \times \text{TIF}]$  represents a significant portion (48-78%) of the nucleophile carbon KIE and that  $[\text{KIE}_T \times \text{TIF}]$  contribution to the total KIE decreases with a poorer leaving group, i.e., from a high of 78.3% to a low of 48% of the nucleophile carbon KIE. This significant contribution of the  $[\text{KIE}_T \times \text{TIF}]$  to the KIE has been reported previously.<sup>38</sup> Another observation is that the  $[\text{KIE}_T \times \text{TIF}]$  decreases as the NC-C $_{\alpha}$  bond in the transition state shortens. Because the  $[\text{KIE}_T \times \text{TIF}]$  varies with transition state structure in the same way as the  $\text{TDF}^{\ddagger}$  and accounts for a significant portion of the nucleophile carbon KIE, the effect of changing to a poorer leaving group is that observed experimentally, i.e., a shorter NC-C $_{\alpha}$  bond is found in the transition state with a poorer leaving group.

## 7.4 Conclusions

Interpreting the experimental nucleophile carbon  $k^{11}/k^{14}$  and secondary  $\alpha$ -deuterium KIEs in the usual fashion suggests that changing to a poorer leaving group leads to a tighter transition state with a slightly shorter Nu-C $_{\alpha}$  bond and a much shorter C $_{\alpha}$ -LG bond. It is important to note that this is exactly the change in transition state structure predicted by theory. The results also confirm that nucleophile carbon  $k^{11}/k^{14}$  KIEs can be used to determine transition state structure and that the usual method of interpreting these KIEs is correct. For the secondary  $\alpha$ -deuterium KIEs, the results also show that the magnitude of the experimental KIE decreases (the C $_{\alpha}$ -LG transition state

bond is shorter) when a poorer halogen leaving groups is used. Also, the experimental KIEs decreases with the  $R_{TS}$  (Nu - LG distance) in the  $S_N2$  transition state for the reactions with the *halogen* leaving group. However, the changes in the experimental and theoretical KIEs with leaving group ability are in opposite directions. Finally, neither the experimental nor the theoretical secondary  $\alpha$ -deuterium KIEs for the ethyl tosylate reaction fit the trend found for the reactions with a halogen leaving group. This presumably is found because of the bulky (sterically hindered) leaving group in the tosylate reaction. From every perspective, the tosylate reaction is too different from the halogen reactions to be compared.

## 7.5 References

- (1) Westaway, K. C.; Ali, S. F., *Can. J. Chem.*, **1979**, *57*, 1354.
- (2) Ando, T.; Tanabe, H.; Yamataka, H., *J. Am. Chem. Soc.* **1984**, *106*, 2084.
- (3) Lee, I.; Koh, H. J.; Lee, B.-S.; Sohn, D. S.; Lere, B. C., *J. Chem. Soc., Perkin Trans, 2*, **1991**, 174.
- (4) Matsson, O.; Persson, J.; Axelsson, B. S.; Langstrom, B.; Fang, Y.; Westaway, K.C., *J. Amer. Chem. Soc.*, **1996**, *118*, 6350.
- (5) Szyllabel-Godala, A.; Madhavan, S.; Rudzinski, J., O'Leary, M. H.; Paneth, P., *J. Phys. Org. Chem.*, **1996**, *9*, 35.
- (6) Westaway, K. C., in *Advances in Physical Organic Chemistry*, Vo. 41, J. Richards, Editor, Elsevier, 2006, pp. 257 - 259.

- (7) Kato, S.; Davico, G. E.; Lee, H. S.; DePuy, C. H.; Bierbaum, V. M., *Int. J. Mass Spectrom*, **2001**, 210/211, 223.
- (8) Hargreaves, R. T.; Katz, A. M.; Saunders, W. H. Jr., *J. Amer. Chem. Soc.* **1976**, *98*, 2614.
- (9) Lynn, K. R.; Yankwich, P. E., *J. Amer. Chem. Soc.*, **1961**, *83*, 3220.
- (10) Koerner, T.; Fang, Y-r.; Westaway, K. C., *J. Amer. Chem. Soc.*, **2000**, *122*, 7342.
- (11) Willey, J. F.; Taylor, J. W., *J. Am. Chem. Soc.* **1980**, *102*, 2387.
- (12) Shiner, V. J.; Wilgis, F. P., in *Isotopes in Organic Chemistry*, Buncl, E. Saunders, W. H. Jr., Eds., Vol. 8, Elsevier, New York, 1992, p. 239-335.
- (13) Dybala-Defratyka, A.; Rostkowski, M.; Matsson, O.; Westaway, K. C.; Paneth, P., *J. Org. Chem.*, **2004**, *69*, 4900.
- (14) Melander, L., in *Isotope Effects on Reaction Rates*, The Ronald Press, New York, N. Y., **1960**, pp 15 and 34.
- (15) Fang, Y.; S. MacMillar, S.; Eriksson, J.; Kołodziejska-Huben, M.; Dybala-Defratyka, A.; Paneth, P.; Matsson, O.; Westaway, K. C., *J. Org. Chem.*, **2006**, *71*, 4742 .
- (16) Fang, Y.; Gao, Y.; Ryberg, P.; Eriksson, J.; Kołodziejska-Huben, M.; Dybala-Defratyka, A.; Madhavan, S.; Danielsson, R.; Paneth, P.; Matsson, O.; Westaway, K. C., *Chem. Eur. J.*, **2003**, *9*, 2696.
- (17) Gaussian 03, Revision B.05, Frisch, M. J.; Trucks, G. W.; Schlegel, H. B.; Scuseria, G. E.; Robb, M. A.; Cheeseman, J. R.; Montgomery, Jr., J. A.; Vreven, T.; Kudin, K. N.; Burant, J. C.; Millam, J. M.; Iyengar, S. S.; Tomasi, J.; Barone, V.; Mennucci, B.; Cossi, M.; Scalmani, G.; Rega, N.; Petersson, G. A.; Nakatsuji, H.; Hada, M.; Ehara, M.;

Toyota, K.; Fukuda, R.; Hasegawa, J.; Ishida, M.; Nakajima, T.; Honda, Y.; Kitao, O.; Nakai, H.; Klene, M.; Li, X.; Knox, J. E.; Hratchian, H. P.; Cross, J. B.; Bakken, V.; Adamo, C.; Jaramillo, J.; Gomperts, R.; Stratmann, R. E.; Yazyev, O.; Austin, A. J.; Cammi, R.; Pomelli, C.; Ochterski, J. W.; Ayala, P. Y.; Morokuma, K.; Voth, G. A.; Salvador, P.; Dannenberg, J. J.; Zakrzewski, V. G.; Dapprich, S.; Daniels, A. D.; Strain, M. C.; Farkas, O.; Malick, D. K.; Rabuck, A. D.; Raghavachari, K.; Foresman, J. B.; Ortiz, J. V.; Cui, Q.; Baboul, A. G.; Clifford, S.; Cioslowski, J.; Stefanov, B. B.; Liu, G.; Liashenko, A.; Piskorz, P.; Komaromi, I.; Martin, R. L.; Fox, D. J.; Keith, T.; Al-Laham, M. A.; Peng, C. Y.; Nanayakkara, A.; Challacombe, M.; Gill, P. M. W.; Johnson, B.; Chen, W.; Wong, M. W.; Gonzalez, C.; and Pople, J. A.; Gaussian, Inc., Wallingford CT, 2004.

(18) Rassolov, V. A.; Ratner, M. A.; Pople, J. A.; Redfern, P. C.; Curtiss, L. A., *J. Computational Chemistry*, **2001**, *22*, 976.

(19) Binning Jr, R. C.; Curtiss, L. A., *J. Comp. Chem.*, **1990**, *11*, 1206.

(20) (a) Shahidul M. Islam, Stephanie D. Huelin, Margot Dawe and Raymond A. Poirier, *Journal of Chemical Theory and Computation*, **2008**, *4*, 86; (b) Shahidul M. Islam and Raymond A. Poirier, *J. Phys. Chem. A*, **2007**, *111*, 13218; (c) Shahidul M. Islam, Joshua W. Hollett and Raymond A. Poirier, *J. Phys. Chem. A*, **2007**, *111*, 526.

(21) Wigner, E., *Z. Phys. Chem.*, **B**, **1932**, *19*, 203.

(22) Anisimov, V; Paneth, P., *J. Math. Chem.*, **1999**, *26*, 75.

(23) Axelsson, S; Matsson, O; Långström, B., *J. Amer. Chem. Soc.* **1990**, *112*, 6661.

- (24) Westaway, K. C.; Fang, Y.-r.; Persson, J.; Matsson, O., *J. Amer. Chem. Soc.*, **1998**, *120*, 3340.
- (25) Westaway, K. C.; Jiang, W., *Can. J. Chem.*, **1999**, *77*, 879.
- (26) Koshy, K. M.; Robertson, R. E., *J. Amer. Chem. Soc.*, **1974**, *96*, 914.
- (27) Shiner, V. J. Jr.; Dowd, W.; Fisher, R. D.; Hartshorn, S. R.; Kessik, M. A.; Milakofsky, L.; Rapp, M. W., *J. Amer. Chem. Soc.*, **1969**, *91*, 4838.
- (28) Poirier, R. A.; Wang, Y.; Westaway, K. C., *J. Amer. Chem. Soc.*, **1994**, *116*, 2526.
- (29) Kato, S.; Davico, G. E.; Lee, H. S.; DePuy, C. H.; Bierbaum, V. M., *Int. J. Mass Spectrom.*, **2001**, *210/211*, 223.
- (30) Reference 6, pages 230- 248.
- (31) Westaway, K. C.; Ali, S. F., *Can. J. Chem.*, **1979**, *57*, 1089.
- (32) Westaway, K. C. in *Isotopes in Organic Chemistry*, Buncl, E. Lee, C. C., Eds., Vol. 7, Elsevier, New York, **1987**, p. 311 – 315 and 355 – 357.
- (33) Abraham, M. H.; McLennan, D. J., *J. Chem Soc., Perkin 2*, **1977**, 873.
- (34) Westaway, K. C.; *Can. J. Chem.*, **1993**, *71*, 2084.
- (35) Andzelm J., Klobukowski M., Radzio-andzelm E., Sakai Y., Tatewaki H. in *Physical Sciences Data 16 Gaussian Basis Sets for Molecular Calculations*, edited by Huzinaga S., (Elsevier Science Publishers), **1984**, p 295.
- (36) Paneth, P., *Computers Chem.*, **1995**, *19*, 231.
- (37) Jobe, D. J.; Westaway, K. C., *Can. J. Chem.*, **1993**, *71*, 1353.
- (38) Westaway, K. C.; Fang, Y.; MacMillar, S.; Matsson, O.; Poirier, R. A.; Islam, S. M. *Journal of Physical Chemistry A*, **2007**, *111*, 8110.

**Table 7.1. The rate constants and the nucleophile carbon  $k^{11}/k^{14}$  KIEs for the  $S_N2$  reactions between cyanide ion and ethyl chloride, bromide, iodide and tosylate in anhydrous DMSO at 20°C.**

Substrate	Average k ( $M^{-1}.s^{-1}$ )	$k^{12}/k^{13}$	$k^{11}/k^{14}$ <sup>a</sup>
Ethyl iodide	$2.024 \times 10^{-1}$		$1.0066 \pm .0008^c (6)^d$
Ethyl bromide	$3.576 \times 10^{-2}$		$1.0028 \pm .0015^c (8)^d$
Ethyl chloride <sup>b</sup>	$4.232 \times 10^{-4b}$	$1.0009 \pm .0007^c (18)^d$	1.0027
Ethyl tosylate	$4.828 \times 10^{-3}$		$1.0015 \pm .0011^c (6)^d$

<sup>a</sup>The substrate and nucleophile concentrations in these experiments were approximately 0.08 M and 0.1 M, respectively.

<sup>b</sup>This data is taken from reference 16. The KIE was measured at 30°C in anhydrous DMSO.

<sup>c</sup>Standard deviation.

<sup>d</sup>The number of separate evaluations of the KIE used to calculate the average KIE.

<sup>e</sup>Estimated using the method in reference 23.

**Table 7.2. The secondary  $\alpha$ -deuterium KIEs for the  $S_N2$  reactions between cyanide ion and ethyl chloride, bromide, iodide and tosylate in anhydrous DMSO at 20°C.**

Substrate	Average $k_H$ ( $M^{-1}.s^{-1}$ ) <sup>a</sup>	Average $k_D$ ( $M^{-1}.s^{-1}$ ) <sup>a</sup>	$(k_H/k_D)_\alpha$ <sup>a</sup>
Ethyl iodide <sup>b</sup>	$2.024 \times 10^{-1}$	$1.961 \times 10^{-1}$	$1.0318 \pm 0.0036$ <sup>d</sup>
Ethyl bromide <sup>b</sup>	$3.576 \times 10^{-2}$	$3.552 \times 10^{-2}$	$1.0065 \pm 0.0005$
Ethyl chloride <sup>c</sup>	$4.232 \times 10^{-4}$	$4.274 \times 10^{-4}$	$0.990 \pm 0.004$
Ethyl tosylate <sup>b</sup>	$4.828 \times 10^{-3}$	$4.548 \times 10^{-3}$	$1.0617 \pm 0.0005$

<sup>a</sup>The rate constants from three separate experiments were used in calculating the average rate constant.

<sup>b</sup>The substrate and nucleophile concentrations in these experiments were approximately 0.003 M and 0.005 M, respectively, for the ethyl iodide reactions, 0.0037 M and 0.0073 M, respectively, for the ethyl bromide reactions and 0.034 M and 0.06 M, respectively, for the ethyl tosylate reactions

<sup>c</sup>This data is taken from reference 16. The KIE was measured at 30°C in anhydrous DMSO. The temperature effect on these KIEs is very small<sup>25-27</sup> and can be ignored.

<sup>d</sup>The error in the KIE is  $1/k_D[(\Delta k_H)^2 + (k_H/k_D)^2 \times (\Delta k_D)^2]^{1/2}$ , where  $\Delta k_H$  and  $\Delta k_D$  are the standard deviations for the average rate constants for the reactions of the undeuterated and deuterated substrates, respectively.<sup>1</sup>

**Table 7.3.** The calculated  $C_{\alpha}$ -LG and NC- $C_{\alpha}$  transition-state bond lengths for the  $S_N2$  reactions between cyanide ion and ethyl iodide, ethyl bromide, ethyl tosylate and ethyl chloride at 25°C.

Substrate	$(C_{\alpha}$ -LG) $^{\ddagger}$ bond length (Å)			$(NC-C_{\alpha})^{\ddagger}$ bond length (Å)			$(C-C_{\alpha} + C_{\alpha}$ -LG) $^{\ddagger}$ = $R_{TS}$ (Å) $^d$
	RHF /6-31+G(d)	B3LYP /6-31+G(d)	B3LYP /aug-cc-pVDZ	RHF /6- 31+G(d)	B3LYP /6- 31+G(d)	B3LYP /aug-cc-pVDZ	
Et-I $^a$	2.6841	2.6129	2.5966 (18.9%) $^b$	2.4937	2.4452	2.4175 (65.7%) $^c$	5.0141
Et-Br	2.4709	2.4048	2.4183 (21.7%)	2.3724	2.3379	2.3969 (64.3%)	4.8152
Et-Cl	2.3623	2.2996	2.2910 (25.3%)	2.3708	2.3477	2.3417 (60.5%)	4.6327
Et-OTs	1.9313	1.8664	1.8710 (28.3%)	2.4425	2.4273	2.4048 (64.8%)	4.2758
Leaving group effect (I-Cl)	0.3218	0.3133	0.3056 (-6.4%)	0.1229	0.0975	0.0758 (5.2%)	0.3814

$^a$  Huzinaga's double zeta basis set $^{35}$  was used for iodine.

$^b$  The % extension of the  $C_{\alpha}$ -LG bond on going to the transition state =  $\{(C_{\alpha}$ -LG bond length in the transition state -  $C_{\alpha}$ -LG bond length in the reactant)/ $C_{\alpha}$ -LG bond length in the reactant}. The  $C_{\alpha}$ -LG bond lengths in the reactant were  $C_{\alpha}$ -I = 2.1834 Å, the  $C_{\alpha}$ -Br = 1.9878 Å, the  $C_{\alpha}$ -Cl = 1.8279 Å, and the  $C_{\alpha}$ -O = 1.4584 Å.

$^c$  The % extension of the NC- $C_{\alpha}$  bond in the transition state =  $\{(NC-C_{\alpha}$  bond length in the transition state - NC- $C_{\alpha}$  bond length in the product)/NC- $C_{\alpha}$  bond length in the product}. The NC- $C_{\alpha}$  bond length in the product was 1.459 Å.

$^d$  At the B3LYP/aug-cc-pVDZ level of theory.

**Table 7.4. The nucleophile carbon ( $k^{11}/k^{14}$ ) KIEs for the  $S_N2$  reactions between cyanide ion and ethyl iodide, ethyl bromide, ethyl tosylate and ethyl chloride at 25°C using three different levels of theory.**

Substrate	$k^{11}/k^{14}$			Expt.
	RHF /6-31+G(d)	B3LYP /6-31+G(d)	B3LYP /aug-cc-pVDZ	
Ethyl iodide <sup>a</sup>	0.9811	0.9869	0.9843	1.0066
Ethyl bromide	0.9691 0.9767 <sup>c</sup>	0.9750 0.9828 <sup>c</sup>	0.9845	1.0028
Ethyl chloride	0.9723	0.9793	0.9809	1.0027 <sup>b</sup>
Ethyl tosylate	0.9737	0.9793	0.9800	1.0015
Leaving group effect (I – Cl)	0.0087	0.0076	0.0034	0.0039

<sup>a</sup>Huzinaga's double zeta basis set<sup>35</sup> was used for iodine.

<sup>b</sup>Estimated using the method in reference 23 from the incoming nucleophile  $k^{12}/k^{13} = 1.0009^{16}$ .

<sup>c</sup>Value is obtained by using standard bromine 6-31+G(d) basis set.

**Table 7.5. The secondary  $\alpha$ -deuterium  $[(k_H/k_D)_\alpha]$  KIEs for the  $S_N2$  reactions between cyanide ion and ethyl iodide, ethyl bromide, ethyl tosylate and ethyl chloride at 25°C using three different levels of theory.**

Substrate	$(k_H/k_D)_\alpha$			Expt.
	RHF /6-31+G(d)	B3LYP /6-31+G(d)	B3LYP /aug-cc-pVDZ	
Ethyl iodide <sup>a</sup>	0.9436	0.9723	0.9718	1.0318
Ethyl bromide	0.9474	0.9734	0.9762	1.0065
	0.9545 <sup>c</sup>	0.9804 <sup>c</sup>		
Ethyl chloride	0.9655	0.9987	0.9899	0.990 <sup>b</sup>
Ethyl tosylate	1.0188	1.0206	1.0009	1.0617
Leaving group effect (I – Cl)	-0.0220	-0.0265	-0.0182	0.0418

<sup>a</sup>Huzinaga's double zeta basis set<sup>35</sup> was used for iodine.

<sup>b</sup>This value was measured in anhydrous DMSO at 30°C.<sup>16</sup> The temperature effect on these KIEs is very small<sup>25-27</sup> and can be ignored.

<sup>c</sup>Value is obtained by using standard bromine 6-31+G(d) basis set.

**Table 7.6. Free energies of activation for the S<sub>N</sub>2 reactions between cyanide ion and ethyl chloride, bromide, iodide and tosylate at 20°C.**

Substrate	$\Delta G^\ddagger$ (kJ mol <sup>-1</sup> )				Expt.
	Gas phase		DMSO		
	B3LYP/ 6-31G(d)	B3LYP/ aug-ccpVDZ	B3LYP/ 6-31G(d)	B3LYP/ aug-cc-pVDZ	
Ethyl iodide	12.4	6.7	91.2	87.7	77.0
Ethyl bromide	21.4	19.1	93.2	91.6	81.3
Ethyl chloride	39.4	34.7	102.4	99.8	92.3
Ethyl tosylate	36.8	36.0	122.9	131.1	86.2

<sup>a</sup>B3LYP/aug-cc-pVDZ

<sup>b</sup>Calculated from the average experimental rate constants in Table 7.1.

<sup>c</sup>Huzinaga's double zeta basis set<sup>35</sup> was used for iodine.

**Table 7.7.** The calculated  $C_{\alpha}$ -LG and NC- $C_{\alpha}$  transition-state bond lengths for the  $S_N2$  reactions between cyanide ion and ethyl iodide, ethyl bromide, ethyl tosylate and ethyl chloride in DMSO at 25°C.

Substrate	$(C_{\alpha}\text{-LG})^{\ddagger}$ bond length (Å)			$(\text{NC-}C_{\alpha})^{\ddagger}$ bond length <sup>d</sup> (Å)			$(C\text{-}C_{\alpha} + C_{\alpha}\text{-LG})^{\ddagger}$ = $R_{\text{TS}}$ (Å) <sup>d</sup>
	RHF /6-31+G(d)	B3LYP /6-31+G(d)	B3LYP /aug-cc-pVDZ	RHF /6-31+G(d)	B3LYP /6-31+G(d)	B3LYP /aug-cc-pVDZ	
Et-I <sup>a</sup>	2.7819	2.6762	2.6557 (21.0%) <sup>b</sup>	2.5150	2.3806	2.3490 (60.2%) <sup>c</sup>	5.0047
Et-Br	2.5384	2.4405	2.4654 (23.1%)	2.4115	2.3107	2.3650 (61.3%)	4.8304
Et-Cl	2.4271	2.3295	2.3227 (25.9%)	2.4481	2.3517	2.3387 (59.5%)	4.6614
Et-OTs	2.0270	1.9446	1.9453 (32.6%)	2.4268	2.3552	2.3320 (59.1%)	4.2773

<sup>a</sup> Huzinaga's double zeta basis set<sup>35</sup> was used for iodine.

<sup>b</sup> The % extension of the  $C_{\alpha}$ -LG bond on going to the transition state =  $\{(C_{\alpha}\text{-LG bond length in the transition state} - C_{\alpha}\text{-LG bond length in the reactant})/C_{\alpha}\text{-LG bond length in the reactant}\}$ . The  $C_{\alpha}$ -LG bond lengths in the reactant were  $C_{\alpha}\text{-I} = 2.1949$  Å, the  $C_{\alpha}\text{-Br} = 2.0033$  Å, the  $C_{\alpha}\text{-Cl} = 1.8444$  Å, and the  $C_{\alpha}\text{-O} = 1.4669$  Å at B3LYP/aug-cc-pVDZ.

<sup>c</sup> The % extension of the NC- $C_{\alpha}$  bond in the transition state =  $\{(\text{NC-}C_{\alpha} \text{ bond length in the transition state} - \text{NC-}C_{\alpha} \text{ bond length in the product})/\text{NC-}C_{\alpha} \text{ bond length in the product}\}$ . The NC- $C_{\alpha}$  bond length in the product was 1.4660 Å at B3LYP/aug-cc-pVDZ.

<sup>d</sup> At the B3LYP/aug-cc-pVDZ level of theory.

**Table 7.8.** The nucleophile carbon ( $k^{11}/k^{14}$ ) KIEs for the  $S_N2$  reactions between cyanide ion and ethyl iodide, ethyl bromide, ethyl tosylate and ethyl chloride in DMSO at 25°C using three different levels of theory.

Substrate	$k^{11}/k^{14}$			Expt.
	RHF /6-31+G(d)	B3LYP /6-31+G(d)	B3LYP /aug-cc-pVDZ	
Ethyl iodide <sup>a</sup>	0.9878	0.985-	0.9787	1.0066
Ethyl bromide	0.9758 0.9841 <sup>d</sup>	0.9751 0.9826 <sup>d</sup>	0.9820	1.0028
Ethyl chloride	0.9523	0.9749	0.9793	1.0027 <sup>b</sup>
Ethyl tosylate	0.9778	0.9778	0.9778	1.0015
Leaving group effect (I – Cl)	0.0355	0.0101	-0.0006 0.0027 <sup>c</sup>	0.0039

<sup>a</sup> Huzinaga's double zeta basis set<sup>35</sup> was used for iodine.

<sup>b</sup> Estimated using the method in reference 23 from the incoming nucleophile  $k^{12}/k^{13} = 1.0009^{16}$ .

<sup>c</sup> Leaving group effect (Br – Cl)

<sup>d</sup> Value is obtained by using standard bromine 6-31+G(d) basis set.

**Table 7.9. The secondary  $\alpha$ -deuterium  $(k_I/k_D)_\alpha$  KIEs for the  $S_N2$  reactions between cyanide ion and ethyl iodide, ethyl bromide, ethyl tosylate and ethyl chloride in DMSO at 25°C using three different levels of theory.**

Substrate	$(k_I/k_D)_\alpha$			Expt.
	RHF /6-31+G(d)	B3LYP /6-31+G(d)	B3LYP /aug-cc-pVDZ	
Ethyl iodide <sup>a</sup>	1.0067	0.9611	0.9517	1.0318
Ethyl bromide	1.0128 1.0332 <sup>c</sup>	0.9722 0.9818 <sup>c</sup>	0.9722	1.0065
Ethyl chloride	1.0540	1.0090	0.9920	0.990 <sup>b</sup>
Ethyl tosylate	1.0923	1.0043	0.9892	1.0617
Leaving group effect (I – Cl)	-0.0473	-0.0479	-0.0402	0.0418

<sup>a</sup> Huzinaga's double zeta basis set<sup>35</sup> was used for iodine.

<sup>b</sup> This value was measured in anhydrous DMSO at 30°C.<sup>16</sup> The temperature effect on these KIEs is very small<sup>25-27</sup> and can be ignored.

<sup>c</sup> Value is obtained by using standard bromine 6-31+G(d) basis set.

**Table 7.10.** The individual contributions to the calculated nucleophile carbon ( $k^{11}/k^{14}$ ) KIEs for the  $S_N2$  reactions between cyanide ion and ethyl iodide, ethyl bromide, ethyl tosylate and ethyl chloride at 25°C in the gas phase at the B3LYP/aug-cc-pVDZ level of theory.

Substrate	TDF <sub>R</sub>	KIE <sub>T</sub>	TIF <sup>‡</sup>	KIE <sub>T</sub> x TIF <sup>‡</sup>	TDF <sup>‡</sup>	KIE <sup>‡</sup> = {KIE <sub>T</sub> .TIF <sup>‡</sup> .TDF <sup>‡</sup> }	Total k <sup>11</sup> /k <sup>14</sup>	% (KIE <sub>T</sub> x TIF <sup>‡</sup> )/k <sup>11</sup> /k <sup>14</sup>
Ethyl iodide	1.2964	1.0021	1.0102	1.0123	0.7501	0.7593	0.9844	78.3
Ethyl bromide	1.2964	1.0022	1.0094	1.0116	0.7507	0.7594	0.9845	74.8
Ethyl chloride	1.2964	1.0025	1.0089	1.0115	0.7481	0.7566	0.9810	60.2
Ethyl tosylate	1.2964	1.0025	1.0071	1.0096	0.7488	0.7560	0.9801	48.0
Leaving group effect (I-Cl)	0.0000	-0.0004	0.0013	0.0008	0.002	0.0027	0.0034	18.1

## CHAPTER 8

### Concluding Remarks

This research involves investigation of the mechanisms and thermodynamics of various reactions, finding the unknown heats of formation of different compounds, and characterizing transition states using the kinetic isotope effect. We have performed quantum-mechanical computations with *ab initio*, DFT and Gaussian-n theories. The performance of each level of theory was also compared to experimental data, where available. A summary of my research is as follows:

#### **Computational Study of the Reactions of SiH<sub>3</sub>X (X = H, Cl, Br, I) with HCN:**

A Computational study of the reactions of SiH<sub>3</sub>X (X = H, Cl, Br, I) with HCN was carried out to add valuable knowledge to the rapidly growing field of silicon

chemistry, through study of a reaction which is quite difficult to carry out experimentally. Silane, halosilanes and HCN are also found in abundance in space and are therefore of great interest in interstellar chemistry. Ab initio and DFT calculations were performed for the mechanistic and thermodynamic study of these reactions. Geometries of the reactants, transition states, intermediates and products were optimized at HF, MP2 and B3LYP levels of theory using the 6-31G(d) and 6-31G(d,p) basis sets. Energies were also obtained using G3MP2 and G3B3 levels of theory. The following remarks could be made from this investigation:

1. It was found that HCN can react with silane and halosilanes via three different mechanisms. One involves HX elimination by a one-step pathway producing  $\text{SiH}_3\text{CN}$ . The second mechanism consists of  $\text{H}_2$  elimination, producing  $\text{SiH}_2\text{XCN}$  via a one-step pathway or three multiple-step pathways. The third mechanism involves dissociation of  $\text{SiH}_3\text{X}$  to various products, which can then react with HCN.
2. The reaction of  $\text{SiH}_3\text{X}$  with HCN produces different products depending on substituent X. For  $\text{X} = \text{H}$  and Br, the decomposition mechanism is preferred ( $\text{SiH}_4 \rightarrow \text{SiH}_2 + \text{H}_2$ ) and ( $\text{SiH}_3\text{Br} \rightarrow \text{SiHBr} + \text{H}_2 \rightarrow \text{SiH}_2 + \text{HBr}$ ) and the reaction of  $\text{SiH}_2$  with HCN will form  $\text{SiH}_3\text{CN}$ . For  $\text{X} = \text{Cl}$ ,  $\text{H}_2$  elimination ( $\text{SiH}_3\text{Cl} + \text{HCN} \rightarrow \text{SiH}_2\text{ClCN} + \text{H}_2$ ) is slightly favoured forming the  $\text{SiH}_2\text{ClCN}$  product, while for  $\text{X}=\text{I}$ , mainly  $\text{SiH}_3\text{CN}$  product should be formed via an HI elimination reaction ( $\text{SiH}_3\text{I} + \text{HCN} \rightarrow \text{SiH}_3\text{CN} + \text{HI}$ ) and decomposition reaction ( $\text{SiH}_3\text{I} \rightarrow \text{SiHI} + \text{H}_2 \rightarrow \text{SiH}_2 + \text{HI}$ ).
3. We have found that the standard 6-31G(d) bromine basis set gave results which were in better agreement with the G3MP2 results than for the Binning-Curtiss basis set.

4. Computed heats of formation ( $\Delta H_f$ ) for  $\text{SiH}_3\text{CN}$ ,  $\text{SiH}_3\text{NC}$ ,  $\text{SiH}_2\text{ClCN}$ ,  $\text{SiH}_2\text{BrCN}$ ,  $\text{SiH}_2\text{ICN}$ ,  $\text{SiHCl}$ ,  $\text{SiHBr}$ , and  $\text{SiHI}$  were found to be 133.5, 150.8, -34.4, 23.6, 102.4, 48.7, 127.1, and 179.8  $\text{kJ mol}^{-1}$ , respectively. From enthalpies calculated at G3MP2, we predict the  $\Delta H_f$  for  $\text{SiH}_2$  to be 262.8  $\text{kJ mol}^{-1}$  compared to the experimental value of  $273.8 \pm 4.2 \text{ kJ mol}^{-1}$ .

**New insights into the bromination reaction for a series of alkenes - A computational study:**

A computational study of the addition of bromine to alkenes was carried out with the aim of discovering the actual mechanism of the reaction. From an extensive literature search, we found that there was very little computational studies of this reaction. Moreover, the existing data did not agree with experiment. Since it is impossible for the experimentalist to conclusively propose a reaction mechanism, we have decided to investigate the reaction computationally. *Ab initio* calculations were carried out for the reaction of  $\text{Br}_2$  with ethene, propene, isobutene, fluoroethene, chloroethene, (E)-1,2-difluoroethene and (E)-1,2-dichloroethene. For ethene, the calculations were also carried out for the reaction with  $2\text{Br}_2$ . Geometries were optimized at HF, MP2 and B3LYP using the 6-31G(d) and 6-31+G(d) basis sets whereas for Br both the standard 6-31G and the Binning-Curtiss bromine basis sets were used. Single point energies were also calculated at G3MP2 and G3MP2B3. The complete reaction pathways for all the proposed mechanisms have been verified using IRC analysis. Activation energies, free energies and enthalpies of activation along with thermodynamic properties ( $\Delta E$ ,  $\Delta H$ , and  $\Delta G$ ) for

each reaction were calculated. Free energies of activation and of reaction for the addition reaction of bromine to alkenes in  $\text{CCl}_4$ ,  $\text{CH}_2\text{Cl}_2$ ,  $\text{CH}_2\text{Cl}-\text{CH}_2\text{Cl}$  and  $\text{CH}_3\text{OH}$  were calculated with the polarizable continuum model (PCM). The investigation has resulted in several conclusions:

1. For the reaction of alkenes with a single  $\text{Br}_2$ , one mechanism involves a perpendicular attack by  $\text{Br}_2$  on the  $\text{C}=\text{C}$  bond and a second mechanism consists of sidewise attack by  $\text{Br}_2$ .
2. The sidewise attack by  $\text{Br}_2$  is found to be the favourable mechanism for the reactions involving a single  $\text{Br}_2$  and alkenes.
3. Alkenes can react with  $2\text{Br}_2$  via several mechanisms all leading to the dibromo product. The most likely pathway for the reaction of ethene and  $2\text{Br}_2$  involves a trans addition of a Br atom from  $\text{Br}_3^-$  to one of the bromonium ion carbons.
4. Our results indicate that the reaction of ethene with  $2\text{Br}_2$  is favoured over reaction with only  $\text{Br}_2$  both in gas phase and in  $\text{CCl}_4$ .
5. There is excellent agreement between the calculated free energies of activation for the reaction of ethene and  $2\text{Br}_2$  with experiment in non-polar aprotic solvents ( $\text{CH}_2\text{Cl}_2$ ,  $\text{CH}_2\text{Cl}-\text{CH}_2\text{Cl}$ ).
6. On the other hand, the free energies of activation for the reaction with a single  $\text{Br}_2$  agrees well with the experimental results for polar protic solvents ( $\text{CH}_3\text{OH}$ ) only when the reaction is mediated by a solvent molecule.
7. A kinetic expression is proposed that accounts for the difference between bromination of alkenes in protic and aprotic solvents.

8. Previously unknown heats of formation for trans-CHFBr-CH<sub>2</sub>Br, trans-CHClBr-CH<sub>2</sub>Br, trans-CHFBr-CHFBr and trans-CHClBr-CHClBr were calculated to be -214.8, -63.4, -400.1 and -61.8 kJ mol<sup>-1</sup>, respectively.

**The addition reaction of adamantylideneadamantane with Br<sub>2</sub> and 2Br<sub>2</sub> - A Computational Study:**

The mechanism for the addition reaction of adamantylideneadamantane with Br<sub>2</sub> and 2Br<sub>2</sub> was investigated at HF and B3LYP levels of theory using the 6-31G(d) basis set. Energies were also obtained using single point calculations at MP2/6-31G(d)//HF/6-31G(d), MP2/6-31G(d)//B3LYP/6-31G(d) and B3LYP/6-31+G(d)//B3LYP/6-31G(d) levels of theory. Intrinsic reaction coordinate (IRC) calculations were performed to characterize the transition states on the potential energy surface. Activation energies, free energies and enthalpies of activation along with the relative stability of products for each reaction pathway were calculated. This reaction has yielded several conclusions:

1. Only one pathway is found for the reaction of Ad=Ad with one Br<sub>2</sub> producing a bromonium/bromide ion pair.
2. Three mechanisms for the reaction of Ad=Ad with 2Br<sub>2</sub> were found leading to three different structural forms of the bromonium/Br<sub>3</sub><sup>-</sup> ion pair.
3. The reaction of Ad=Ad with 2Br<sub>2</sub> is strongly favoured over reaction with only one Br<sub>2</sub>. This is in agreement with our previous study on the bromination reaction of ethene.

4. According to B3LYP/6-31G(d) and single point calculations at MP2, the most stable bromonium/ $\text{Br}_3^-$  ion pair would form spontaneously.
5. The most stable of the three bromonium/ $\text{Br}_3^-$  ion pairs has a structure very similar to the observed X-ray structure.
6. Free energies of activation and relative stabilities of reactants and products in  $\text{CCl}_4$  and in  $\text{CH}_2\text{ClCH}_2\text{Cl}$  were also calculated with PCM using the united atom (UA0) cavity model and, in general, results similar to gas phase were obtained.
7. An optimized structure for the trans-1,2-dibromo product is also found at all the levels of theory both in gas phase and in solution, but no transition state leading to the trans-1,2-dibromo product was obtained.

**A comparison of the Standard 6-31G and Binning-Curtiss Basis Sets for Third Row Elements:**

A comparison of the standard 6-31G and Binning-Curtiss (BC6-31G) basis sets for third row elements was carried out to aid other researchers in choosing the best 6-31G basis set. From our previous research on the reaction of silanes with HBr and the bromination reactions of alkenes, we found that the energies obtained from using the bromine BC6-31G basis set did not agree with experiment. Therefore we investigated these basis sets more thoroughly. *Ab initio* and DFT calculations were carried out for isogyric reactions involving the 3<sup>rd</sup> row elements, Ga, Ge, As, Se, and Br. Geometries of all the reactants and products were optimized at HF, MP2, and B3LYP levels of theory using the 6-31G(d) and 6-31G(d,p) basis sets. For molecules containing 3<sup>rd</sup> row elements,

geometries, frequencies and thermodynamic properties were calculated using both the standard 6-31G and the Binning-Curtiss (BC6-31G) basis sets. In order to determine the performance of these basis sets, the calculated thermodynamic properties were compared to G3MP2 values and where possible to experimental values. The research has resulted in several major findings:

1. Geometries and frequencies calculated with the standard 6-31G and the BC6-31G basis sets were found to differ significantly.
2. Frequencies calculated with the standard 6-31G basis set were generally in better agreement with the experimental values (MAD= 40.1cm<sup>-1</sup> at B3LYP/6-31G(d,p) and 94.2 cm<sup>-1</sup> at MP2/6-31G(d,p) for unscaled frequencies and 29.6 cm<sup>-1</sup> and 24.4 cm<sup>-1</sup>, respectively for scaled frequencies).
3. For all the reactions investigated, the thermodynamic properties calculated with the standard 6-31G basis set were found to consistently be in better agreement with the G3MP2 and the available experimental results. However, the BC6-31G basis set performs poorly for the reactions involving both 2<sup>nd</sup> and 3<sup>rd</sup> row elements. Since, in general, the standard 6-31G basis set performs well for all the reactions, we recommend that the standard 6-31G basis set be used for calculations involving 3<sup>rd</sup> row elements.
4. Using G3MP2 enthalpies of reaction and available experimental heats of formation ( $\Delta H_f$ ), previously unknown  $\Delta H_f$  values for CH<sub>3</sub>SeH, SiH<sub>3</sub>SeH, CH<sub>3</sub>AsH<sub>2</sub>, SiH<sub>3</sub>AsH<sub>2</sub>, CH<sub>3</sub>GeH<sub>3</sub> and SiH<sub>3</sub>GeH<sub>3</sub> were found to be 18.3, 18.0, 38.4, 82.4, 41.9 and 117.4 kJ mol<sup>-1</sup>, respectively.

**A new insight into using chlorine leaving group and nucleophile carbon kinetic isotope effects to determine substituent effects on the structure of S<sub>N</sub>2 transition states:**

Chlorine leaving group  $k^{35}/k^{37}$ , nucleophile carbon  $k^{11}/k^{14}$  and secondary  $\alpha$ -deuterium  $[(k_H/k_D)_\alpha]$  kinetic isotope effects (KIEs) have been calculated for the S<sub>N</sub>2 reactions between *para*-substituted benzyl chlorides and cyanide ion to determine whether these isotope effects can be used to determine the substituent effect on the structure of the transition state. The calculations were done at the RHF/6-31+G(d), the B3LYP/6-31+G(d) and the B3LYP/aug-cc-pVDZ level of theory. KIEs were calculated with the program ISOEFF98. With a combination of computational and experimental results, we were able to provide a new theory on the relationship between the effects of substituents on the transition-states and the KIE in a series of S<sub>N</sub>2 reactions. We can make the following remarks on the basis of our investigation:

1. The experimental secondary  $\alpha$ -deuterium KIEs indicate the transition states for these reactions are unsymmetric. The theoretical calculations at the B3LYP/aug-cc-pVDZ level of theory support this conclusion, i.e., they suggest that the transition states for these reactions are unsymmetric with a long NC-C <sub>$\alpha$</sub>  and reasonably short C <sub>$\alpha$</sub> -Cl bonds.
2. The calculated chlorine isotope effects suggest that these KIEs can be used to determine the substituent effects on transition state structure with the KIE decreasing

when a more electron-withdrawing *para*-substituent is present. This conclusion is also supported by experiment.

3. The experimental nucleophile carbon  $k^{11}/k^{14}$  KIEs for these reactions do not change significantly with substituent and therefore do not appear to be useful for determining how the NC-C $_{\alpha}$  transition-state bond changes with substituent. The theoretical calculations on the other hand indicate that the NC-C $_{\alpha}$  bond shortens as a more electron-withdrawing substituent is placed on the benzene ring of the substrate. However, the changes in the NC-C $_{\alpha}$  transition-state bond with substituent are very small and may not be measurable.
4. Finally, through a theoretical approach, it was possible to determine if chlorine leaving group and nucleophile carbon KIEs can be used to determine the substituent effect on an S $_N2$  transition state structure. A correct and measurable substituent effect on leaving group KIEs will only be found for a very reactant-like or for a very product-like S $_N2$  TS. Similarly, the substituent effect on nucleophile KIEs will only be found when the Nu-C $_{\alpha}$  bond formation in the TS is well advanced i.e., in a product-like S $_N2$  TS.
5. These KIEs can also indicate whether an S $_N2$  reaction has a reactant-like, a product-like, or a central transition state.
6. Experimental chemists must ensure that only S $_N2$  products are formed from the reaction.

**Can incoming nucleophile carbon kinetic isotope effects be used to determine the transition state structure for different S<sub>N</sub>2 reactions?:**

Nucleophile carbon  $k^{11}/k^{14}$  and secondary  $\alpha$ -deuterium  $[(k_H/k_D)_\alpha]$  kinetic isotope effects (KIEs) have been measured for S<sub>N</sub>2 reactions between tetrabutylammonium cyanide and ethyl iodide, bromide, chloride and tosylate in anhydrous DMSO to determine whether these isotope effects can be used to determine the structure of the S<sub>N</sub>2 transition states. PCM was used for the calculations in solvent (DMSO). This reaction has yielded several conclusions:

1. The experimental KIEs suggests that the transition state is tighter with a slightly shorter NC-C<sub>a</sub> bond and a much shorter C<sub>a</sub>-LG bond when the substrate has a poorer halogen leaving group. Theoretical calculations at the B3LYP/aug-cc-pVDZ level of theory support this conclusion.
2. The results show that the nucleophile carbon  $k^{11}/k^{14}$  KIEs can be used to determine transition state structure in different reactions and that the usual method of interpreting the experimental  $k^{11}/k^{14}$  KIEs is correct.
3. The magnitude of the experimental secondary  $\alpha$ -deuterium KIE is related to the nucleophile – leaving group distance in the S<sub>N</sub>2 transition state ( $R_{TS}$ ) for reactions with a halogen leaving group. However, the calculated and experimental  $\alpha$ -deuterium KIEs change oppositely with leaving group ability.
4. Neither the experimental nor the theoretical secondary  $\alpha$ -deuterium KIEs for the ethyl tosylate reaction fit the trend found for the reactions with a halogen leaving group. This presumably is found because of the bulky (sterically hindered) leaving group in

the tosylate reaction. From every prospective, the tosylate reaction is too different from the halogen reactions to be compared.

**Future work:**

The secondary  $\alpha$ -deuterium  $[(k_H/k_D)_\alpha]$  kinetic isotope effects (KIEs) for the  $S_N2$  reactions between tetrabutylammonium cyanide and ethyl iodide, bromide, chloride and tosylate were calculated to determine the structure of the  $S_N2$  transition states. The KIEs did not agree with the experimental observations. We think that the calculation of KIE is not straightforward and has some limitation. The equation used for the calculation of KIE may not be able to give the correct KIE if there are high frequency modes involved. More analysis is required to explore the limitations of KIE. The future work may also provide new theoretical approaches on the calculation of the KIEs where the conventional approach fails. The calculated kinetic isotope effect also suggests that the existing basis sets for iodine needs to be reevaluated. Apparently, there is no standard 6-31G or aug-cc-pVDZ basis set for fourth row elements such as iodine. It is very important to implement basis sets for fourth row elements that are consistent with the basis sets for 1<sup>st</sup>, 2<sup>nd</sup> and 3<sup>rd</sup> row elements. Since the KIEs are very sensitive to basis sets, they may also be used to evaluate the performance of new basis sets.

## Appendix A

### Input for Solvent Calculation in Gaussian:

# B3LYP/6-31G(d) OPT SCRF=(PCM,solvent=carbontetrachloride) FREQ

Ethene

```
0 1
C,0,0,0.,-0.6656073523
C,0,0,0.,0.6656073523
H,0,0.9236858228,0.,1.2394677393
H,0,-0.9236858228,0.,1.2394677393
H,0,0.9236858228,0.,-1.2394677393
H,0,-0.9236858228,0.,-1.2394677393
```

### Output from Gaussian:

===

Optimized Geometry:

```
C,0,0,0.,0.6656073523
C,0,0,0.,-0.6656073523
H,0,0,0.9236858228,-1.2394677393
H,0,0,-0.9236858228,-1.2394677393
H,0,0,0.9236858228,1.2394677393
H,0,0,-0.9236858228,1.2394677393
```

===

Total free energy in solution:

with all non electrostatic terms (a.u.) = -78.583014

===

Zero-point correction =	0.051154 (Hartree/Particle)
Thermal correction to Energy =	0.054198
Thermal correction to Enthalpy =	0.055142
Thermal correction to Gibbs Free Energy =	0.030278
Sum of electronic and zero-point Energies =	-78.536892

Sum of electronic and thermal Energies =	-78.533848
Sum of electronic and thermal Enthalpies =	-78.532904
Sum of electronic and thermal Free Energies=	-78.557768

===

Therefore,

The free energy of ethene in CCl<sub>4</sub> at B3LYP/6-31G(d) level of theory is the summation of the above shaded values., i.e.  $-78.583014 + 0.030278 = -78.552736$ .

## Appendix B

[The experimental KIEs were measured by Prof. Kenneth C. Westaway and his group at Laurentian University, Canada and Prof. Olle Matsson and his group at Uppsala University, Sweden]

**Experimental Procedure for determining the secondary  $\alpha$ -deuterium- ( $k_H/k_D$ ) $_{\alpha}$ , the chlorine leaving group- ( $k^{35}/k^{37}$ ) and the nucleophile carbon  $k^{11}/k^{14}$  KIEs for the  $S_N2$  reaction between cyanide ion and *para*-substituted benzyl chlorides:**

**Secondary  $\alpha$ -deuterium KIEs:** Approximately 0.9g of tetrabutylammonium cyanide was dissolved in 50 mL of anhydrous THF under a nitrogen atmosphere in an I<sup>2</sup>R glove bag. Then, a 0.060 – 0.70 M. stock solution of benzyl chloride was prepared in a sample vial that had been pre-filled with 10 mL of anhydrous THF and sealed with a rubber septum under a nitrogen atmosphere in the glove bag by injecting 1 mL of benzyl chloride into the sample vial. The exact concentration of the benzyl chloride stock solution was calculated from the accurate weight of the vial before and after the benzyl chloride was added. Then, 20 mL of the tetrabutylammonium cyanide stock solution was transferred into a reaction flask fitted with a serum cap in the glove bag and the reaction flask and the benzyl chloride stock solution were cooled in a distilled ice-water bath for an hour. The reaction was started by injecting 1.00 mL of the benzyl chloride stock solution into the reaction flask. One mL samples of the reaction mixture solution were taken at various times throughout the reaction and injected into 25 mL of 0.0025 M nitric

acid to quench the reaction by converting the unreacted cyanide ion into HCN. The acidic solution was stirred in the fume hood for at least an hour to completely remove the HCN and then the chloride ion in the sample was analyzed in a potentiometric titration using a standard 0.005 M silver nitrate solution.

The same procedure was used to measure the secondary  $\alpha$ -deuterium KIE except that the tetrabutylammonium cyanide stock solution was prepared by dissolving 0.5g of tetrabutylammonium cyanide in 50 mL of anhydrous THF and that the 4-chlorobenzyl chloride solution was prepared by injecting 0.58 mL of 4-chlorobenzyl chloride in a sample vial containing 10 mL of anhydrous THF.

**Chlorine Leaving Group KIEs:** The procedure used in measuring these KIEs is described in the article:

Koerner, T.; Fang, Y.; Westaway, K. C., *J. Amer. Chem. Soc.*, **2000**, 122, 7342-7350.

**Nucleophile Carbon  $^{11}\text{k}/^{14}\text{k}$  KIEs:**

Reagents: The aldehyde impurities in the *para*-substituted benzyl chlorides were removed by treatment with sodium bisulfite.<sup>41, 42</sup> Then, the purified compounds were distilled under reduced pressure and stored in an air-tight container in the refrigerator.  $^1\text{H}$  NMR showed negligible levels of aldehyde after a week. The THF was distilled over sodium and benzophenone. The tetrabutylammonium cyanide (TBACN) was stored in a desiccator over  $\text{P}_2\text{O}_5$ . In order to avoid a build up of [ $^{14}\text{C}$ ]formic acid, small aliquots of the solid [ $^{14}\text{C}$ ]potassium cyanide (2.04 GBq/mmol, American Radiolabeled Chemicals,

Inc.) were withdrawn and dissolved in distilled water on the day of a kinetic run. Any unused  $K[^{14}C]N$  solution was refrigerated and used within two days. The  $^{11}C$ -labelled cyanide was produced employing the Scanditronix MC-17 Cyclotron at Uppsala Imanet AB. Proton bombardment of nitrogen,  $^{14}N(p,\alpha)^{11}C$ , in the presence of trace amounts of oxygen afforded  $[^{11}C]O_2$  which was converted to hydrogen  $[^{11}C]$ cyanide utilizing an on-line gas-processing synthesis.<sup>43, 44</sup> Prior to trapping in distilled water (1 mL at 0° C) the  $H[^{11}C]N$  was passed through a 50% aqueous sulfuric acid at 70° C and then sicapent<sup>®</sup>. All the work with  $^{11}C$ -materials was performed behind 5 cm thick lead shields. Generally, the resulting activity of the  $H[^{11}C]N$  solution was 2.0 - 4.0 GBq.

After transport to the laboratory in a lead-lined trolley, sufficient  $[^{14}C]$ potassium cyanide to yield a  $^{14}C$ -activity of over 10,000 counts per minute at 50% reaction of a kinetic run) was added to the  $[^{11}C]$ hydrogen cyanide solution. Impurities mostly formed in the synthesis of  $H[^{11}C]N$  were removed by employing a preparative HPLC system equipped with a  $\beta^+$ -detector. A C18 column (Phenomenex, Luna 10  $\mu$  250  $\times$  10 mm) operated at a flow of 4 ml/min. The isocratic mobile-phase system consisted of ammonium formate (50 mM, pH 3.5) 95% and acetonitrile 5%. Hydrochloric acid (0.3 mL, 0.11 mM) was added to the collected fraction of HCN ( $t_R = 4.5 - 5.1$  min). Then, the HCN was transferred to the reaction solvent by first heating it to 75°C and passing a gentle stream of nitrogen (< 10 mL/min) through the solution. The HCN was dried with sicapent<sup>®</sup> before being trapped in an anhydrous THF solution of TBACN (1.0 mL, 0.05

M) at - 42°C. The activity of the THF solution was usually 150 – 300 MBq after 7 min of distillation.

**Kinetic Procedure.** Two portions (100  $\mu$ L and 700  $\mu$ L) of the labeled THF solution were withdrawn and transferred to septum-capped 1.5 mL vials. A 10  $\mu$ L aliquot was taken from the 700  $\mu$ L portion and mixed with 90  $\mu$ L of 30% acetonitrile in water. Dilution with water was necessary in order to prevent substantial tailing of the HCN peak and the acetonitrile was needed to assure full solubility of the *para*-substituted benzyl cyanides. Ten  $\mu$ L of the diluted cyanide solution was injected into an HPLC equipped with a  $\beta^+$ -flow detector. The HPLC consisted of a C18 column (Phenomenex, Synergy 4  $\mu$  Hydro-RP 80 Å, 150  $\times$  4.60 mm) operating at a flow rate of 1 mL/min. The mobile-phase system consisted of ammonium formate, 50 mM at pH 3.5 (A) and acetonitrile (B). The gradient system used was from 0 to 2 min: 7% B, from 2 to 3 min: 7 to 80% B, 3 – 8 min: 80% B, 8 –9 min: 80 to 7% B, 9 – 16 min: 7% B. The product fraction (X = H, 6.8 – 8.5 min; CH<sub>3</sub>, 6.3 – 8.0; Cl, 6.6 – 8.3 min) was collected to serve as a correction for <sup>14</sup>C-impurities (see below). In order to achieve flexible and clean collection, a manual procedure was employed. The outlet from the  $\beta^+$ -detector was elongated by Teflon tubing so that it could be directly immersed into a polyethylene scintillation vial containing 14 mL of Zinsser Analytic QUICKSAFE A scintillation cocktail. Immediately after collection, the outlet tube from the detector was withdrawn, the vial capped and shaken vigorously.

Sufficient *para*-substituted benzyl chloride (X = H, 6  $\mu$ L; CH<sub>3</sub>, 6.5  $\mu$ L; Cl, 6  $\mu$ L) to react with between 25 and 60% of the hydrogen cyanide was added to the capped vial containing the 700  $\mu$ L solution. After vortex mixing, the vial was placed in an autoinjector rack connected to a temperature bath at  $20 \pm 0.01^\circ\text{C}$ . Every twenty minutes, a 10-20  $\mu$ L aliquot of the diluted reaction-mixture was injected into the HPLC and the product fraction was collected as described above. Care was taken to reseal the reaction vial with parafilm after each injection. Twenty  $\mu$ L of the neat *para*-substituted benzyl chloride was added to the 100  $\mu$ L solution at the beginning of the experiment. This amount ensured complete reaction of the cyanide. At the end of the experiment, a 10  $\mu$ L aliquot of this solution was withdrawn, diluted with 90  $\mu$ L of acetonitrile (no water was added as to ensure full solubility of the *para*-substituted benzyl nitriles) and 20  $\mu$ L of the resulting solution was injected into the HPLC and the product fraction collected as described above.

The total amount of radioactivity ( $^{11}\text{C} + ^{14}\text{C}$ ) in the collected fractions was measured by liquid scintillation at a wide mode for 2.5 min. Usually, the activity was 20,000 – 300,000 cpm (counts per minute). When all the  $^{11}\text{C}$  had decayed, each sample was remeasured to obtain the  $^{14}\text{C}$ -activity (wide mode, 50 min), which normally was 10,000 – 50,000 cpm. The time for each measurement was adjusted so that the relative error of the activity was less than 1%. In order to correct for possible  $^{14}\text{C}$ -contaminants co-eluting with the *para*-substituted benzyl cyanides, the initial labeled cyanide solution was injected twice and fractions were taken at the  $t_R$  of the *para*-substituted benzyl

cyanide. The mean of these activities and the activity of the product fraction from the unreacted cyanide solution, was subtracted from the  $^{14}\text{C}$ -activity. The  $^{11}\text{C}$ -activity was obtained by subtracting the uncorrected  $^{14}\text{C}$ -activity from the ( $^{11}\text{C} + ^{14}\text{C}$ )-value. Finally, the  $^{11}\text{C}$ -activity was decay corrected.

Data evaluation: The kinetic isotope effect was calculated with equation 1. The isotopic

$$k^{11}/k^{14} = \ln(1-f) / \ln[1-f(R_f/R_0)] \quad (1)$$

ratio  $R_f$  was calculated by dividing the corrected  $^{14}\text{C}$ - and  $^{11}\text{C}$ -values at fraction of reaction,  $f$ , and  $R_0$  was the ratio of the corrected  $^{14}\text{C}$ - and  $^{11}\text{C}$ -values at 100% reaction. The  $f$  value was obtained from the peak areas in the  $\beta^+$ -detector chromatograms. A  $^{11}\text{C}$ -impurity coeluted with the hydrogen cyanide. The amount of impurity was obtained from the chromatogram of the 100% reaction sample and subtracted from the area of the reactant peak in each reaction chromatogram. Usually, the impurity represented 2.0 – 2.5% of the total activity. Since the impurity did not react and was constant throughout the experiment, the impurity, although unidentified, did not affect the results.

## Appendix C

[The experimental KIEs were measured by Prof. Kenneth C. Westaway and his group at Laurentian University, Canada and Prof. Olle Matsson and his group at Uppsala University, Sweden]

**Experimental Procedure for determining the nucleophile carbon  $k^{11}/k^{14}$  and the secondary  $\alpha$ -deuterium- ( $k_H/k_D$ ) $_{\alpha}$  KIEs for the  $S_N2$  reactions between cyanide ion and ethyl chloride, bromide, iodide and tosylate in anhydrous DMSO at 20°C:**

### **Nucleophile Carbon $k^{11}/k^{14}$ KIEs**

Reagents: The ethyl chloride, bromide and iodide were used as received. The ethyl tosylate was distilled under reduced pressure before use. The anhydrous DMSO (Aldrich 99.9 +%, <0.005% water cont.) was used as received and stored under extra-dry nitrogen. The tetrabutylammonium cyanide (TBACN) was stored in a desiccator over  $P_2O_5$ . In order to avoid build up of [ $^{14}C$ ]formic acid, small aliquots of the solid [ $^{14}C$ ]potassium cyanide (2.04 GBq/mmol, American Radiolabeled Chemicals, Inc.) were withdrawn and dissolved in distilled water on the day of a kinetic run. The preparation and purification of the  $H[^{11}C]N$  is described elsewhere.<sup>38</sup> The only difference being that the labelled hydrogen cyanides were trapped in 0.9 mL of anhydrous DMSO instead of 1.0 mL of THF. Transfer of the labeled HCN solution to a capped vial with TBACN in anhydrous DMSO (1.0 M, 0.1 mL) resulted in a 0.1 M solution of cyanide ion. The obtained activity radioactivity was usually between 30 and 300 MBq after 7 min of distillation.

**Kinetic Procedure:** Two portions (600  $\mu\text{L}$  and 150  $\mu\text{L}$ ) were withdrawn from the labeled cyanide solution and transferred to septum-capped 1.5 mL vials. A 10  $\mu\text{L}$  aliquot was injected into an HPLC system equipped with a  $\beta^+$ -flow detector. A C18 column (Phenomenex, Synergy 4  $\mu$  Hydro-RP 80  $\text{\AA}$ , 150  $\times$  4.60 mm) was used with a flow of 1 mL/min. The mobile-phase system consisted of ammonium formate, 50 mM at pH 3.5 (A) and acetonitrile (B). The gradient system used was from 0 to 2 min: 7% B, from 2 to 3 min: 7 to 80% B, 3 – 8 min: 80% B, 8 –9 min: 80 to 7% B, 9 – 16 min: 7% B. The product fraction, 5.0 – 6.5 min, was collected to serve as a correction for  $^{14}\text{C}$ -impurities (see below). For this reason, 70  $\mu\text{L}$  of reaction medium was put aside to enable further injections at a later stage. In order to achieve flexible and clean collection a manual procedure was employed. The outlet from the  $\beta^+$ -detector was elongated by Teflon tubing so that it could be directly immersed into a polyethylene scintillation vial containing 14 mL of Zinsser Analytic QUICKSAFE A scintillation cocktail. A lid was thread over the tubing, capping the vial during collection. Immediately after collection, the outlet was withdrawn, the vial recapped and vigorously shaken.

An adjusted (see below) quantity of substrate dissolved in anhydrous DMSO was introduced to the 600  $\mu\text{L}$  portion of cyanide solution. After vortex mixing, the vial was placed in an autoinjector rack connected to a temperature bath at  $20.00 \pm 0.01$   $^{\circ}\text{C}$ . Aluminum foil was used to screen the reaction vial from light. Every twenty minutes an aliquot of 10 - 30  $\mu\text{L}$  was injected and the product fraction was collected as described above. Care was taken to reseal the reaction vial with parafilm after each injection as the

septum became increasingly pierced. The intent was to achieve a spread of cyanide conversion (30 – 60%) within one experimental run. For the slowly reacting ethyl tosylate, one addition (10 mg in 25  $\mu$ L DMSO) sufficed. The ethyl halides however, required addition in a cumulative fashion. For example, 7 min after a first addition of ethyl iodide (7  $\mu$ L, 20 v/v% in DMSO), 30% of the cyanide ion had been consumed. After this sample had been analyzed, more substrate was added and the reaction continued.

To ensure complete reaction with respect to cyanide ion, 20  $\mu$ L of neat ethyl chloride was introduced to the 150  $\mu$ L portion of cyanide ion solution at the beginning of the experiment. At the end of the experiment, a 25  $\mu$ L aliquot of the reaction mixture was withdrawn and injected into the HPLC. The product fraction was collected as described above.

The procedure used for counting the samples and calculating the kinetic isotope effect is described in the article:

Westaway, K. C.; Fang, Y.; MacMillar, S.; Matsson, O.; Poirier, R. A.; Islam, S. M. A new insight into using chlorine leaving group and nucleophile carbon kinetic isotope effects to determine substituent effects on the structure of  $S_N2$  transition states, *Journal of Physical Chemistry A*, **2007**, *111*, 8110-8120.

### **Secondary $\alpha$ -Deuterium KIEs**

Reagents: The preparation of the  $[1,1\text{-}^2\text{H}_2]$ ethyl chloride is described in reference 16. The  $[1,1\text{-}^2\text{H}_2]$ ethyl bromide  $[1,1\text{-}^2\text{H}_2]$ ethyl iodide were used as received from Sigma-Aldrich. The  $[1,1\text{-}^2\text{H}_2]$ ethyl tosylate was prepared by adding 5g of  $[1,1\text{-}^2\text{H}_2]$ ethyl alcohol dropwise to a solution of 22 g tosyl chloride in 88 mL of dry pyridine at  $-10\text{ }^\circ\text{C}$ . The temperature rose to  $-6\text{ }^\circ\text{C}$  after 2 minutes and then fell to  $-10\text{ }^\circ\text{C}$ . After the mixture was stirred for at  $-10\text{ }^\circ\text{C}$  for 30 minutes, 250 mL of 5 N sulfuric acid cooled to  $0\text{ }^\circ\text{C}$ , was added rapidly. On cooling, the product crystallized out. It was filtered, washed with water, and dried overnight in a vacuum desiccator. The crude tosylate (14g).was distilled at  $135\text{ }^\circ\text{C}/1.5\text{mm Hg}$  before use.

### **Kinetic Procedure:**

Ethyl Chloride Reaction: The following solutions were prepared under an extra-dry nitrogen atmosphere in a  $I^2R$  glove bag. One gram of tetrabutylammonium cyanide was dissolved in 15 mL of anhydrous DMSO giving a 0.25 M solution and 400  $\mu\text{L}$  of ethyl chloride was injected with a 500  $\mu\text{L}$  syringe that had been cooled in a deep freeze, into a sample vial containing 15 mL of DMSO giving a 0.12 M ethyl chloride stock solution. The free space above the solvent in the vial was kept to less than 1 mL to reduce the risk of evaporation of the ethyl chloride. The amount of ethyl chloride added to the vial was determined by accurately weighing the vial before and after the ethyl chloride was added.

After these solutions had been temperature equilibrated in a constant temperature bath at  $30.000 \pm 0.002^\circ\text{C}$  for 1 h, the reaction was started by injecting 5 mL of the ethyl chloride stock solution into the tetrabutylammonium cyanide solution. One mL aliquots of the reaction mixture were taken and injected into 30 mL of 0.013 M nitric acid. This quenched the reaction by protonating the nucleophile and making it unreactive. **The acidic solution containing HCN from the unreacted cyanide ion was stirred in the fume hood for at least an hour so the hydrogen cyanide was completely removed.** Finally, the concentration of chloride ion was determined using a potentiometric titration and a standard 0.005 M silver nitrate solution.

Ethyl Bromide Reaction: The procedure used for the ethyl chloride reaction was used to measure the rate constants for the ethyl bromide reaction. The only difference was that the stock solutions had different concentrations. A 0.018 M stock solution of ethyl bromide was prepared by injecting 10  $\mu\text{L}$  of ethyl bromide into a sample vial containing 7.00 mL of anhydrous DMSO and a 0.009 M tetrabutylammonium cyanide stock solution was prepared by dissolving approximately 0.126 g of tetrabutylammonium cyanide (accurately weighed) in 50.00 mL of anhydrous DMSO. Finally, 20.00 mL of the tetrabutylammonium cyanide solution was transferred into a reaction flask fitted with a serum cap.

After both stock solutions had been temperature equilibrated at  $20.000 \pm 0.002^\circ\text{C}$  for one hour, the reaction was started by injecting 5.00 mL of the ethyl bromide stock

solution into the reaction flask. Finally, the bromide ion in the sample was determined via a potentiometric titration using a standard 0.0005 M silver nitrate solution.

**Ethyl Iodide Reaction:** The procedure used for the ethyl chloride reaction was used to measure the rate constants for the ethyl iodide reaction. The only difference was that the stock solutions had different concentrations. A 0.011M ethyl iodide stock solution was prepared by injecting 10  $\mu$ L of ethyl iodide into a sample vial containing 10.00 mL of anhydrous DMSO and a 0.006 M tetrabutylammonium cyanide stock solution was prepared by dissolving approximately 0.088 g of tetrabutylammonium cyanide (accurately weighed) in 50.00 mL of anhydrous DMSO. Finally, 20.00 mL of the tetrabutylammonium cyanide solution was transferred into a reaction flask fitted with a serum cap.

After the stock solutions had temperature equilibrated at  $20.000 \pm 0.002^{\circ}\text{C}$  for 1 h., the reaction was started by injecting 5 mL of the ethyl iodide stock solution into the reaction flask. The iodide ion in the sample was analyzed using a potentiometric titration and a 0.0005 M silver nitrate solution.

**Ethyl p-toluenesulfonate Reaction:** The procedure used for the ethyl chloride reaction was used to measure the rate constants for the ethyl tosylate reaction. The only difference was that the stock solutions had different concentrations. A 0.17 M ethyl-p-toluenesulfonate stock solution was prepared by dissolving approximately 0.24g of ethyl p-toluenesulfonate (accurately weighed) in 7.00 mL of anhydrous DMSO and a 0.08 M

tetrabutylammonium cyanide stock solution was prepared by dissolving approximately 1.12 g of tetrabutylammonium cyanide (accurately weighed) in 50.00 mL of anhydrous DMSO. Finally, 20.00 mL of the tetrabutylammonium cyanide solution was transferred into a reaction flask fitted with a serum cap.

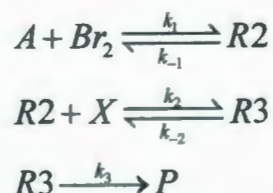
After the reaction flask and the ethyl p-toluenesulfonate stock solution had been temperature equilibrated at  $20.000 \pm 0.002^{\circ}\text{C}$  for 1 hour, the reaction was started by injecting 5mL of the ethyl p-toluenesulfonate stock solution into the reaction flask. Then, 1.00 mL aliquots of the reaction solution were taken and quenched in 3 mL of a methanol solution that was 0.0045 M in the internal standard, methyl benzoate. Five  $\mu\text{L}$  of this solution was injected into the Waters HPLC *immediately* and the concentration of the unreacted ethyl-p-toluenesulfonate was determined from the peak areas using a calibration curve. The HPLC analyses were done using a 83% methanol - 17% water mixture as the eluant at a flow rate of 1mL/min. The UV detector was set at 254 nm.

## Appendix D

**Derivation of rate expression for the bromination of alkenes in protic and aprotic solvents:**

Two possible cases exist for the bromination reaction of alkenes:

**Case 1:**



where X can be Br<sub>2</sub> or a solvent molecule.

Rate of formation of product,

$$\frac{dp}{dt} = k_3[R_3] \quad (2)$$

Following the steady-state approximation,

$$\begin{aligned}\frac{dR_2}{dt} &= k_1[A][Br_2] - k_{-1}[R_2] - k_2[R_2][X] + k_{-2}[R_3] = 0 \\[R_2] &= \frac{k_1[A][Br_2] + k_{-2}[R_3]}{k_{-1} + k_2[X]} \quad (3)\end{aligned}$$

Similarly,

$$\begin{aligned}\frac{dR_3}{dt} &= k_2[R_2][X] - k_{-2}[R_3] - k_3[R_3] = 0 \\[R_3] &= \frac{k_2[R_2][X]}{k_{-2} + k_3} \\&= \frac{k_2[X]}{k_{-2} + k_3} \left( \frac{k_1[A][Br_2] + k_{-2}[R_3]}{k_{-1} + k_2[X]} \right) \text{ [Putting the values of [R}_2\text{]]}\end{aligned}$$

$$= \frac{k_1 k_2 [A][Br_2][X] + k_2 k_{-2} [R3][X]}{(k_{-2} + k_3)(k_{-1} + k_2[X])}$$

$$= \frac{k_1 k_2 [A][Br_2][X]}{(k_{-2} + k_3)(k_{-1} + k_2[X])} + \frac{k_2 k_{-2} [R3][X]}{(k_{-2} + k_3)(k_{-1} + k_2[X])}$$

$$[R3] - \frac{k_2 k_{-2} [R3][X]}{(k_{-2} + k_3)(k_{-1} + k_2[X])} = \frac{k_1 k_2 [A][Br_2][X]}{(k_{-2} + k_3)(k_{-1} + k_2[X])}$$

Since  $k_{-2} \gg k_3$ ,

$$[R3] - \frac{k_2 k_{-2} [R3][X]}{k_{-2}(k_{-1} + k_2[X])} = \frac{k_1 k_2 [A][Br_2][X]}{k_{-2}(k_{-1} + k_2[X])}$$

$$[R3][k_{-2}(k_{-1} + k_2[X])] - k_2 k_{-2} [R3][X] = k_1 k_2 [A][Br_2][X]$$

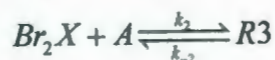
$$k_{-1} k_{-2} [R3] + k_{-2} k_2 [R3][X] - k_2 k_{-2} [R3][X] = k_1 k_2 [A][Br_2][X]$$

$$[R3] = \frac{k_1 k_2}{k_{-1} k_{-2}} [A][Br_2][X] \quad (4)$$

Putting the value of [R3] from eq (4) in eq. (2),

$$\frac{dP}{dt} = \frac{k_1 k_2 k_3}{k_{-1} k_{-2}} [A][Br_2][X] \quad (5)$$

## Case 2:



where X can be Br<sub>2</sub> or a solvent molecule.

Rate of formation of product,

$$\frac{dp}{dt} = k_3 [R3] \quad (6)$$

Following the steady-state approximation,

$$\frac{d[Br_2X]}{dt} = k_1[Br_2][X] - k_{-1}[Br_2X] - k_2[Br_2X][A] + k_{-2}[R3] = 0$$

$$[Br_2X] = \frac{k_1[Br_2][X] - k_{-2}[R3]}{k_{-1} + k_2[A]} \quad (7)$$

Similarly,

$$\frac{d[R3]}{dt} = k_2[Br_2X][A] - k_{-2}[R3] - k_3[R3] = 0$$

$$[R3] = \frac{k_2[Br_2X][A]}{k_{-2} + k_3}$$

$$= \frac{k_2[A]}{(k_{-2} + k_3)} \left( \frac{k_1[Br_2][X] + k_{-2}[R3]}{k_{-1} + k_2[A]} \right) \text{ [Putting the values of } [Br_2X] \text{]}$$

Since  $k_{-2} \gg k_3$

$$= \frac{k_1 k_2 [A] [Br_2] [X] + k_2 k_{-2} [A] [R3]}{k_{-2} (k_{-1} + k_2 [A])}$$

$$k_{-2} (k_{-1} + k_2 [A]) [R3] = k_1 k_2 [A] [Br_2] [X] + k_2 k_{-2} [A] [R3]$$

$$k_{-1} k_{-2} [R3] + k_2 k_{-2} [A] [R3] - k_2 k_{-2} [A] [R3] = k_1 k_2 [A] [Br_2] [X]$$

$$[R3] = \left( \frac{k_1 k_2}{k_{-1} k_{-2}} \right) [A] [Br_2] [X] \quad (8)$$

Putting the value of [R3] from eq (8) in eq. (6),

$$\frac{dP}{dt} = \frac{k_1 k_2 k_3}{k_{-1} k_{-2}} [A] [Br_2] [X] \quad (9)$$

Therefore both case 1 and 2 gives the same rate expressions, eq. (5) and (9).







